BEHAVIOR OF GRANULAR MATERIALS UNDER CYCLIC AND REPEATED LOADING

A

Thesis

Presented to the Faculty

of the University of Alaska Fairbanks

in Partial Fulfillment of the Requirements

for the Degree of

DOCTOR OF PHILOSOPHY

By

George H. Minassian, B.S., M.S.

Fairbanks, Alaska

December 2003

BEHAVIOR OF GRANULAR MATERIALS UNDER CYCLIC AND REPEATED LOADING

By

George H. Minassian

RECOMMENDED:

Advisory Committee Chair

Chair, Department of Civil & Environmental Engineering

APPROVED:

Dean, College of Science Engineering and Mathematics

Dean of Graduate School

December 15, 2003

Date

Abstract

Granular layers are essential contributors to the structural integrity of the pavement system, their premature deformation radically decrease support of the asphalt concrete surface layer, thus leading to the early deterioration of the overall pavement structure. This research was conducted to better understand the behavior of granular materials when subjected to the complex nature of traffic loading.

Long-term triaxial tests were conducted on typical Alaskan base course material using both repeated as well as cyclic loading to also account for the shear reversal effects induced by wheel load. Results show that the shear reversal component of the traffic loads, which have been ignored so far, induces considerable damage to the granular layers. Models were presented to predict the different soil moduli while also accounting the effect of strain hardening or densification due to the repetitive nature of the loads applied. Moreover, a simple yet powerful model was presented to predict accumulated permanent strains as function of the stress state, number of load repetitions and the strength level applied.

The results obtained in this study also show a clear indication of the existence of given stress level limit beyond which incremental collapse of the system takes place. Furthermore, regions of instability of granular layers subjected to dynamic loading have been defined using a simple response parameter and monotonic shear strength of the soil. An effort was made to explain the instability zones identified in this research by the shakedown theory.

Table of Contents

List of Figures

List of Tables

List of Appendices

List of Other Materials

Acknowledgements

The author wishes to express his sincere gratitude to the members of the advisory committee and mainly to his major advisor Professor Lutfi Raad for his invaluable advice, guidance and input throughout the course of this research. Special thanks are due to the Civil and Environmental Engineering Department, the Transportation Research Center, and the Geophysical Institute at the University of Alaska Fairbanks, all for financial support provided through teaching and research assistantships, which made the completion of this dissertation possible. This research would not have been possible to carry out without the technical support received from Howard Fruhwirth, Eric Johansen, Thomas McCarty, and Gary Porter.

The author would also like to recognize the support and understanding he continuously receives from his family and friends. Especially for the encouragement and help received during tough times. Thanks go to Steve Saboundjian, Saber Ebadpour, Steve Brunanski, Hilary Fletcher, Rune Storvold, Kevin Engle, Hillevi Mörtberg, Huan Luong, Fiona Danks, Judy Atkinson, Joe Kemp, Sarah Wolf, and Ryan Woodard. These and many other friends have truthfully proved, time and time again, that friendship multiplies joys and divides griefs.

The author wishes to dedicate this dissertation to his parents, Haroutune and Josephine, and sisters, Maria and Maggie, for their continuous support and never ending sacrifice during the course of his education.

Chapter One

Introduction

1.1 Background

Currently, there are approximately 4 million miles (6.44 million kilometers) of roads in the United States. Roughly sixty three percent are paved ninety four percent of these paved roads have a flexible wearing surface while the rest have a rigid top surface (FHWA 2001). Flexible pavements are asphalt concrete (AC) pavements and are named so, because they are designed such that the total pavement structure deflects, or flexes, under traffic loading. Whereas in rigid pavements, the driving surface is made of Portland concrete (PC) which is quite stiff. Therefore, rigid pavements do not deflect appreciably to accommodate traffic loads.

A flexible pavement structure is typically composed of several layers of different materials. Each layer receives loads from the layer above, spreads them out, and passes on these loads to the next layer below. Thus, the further down in the pavement structure a particular layer is, the less load (in terms of force per area) it must carry and consequently it can be of lower structural quality.

Granular materials are used in base course and subbase layers in a pavement structure. A base course layer is, by definition, the layer of material that lies directly under the wearing surface; and the subbase is the layer that lies between the base course and the natural soil or the subgrade soil. Traditionally, subbase layers are composed of lesser quality granular materials.

The role of granular materials in a pavement section is to distribute the wheel load over a larger area in order to reduce traffic induced stresses in the subgrade layer and also provide the asphalt layer with adequate support to increase its fatigue life or

to prevent pumping when the wearing surface is rigid. Furthermore, the base course layer is designed to provide frost protection and drainage to the system.

The particulate nature of granular material in base and subbase layers provides the necessary properties to perform the role of these layers in a pavement structure. Unbound granular layers are easy to lay down and compact without the need of sophisticated machinery. This expedites construction. Furthermore, the grain-to-grain contact between the particles provides the necessary stability to support the wearing surface and the voids between the aggregates facilitates the drainage function of base course layers. In order to optimize the quality and value of the base course material, special care is taken to choose type, shape, and size distribution of the aggregates and their source proximity to the project at hand.

Most of flexible pavement design procedures presently in use are based on empirical methods developed either from test sections (such as AASHO Road Test, MnRoad, etc...) or laboratory tests (simple shear tests, triaxial tests, etc...). These methods have been more or less satisfactory. However, with an increase in traffic volume and more significant increases in traffic load, better design methods are needed to lengthen the design life of pavement structures in general and unbound granular layers in particular. Data published by the Federal Highway Administration (FHWA 2001), shows that over a three-year period the traffic volume on rural roads increased by 13% and the traffic load on these same roads increased by 28.6% (Figure 1.1).

Since the demand on the highway system to perform is getting higher by the day and in lieu of the shrinking federal and local government budgets geared towards building new highways and maintaining existing ones, it is imperative to update the current pavement design procedures by including more efficient material behavior models.

In this research, an attempt will be made to understand the mechanisms behind the development of deformation in granular materials resulting from applied stress levels.

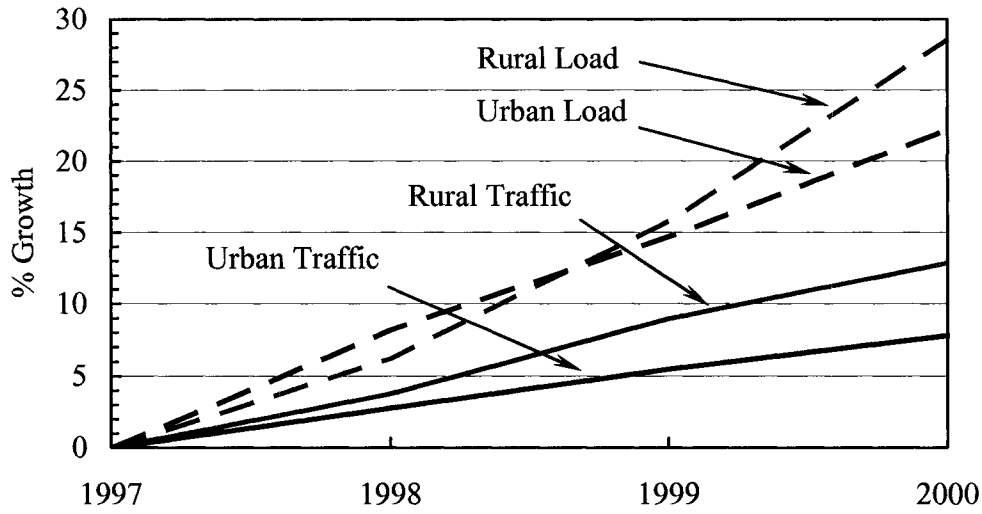

Figure 1.1: Traffic Volume and Load Growth on Urban and Rural Roads (FHWA 2001).

1.2 Problem Statement

Granular layers are essential contributors to the structural integrity of the pavement system. Their premature deformation radically decreases support for the asphalt concrete surface thus leading to early deterioration of the overall pavement structure.

Current granular material models are based on observations made during laboratory testing trying to simulate traffic loads in the field. These models are based on the idea that granular soils generally behave elastically under long term loading. This leads to the use of the material resilient properties in pavement design methods. These same laboratory tests are also used to estimate the amount of the permanent strain accumulated in the system. In this estimation, mostly a relationship between the number of load applications and the permanent vertical strain are derived.

On the other hand, even though the strength of soils subjected to monotonic or static loading have been extensively studied resulting in sound models, the dynamic strength of soils still has not been convincingly addressed. Granular layers in pavement structures are repeatedly subjected to dynamic loads with magnitudes far below the static strength of the material, and yet they still fail.

Understanding the true nature of deformation in granular materials when subjected to dynamic loading and accordingly choosing a suitable model for design is seriously needed. Behavioral insight of these soils will be helpful in predicting pavement performance and designing longer lasting pavement structures.

1.3 Objectives and Limitations of this Study

The major research objectives addressed in this study are:

1. Investigate the stability of granular material under long term dynamic loading and how it relates to static strength.
2. Address the influence of strain rate on static strength and the effect of repetitions on rapid shear strength as part of trying to understand failure under repeated (one-way) and cyclic (two-way) dynamic loading.
3. Examine the effect of shear stress reversal (induced by traffic loading) on resilient behavior and accumulation of permanent strains in granular base course materials.
4. Develop improved relationships that define constitutive modeling (resilient modulus, total modulus – both axial and shear) and improved performance modeling taking into consideration shear stress reversal effects.
5. Provide a possible explanation for the stability of granular material using Shakedown concept terminology.

Due to the meticulous nature of the tests conducted and the aim of obtaining duplicate samples, only one type of soil was considered. The soil used represents a typical Alaskan unbound base course material.

1.4 Organization of the Thesis

The dissertation at hand reports the results and observations of laboratory tests conducted on typical Alaskan Base Course material. After this introduction, Chapter two provides the reader with a literature review on various aspects concerning granular materials in general and their behavior under both static and dynamic loads. Chapter three outlines the experimental setup used to conduct the laboratory tests and presents classical soil mechanics properties of the tested soils. Chapter four presents the results obtained during the course of this research. The results are analyzed and discussed at length in Chapter five, where adequate models are recommended for use in pavement analysis. Moreover, an attempt is made to define the different stages of stability of granular soils when subjected to repeated dynamic loading.

Finally, Chapter six summarizes the contributions from this research. In addition, recommendations for future work are presented.

Chapter Two

Literature Contribution

2.1 Introduction

This chapter presents a historical review of the state of knowledge in granular base material behavior characterization in pavement structures. Resilient and long-term behavioral models, as well as several constitutive models, are presented.

2.2 Resilient Behavior Characterization of Granular Layers.

The deformation of a pavement structure due to the stress induced by a wheel load is conveniently divided into two types: resilient (or recoverable) deformation, and plastic (or permanent) deformation. The resilient response of granular materials has been the topic of many research projects since the 1960's. This behavior was found to be dependent on several factors with varying degrees of importance. These factors are outlined and their effects are explained in the following paragraphs.

2.2.1 Stress Level

The resilient behavior of granular materials is largely dependent on its state of stress. Based on results from triaxial tests, Kasianchuk (1968), Monismith et al. (1967), and Hicks (1970), found that the confining pressure has the most significant effect on the resilient properties of unbound aggregates. Hicks and Monismith (1971) noted an increase of 250 percent in resilient modulus when confining pressure is

increased from 14kPa (2psi) to 70kPa. (10psi). The deviator stress (or shear stress) was also found to affect the resilient modulus but at a relatively lesser degree than the confining pressure. An increase in deviatoric stress from 70kPa (10psi) to 210kPa (30psi) resulted in an increase of 130 percent in resilient modulus at a given confining stress (Hicks and Monismith 1971).

The stress level also affects the resilient Poisson's ratio. Hicks and Monismith (1971), Sweere (1990) and Kolisoja (1997) noticed that Poisson's ratio decreases with an increase in confining pressure and increases with an increase in deviatoric stress.

2.2.2 Gradation, Aggregate Type and Shape

The higher the internal friction in granular materials, the better is their resistance to deformation under loading. Internal friction is dependent on aggregate gradation, type and shape.

The size distribution of the aggregate has the largest influence. Stability in a granular soil is achieved primarily from grain-to-grain contact. The overall deformation in these materials increases with the number of grain-to-grain contacts (corresponding to an increase in probable slippage areas) resulting in lower material stiffness. Therefore, aggregates with high percentage of fines will result in low stability granular base layers. Based on laboratory tests, Kalcheff (1976) and Kolisoja (1997) noted that the rigidity of the aggregate material could be improved by increasing the aggregate nominal size. Barksdale (1972) reported an important reduction in resilient modulus resulting from an increase in fines content from 3 percent to 11.25 percent. Hicks and Monismith (1971) noticed that the resilient modulus, M_R, varied with the percent passing No. 200 sieve and aggregate type. For partially crushed aggregates, it was found that M_R decreased as the percentage of fines increased. However, for crushed aggregates, M_R slightly increased with percent

passing No. 200 sieve. Raad et al. (1992) found out that an increase of fines content led to a decrease of resilient modulus, especially at low values of bulk stresses.

Poisson's ratio is also influenced by gradation. An increase in the content of fines resulted in a decrease in the mean value of Poisson's ratio (Hicks 1970). This decrease was larger in the case of the crushed aggregates.

The influence of aggregate type and shape on the behavior of granular materials was also studied (Barksdale and Itani 1988). These studies concluded that aggregate type significantly influenced M_R. At low values of bulk stress, the resilient moduli of the rough, angular materials were about 50 percent higher than rounded gravel. At high bulk stresses, the resilient modulus of angular granite was about 25 percent higher than that of gravel.

2.2.3 Density

For the same magnitude of stress, as the density of the granular base increases, its resilient response increases.

Based on results of slow repeated cyclic tests on poorly graded sand, Trollope et al. (1962) concluded that the resilient modulus of sand increased with an increase in dry density. The difference in moduli between loose and dense sand was reported to be as much as 50 percent. Similar findings were published by Coffman et al. (1964), who reported that for an increase in dry density from 2180 to 2250 kg/m^3, the resilient modulus increased by 27 percent. Repeated triaxial compression tests carried out by Hicks and Monismith (1971) indicated that M_R increases significantly more with increasing density for the case of partially crushed aggregates than for fully crushed aggregates. Furthermore, the effect of density on the resilient modulus of partially crushed aggregates was found to be less pronounced as the percentage of fines increased in the mix. Barksdale and Itani (1988) noticed that M_R increased with density only at low stress levels whereas this effect was much less at high stress

levels. After testing several types of aggregates, Knutson et al. (1977) concluded that density does not have a significant effect on the resilient behavior of granular mixes. Poisson's ratio is affected only slightly by changes in density (Hicks 1970, Allen and Thompson 1974). In general, an increase in relative density of a mix decreased the Poisson's ratio by a small factor (Hicks and Monismith 1971).

2.2.4 Degree of Saturation

The granular base course in pavement sections can gain moisture from different sources:

- From the top, water may enter joints and cracks in the pavement surface and seep down to the base course.
- From the sides and shoulders, especially when the surface drainage facilities are either absent or inadequate.
- From the bottom, as the water table rises (specially during spring) or through capillary action.

As to the effect of the degree of saturation on the behavior of granular materials, it was noted that the value of M_R decreased with an increase in the degree of saturation (Hicks and Monismith 1971) and this decrease was substantial at very high saturation conditions (Barksdale and Itani 1988, Hayes and Yoder 1963, Dawson et al. 1996).

Hicks and Monismith (1971) noticed that the saturation in the base layer influenced surface deflection, which increased by 15 to 20 percent while measured subgrade deflections remained nearly the same after the base layer was saturated. Other experimental results (Barksdale 1972) also indicated an increase of 68 percent

in the plastic strain for soaked aggregate samples as compared to moist compacted specimens.

Monismith (1966) has suggested the possibility of liquefaction of granular material under repeatedly applied loads if the material is close to saturation and if the drainage is impeded. Hayes and Yoder (1963) reported results for undrained repeated load triaxial tests on gravel and crushed stone similar to the ones used at the AASHO road test. Specimens tested were prepared to in-situ densities. The results show that for crushed stone the resilient modulus decreased slightly as the degree of saturation increased. The modulus of gravel, however, was more sensitive to degree of saturation and decreased to about one half its original value with increased degree of saturation.

Thompson (1969) ran tests on crushed stone material from the AASHO road test at varying degrees of saturation. A substantial increase in permanent deformation was noticed with increased degree of saturation.

Kasianchuk (1968) and Raad et al. (1992) also tested granular aggregates under undrained repeated loading. Pore pressures were measured throughout the tests. It was reported that with increasing number of repeated stresses, an excess pore water pressure tended to develop, which resulted in a reduction of the effective confining stress and the resilient modulus.

Results reported from field tests suggest that both the resilient and total deformations are influenced by the degree of saturation. At the AASHO road test, 80 percent of the failures of the flexible pavements occurred during spring, whereas failures in rigid pavements were distributed uniformly throughout the year (HRB 1962). Similar results were reported at the WASHO road test (HRB 1955) where it was also noticed that more than 50 percent of the total rut depth occurred in the base and subbase layers.

2.2.5 Load History, Frequency, and Duration

In general, researchers agree that the resilient modulus of granular materials is independent of stress history.

Knutson et al. (1977) compared the resilient moduli of different types of aggregates at different densities, before and after they were subjected to 5,000 load repetitions. Due to the scatter and inconsistency of results obtained, they concluded that there is no evidence of any effect of load history on the resilient behavior of granular mixes.

Dehlen (1969) noted that irregular variations in M_R values of granular materials are observed after a few number of load applications. As the number of repetitions increases, these materials tend to densify and become stiffer if the initial void ratio of the mix is above the critical value for the confining pressure applied. Moore et al. (1970) also observed an increase in resilient modulus of crushed limestone due to repeated load. Other investigators (Hicks 1970, Hayes and Yoder 1963) reported that load repetitions, as well as loading sequence (Hicks 1970, Dehlen 1969), did not seem to have any significant effect on the resilient behavior of unbound granular materials. Duration and frequency of loading, however, do not have any significant effect on the resilient modulus and Poisson's ratio (Dehlen 1969, Hicks 1970, and Moore et al. 1970).

2.3 Resilient Behavior Models

Resilient modulus is used to describe the resilient stress-strain relationship of granular materials. This modulus is defined as the ratio of repeated axial (deviator) stress applied, σ_d, divided by the recoverable axial strain, ε_r.

$$M_R = \frac{\sigma_d}{\varepsilon_r} \tag{2.1}$$

Since the resilient modulus was found to be primarily dependent on the confining pressure σ_3, and almost independent of σ_d provided that the latter is not large enough to cause excessive plastic deformation (Dehlen 1969), Dunlap (1963) suggested the following linear relationship:

$$M_R = K_1 + K_2 \cdot (\sigma_r + \sigma_\theta) \tag{2.2}$$

Where σ_r and σ_θ are respectively the radial and tangential stresses. K_1 and K_2 are material dependent constants.

Shortly after, several researchers (Dunlap 1963, Monismith et al. 1967, Dehlen 1969) suggested the use of a simpler expression based on more convenient triaxial test parameters:

$$M_R = K_3 \cdot \sigma_3^{K_4} \tag{2.3}$$

Where K_3 and K_4 are material parameters.

Biarez (1962) had previously suggested the using the first stress invariant (or sum of principal stresses) instead of σ_3 in the Equation 2.3. This was adopted by several investigators (Monismith et al. 1967, Seed et al. 1967, Kasianchuk 1968, Hicks 1970, Hicks and Monismith 1971) and soon after became the most popular expression of M_R, referred to simply as the K-θ model:

$$M_R = K_5 \cdot \theta^n \tag{2.4}$$

Where θ is the sum of principal stresses. K_5 and n are material constants.

After extensive testing Allen and Thompson (1974) concluded that the K-θ model expressed in Equation 2.4 resulted in the highest correlation coefficients and the lowest standard error of estimate when compared to Equation 2.3. It was also shown that the data scatter associated with the model given by Equation 2.3, is due to neglecting the effect of the deviatoric stress, and that an inverse correlation exists between the material constants K_5 and n in Equation 2.4 (Rada and Witczak 1981). Garg and Thompson (1997) suggested a modified version of the Equation 2.3 by including the deviator stress:

$$M_R = K_6 \cdot q^N \cdot \sigma_3^{N_1} \tag{2.5}$$

Where: q = deviator stress,

σ_3 = confining stress,

K_5, N, and N_1 are material dependent parameters.

On the other hand, many authors have criticized the K-θ model (May and Witczak 1981, Brown and Pappin 1985, Uzan 1985). May and Witczak (1981) modified the K-θ model by adding a correction factor to obtain better agreement between the measured and predicted values. This correction factor was found to be a function of the shear strain induced in the granular layer. Therefore, the resilient modulus is not only dependent on the state of stress but also on the magnitude of shear strain induced.

Brown and Pappin (1981) studied the limitations of this model and developed a more complex nonlinear stress-strain relationship known as the contour model, which takes

into consideration the effective, mean, and deviator stress as well as the effect of the stress path followed. In this model, the resilient strain is divided into volumetric and shear components, which are expressed in terms of mean and deviatoric stresses:

$$\varepsilon_{vr} = \left(\frac{p}{A}\right)^{m} \cdot \left[1 - B\left(\frac{q}{p}\right)^{n_1}\right] \tag{2.6}$$

$$\gamma_{nr} = \frac{\gamma_r}{F} = \frac{Cq}{(p+D)} \tag{2.7}$$

Where: ε_{vr} = resilient volumetric strain

p = mean normal stress

q = deviatoric stress

γ_{nr} = normalized resilient shear strain

γ_r = resilient shear strain

F = correction factor for stress path length *l*, given by:

$$F = \left[\frac{l}{\frac{1}{2}(p_1 + p_2)}\right]^{r}; \quad l = \sqrt{(p_1 - p_2)^2 + (q_2 - q_1)^2} \tag{2.8}$$

And, *A, B, C, D, m,* and n_1 are material constants.

Using the equations above, initial volumetric and shear strain values are obtained. These are used to find initial material properties defined by the bulk and shear moduli from the following equations:

$$K = \frac{p}{\varepsilon_{vr}} = \frac{E}{3(1-2\nu)} \tag{2.9}$$

And

$$G = \frac{q}{3\gamma_{nr}} = \frac{E}{2(1+\nu)} \tag{2.10}$$

Where: K = bulk modulus,

p = mean normal stress

q = deviatoric stress

E = Young's modulus

ν = Poisson's ratio

ε_{vr} = resilient volumetric strain

G = shear modulus

γ_{nr} = normalized resilient shear strain

The load is then applied incrementally and the stresses for each incremental step are calculated using the moduli from the previous iteration. Next, the volumetric and shear strains are calculated from the contour model and are used, along with the stresses, to update the material properties. These steps are repeated until convergence in material properties is achieved.

Uzan (1985) noticed that for a given constant confining pressure, the resilient modulus decreased with increasing deviatoric stress. This led him to the same

conclusion as May and Witczak (1981) and consequently he proposed the following model:

$$M_R = K_7 \cdot \theta^{n_2} \cdot \varepsilon_a^{n_3} \tag{2.11}$$

Or

$$M_R = K_8 \cdot \theta^{n_2} \cdot \sigma_d^{n_4} \tag{2.12}$$

Where ε_a = resilient axial vertical strain,

σ_d = repeated deviatoric vertical stress, and,

K_7, K_8, n_2, n_3 and n_4 are material parameters.

Later Witczak and Uzan (1988) rewrote Equation 2.12 by substituting the deviatoric stress, σ_d, by the octahedral shear stress, τ_{oct}, in order to use it in three dimensional pavement analyses. Kolisoja (1997) showed that Uzan's model is far better predictive than the K-θ model and he modified both models to include a correction factor for density, reflected by a porosity term, as follows:

$$M_R = H\left(\eta_{\max} - \eta\right) p_0 \left(\frac{\theta}{p_0}\right)^{0.5} \tag{2.13}$$

And,

$$M_R = L\left(\eta_{\max} - \eta\right) p_0 \left(\frac{\theta}{p_0}\right)^{0.7} \left(\frac{q}{p_0}\right)^{-0.2} \tag{2.14}$$

Where: η_{max} = maximum porosity

η = porosity of base course mix

θ = sum of principal stresses

p_0 = atmospheric pressure

q = deviator stress

H and L are material dependent parameters

Another limitation of the K-θ model is that it assumes a constant Poisson's ratio, which is then used to predict the radial strains. Sweere (1990) used the K-θ model and although he reported good predictions of axial strains, his predictions of the radial resilient strains and, hence, the volumetric strains were rather poor. This is of course due to the assumption of a constant, stress independent Poisson's ratio where in fact it has been proven to be very much dependent on the state of stress. Hicks and Monismith (1971) approximated the variation of Poisson's ratio by a third-degree polynomial function of state of stress, as:

$$\nu_r = A_0 + A_1\left(\frac{\sigma_1}{\sigma_3}\right) + A_2\left(\frac{\sigma_1}{\sigma_3}\right)^2 + A_3\left(\frac{\sigma_1}{\sigma_3}\right)^3 \qquad (2.15)$$

Where A_0, A_1, A_2 and A_3 are regression constants.

The values of Poisson's ratio vary largely and have been reported to be sometimes greater than 0.5 (Sweere 1990). Even though this does seem to violate the laws of thermodynamics, it is due to the fact that the granular media is composed of discrete and unconnected elements, which can dilate and occupy a bigger volume during a stress pulse.

2.4 Limiting Criteria - Permanent Deformation Behavior

The permanent deformation of granular materials has not been explored as much as the resilient behavior has. This is largely due to the fact that permanent deformation studies require long term testing that is both, time consuming and more expensive than resilient testing.

Whereas the resilient behavior is used to obtain a strength parameter needed to design the adequate height of granular layers in a pavement structure, the permanent deformation study helps in predicting the amount of non-recoverable deformation expected to accumulate in granular layers after a certain number of load repetitions. These accumulated permanent deformations lead to rutting in the pavement structure and eventual cracking of the surface layer.

The studies conducted in this field show that the accumulation of plastic deformation in granular layers is dependent on many factors such as: stress level, number of load applications, moisture content, density, aggregate type and gradation, fines content, and stress history. The effect of these factors will be summarized in the following paragraphs.

2.4.1 Stress Level

Researchers agree that stress level is the most important factor affecting the amount and rate of permanent deformation. In general, accumulated plastic deformation increases with an increase in deviator stress levels, and decreases with increasing confining stresses. Based on triaxial testing on clayey subgrade soils, Seed et al. (1955) concluded that as the repeated stress level increased so did the amount of accumulated permanent deformation. Barksdale (1972) showed that for any given number of load applications, higher deviator stress levels yielded much larger accumulated plastic strains. Brown and Hyde (1975) found that the measured axial

plastic strain settled down to a constant value directly related to the ratio of deviatoric stress to confining stress.

2.4.2 Number of Load Applications

Based on testing several different types of dense graded granular materials, Barksdale (1972) concluded that for low deviator stresses the rate of plastic strain accumulation decreases as the number of load applications increases, but beyond a certain critical value of the deviator stress, the rate of the plastic strain accumulation increases with increasing number of load applications. Based on results obtained after extensive testing of base course materials, Knutson et al. (1977) found that the increase in plastic strain in general is inversely proportional to the number of load applications.

2.4.3 Moisture

Barksdale (1972) compared the results of "soaked" specimens of different base course materials with "as compacted" aggregates. He concluded that "soaked" specimens exhibited, on the average, 68 percent more plastic strains than the "as compacted" specimens. The soaked specimens had high degree of saturation but were not completely saturated. Furthermore these specimens were tested under free draining conditions, which means that significant pore pressure build up was not likely during the test.

Dawson et al. (1996) noticed that changes in moisture content affected the amount of accumulated permanent deformation as well as the value of Poisson's ratio. With increasing moisture content, higher permanent strains were recorded and a significant increase in Poisson's ratio was noticed. The magnitude of the effects,

led them to conclude that changes in moisture content may cause much greater changes in permanent deformation than would be caused by changes in magnitude of applied loading.

2.4.4 Density

In general, materials compacted at higher densities offer better resistance to plastic deformation (Knutson et al. 1977, Allen 1973). Barksdale (1972) reports that specimens compacted at 95 percent of maximum compaction density, accumulated on the average 185 percent more plastic strains when compared with specimens compacted at 100 percent of maximum density. However, for densities beyond the maximum density, the change in plastic strain accumulation was minimal.

2.4.5 Aggregate Type, Gradation and Fines Content.

At low confining pressures, angular materials tend to resist permanent deformation better than do rounded materials (Knutson 1977), however this is not necessarily the case at high confining pressures. Allen (1973) reported that crushed aggregates experienced less plastic strain than gravel.

For a given gradation, Barksdale (1972) reports a distinctive difference in the amount of plastic deformation accumulated for two different types of gravel. Knutson et al. (1977) acknowledge the effect of gradation on the amount of accumulated plastic strain, however this effect is not found to be as significant as the effect of stress level and number of load applications.

Plastic strains increased significantly as the percentage of fines increased, with greater differences occurring at larger deviator stress levels (Barksdale 1972).

Brown and Hyde (1975) concluded that loading history has a considerable effect on permanent strain accumulation.

2.5 Permanent Deformation Models

Since stress level and the number of load applications were identified as being major factors affecting the accumulation of permanent deformation in a granular layer, research has been focusing on using either, or both factors to come up with adequate models.

Barksdale (1971) took the hyperbolic model (originally proposed by Kodner et al. (1965) and later developed by Duncan and Chan (1970)) to model static stress-strain relationship), and used it to predict the permanent strains due to repeated loading:

$$\varepsilon_a^p = \frac{(\sigma_1 - \sigma_3) \Big/ K_9 \sigma_3^{n_5}}{1 - \left[\frac{(\sigma_1 - \sigma_3) \cdot R_f}{2(c.\cos\phi + \sigma_3 \cdot \sin\phi)/(1 - \sin\phi)} \right]} \qquad (2.16)$$

Where:

ε_a^p = axial plastic strain for a given number of load applications N,

$K_9\ \sigma_3^{n5}$ = relationship defining the initial tangent modulus as a function of confining pressure σ_3 (K_9 and n_5 are constants),

c = cohesion

ϕ = angle of friction, and

R_f = ratio of measured strength to an asymptotic stress difference.

Barksdale (1972) used repeated triaxial test to study large variety of granular material types under different conditions. Based on the results obtained, he proposed a simple expression to predict permanent axial strains as a function of the number of load applications:

$$\varepsilon_a^p = a + b \cdot \log(N) \tag{2.17}$$

Where:

ε_a^p = accumulated axial plastic strain,

N = number of load applications, and,

a and b are regression parameters

Monismith et al. (1975) used a log-log version of Barksdale's expression which was proved later by Sweere (1990) to better predict permanent strains specially at large values of N, beyond 100,000 repetitions. This expression is simply given by:

$$\varepsilon_a^p = aN^b \tag{2.18}$$

Majidzadeh et al. (1978) studied the development of permanent deformation, ε_a^p, in subgrade soils under repeated loading. This study concluded the following relationship:

$$\frac{\varepsilon_a^p}{N} = a \cdot N^{-b} \tag{2.19}$$

Later, Khedr (1985) successfully applied this same relationship to granular materials.

Research done in South Africa (Theyse 1999, Wolff and Visser 1994) using full-scale Heavy Vehicle Simulator Tests (HVS), suggested a relationship which is argued to be more accurate for predicting permanent deformations after very large number of load repetitions, as follows:

$$\varepsilon_a^p = (cN + a)\left(1 - e^{-bN}\right) \tag{2.20}$$

Where a, b, and c are regression parameters.

Paute et al. (1996) suggested an expression combining the effects of both stress level and number of load applications. This expression assumes that the permanent strain in a granular mix accumulates asymptotically to a certain maximum value, which is a function of the static strength of the material. The model adds the measured permanent strain accumulated after 100 load cycles to the amount predicted, ε_a^p*, to occur from thereafter.

$$\varepsilon_a^p(N) = \varepsilon_a^p(100) + \varepsilon_a^{p*}(N) \tag{2.21}$$

And,

$$\varepsilon_a^{p*}(N) = A\left[1 - \left(\frac{N}{100}\right)^{-B}\right] \tag{2.22}$$

A and B, in the above equation, are positive regression parameters. As the number of load applications, N, increases ε_a^p* reaches a limit value equal to A. The value of A is dependent on the static strength of the material and given by the following hyperbolic function:

$$A = \frac{\left(\frac{q_{max}}{p_{max} + p^*}\right)}{a - b \cdot \left(\frac{q_{max}}{p_{max} + p^*}\right)} \tag{2.23}$$

Where:

p_{max} is the maximum mean normal stress during repeated loading, given by:

$$p_{max} = \frac{\sigma_1' + \sigma_3'}{2} \tag{2.24}$$

q_{max} is the maximum deviator stress during repeated loading, given by:

$$q_{max} = \frac{\sigma_1' - \sigma_3'}{2} \tag{2.25}$$

p^* = stress parameter related to failure line of the material (Figure 2.1),

a and b are positive material parameters

p_{max} and q_{max} define the stress pass length and the static failure line is defined by q_f as shown in Figure 2.1, or given by:

$$q_f = m \cdot p + s = m \cdot (p + p^*) \tag{2.26}$$

Lekarp et al. (1997) examined the model presented by Paute et al. (1996) and concluded that whereas the permanent strain prediction part of the model seems successful, the limiting value it asymptotically reaches is not dependent on the stress ratio presented. They believe there is no indication that the total permanent axial strain is in any way dependent on the static strength of the material. This said, Lekarp et al. (1997) still agree that a certain stress ratio, greater or smaller than the static strength, indeed seems to have a significant impact on the plastic deformation development.

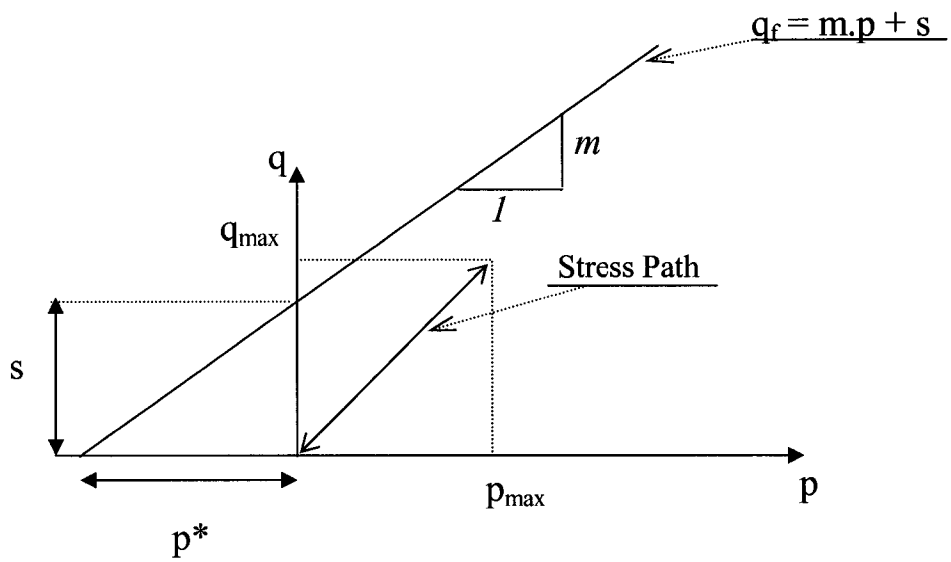

Figure 2.1: Stress Path and Static Failure Line as Defined by Paute et al. (1996)

Pappin (1979) had previously tried to express the accumulated permanent strain rate for a given number of load applications, to the length of the repeated stress path applied. Using the same principal, Lekarp and Dawson (1997) presented a simple expression, given by:

$$\frac{\varepsilon_a^p\left(N_{ref}\right)}{L/p_0} = a \cdot \left(\frac{q}{p}\right)_{max}^{b} \qquad (2.27)$$

Where:

ε_a^p (N_{ref}) = accumulated permanent axial strain after N_{ref} number of cycles,

N_{ref} = any given number of load cycles greater than 100

L = length of stress path in *q-p* space,

p_0 = reference stress, e.g. atmospheric pressure,

q_{max} = maximum deviator stress,

p_{max} = maximum mean normal stress, and

a and *b* are regression parameters

2.6 Cyclic Shear Behavior

The dynamic repetitive nature of cyclic loading is the cause of several soil behavior features that are not encountered when the soil is subjected to monotonic or slowly applied loads.

Repeated cyclic shear straining of loose to medium dense sand under drained conditions causes densification. This densification increases with every repetition at a decreasing rate, as shown in Figure 2.2, and is the result of soil particles being rearranged during the back and forth straining (Youd 1972). In the case of saturated soils, the cyclic loading applied causes the soil structure to decrease in volume. However, due to the presence of incompressible fluid (water) in the voids within the soil fabric and the fact that its movement is prevented (undrained condition), densification cannot take place. Instead, part of the stress applied is transferred to the pore water, which translates, into a decrease in the effective stress of the sample. The pore water pressure increases with load application until it becomes equal to the initial confining pressure; this condition is termed as *liquefaction*. The number of load cycles needed to reach this condition is dependent on many factors such as initial relative density of the soil and the magnitude or level of the cyclic load (or deformation) applied.

Based on results of a variety of tests (e.g. cyclic simple shear, shaking table, resonant column and cyclic triaxial tests) researchers (Silver and Seed 1971, Youd 1972) have argued that the process of densification is controlled by the amplitude of

cyclic strain rather than by the level of cyclic stress applied. Furthermore, the existence of a threshold shear strain, γ_t, below which no densification occurs regardless of the number of load repetitions, was determined (Hardin and Black 1968, Drnevich and Richard 1970, Youd 1972) to be approximately 0.01% (Yokel et al. 1980, Dobry et al.1981) regardless of the initial relative density of the soil, as can be seen in Figure 2.3.

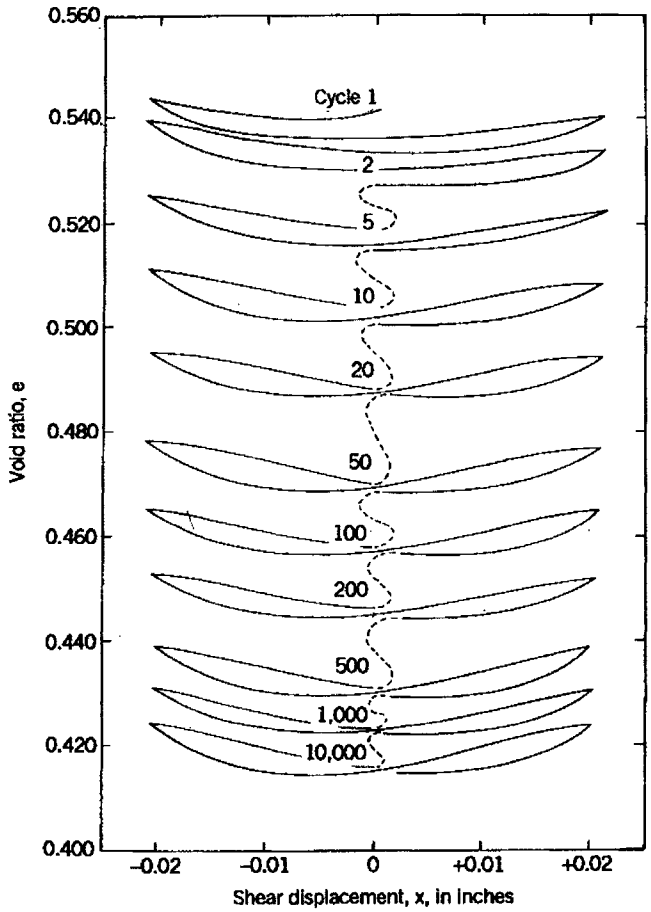

Figure 2.2: Densification of Sand Due to Cyclic Shear Displacement.
Source: Youd (1972)

Vucetic (1994) suggested the existence of two separate threshold shear strains that affect the behavior of soils under cyclic loading; these are, the linear cyclic

threshold shear strain γ_{tl}, and the volumetric threshold shear strain γ_{tv} with γ_{tv} being greater than γ_{tl}. He further suggested that these represent boundaries between fundamentally different categories of cyclic soil behavior. For cyclic shear strains below γ_{tl}, soil behaves essentially as a linearly elastic material. Between γ_{tl} and γ_{tv}, soil becomes more and more nonlinear but remains elastic, and for shear strains above γ_{tv} soil behaves as a nonlinear inelastic material. According to Vucetic's definition, γ_{tv} is the same threshold shear strain previously denoted as γ_t.

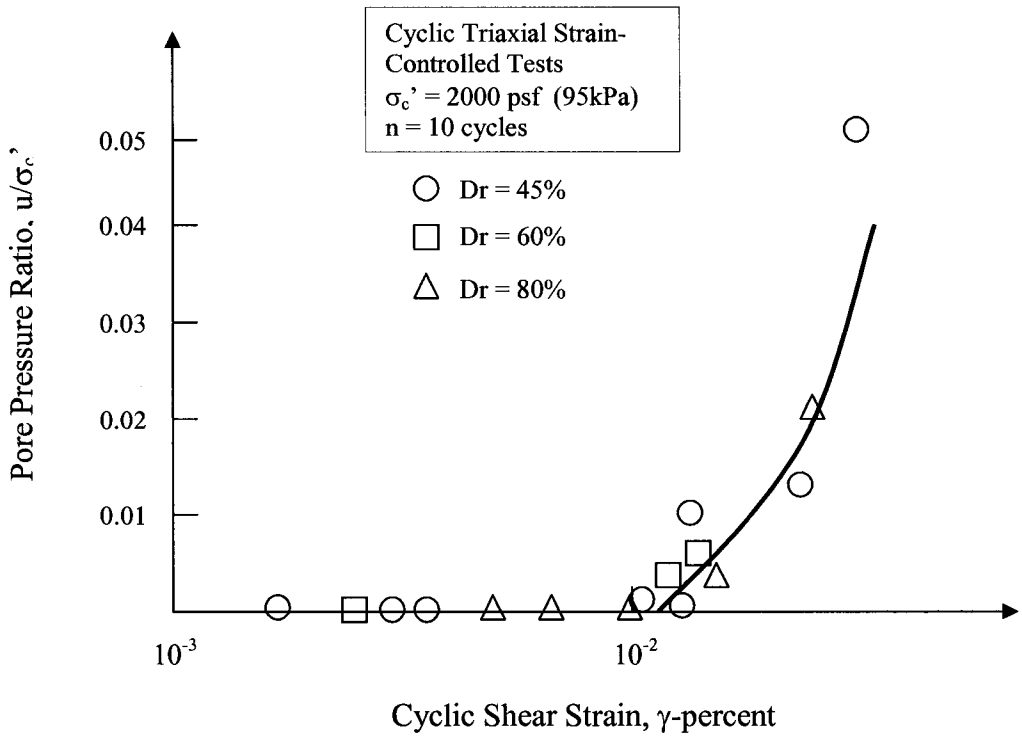

Figure 2.3: Pore Pressure Buildup versus Cyclic Shear Strain Showing the Existence of a Threshold Shear Strain. Source: Yokel et al. (1980)

For non-cohesive soils, researchers reported values of γ_{tv} ranging anywhere from 0.005 % to 0.03 % with an average value of γ_{tv} equal to 0.01 %. As for cohesive soils, the reported values are somehow higher and range between 0.04 % and 0.2 %

(refer to Table 2.1). Vucetic (1994) concluded that the value of γ_{tv} generally increases as the size of the particle increases. Accordingly, both linear and volumetric threshold shear strains were found to increase with the plasticity index of a soil.

Table 2.1: Summary of γ_{tv} Values for Different Soils.

Soil	Test	Relative Density	γ_{tv} (%)	Reference
Saturated Gravel	Undrained Triaxial	25% - 45%	0.005 – 0.02	Hynes-Griffin (1988)
Dry Clean Sand	Drained Simple Shear	45% - 80%	0.02 – 0.03	Silver and Seed (1971)
Saturated Clean Sand	Drained Simple Shear	77 %	0.01 – 0.02	Youd (1972)
Saturated Clean Sand	Undrained Triaxial	60%	0.012 – 0.028	Dobry et al. (1981)
Saturated Clean Sands	Undrained Triaxial	45% - 80%	0.01 – 0.015	Dobry et al. (1982)
Saturated Clay	Undrained Triaxial	55%	0.10	Matsui et al. (1980)
Saturated Clays	Undrained Torsional	?	0.04	Macky and Saada (1984)
Partially Saturated Clayey Sand	Drained Simple Shear	Different D_r.	0.10	Pyke et al. (1973)
Partially Saturated Clay	Drained Simple Shear	Different D_r.	0.07-0.20	Chu and Vucetic (1992)

While shear strain is widely recognized to be the governing parameter responsible for triggering phase change in soils subjected to cyclic loading, some researchers tried to look at the stress level applied to come up with a certain threshold level separating different behavior patterns of soil under cyclic loading. The first of such studies was done by Roscoe et al. (1958) at Cambridge University, which eventually led to a well-known soil model known as the Cam-clay model. However, the pioneering work in this field was done in France by Habib and Luong (1978) (Characteristic state) and in Japan by Tasuoka and Ishihara (1974) (phase transformation), others include Castro (1969) (steady state).

When a saturated soil mass is subjected to cyclic loading, the progressive decrease in effective stress results in an increase in permanent shear strain under constant stress cyclic loading or a decrease in the cyclic stress if subjected to a controlled strain test. For both cases, the most popular way to represent the strength degradation of saturated soils when subjected to cyclic loading is to plot the ratio of cyclic shear stress applied (τ) to the initial effective confining pressure (σ_0') versus the number of load repetitions needed to cause liquefaction.

2.7 Shakedown Considerations

The classic question addressed by shakedown theory is whether under a certain domain of load variations applied to a given structure, a state is reached where the accumulation of plastic strains in the structure cease and all subsequent load applications will only produce elastic changes in stresses and deformations. In this case the structure is said to have reached a stable response and a shakedown condition is attained.

The static shakedown theorem, originally developed by Melan (1936), states that a system will shakedown under repeated cyclic loads if a self-equilibrated residual stress field could be found such that equilibrium conditions, boundary conditions, and yield conditions are point wise satisfied. The material in this case is

assumed to be elastic-perfectly plastic with convex yield surface and applicable normality condition and that viscous and inertia effects are negligible. Numerical methods for the application of the static shakedown theorem in pavement structures have been proposed by a number of investigators (Sharp and Booker 1984, Sharp 1985, Raad et al. 1988, Raad et al. 1989, Weichert and Raad 1992, Raad and Weichert 1995, Boulbibane and Weichert 1997, Boulbibane et al. 2000), while others (Lekarp and Dawson 1997, Werkmeister 2001) tried to explain observed laboratory behavior of granular materials in particular using static shakedown concept and terminology. All of these efforts appear to bear encouraging results.

2.8 Failure and Constitutive Models

2.8.1 Static versus Dynamic Problems of Soils

In order to evaluate the strength of soils, classical soil mechanics considered mainly static forces applied to a system such as forces involved in the evaluation of the degree of safety of foundations or soil structures against failure. A common approach has been to evaluate available strength of soils (mostly using Möhr-Coulomb criteria) and to compare it against the stresses induced by external loading. Thus attention has been centered to evaluate the strength of soil. The other major concern in the field has been the amount and rate of settlements of the ground or structures associated with the deformation of soils.

In contrast, in soil dynamics, the subject of study is the state of soil in motion, which introduces the inertia force as an important factor that cannot be neglected. This force plays an increasingly significant role as the time interval at which deformation occurs becomes shorter. Consequently, even if the level of strain (or deformation) is small, the inertia force could become significantly great with increasing speed of loading (and/or number of repeated load application) to a point

where its influence can no longer be neglected in engineering practice. For this reason it becomes necessary in soil dynamics to draw attention to the behavior of soils subjected to very small strain levels, which are completely neglected in conventional soil mechanics dealing with static loading. This is one of the most important aspects that distinguish dynamic problems from the static ones.

Since the 1960's, as interest in studying the detrimental effects and mechanism of dynamic loading increased, a lot of effort has been directed towards acquiring a better understanding of soil behavior. Digital computer technology and numerical techniques encouraged researchers to explore further and expand the horizon of the field. They have developed with numerous numerical formulations that rely mainly on mechanics in general and continuum mechanics in particular. The following is a comprehensive overview of soil constitutive models.

2.8.2 Historical Background

The earliest attempt to rationalize the behavior observed in laboratory soil tests was done at Cambridge (Roscoe et al. 1958). The work was performed mostly on clays but several of the concepts they developed found applications to granular materials. The development of the Cambridge model included the "critical state" theory and the "Cam Clay" (elasto-plastic constitutive soil) model. The Cambridge model can account for such experimental observations as:

a) Permanent volumetric deformation occurring under hydrostatic loading conditions.
b) Existence of a coupling between volumetric changes and changes in the shear stress.
c) Dense soils expand in volume during shear whereas loose soils contract.

The most obvious limitations of this model are:

a) It does not adequately model structural and stress-induced anisotropy.
b) It is not applicable to cyclic shear loading conditions.
c) It does not reflect the strong dependency of the shear dilatancy on the effective stress ratio.
d) It does not account for the viscous time-dependent stress-strain response of cohesive soils.

Since then, more elaborate constitutive models have been constructed to remove some of the limitations of the original model. Several elastic, micro-mechanical and many elastic-plastic models with various degrees of complexity have been proposed. Other models, which have been proposed, include: simple nonlinear elastic stress-strain models like the hyperbolic model that have been applied to various types of soil with different degrees of success (Kodner and Zelasko 1963, Hardin and Drnevich 1972, Griffiths and Prevost 1990); and many other empirical models which rely on analytical relations based on experience and/or experimental observations. However, the most promising models for granular materials seem to be the Cap models. For a detailed review of constitutive models in soils, the reader is referred to an excellent review written by R. Scott (1985).

2.8.3 Cap Models

The most popular and widely used soil models are Cap models based on classical isotropic plasticity theory, and are variations and refinements of the basic Cap model introduced by Drucker, Gibson and Henkel (1957). Important limitations of these Cap models are:

- They do not adequately model stress-induced anisotropy.
- They are not applicable to cyclic loading conditions.

Later more powerful and flexible material models were achieved by using a set of nested yield surfaces in stress space to account for continuous yielding combined with kinematic and isotropic hardening/softening plastic rules (Prévost 1978).

In Cap models, the yield function is assumed to be composed of two parts: (1) a failure envelope beyond which only ideal plastic deformation occurs, and (2) a strain hardening cap usually modeled as an ellipse or sphere (or flat as suggested by Vermeer 1980) that expands isotropicly with plastic strains. A typical Cap model in I_1 - $J_2^{1/2}$ space is shown in Figure 2.4.

The failure envelope is usually stationary (although some models use expanding envelopes) and the most popular failure envelopes used are the Möhr-Coulomb, the Drucker-Prager and the Lade-Duncan envelopes. These models are compared to each other in Figure 2.5 and their advantages and disadvantages are summarized in Table 2.2.

The Coulomb failing criterion dates back to 1773 and certainly is the best-known failure criterion in soil mechanics. It was proposed for geotechnical materials and takes into effect the hydrostatic pressure on the strength of granular materials. This criterion states that failure occurs when the shear stress τ and the normal stress σ acting on any element in the material satisfy the linear equation

$$\tau - \sigma \cdot \tan\phi - c = 0 \qquad (2.28)$$

Where c and ϕ are respectively the cohesion and the angle of friction of the material. For a given state of stress (σ_1, σ_2, σ_3) and if $\sigma_1 > \sigma_2 > \sigma_3$, the Möhr-Coulomb criteria can be written as:

$$\tfrac{1}{2}(\sigma_1-\sigma_3)=-\tfrac{1}{2}(\sigma_1+\sigma_3)\cdot\sin\phi+c\cdot\cos\phi \qquad (2.29)$$

Each principal stress can be expressed in terms of the stress invariants I_1 and J_2 and the Lode angle θ, and we obtain:

$$\begin{aligned}\sigma_1&=\frac{2}{\sqrt{3}}\sqrt{J_2}\cdot\cos\theta+\frac{1}{3}I_1\\ \sigma_2&=\frac{2}{\sqrt{3}}\sqrt{J_2}\cdot\cos(\theta-\frac{2}{3}\pi)+\frac{1}{3}I_1\\ \sigma_3&=\frac{2}{\sqrt{3}}\sqrt{J_2}\cdot\cos(\theta+\frac{2}{3}\pi)+\frac{1}{3}I_1\end{aligned} \qquad (2.30)$$

Where:

I_1 = the first invariant of the stress tensor.

J_2 = the second invariant of the deviatoric stress tensor.

And the Lode angle θ, can be expressed in terms of the second (J_2) and third (J_3) invariants of deviatoric stress, and is given by:

$$\theta=\frac{1}{3}\cos^{-1}\left[\frac{3\sqrt{3}}{2}\frac{J_3}{J_2^{3/2}}\right] \qquad (2.31)$$

Therefore substituting the σ_1, σ_2 and σ_3 expressions in equation 2.27, we obtain:

$$I_1\cdot\sin\phi+\frac{1}{2}\left[3\cdot(1-\sin\phi)\cdot\sin\theta+\sqrt{3}\cdot(3+\sin\phi)\cdot\cos\theta\right]\sqrt{J_2}-3\cdot c\cdot\cos\phi=0$$

Or,

$$\sqrt{J_2} = \frac{-2I_1 \sin\theta + 6c \cos\theta}{3(1-\sin\phi)\sin\theta + \sqrt{3}(3+\sin\phi)\cos\theta} \qquad (2.32)$$

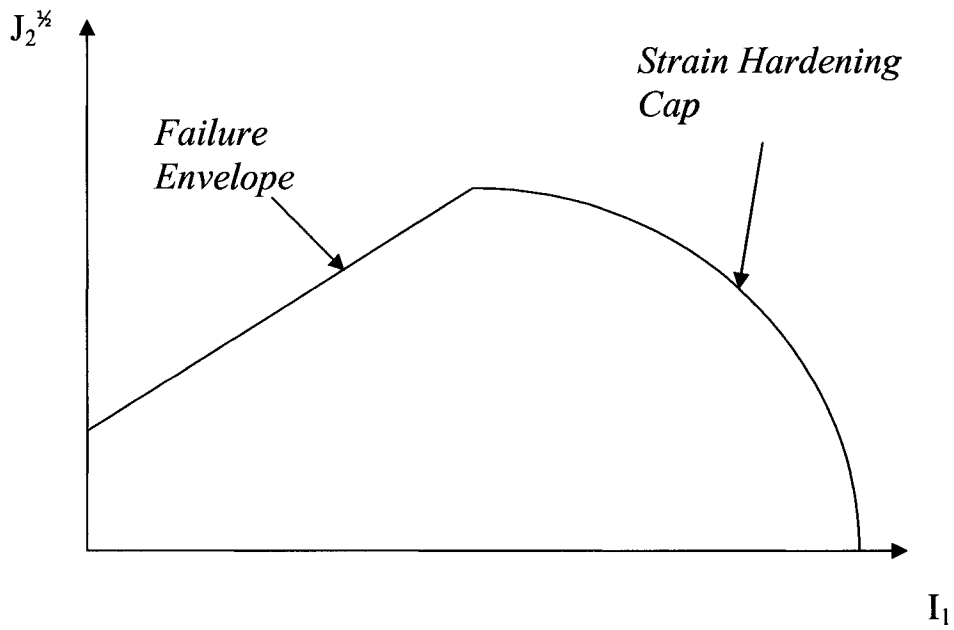

Figure 2.4: Schematic Representation of a Typical Cap Model

The Von Mises yield criterion for metals was modified by Drucker and Prager (1952) so that it would be applicable for soils. The yield surface of this Drucker-Prager model (also known as extended Von Mises criterion) in principal stress space is a right circular cone equally inclined to the principal axes. The intersection of the π-plane with this yield surface is a circle as shown in Figure 2.5. The failure function used by Drucker and Prager to describe this cone has the form:

$$\alpha \cdot I_1 + \sqrt{J_2} - k = 0 \tag{2.33}$$

Where α and k are material constants and can be related to cohesion c and friction angle ϕ (for compressive meridian case) with the following equations:

$$\alpha = \frac{2\sin\phi}{\sqrt{3}(3-\sin\phi)} \tag{2.34}$$

$$k = \frac{6 \cdot c \cdot \cos\phi}{\sqrt{3} \cdot (3-\sin\phi)} \tag{2.35}$$

Lade and Duncan (1973, 1975) investigated the characteristics of *Monterey Sand No. 0* by means of cubical triaxial tests. Failure states were examined for different relative magnitudes of intermediate principal stress, b, defined as:

$$b = \frac{\sigma_2 - \sigma_3}{\sigma_1 - \sigma_3} \tag{2.36}$$

Where σ_1, σ_2, σ_3 are the principal stresses and the value of b varies between zero and unity. Based on results of tests conducted on specimens with a variety of densities, ranging from loose to very dense, Lade and Duncan proposed a failure criterion that can be simply expressed as:

$$\kappa_1 = \frac{I_1^3}{I_3} \tag{2.37}$$

Where I_1 and I_3 are respectively the first and third invariants of the stress tensor, and κ_1 is a value of stress level at failure, which depends on the density of granular materials.

Table 2.2: Comparison of Different Failure Envelopes Used in Cap Models.

Failure Surface	**Shape on π-plane**	**Advantage**	**Disadvantage**	**Variables**
Möhr- Coulomb	Irregular hexagonal	• Simple • All Soils	Singularities due to corners	ϕ and c
Drucker - Prager	Circle	• Simple • Smooth Function	Neglects effect of I_3	k and α
Lade-Duncan	Ellipsoidal triangle	• Smooth Function • Includes effect of I_3	Based on true triaxial test results	κ_1

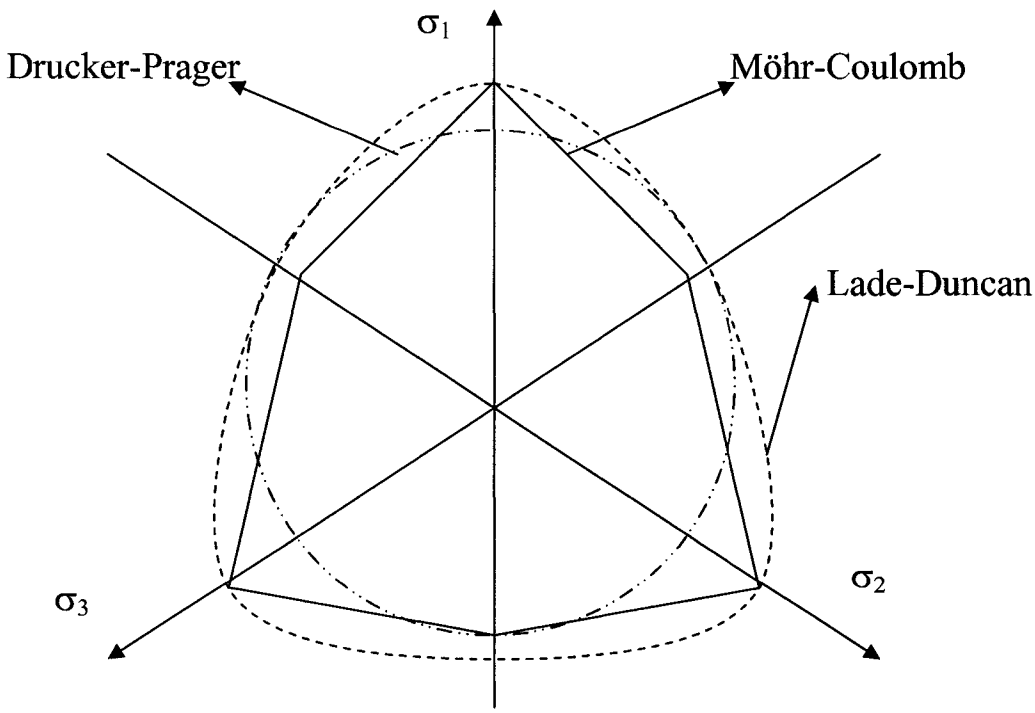

Figure 2.5: Projection of the Failure Surfaces with the π-plane ($\sigma_1 + \sigma_2 + \sigma_3 = 0$)

2.8.4 Specific Models

In this section, some Cap models that best seem to apply to granular materials are presented. These models are compared to each other and their advantages and disadvantages are given.

2.8.4.1 Desai-Bonaquist Model

The basic hierarchical model presented by Desai et al. (1986) was developed only for monotonic loading conditions and assumed effective stresses. Furthermore, Desai et al. only included equations for the plastic strains and did not provide specific constitutive forms for the elastic strains but envisioned that these would be functions of stress or strain invariants.

For his research, Bonaquist (1996) took Desai's model and modified it to enhance its predictive capability for plastic strains and checked its sensitivity for the range of granular material used (base course, subbase, and subgrade materials) in pavement structures. He also presented equations describing the resilient strains as function of the same stress invariants used in the yield surfaces. Finally, he developed a cyclic hardening model to account for the accumulated permanent deformation behavior of these granular materials during repeated loading.

The basic hierarchical model used in Bonaquist's research, is an isotropic hardening model with associated flow. The model consists of a series of yield surfaces, which expands with increasing plastic strains. The final form of the equation used by Bonaquist to describe these yield surfaces is:

$$\frac{J_2}{p_0^2} - \left[\alpha \left(\frac{I_1 + \frac{k}{\sqrt{\alpha}}}{p_0} \right)^2 - 0.002408 \frac{\sqrt{\alpha}}{\xi^{0.45}} \left(\frac{I_1 + \frac{k}{\sqrt{\alpha}}}{p_0} \right)^{3.05} \right] = 0 \qquad (2.38)$$

Where:

J_2 = Second deviatoric invariant of stress.

I_1 = First stress invariant.

p_0 = Atmospheric pressure

k, α = Drucker- Prager material failure parameters, obtained from a series of monotonic triaxial drained tests.

ξ = Plastic strain trajectory, and given by,

$$\xi = \int \left(d\varepsilon_1^p + 2 d\varepsilon_3^p \right)^{1/2} \qquad (2.39)$$

Where $d\varepsilon^p{}_1$ and $d\varepsilon^p{}_3$ are respectively the permanent axial and radial strain increments.

The yield surfaces and flow rule describe the plastic portion of the elastic-plastic response of the basic hierarchical model. The elastic strains in this model are assumed to follow an incremental form of Hook's law, where the elastic constants are expressed in terms of stress or strain invariants. The model, representing the elastic behavior is given by:

$$\gamma_{oct} = g_1 \left(\frac{I_1}{p_a} \right)^{g_2} \left(\frac{\sqrt{J_2}}{p_a} \right)^{g_3} \qquad (2.40)$$

Where:

γ_{oct} = Octahedral shear strain

g_1, g_2, g_3 = Fitting parameters which were found to be highly dependent on the Drucker-Prager failure parameters and consequently can be obtained by:

$$g_1 = \frac{0.00146}{\alpha^{0.62}} \tag{2.41}$$

$$g_2 = 0.425 - 3.91\sqrt{\alpha} \tag{2.42}$$

$$g_3 = 0.552 + 2.98\sqrt{\alpha} \tag{2.43}$$

And since the octahedral shear stress is given by:

$$\tau_{oct} = \frac{\sqrt{2}}{3}\sqrt{J_2} \tag{2.44}$$

Consequently, the secant shear modulus G_s can be expressed by:

$$G_s = \sqrt{\frac{2}{3}}\frac{\sqrt{J_2}}{g_1}\left(\frac{I_1}{p_a}\right)^{-g_2}\left(\frac{\sqrt{J_2}}{p_a}\right)^{-g_3} \tag{2.45}$$

And the Poisson's ratio is given by:

$$\upsilon = 0.447 - 0.345\left[\frac{\sqrt{J_2}}{\alpha^{1/2}I_1 + k}\right] + 0.404\left[\frac{\sqrt{J_2}}{\alpha^{1/2}I_1 + k}\right]^{4.44} \tag{2.46}$$

Since isotropic hardening models such as the hierarchical model were developed for monotonic loading conditions, modifications were required to apply these models to repeated or cyclic loading.

This modification was achieved by choosing a bounding yield surface concept presented by Mroz et al. (1978). In this approach, two yield surfaces are used. The first yield surface is the initial surface, which describes the past loading history of the material. The second yield surface is the bounding surface, which describes the current stress state. During repeated loading, the initial surface expands while the bounding surface remains stationary. Elastic behavior is assumed for stresses below the initial yield surface and elastic-plastic behavior is assumed for stresses between the initial and bounding yield surfaces. When the initial and bounding surfaces coincide, the response is purely elastic and no additional permanent deformation occurs.

The location of the bounding yield surface is dependent on the state of stress and is characterized by ξ_b, given by:

$$\xi_b = \left[\frac{a_1 \left(\frac{I_1}{p_a} \right)^n}{\left(\frac{\alpha I_1^2 - J_2}{p_a^2} \right)} \right]^{\frac{1}{\eta_1}} \tag{2.47}$$

Whereas the initial yield surface depends on the past loading history and is characterized by ξ_i given by:

$$\xi_i = \xi_0 + \left(1 - \frac{1}{N^{a_2}} \right) \cdot (\xi_b - \xi_0) \tag{2.48}$$

Where:

ξ_i = location of the initial surface

ξ_b = location of the bounding surface

ξ_0 = initial location of the initial surface

N = number of repetitions

a_2 = hardening coefficient = $1.09\ (1 - r^5)^{1/3}$

and r = stress to strength ratio

2.8.4.2 Lade Model

Lade and Duncan (1975) studied the characteristics of cohesionless soils performing cubical triaxial tests on Monterey Sand. Based on these tests (loose and dense sand), they developed the isotropic elastic-plastic work-hardening model, based on failure criterion mentioned above. The model was also verified by plotting data from several other researches. Their model contains subsequent yield (or loading) surfaces and a failure surface. The form of the failure surface f_f is again expressed in terms of the stress invariants I_1 and I_3.

$$f_f = I_1^3 - k_1 I_3 \tag{2.49}$$

Or using the other stress invariants,

$$f_f = J_3 - \frac{1}{3} I_1 J_2 + \left(\frac{1}{27} - \frac{1}{k_1} \right) I_1^3 = 0 \tag{2.50}$$

Similarly, the form of the loading surfaces f_l, is given by:

$$f_l = J_3 - \frac{1}{3} I_1 J_2 + \left(\frac{1}{27} - \frac{1}{k} \right) I_1^3 = 0 \qquad (2.51)$$

Where k is a value, which is determined from the current stress level and varies from 27 for hydrostatic stress condition ($\sigma_1 = \sigma_2 = \sigma_3$) up to a value of k_l at failure. Consequently, the loading surface expands isotropicly around the hydrostatic axis as the applied stress level approaches the failure condition.

In the three-dimensional principal stress view, this failure surface is conical with a smooth triangular-elliptic base. On the π-plane, the triangular-elliptic shape looks like a smooth-edged approximation of the Möhr-Coulomb failure surface (Figure 2.5).

Further investigations led Lade and Duncan to introduce a plastic potential function g similar to the failure form:

$$g = J_3 - \frac{1}{3} I_1 J_2 + \left(\frac{1}{27} - \frac{1}{k_2} \right) I_1^3 = 0 \qquad (2.52)$$

Where k_2 has a constant value for a given stress level and related to the directions of the plastic strain in the triaxial plain (for both triaxial compression and tension) which were found to be at acute angles to the failure surface thus not satisfying the normality condition of classical plasticity theory.

Based on several experimental results, k_2 variation was expressed as a function of the current stress level, k, as:

$$k_2 = A \cdot k + 27(1 - A) \qquad (2.53)$$

Where A is the inclination of straight line which can be determined from experimental data. The value of k_2 varies from 27 (for k = 27) under hydrostatic stress to a value of $A\ (k_1\text{-}27) + 27$ for $k = k_1$ at failure.

A relation between the plastic work W_p given by:

$$W_p = \int \sigma_{ij}\ d\varepsilon_{ij}^p \tag{2.54}$$

and the current stress level, $k = I_1^3/I_3$, was examined from experimental results and a hyperbolic relationship was suggested, such as:

$$k - k_t = \frac{W_p}{\left(a + dW_p\right)} \tag{2.55}$$

Where k_t is a threshold stress level. The assumption is that for the value 27 up to k_t, no plastic strain occurs and no plastic work is done. Only elastic behavior dominates until the stress level reaches $k = k_t$. The parameter a may be expressed as:

$$a = M \cdot p_0 \left(\sigma_3 / p_0\right)^l \tag{2.56}$$

Where p_0 is the atmospheric pressure, and σ_3 is the initial confining pressure. Both M and l are dimensionless numbers, which may be determined by plotting the a-values versus the σ_3-values on a log-log scale.

Once knowing the current value of stress level and the difference in k between two successive stress states, dW_p can be calculated from:

$$dW_p = \frac{a\ dk}{\left[1 - d\left(k - k_t\right)\right]^2} \tag{2.57}$$

And then from the non-associated flow rule assumption, the plastic strain increments, $d\varepsilon_{ij}^p$, are calculated as follows:

$$d\varepsilon_{ij}^p = d\lambda \frac{\partial g}{\partial \sigma_{ij}} \tag{2.58}$$

Where the positive scalar function $d\lambda$ is expressed as:

$$d\lambda = \frac{dW_p}{3g} \tag{2.59}$$

And the elastic strain increments are calculated from Hook's law, using the unloading-reloading moduli developed by Duncan and Chang (1970).

The Lade-Duncan model described above is a classical isotropic hardening model without any cap. Lade (1977) modified this model, by adding a cap and by allowing isotropic hardening of both the cap and the cone. He also used a curved-conical yield surface instead of the conventional yield surface with a straight meridian line. In this model, The total strain increments, $d\varepsilon_{ij}$, are divided into an elastic component, $d\varepsilon_{ij}^e$, a plastic collapse component, $d\varepsilon_{ij}^c$, and a plastic expansive component, $d\varepsilon_{ij}^p$, such that:

$$d\varepsilon_{ij} = d\varepsilon_{ij}^e + d\varepsilon_{ij}^c + d\varepsilon_{ij}^p \tag{2.60}$$

These strain components are calculated separately, the elastic strains by Hooke's law, the plastic collapse strains by a plastic stress-strain theory involving a cap-type yield surface, and the plastic expansive strains by a stress-strain theory which involves a conical yield surface with apex at the origin of stress space.

In order to make the failure surface curved (as observed for most cohesionless soils), the frictional angle ϕ is assumed to decrease with increasing hydrostatic pressure.

The modified yield surface is given by:

$$f_p = \left(\frac{I_1^3}{I_3} - 27\right)\left(\frac{I_1}{p_a}\right)^m \tag{2.61}$$

Where f_p has a value of η_I at failure. η_I and m can be determined by plotting $(I_1^3/I_3 - 27)$ vs. p_a/I_1 at failure in log-log scale. The curvature of the failure surface increases as the value of m increases, and for $m = 0$, it becomes a straight line (identical to Lade-Duncan).

The cap surface is expressed in terms of the first and second stress invariants as:

$$f_c = I_1^2 - 2I_2 \tag{2.62}$$

The cap surface expands isotropicly as the value of f_c increases. The plastic potential surface corresponding to the yield surface is taken the same as f_c in this portion (associative flow).

The plastic potential of the conical yield surface is expressed in a form similar to the failure or yield function f_p:

$$\eta_2 = \left(\frac{I_1^3}{I_3} - 27\right)\left(\frac{I_1}{p_a}\right)^m \tag{2.63}$$

Where η_2 is a constant for given values of f_p and σ_3, and m is the same constant as in the conical yield function. The value of η_2 can be determined from the directions of the plastic strain increments in the triaxial plane.

The shapes of the plastic potential surfaces are like asymmetric bullets with their apices at the origin of the principal stress space. Their shapes on the π-plane are the same as the Lade-Duncan yield surfaces.

In order to calculate the plastic collapse strains with the associated flow rule, work-hardening relationship is determined from an isotropic compression test. The total plastic work, W_c, accumulated due to the collapse strain is expressed in terms of f_c (cap function):

$$W_c = F_c(f_c) \tag{2.64}$$

Where F_c is a monotonically increasing, positive function, implying that the work-hardening relationship is independent of the stress-path.
For an isotropic compression test, W_c reduces to:

$$W_c = \int \sigma_m \cdot d\varepsilon_{kk}^c \tag{2.65}$$

Where σ_m is the hydrostatic pressure and $d\varepsilon_{kk}{}^c$ is the increment of the volumetric plastic collapse strain. And subsequently, f_c is reduced to:

$$f_c = 3\sigma_m^2 \tag{2.66}$$

For such a simple test, the relationship between W_c and f_c is expressed by:

$$W_c = Cp_0\left(f_c/p_0^2\right)^q \tag{2.67}$$

If this relationship is plotted on log-log scale, it results in a straight line; where the collapse modulus C is determined at $f_c/p_0^2 = 1$. The exponent q is the slope of the straight line and p_0 is the atmospheric pressure.

To calculate the plastic expansive strains using a non-associated flow rule, both isotropic work hardening and work-softening relationships are determined from the triaxial compression tests. The plastic work due to the plastic expansive strains at each stage of the triaxial compression tests can be calculated as:

$$W_p = \int \sigma_{ij}\ d\varepsilon_{ij}^p \tag{2.68}$$

Where $d\varepsilon_{ij}^p$ is an increment of the plastic expansive strains. In a similar manner to that of the hardening relation between f_c and W_c, the following expression corresponding to f_p and W_p can be presented:

$$f_p = a \cdot e^{-bW_p} \cdot \left(\frac{W_p}{p_0}\right)^{1/q},\ q > 0 \tag{2.69}$$

Where the parameters a, b and q are constants for a given value of confining pressure σ_3. Since the value of f_p increases until W_p reaches a peak value of W_p^{peak} after which f_p decreases with further increase in W_p. The above equation is used for both work hardening and work softening behavior of cohesionless soils.

2.7 Limitations

In this chapter a thorough review of the literature was presented in order to illustrate the current state of knowledge.

Upon closer inspection it is safe to say that there exists two distinct schools of thoughts. In general, pavement engineers examined the behavior of granular materials under long-term repeated one-directional loading, which (according to the prevailing assumption) best simulates traffic loads. On the other hand, earthquake-engineers studied the behavior of cohesionless soils (mainly sands) under short-term cyclic two-directional loading which best replicates seismic loading. Therefore, there is lack of available data on the behavior of granular materials under long-term cyclic loading.

Failure of soils under monotonic loading is very well documented, modeled and understood; however, the definition of failure of soils under dynamic loading is still debatable and lacking a comprehensive analysis. The main question asked is how can soils fail under repetitive loads with magnitudes far less than their static strength. Several attempts have been made to relate the dynamic strength of soils to the well-understood and simple case of failure in soils due to monotonic loading. These attempts usually neglect the effect of the repetitive nature of the load applied and concentrate on its magnitude only. Until now such available models do not address satisfactorily the problem at hand.

Chapter Three

Materials, Experimental Study and Testing Program

To carry out the research in this study a series of different tests were carried out to find the various characteristics of the material used and to identify its resilient, as well as, long-term behavior when subjected to certain load patterns.

3.1 Stress-Strain Conditions

Not satisfied with monotonic triaxial testing to study the behavior of materials in pavement structures subjected to repeated loading, Seed et al. (1955) advised the use of a load-on load-off triaxial testing system. They later admitted that even this method is at best a simplification of what occurs in the field under very slow traffic. Barksdale (1975) argued that accurate simulation of what happens in the field requires that more complicated stress versus time functions should be used, such as sinusoidal or triangular shape functions with a pulse duration similar to normal traffic speeds in the field. His research showed that 70 km/hr (45 miles/hr) traffic results in a pulse duration that varies between 0.02 s at the surface of pavement to 0.1 s at a depth of 0.75 m (30 inches).

Allen and Thompson (1974) went one step further and were the first to apply a cyclic confining pressure while subjecting the soil specimen to vertical repeated deviatoric stress, arguing that this better simulates the actual field conditions, since the confining stress acting on the pavement structure is cyclic in nature. Recently, with advances in testing equipment, this type of testing has become more popular.

Brown and Hyde showed that varying confining pressure (σ_3) does not affect

the resilient response nor the long-term permanent deformation of the material when an average value of cyclic σ_3 is used to compare, however, the variation of σ_3 affects the Poisson ratio considerably unless when stresses and strains are separated into volumetric and shear components. In this case the cyclic confining pressure tests and the constant confining pressure tests yielded the same stress-strain relationships for stress ratios that do not cause specimen dilation.

The stress pattern induced by traffic loading in a pavement structure may be approximated by performing a multi-layer elastic analysis using Elsym5 (1972), a computer program capable of solving an elastic multi-layer system with axisymmetric loading. In this solution, the wheel load can be represented by uniform load p acting on a circular area with a radius r, as shown in Figure 3.1. Results of this analysis are given in Figures 3.2 and 3.3 and can be summarized as follows:

- As the load approaches a given point A in the base course, the vertical stress increases to a maximum corresponding to the moment when the wheel passes over point A and then as the wheel keeps moving, the vertical stress decreases symmetrically.
- The horizontal stress increases with the approach of the wheel load and decreases symmetrically as the load departs.
- Shear stress increases to a positive maximum (compressive) value when the wheel is at a distance r from point A, then decreases to a value of zero when the load is over point A and keeps on decreasing to a minimum negative (tensile) value when the wheel is at a distance r away from point A.

Ishihara (1983) obtained similar results when analyzing stresses induced by traffic loading in a pavement structure using Boussinesq plane strain solution.

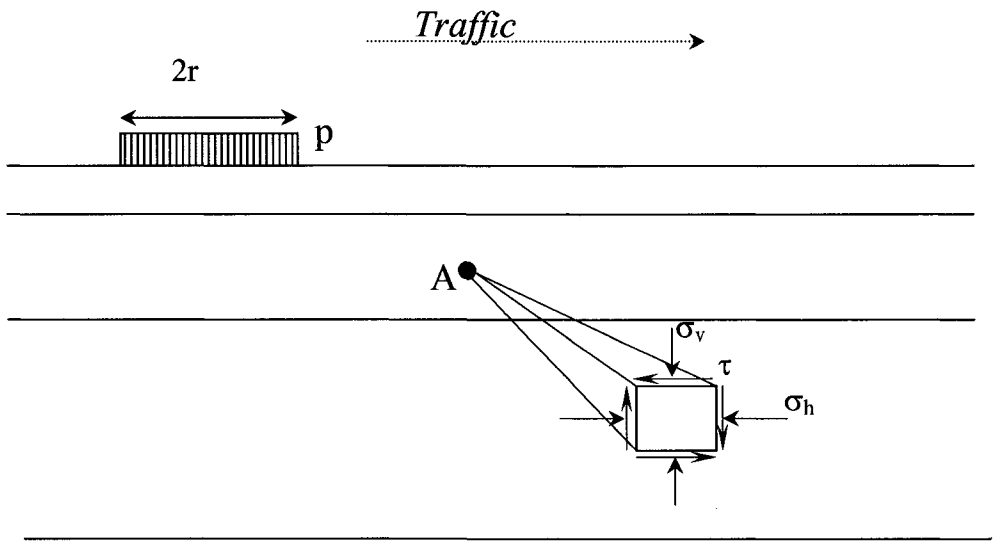

Figure 3.1: Elastic Multi-Layer System Analysis.

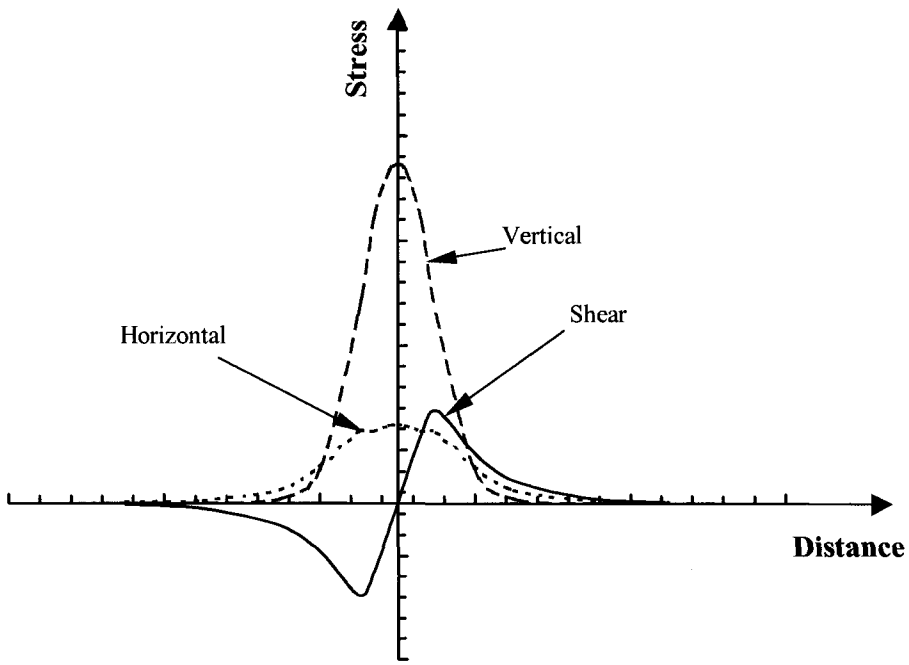

Figure 3.2: Vertical, Horizontal and Shear Stress Variation Due to Wheel Passage.

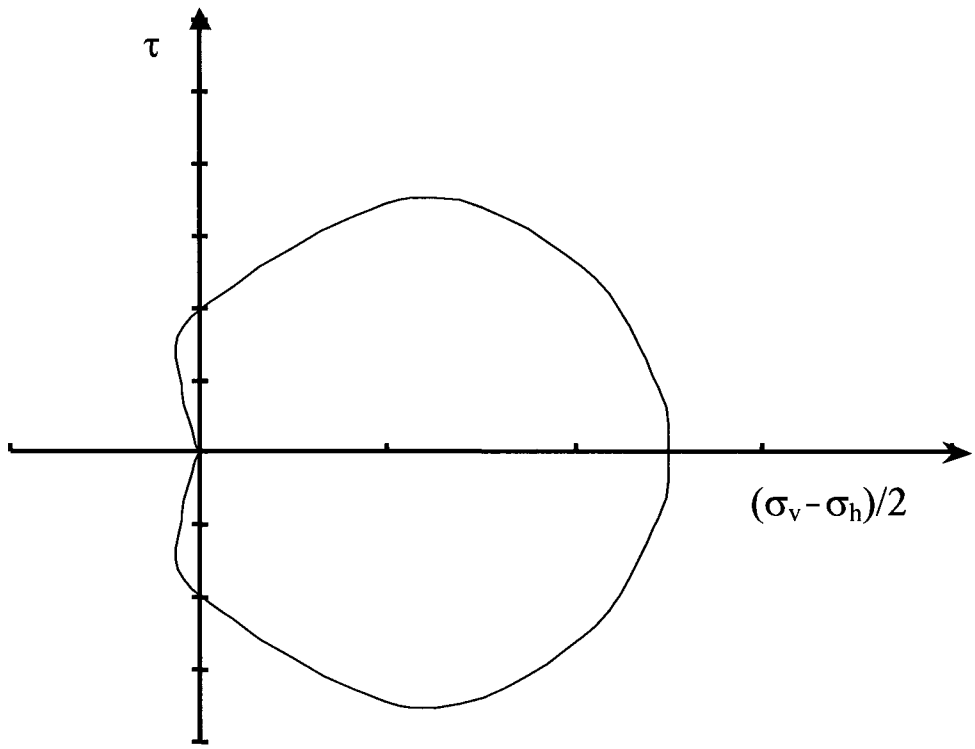

Figure 3.3: Stress Path due to Traffic Loading in τ–σ Space (Ishihara 1996).

Shear stress reversal induced by the traffic load is an important factor that cannot be disregarded. It has been argued that varying the horizontal confinement while subjecting the specimen to repeated vertical haversine loading can simulate this phenomenon. An alternative way of loading would be keeping the horizontal confinement constant while applying a vertical sinusoidal (compressive-tensile) type of loading. The cyclic load, in this case, should be limited to a value not to exceed the confining pressure applied. This is to insure that there is continuous contact between the loading ram and the specimen.

3.2 Laboratory Investigation

The laboratory testing consisted of series of conventional soil mechanics tests to characterize the materials used in this research. Several monotonic triaxial tests were also carried out to determine the strength parameters needed to define the Möhr-Coulomb envelope and the sensitivity of these parameters to the rate of loading, type of loading, and number of load repetitions. Resilient triaxial tests were performed to check the resilient properties of the base course studied and their variation with repetitions. Finally, long term repeated load tests were used to study the accumulation of permanent deformation under different types of loading used in this research.

3.2.1 Material Used

The materials used in this study conforms to the gradation requirements set by the Alaska Department of Transportation for a premium type of unbound base course material designated as D-1 and a surface course material designated as F-1, which will be referred to in this research as '*marginal material*'. All aggregates were crushed river deposits of igneous and metamorphic origin from Tanana Valley, in interior Alaska. A summary of the petrography of the material used is given in Appendix A.

3.2.2 Conventional Tests

Conventional soil mechanics tests were conducted to characterize the material used in this research. These consist of:

- Specific gravity of coarse and fine portion of aggregates,
- Absorption of coarse and fine portion of aggregates,
- Liquid Limit and Plastic Limit of soil used.

- Hydrometer Test on the fine portion (finer than #200 sieve) of material used.
- Modified Proctor Tests to identify the optimum moisture content and the corresponding maximum dry density of mixes used,
- Constant head permeability of the base course and marginal mixes,

The results of these tests are summarized in Tables 3.1 and 3.2 as well as in Figure 3.5; and the grain size distribution of both mixes is shown in Figure 3.4.

Table 3.1: Geotechnical Characterization of the Material Used.

	Coarse Portion (> #4 sieve)	Fine Portion (< #4 sieve)
Specific Gravity	2.712	2.715
Absorption, %	0.65	0.95
Liquid Limit	-	30
Plasticity Index	-	4

Table 3.2: Geotechnical Characterization of the Tested Mixes.

	Base Course	Marginal Material
Gradation (% Finer)		
12.5 mm	100	100
9.5 mm	69	85
# 4 sieve	47	70
# 8 sieve	36	58
# 16 sieve	29	43
# 30 sieve	26	38
# 50 sieve	19	28
#100 sieve	8	19
#200 sieve	4	15
Max. Dry Density, kg/m^3	2185	2250
Optimum Moisture Content, %	6%	7.5%
Permeability, cm/sec	0.01	0.008
AASHTO Classification	A-1-a	A-1-b
Unified Classification	GW	SM

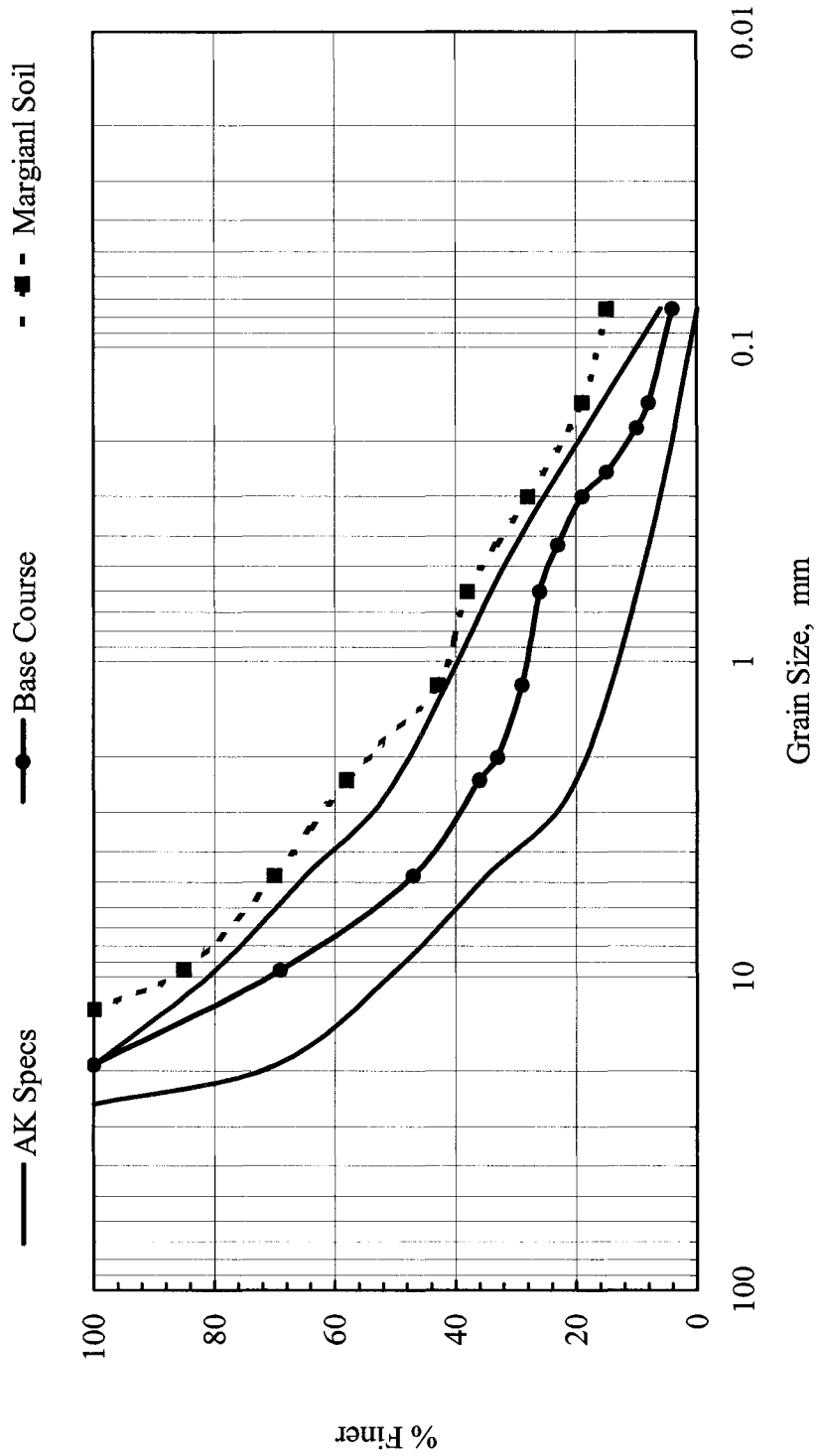

Figure 3.4: Gradation of Soils Tested

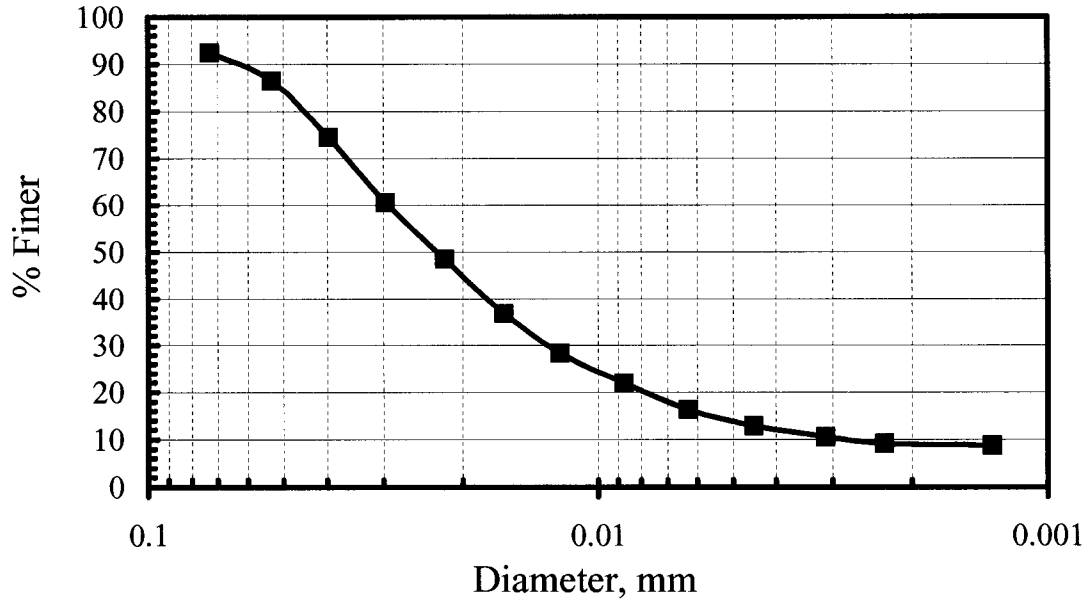

Figure 3.5: Size Distribution of Fines (finer than #200 sieve).

3.2.3 Specimen Preparation

In order to ensure strict compliance with the chosen grain size distribution, the material used to prepare the samples was mixed using eight different size fractions. The maximum aggregate size used was less than 12.7 mm. After mixing the soil with the adequate moisture content, the mix was covered well and set to cure for approximately 30 minutes. Cylindrical specimens, 100 mm in diameter and around 200 mm high, were prepared in a split mold seated on the lower platen using vibratory compaction. Specimens were compacted in five layers; each subjected to 7 kPa surcharge and vibrated at 60 Hz for 60 seconds using a vibrating table. A 0.9 mm-thick rubber membrane was used to encase the compacted specimen.

It was noticed that compacting the 5 layers using equal compaction effort, resulted in denser layers at the bottom of the specimen and looser ones on top. The reason being that compaction of the upper layers further compacted the previous layers. Following the guidelines set by Ladd (1978), The compaction of the specimen was carried out such that the lower layers were under-compacted at ascending degrees of compaction and, of course, the top layer was subjected to the full compaction effort. The controlling variable was chosen to be the duration of compaction. This resulted in a sample compacted at a given uniform final density equal to 98% of T-180. The actual density and moisture content of the specimen prepared were measured and compared to the target range. If these values did not fall within this range, the specimen was disregarded. Overall, around 7% of the specimens prepared were disregarded, at this stage, for this reason.

The split mold was removed once partial vaccum was applied to the specimen. After mounting a circumferential extensometer at the midpoint of the specimen to measure radial deformations, the triaxial cell was assembled and placed on an MTS closed-loop hydraulic testing machine. Two spring-loaded linear variable differential transducers (LVDT) were mounted externally (and equidistant) to opposite sides of the piston rod outside the test chamber, as shown in Figure 3.6, in order to measure the vertical deformation of the sample. The whole triaxial assembly was then elevated using the hydraulic piston and connected to the crosshead. The vaccum line was disconnected and the specimen was subjected to 35 kPa confining pressure for 15 minutes to equilibrate, after which, the specimen was conditioned with 1,000 cycles of repeated deviatoric stress of 35 kPa. All the triaxial tests conducted in this research were under drained conditions.

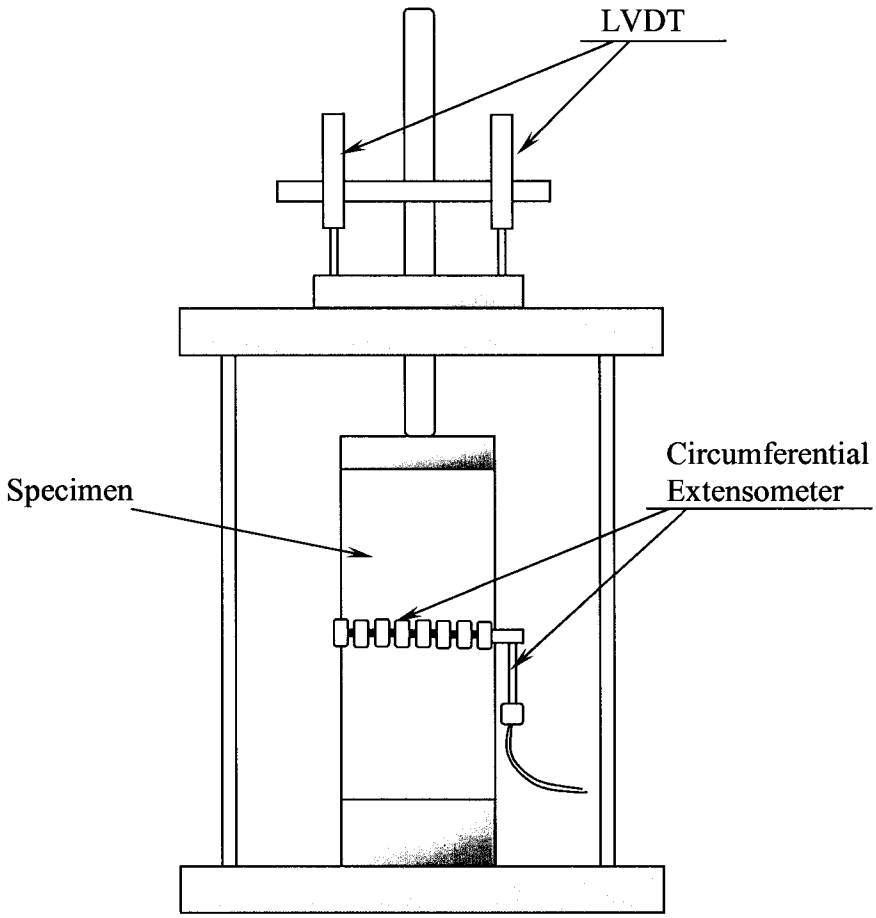

Figure 3.6: Assembled Triaxial Cell (not to scale)

3.2.4 Monotonic Tests

A series of monotonic tests were carried out on compacted specimens under different confining pressures in order to determine the Möhr-Coulomb parameters needed to describe the static strength of the mix. Mainly, rapid shear strength tests with a (strain controlled) rate of loading of 750% strain per minute (causing 5% strain in 400 msec.) were used, as suggested by Thompson and Smith (1990) to best simulate the actual relatively-slow traffic loading encountered in the field.

To address the effect of loading rate on the shear strength of the materials used, specimens compacted at 98%, 95% and 90% of maximum dry density were subjected to various loading rates ranging from 1% per minute to 750% per minute.

3.2.5 Resilient Testing

Resilient testing was carried out according to AASHTO Method T274-82 on compacted specimens to determine the resilient properties of the mix. This method consists of applying several combinations of deviatoric (σ_d) and confining stresses (σ_3). The σ_d applied is haversine in nature with load duration of 0.1 sec followed by a rest period of 0.9 sec. For each σ_3 and σ_d combination, 100 cycles of designated σ_d are applied and the resilient deformation for the last 5 cycles is recorded and its average is used to calculate the corresponding resilient modulus M_R defined as:

$$M_R = \frac{\sigma_d}{\varepsilon_r} \tag{3.1}$$

Where:

σ_d = deviatoric stress, and,

ε_r = resilient strain.

The effect of the number of repetitions and type of loading on the resilient properties of granular materials was also explored. Base course specimens were first subjected to long term loading and afterwards their resilient properties were checked and compared to resilient properties of virgin samples.

3.2.6 Long Term Testing

The objective of the long-term tests is to obtain the accumulated permanent deformation of the base course under different types of loading. Each specimen was subjected to 100,000 repetitions of either repeated or cyclic loading. The different load patterns used were: cyclic stress (CS), cyclic strain (CN), repeated stress (RS), and repeated strain (RN). For a definition of these load patterns, check Figure 3.7.

Accumulated axial and radial deformations were collected at selected intervals. After the completion of a test, the triaxial shear strength of the specimen was obtained using rapid shear strength test. A summary of conducted triaxial tests in this study is presented in Appendix B. A thorough examination of test results is presented in Chapter four.

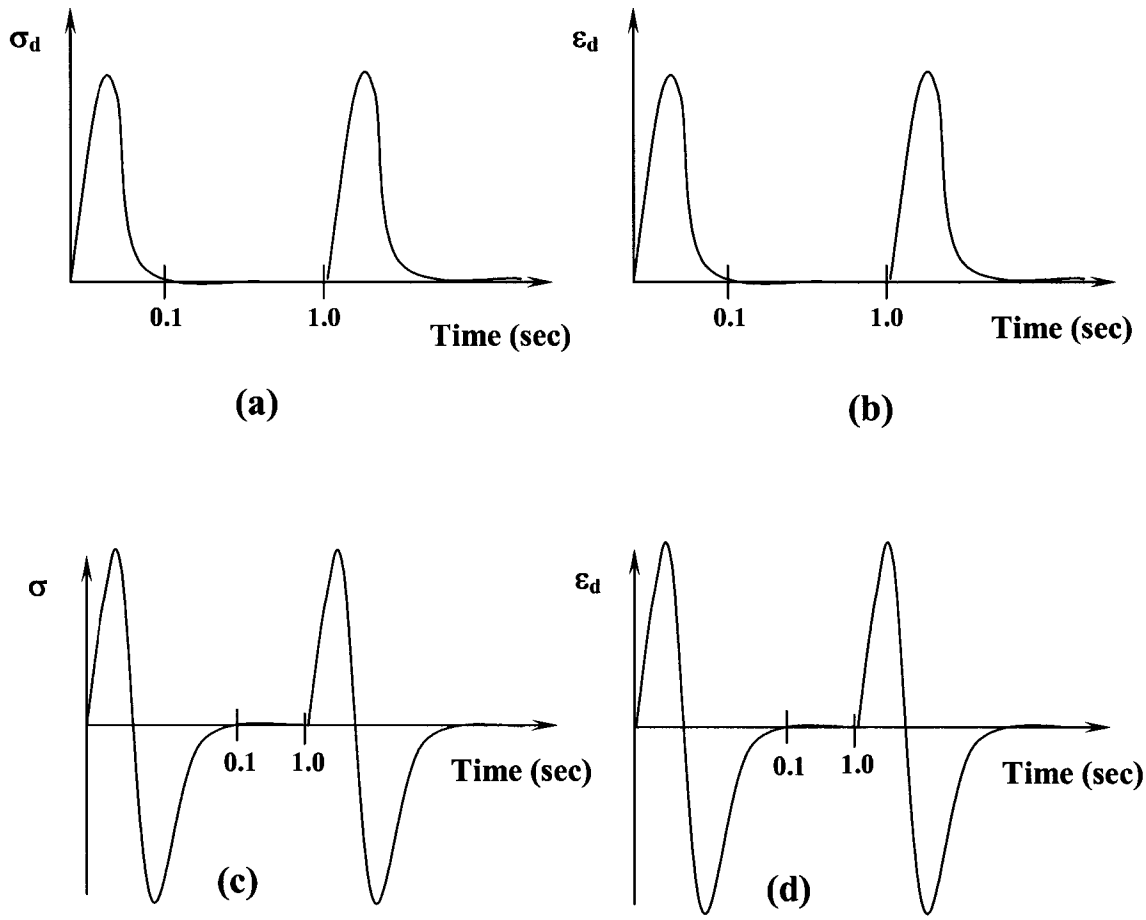

Figure 3.7: Types of Loading Used in this Research: (a) Repeated Stress; (b) Repeated Strain; (c) Cyclic Stress; and (d) Cyclic Strain.

3.3 Definition of Calculated Variables

Before presenting the experimental results obtained in this study, a definition of the variables calculated will be presented in the following sections

3.3.1 Repeated Stress

The repeated stress-load pattern used in this study (see Figure 3.7(a)) results in a response similar to that presented in Figures 3.8 and 3.9 below.

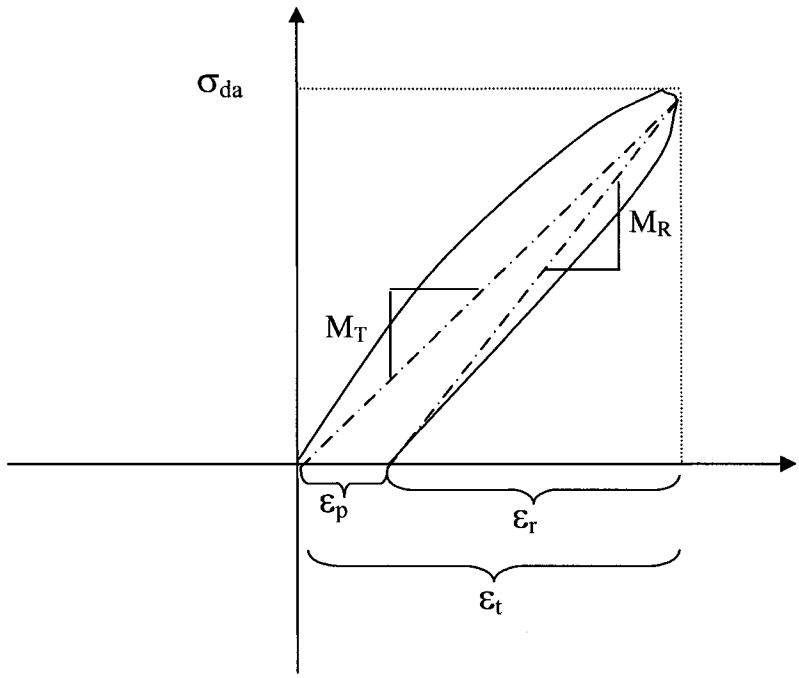

Figure 3.8: Response Parameters for Repeated Stress Load Pattern.

Where:

σ_{da}= Applied Deviatoric Stress,

ε_r = Resilient or Recoverable Strain,

ε_p = Permanent or Plastic Strain,

ε_t = Total Strain,

M_R = Resilient Modulus, and,

M_T = Total Modulus.

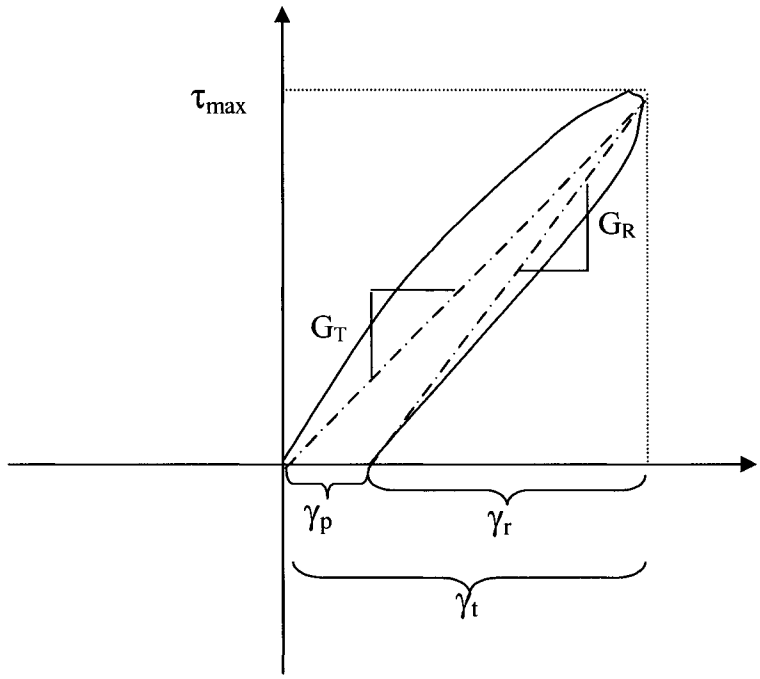

Figure 3.9: Shear Response Parameters for Repeated Stress Load Pattern (45°plane).

Where:

τ_{max} = Maximum shear stress applied,

γ_r = Resilient or recoverable shear strain,

γ_p = Permanent or plastic shear strain,

γ_t = Total shear strain,

G_R = Resilient shear modulus, and,

G_T = Total shear modulus.

3.3.2 Repeated Strain

The repeated strain-load pattern presented in Figure 3.7(b) results in a response similar to that presented in Figures 3.10 and 3.11.

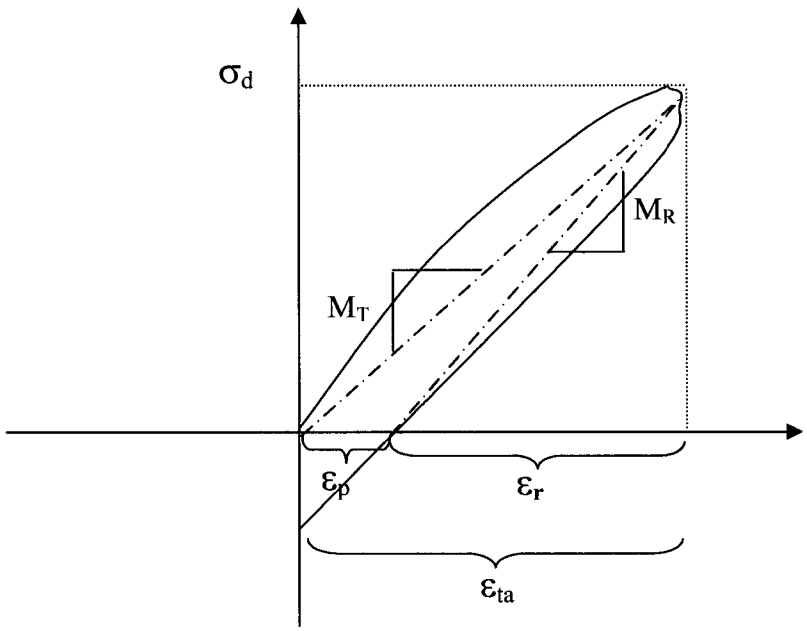

Figure 3.10: Response Parameters for Repeated Strain Load Pattern.

Where:

σ_d = Deviatoric stress,

ε_{ta} = Applied total strain,

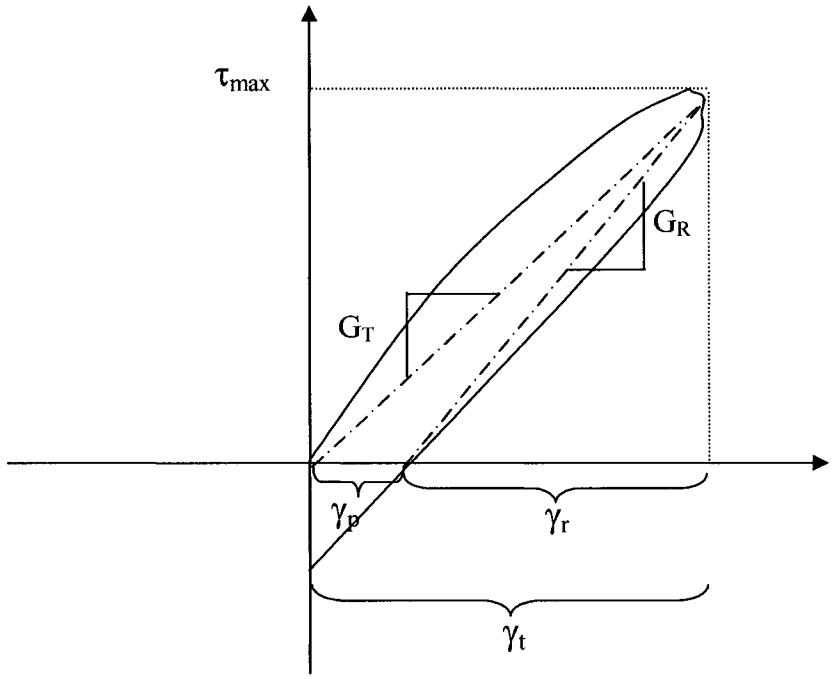

Figure 3.11: Shear Response Parameters for Repeated Strain Load Pattern (45°plane).

3.3.3 Cyclic Stress

In the case of cyclic stress load pattern, the applied load is cycled between two extreme values as presented in Figure 3.7(c). The response of such a load pattern is presented in Figures 3.12 and 3.13. For the purpose of this study, loading is considered positive, whereas, unloading is considered negative. During testing, great care was taken so that the stress during unloading did not exceed the applied confining pressure of the specimen. In fact, the maximum value of the cycled deviatoric stress was set at $0.8 \times \sigma_3$, where σ_3 is the confining pressure.

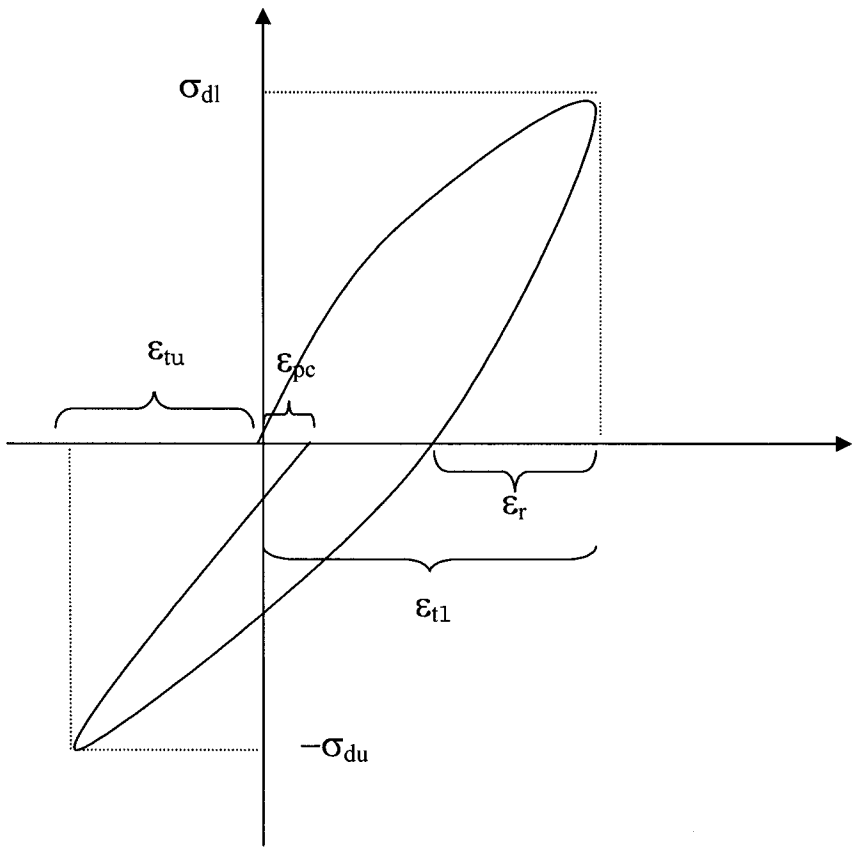

Figure 3.12: Response Parameters for Cyclic Stress Load Pattern.

Where:

σ_{dl} & σ_{du} = Applied cyclic loading and unloading deviatoric stress,

ε_{pc} = Cumulative permanent or plastic strain.

M_T = Total modulus, defined as,

$$M_T = \frac{\sigma_{dl} + |\sigma_{du}|}{\varepsilon_{tl} + |\varepsilon_{tu}|} \tag{3.2}$$

M_R = Loading Resilient Modulus, defined as,

$$M_R = \frac{\sigma_{dl}}{\varepsilon_r} \tag{3.3}$$

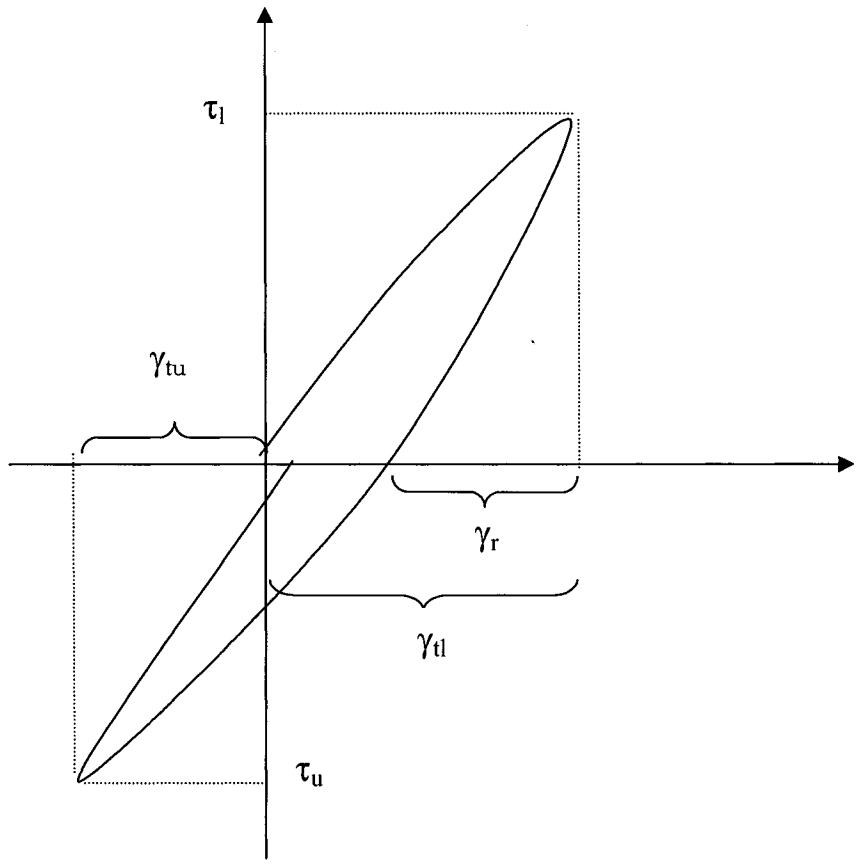

Figure 3.13: Shear Response Parameters for Cyclic Stress Load Pattern (45° plane).

Where:

τ_l & τ_u = Cyclic loading and unloading shear stress,

γ_r = Resilient shear strain, and,

γ_{tl} & γ_{tu} = Total loading and unloading shear strain.

G_T = Total shear modulus, defined as:

$$G_T = \frac{\tau_1 + |\tau_u|}{\gamma_{tl} + |\gamma_{tu}|} \tag{3.4}$$

G_R = Loading Resilient Shear Modulus, defined as,

$$G_R = \frac{\tau_{dl}}{\gamma_r} \tag{3.5}$$

The cyclic strain case was primarily used to check if the load pattern applied had any effect on the shear strength development of the material. Otherwise, it was not used in the study.

Chapter Four

Laboratory Testing Results

4.1 Introduction

In this chapter the results of the various laboratory tests are presented. The main objectives of these tests were: to find the shear strength of the soils tested, to get the resilient and plastic response of the granular material and monitor their variation with the type of loading used. Furthermore, attempts are made to check if there is any relation between the static and dynamic strength of the material.

4.2 Triaxial Shear Strength

Rapid shear monotonic triaxial tests (750% strain per minute) served to compute shear strength parameters for the materials tested. Moreover, load rates ranging from 1% strain per minute to 750% strain per minute were used to check the granular material shear strength dependency on rate of load.

Figures 4.1 and 4.2 depict the variation of the shear strength (strain rate = 750% per minute) of the base course material and the marginal material respectively, in a *q-p* space for both dense (98% AASHTO T180 density) and loose (90% AASHTO T180 density) packed samples. *q'* and *p'* are defined as:

$$q' = \frac{\sigma_1' - \sigma_3'}{2} \tag{4.1}$$

$$p' = \frac{\sigma_1' + \sigma_3'}{2} \tag{4.2}$$

Where: σ_1' = Effective major principal stress
σ_3' = Effective minor principal stress

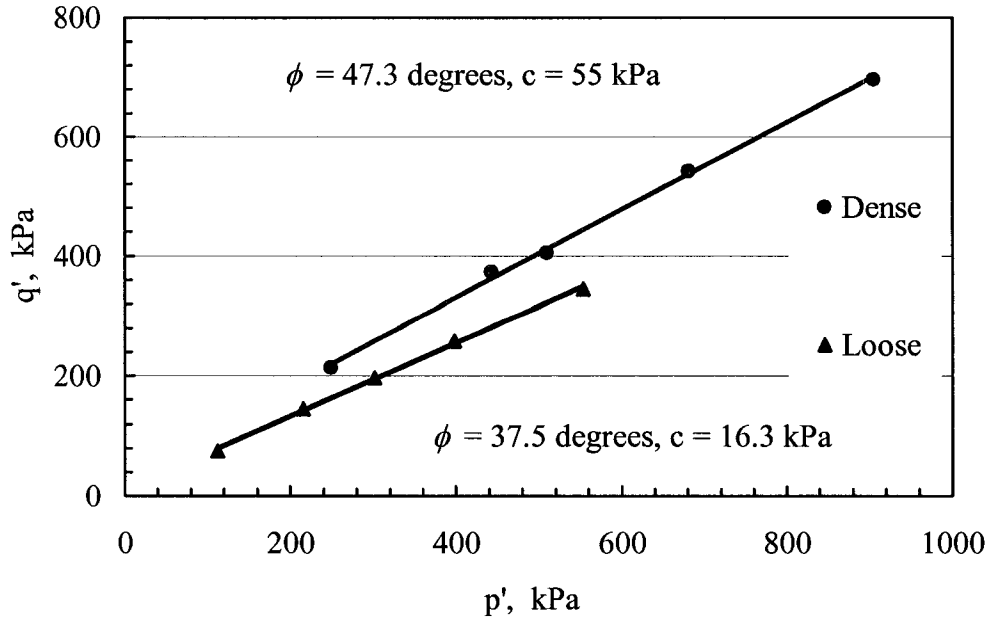

Figure 4.1: Stress Path Curve in *q-p* Space of the Base Course Material

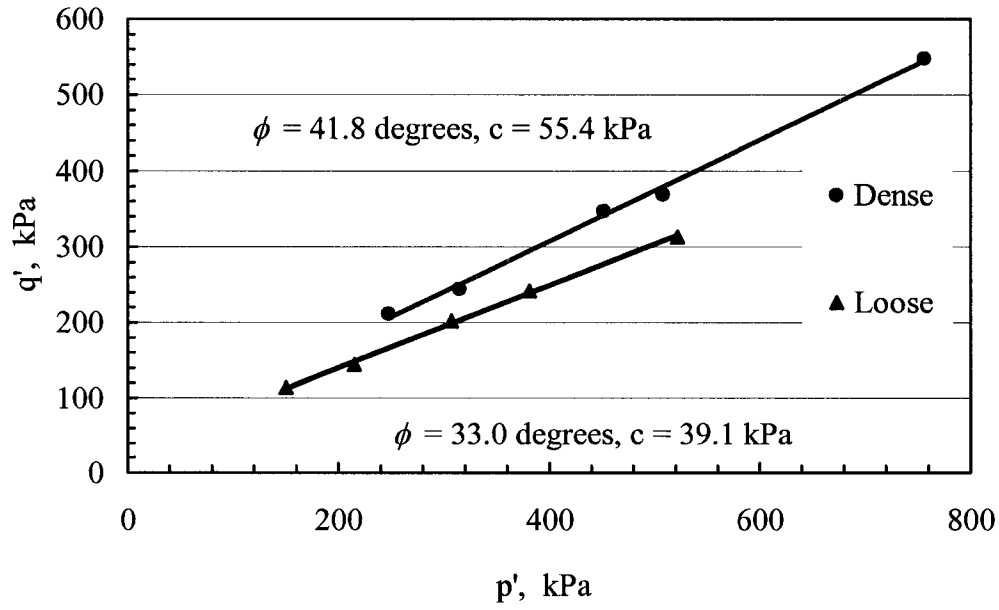

Figure 4.2: Stress Path Curve in *q-p* Space of the Marginal Material

Density variation had an effect on both the cohesion c and the angle of internal friction ϕ (see Figures 4.1 and 4.2). An increase from 90% of AASHTO T180 density to 98% of AASHTO T180 density resulted in increases of 205% and 40% in cohesion respectively for the base course and marginal material mixes. The same increase in density also lead to an increase of 52% and 27% in the angle of friction of base course and marginal material respectively. This fact strengthens the argument that density remains a very important factor in the stability of granular material layers.

Loading rates were studied using four different strain rates and these results are presented for both loose and dense specimens (see Figures 4.3 and 4.4). The resulting shear strength parameters are summarized in Table 4.1.

The test results show that strain rates have minimal effect on shear strength parameters for the granular materials tested. This is true regardless of density. For a given density, monotonic testing of these aggregate mixes, at rates varying from 1% strain per minute to 750% strain per minute, resulted in practically same values of shear strength parameters.

Table 4.1: Base Course Shear Strength Parameters' Variation with Loading Rates.

	Dense		Loose	
Loading Rate (% Strain/Minute)	ϕ (degrees)	c (kPa)	ϕ (degrees)	c (kPa)
1 %	47.4	33.5	35.1	17.6
5 %	47.3	33.2	35.9	16.6
10 %	47.3	37.5	35.5	18.1
750 %	47.3	55.0	37.4	16.3

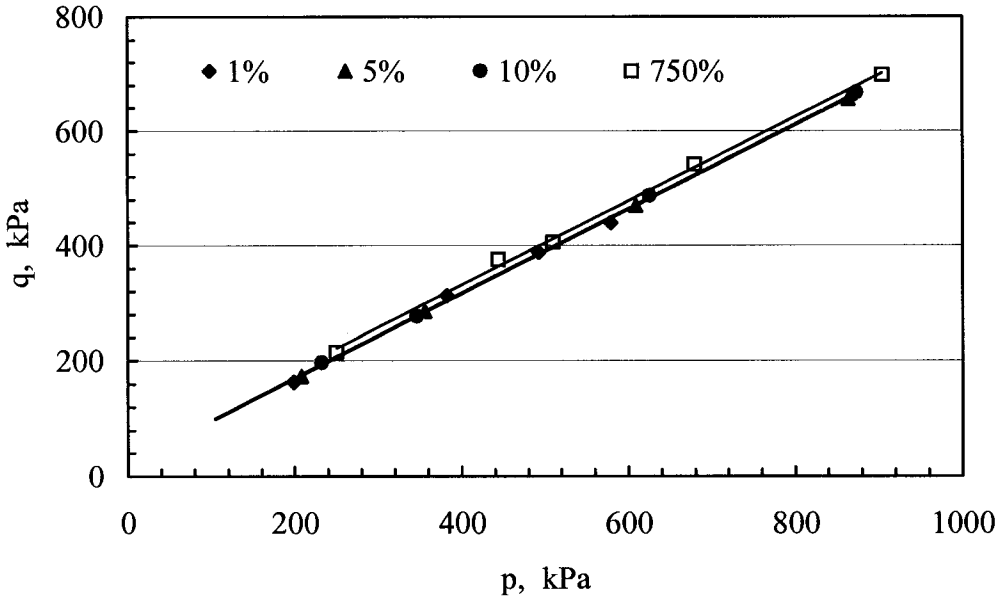

Figure 4.3: Variation of Dense Base Course Stress Path with Loading Rates.

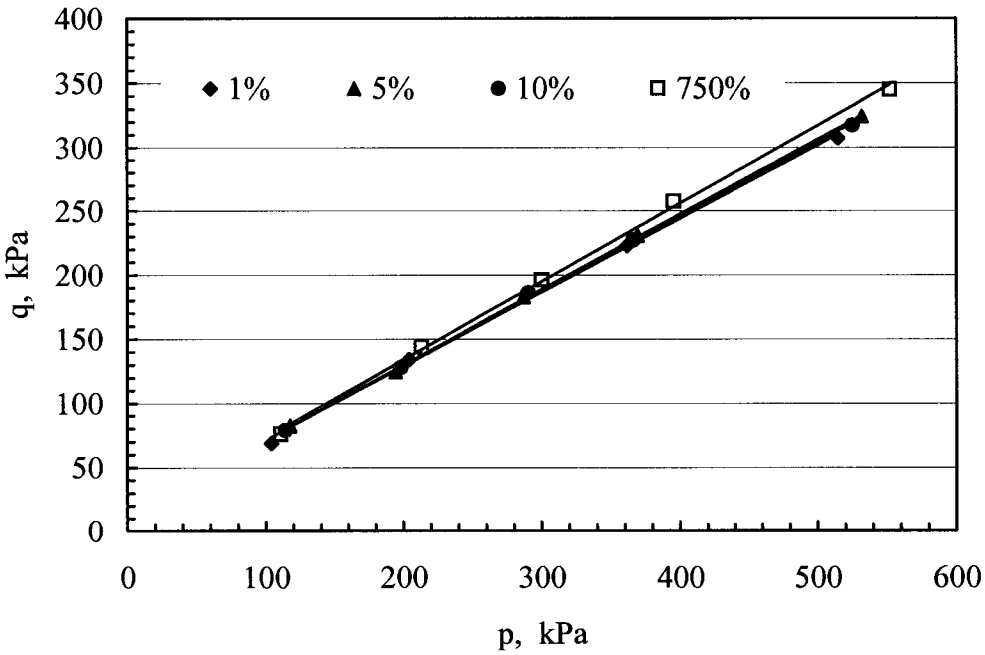

Figure 4.4: Variation of Loose Base Course Stress Path with Loading Rates.

4.3 Resilient Test Results

Resilient modulus test remains the most common laboratory procedure used to characterize pavement materials in current practice. It is by far simpler, faster and thus more economical than long-term dynamic tests. The resilient modulus test provides a mean of characterizing pavement materials in general and granular materials in particular when subjected to a variety of state stresses as well as under other conditions (density, moisture etc...) encountered in the field. The test results are generally used to find the constitutive relationship between the stress and deformation of pavement materials. These values are typically used to perform a structural analysis of the pavement structures.

This study was conducted to answer among other things the question: does the resilient modulus, as determined by AASHTO Method T274-82, change with load repetitions and type of loading? Similarly conditioned samples were subjected to different loading patterns under the same level of stress. The confining stress in all cases was maintained at 35 kPa. In the case of repeated stress, the applied deviatoric stress, σ_d, was 35 kPa. For the repeated strain case, a deviatoric strain, ε_d, was applied such that the initial repetition resulted in a deviatoric stress of 35 kPa; as for the cyclic stress case, the applied σ_d was set at ± 35 kPa.

In order to compare the results obtained, the resilient modulus M_R is plotted versus the first stress invariant θ (where $\theta = \sigma_1 + 2\sigma_3$), and k and n parameters of the k-θ model are obtained. Figures 4.5, 4.6 and 4.7 show the variation of M_R with the number of repetitions for different loading conditions (respectively repeated stress RS, repeated strain RN, and cyclic stress CS). As can be seen from these figures, in the case of repeated stress and repeated strain, no significant difference is detected for a number of repetitions less than 100,000. With repeated strain yielding slightly higher resilient modulus values at 100,000 repetitions. As for the case of cyclic strain, M_R increases markedly with the number of repetitions. Values of resilient modulus, for a given θ (say 275 kPa), almost double in value after applying 100,000

cyclic stress repetitions. This is because cyclic loading results in more densification than repeated loading as discussed in the literature review in Chapter 2.

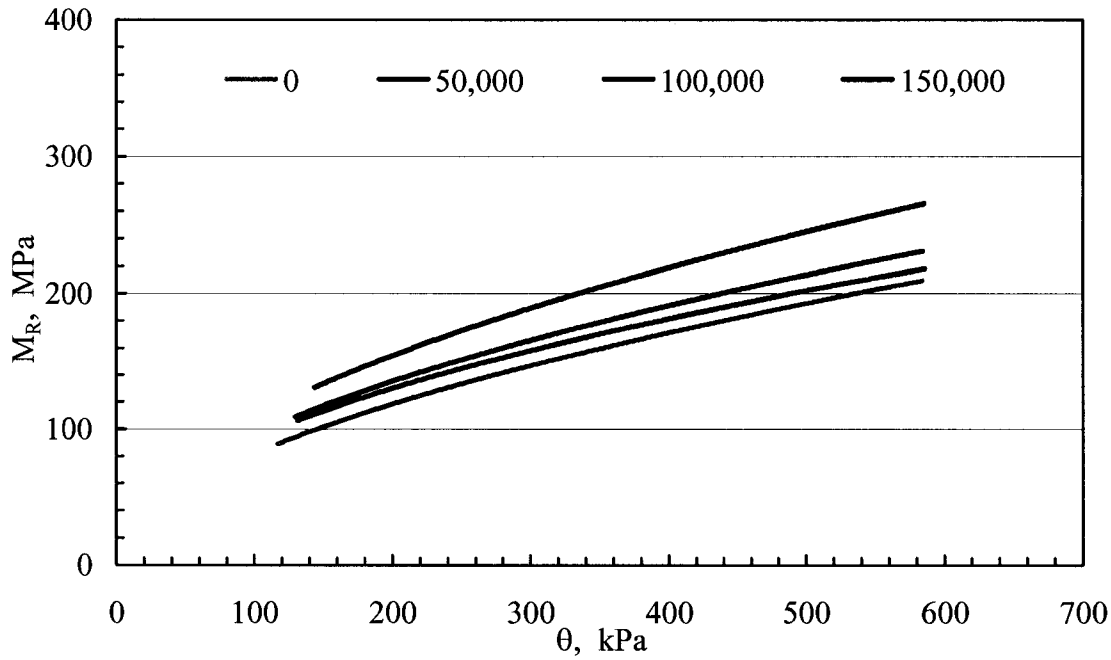

Figure 4.5: Variation of Resilient Modulus with Repeated Stress Repetitions.

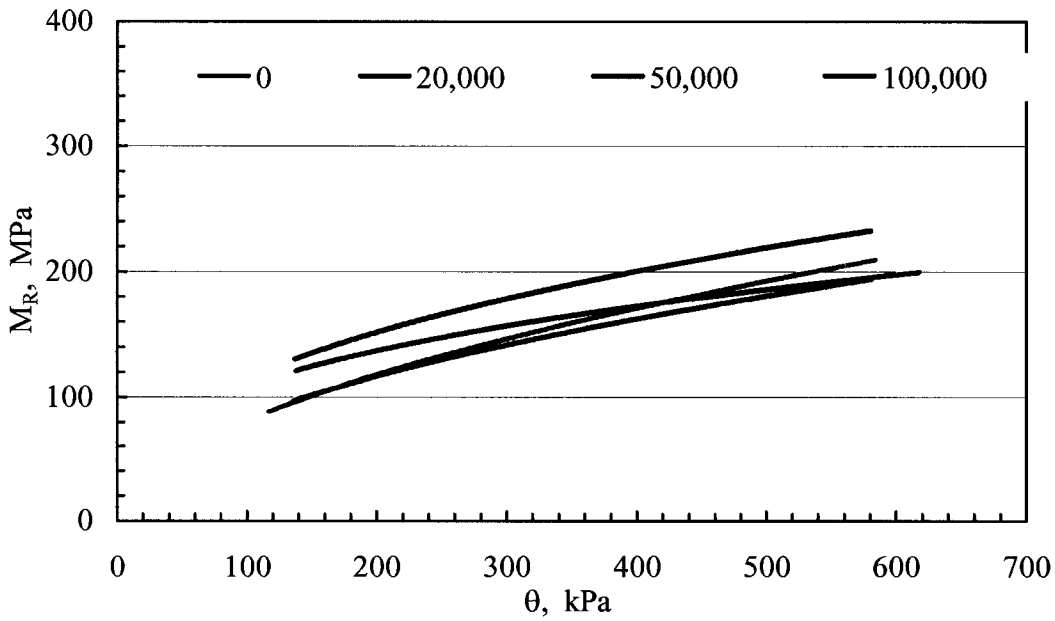

Figure 4.6: Variation of Resilient Modulus with Repeated Stain Repetitions.

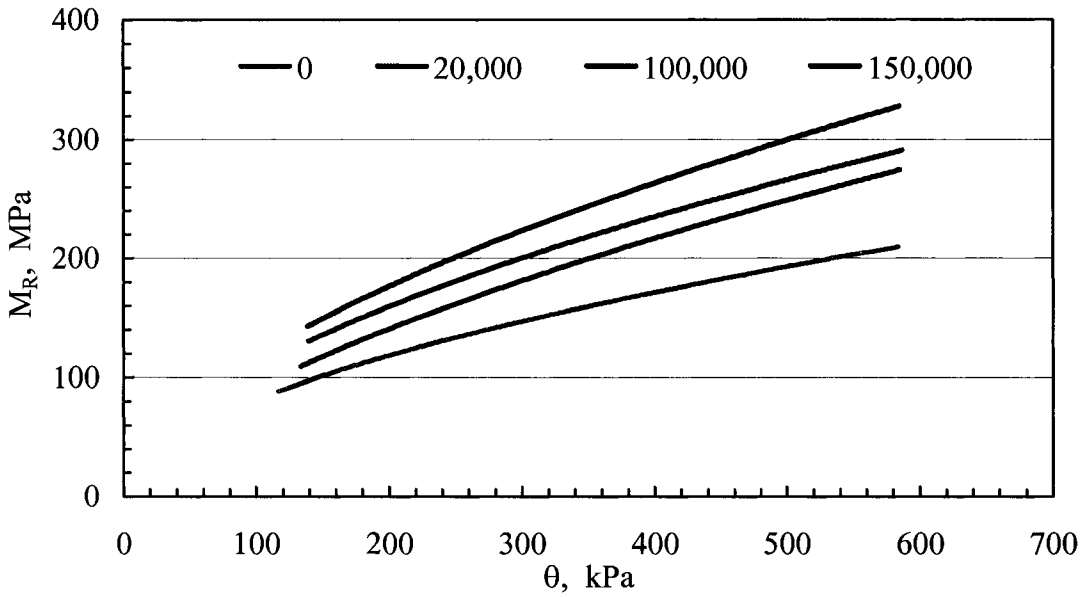

Figure 4.7: Variation of Resilient Modulus with Cyclic Stress Repetitions.

Table 4.2: Resilient Response Parameters for Different Load Types.

	Repeated Strain		Repeated Stress		Cyclic Stress	
Load Repetitions	k (MPa)	n	k (MPa)	n	k (MPa)	n
0	7.073	0.532	7.073	0.532	7.073	0.532
20,000	9.625	0.472	-	-	5.257	0.621
50,000	23.976	0.330	10.231	0.480	-	-
100,000	18.342	0.399	9.715	0.498	8.349	0.557
150,000	-	-	10.625	0.505	8.221	0.579

The various k and n values obtained from these tests are listed in Table 4.2. It is hard to discuss the variation of these parameters individually with number of load repetitions applied, since the combination of both represent a curve fit in a M_R-θ graph.

Knutson et al. (1977) reported similar findings when comparing the resilient moduli of several types of granular materials before and after subjecting them to 5,000 repetitions of repeated stress loading. However, they concluded that the increase in M_R with repetitions is not significant and consistent for all type of mixes used.

The variation of M_R with the type of loading is illustrated in Figure 4.8. In this figure, the resilient modulus of samples that had undergone 100,000 repetitions of a given load pattern are compared. Overall, the specimens that were subjected to cyclic stress (CS) yielded higher resilient moduli than those subjected to either repeated stress (RS) or repeated strain (RN) loading. It is also apparent that the difference between the CS samples and the others increases with an increase in the first stress invariant θ.

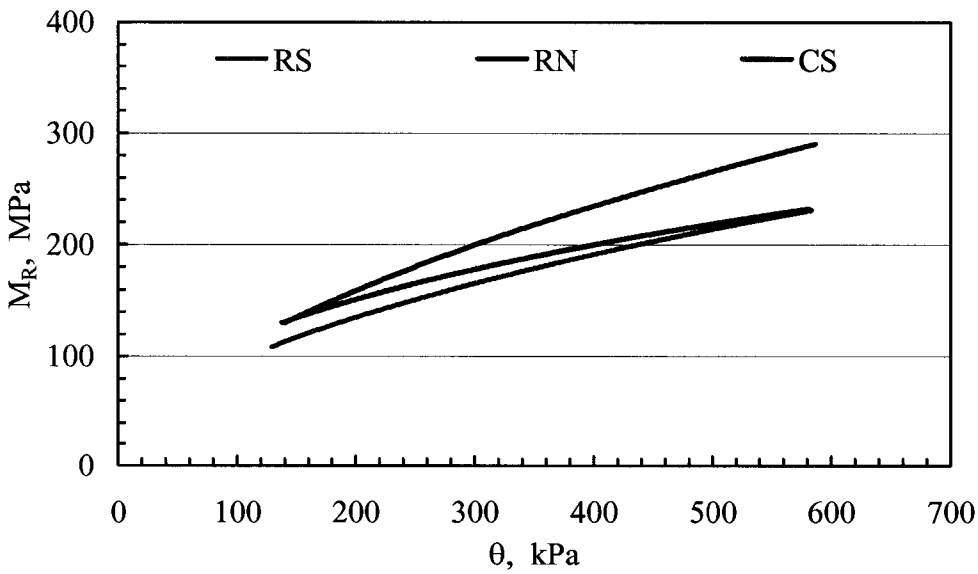

Figure 4.8: Variation of Resilient Modulus with Loading Pattern after 100,000 Repetitions.

4.4 Long Term Dynamic Testing

The stress level induced by traffic loads in a pavement system is far below the static failure stress level of the various materials that constitute the pavement structure. However, failure can be observed in pavements after several years in service. It is believed that this failure is primarily due to the repetitive nature of the applied load. Under repetitive dynamic loads, different materials in the pavement structure either fatigue or, as in the case of granular materials, densify causing significant permanent strains that render the overall structure unusable. Long-term response of these materials was studied for load levels similar to those expected in the field.

The long-term dynamic testing program used in this study consisted of several phases. Conditioned specimens were subjected to 100,000 load repetitions following different load patterns and resulting radial and axial deformations, as well as vertical stresses (in the case of strain controlled test), were measured to evaluate the response of the base course mix tested. On the other hand, similar samples were subjected to the same load patterns repeated 20,000, 50,0000, 100,000 and 150,000 times before subjecting them to rapid monotonic shear tests to check whether the shear strength of this material is affected by applied stress history.

4.4.1 Shear Strength Development

4.4.1.1 Effect of Repetitive Loading

Change of static strength of granular materials with load history was studied for four different load repetitions by evaluating the rapid shear strength of specimens subjected to various types of loading.

Identical specimens were first subjected to load repetitions of 20,000, 50,000, 100,000 and 150,000 using a given load pattern. Immediately after, a rapid shear strength test was conducted, and the static strength of the mix was evaluated. These

tests were conducted at two levels of confining stress, 35 kPa and 100 kPa. Results of these tests are presented in Figures 4.9 and 4.10.

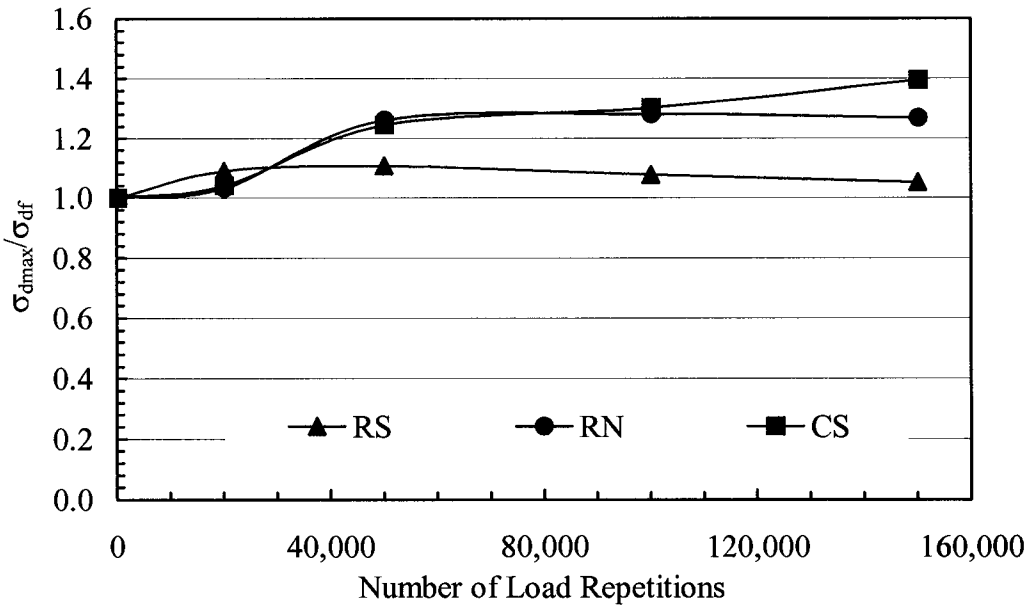

Figure 4.9: Shear Strength Variation with Number of Load Repetitions for Different Dynamic Load Patterns, σ_3 = 35 kPa.

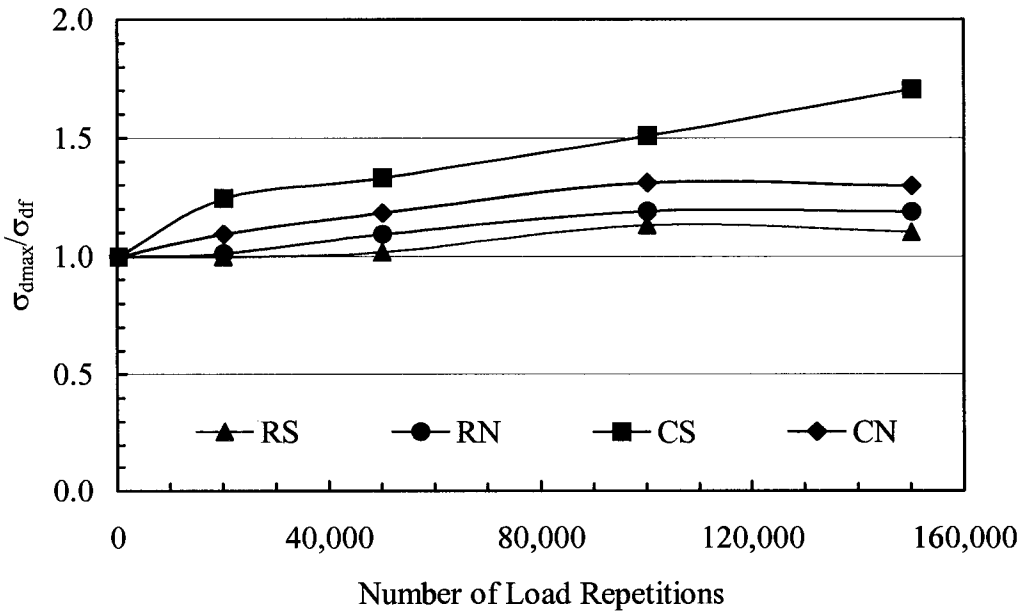

Figure 4.10: Shear Strength Variation with Number of Load Repetitions for Different Dynamic Load Patterns, σ_3 = 100 kPa.

In the figures above the shear strength ratio is expressed as $\sigma_{dmax}/\sigma_{df}$, where the numerator represents the shear strength of the material after being subjected to repetitions and the denominator represents the original shear strength of the material.

Based on Figures 4.9 and 4.10 we can make the following observations:

- In general, shear strength increases with number of load repetitions. It may be argued that this is due to the fact that repetitive loading causes the material to densify, resulting in an increase in the shear strength.
- Specimens subjected to repeated stress load repetitions (RS) were found to have the least amount of shear strength increase.
- Control-strain tests (repeated strain RN, and cyclic strain CN) initially exhibit considerable increase in shear strength with number of load repetitions up to a certain point beyond which the shear strength remains unchanged. This because with densification (therefore, shortening of the specimen), the deviatoric stress applied to the specimen decreases with the number of load repetitions thus limiting the amount of further densification to a point where the latter becomes negligible causing the shear strength to remain the same.
- For the low confining stress case, the specimens subjected respectively to cyclic stress (CS) and repeated strain (RN) result in comparable shear strength gain up to 50,000 load repetitions, afterwards the shear strength of CS keeps on increasing ultimately reaching a shear strength ratio value of 1.4 while the shear strength ratio of specimens subjected to RN remains unchanged.
- At high confining pressure, specimens subjected to CN, RN, and RS loading yield similar patterns of shear strength gain with CN resulting in the greatest gain (shear strength ratio $\approx$ 1.3 at 150,000 load repetitions). While specimens subjected to CS loading witness continuous increase in shear strength ratio with load repetitions, reaching values of $\approx$1.7 for 150,000 load repetitions.

- Samples subjected to cyclic loading (CS and CN) result in higher shear strength ratio values with load repetitions than samples subjected to repeated loading (RS and RN). From this we conclude that a cyclic two-directional type of loading causes more densification than one directional repeated type of loading.

4.4.1.2 Effect of Strength Level

In order to study the effect of strength level on the development of static shear strength of the material, identical samples of the granular base material studied were subjected to 100,000 repetitions of repeated and cyclic stress loading at different stress levels. At the end of the dynamic test, the specimen was directly subjected to rapid shear strength test in order to determine its static shear strength.

In the case of the repeated stress loading, the strength level (σ_d/σ_{df}), which is defined as the ratio of deviatoric stress applied over the shear strength of the material, was varied from 8% to 75% and was determined at three different confining pressures, 35 kPa, 70 kPa and 100 kPa. As for the case of cyclic stress, a restriction on the maximum amount of deviatoric stress ($\pm \sigma_d$) applied exists such that the specimen remains in contact with the platen at all time. The range of strength levels used in this case varied from 6.4% to 10.9% (which corresponds to stress level σ_d/σ_3 values of 0.5 to 0.85) and tests were conducted at a confining stress of 100 kPa. The reason why lower values of confining stress were not used in this case is due to the fact that low σ_3 values do not provide the luxury of using a range of strength or stress levels needed.

The shear strength of specimens subjected to 100,000 repeated RS loading increased with the stress level applied regardless of the confinement used. Figure 4.11 depicts the development of the static shear strength (post dynamic test) with strength levels used. The shear strength in this figure is given in two different terms: on the left y-axis as failure deviatoric strength σ_{df}, and on the right y-axis as strength ratio

(or normalized strength ratio), which is the ratio of static strength after 100,000 repetitions over the shear strength of the sample before any dynamic load application.

This definition of strength ratio facilitates the comparison of shear strength development of the materials tested under all three confining pressures used in this research as shown by Figure 4.12. This figure suggests that regardless of confinement pressure used, the shear strength ratio increases with stress level applied following a unique curve. Figure 4.13 depicts the development of stress-strain curve for different strength levels after 100,000 RS load repetitions.

The results of specimens subjected to cyclic loading are shown in Figure 4.14. In this case, the shear strength ratio also increases in a similar manner with the stress level applied reaching a value of 1.51 at a strength level of 10.9%. The progression of the stress-strain curves in this case (CS case) is presented in Figure 4.15.

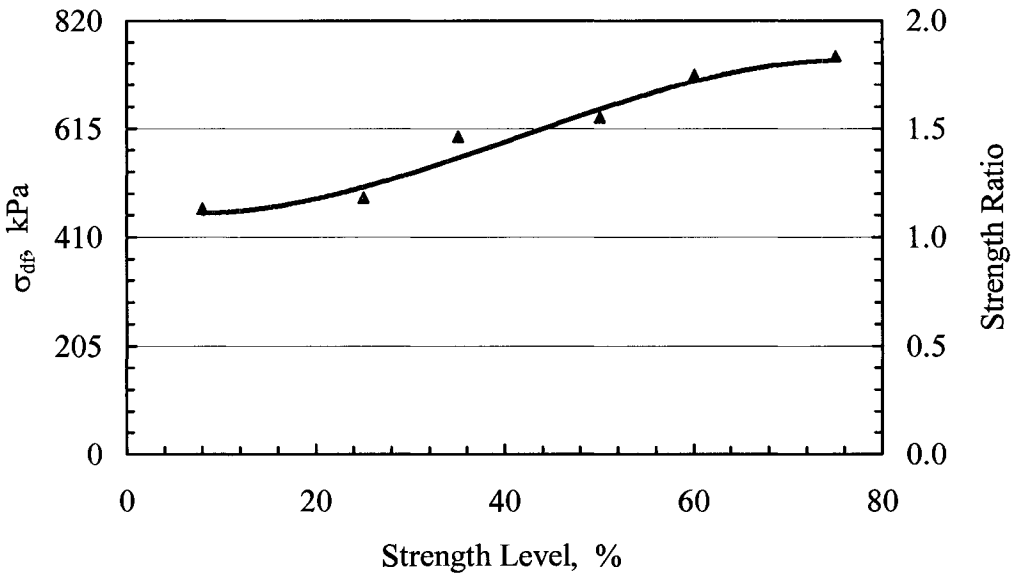

Figure 4.11: Strength Level Effect on Shear Strength Ratio after 100,000 RS Load Repetitions (σ_3 = 35 kPa).

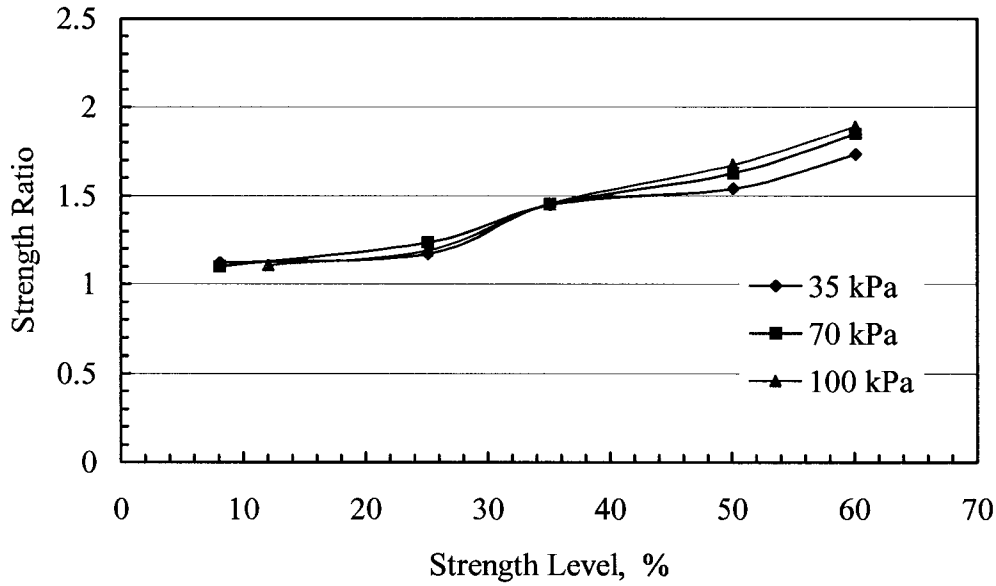

Figure 4.12: Shear Strength Ratio Variation with Strength Level for RS Loading under Different Confinement Stresses.

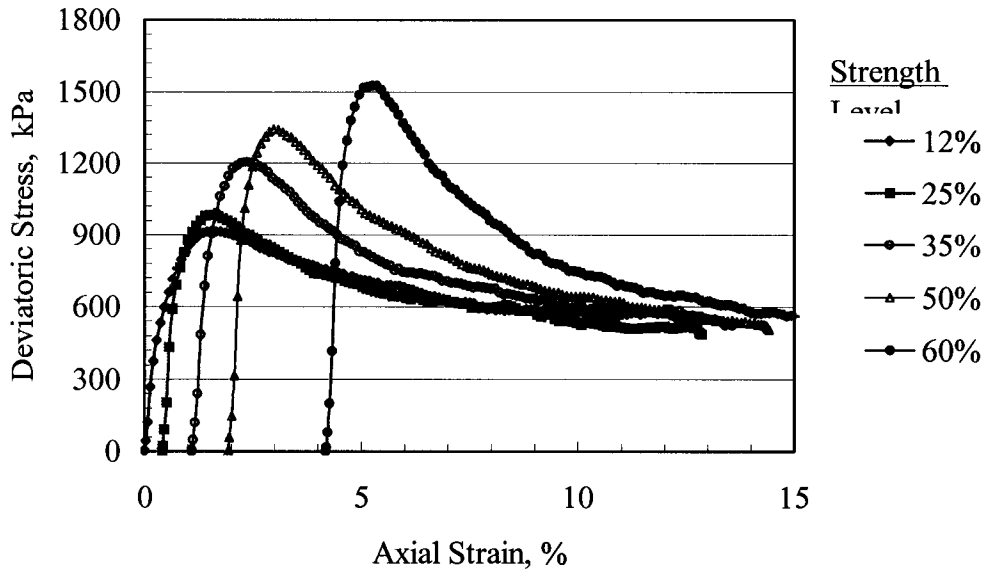

Figure 4.13: Monotonic Stress-Strain Curve for Different *SL* after 100,000 RS Load Repetitions (σ_3 = 100 kPa)

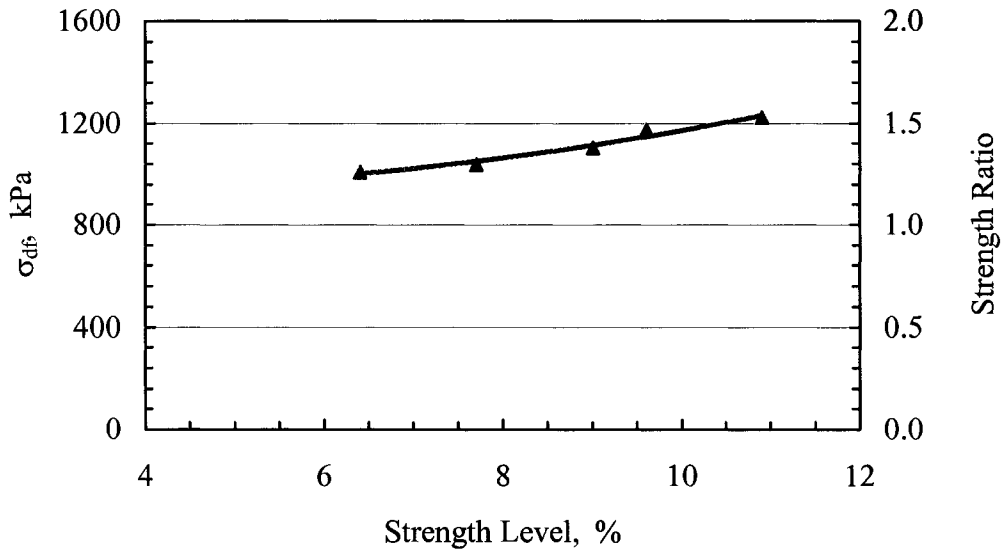

Figure 4.14: Shear Strength Ratio Variation with Strength Level for CS Loading under 100 kPa Confinement.

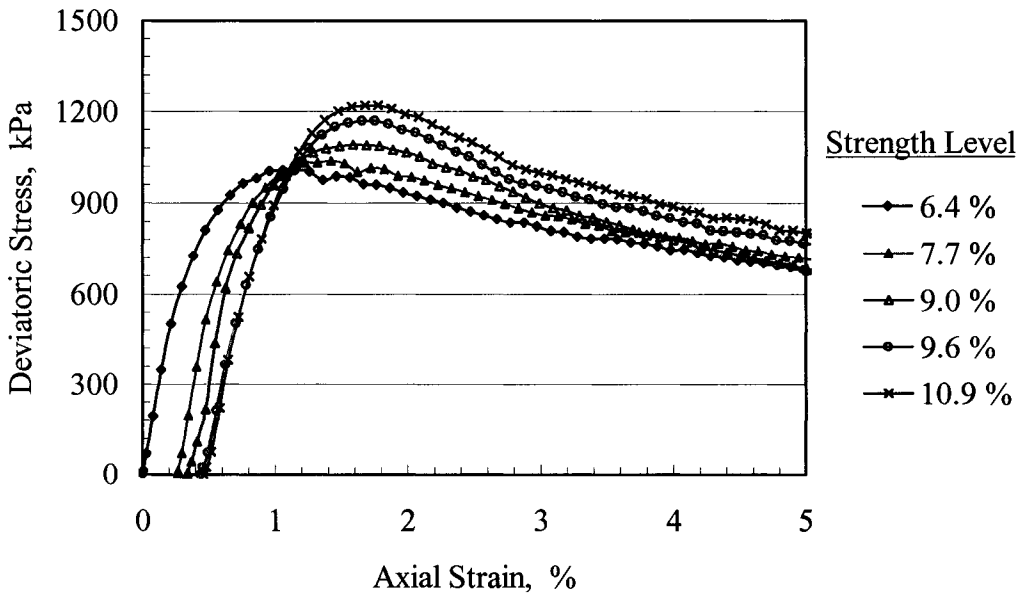

Figure 4.15: Monotonic Stress-Strain Curve for Different *SL* after 100,000 CS Load Repetitions (σ_3 = 100 kPa)

4.4.2 Resilient Strains

4.4.2.1 Resilient Axial Strains

The resilient response of the specimens subjected to long-term loading was monitored. Consistently, specimens that were subjected to repeated load patterns yielded higher resilient axial strains than specimens tested at similar strength level using cyclic loading pattern.

RS loading resulted in 75% higher resilient axial strains than CS loading at low confinement (35 kPa) and approximately 55% higher resilient strains for tests at high confining stress (100 kPa). The resilient axial strain of RS specimens increased with number of load repetitions applied by about 7% to 20% for tests conducted at 35 kPa and 100 kPa respectively (after 100,000 load repetitions), whereas, the resilient response of CS specimens remained basically unchanged for tests at low confinement and increased by about 12% for specimens tested at relatively high confining pressure (Figures 4.16 and 4.17).

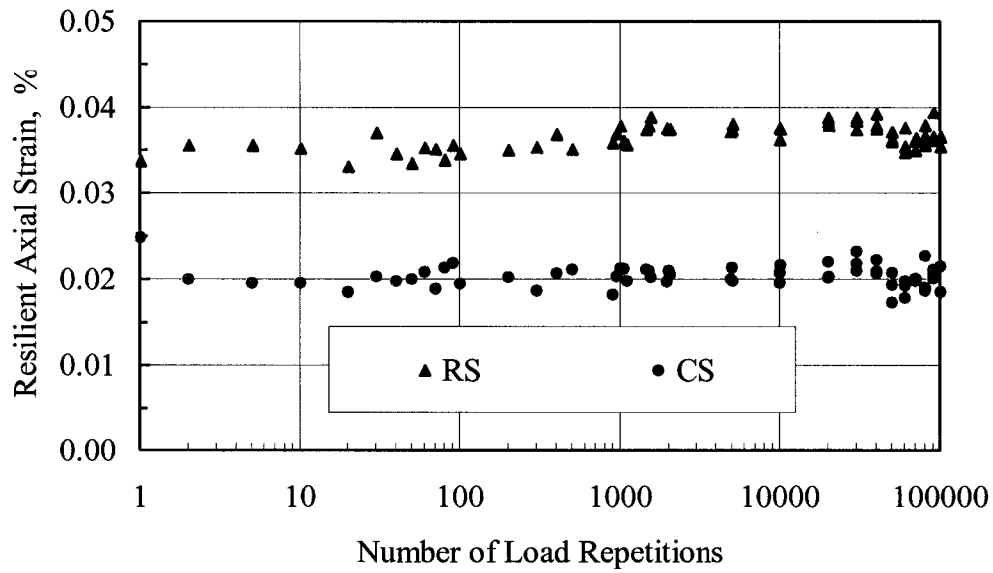

Figure 4.16: Resilient Axial Strain Variation under RS and CS Loading for Same Strength Level = 8% (σ_3 = 35 kPa).

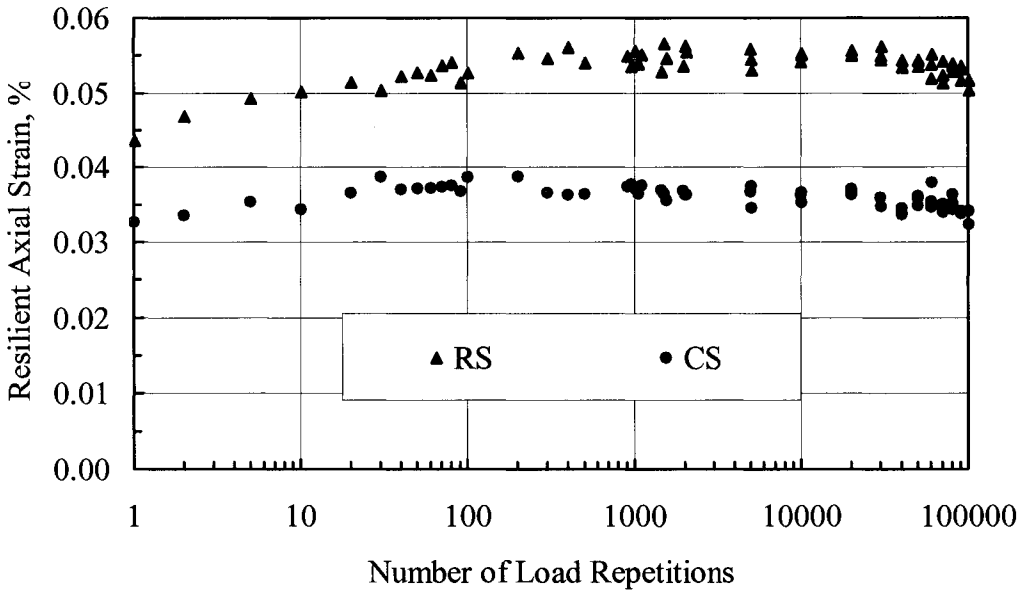

Figure 4.17: Resilient Axial Strain Variation under RS and CS Loading for Same Strength Level =12% (σ_3 = 100 kPa).

The figures above show the comparison between repeated and cyclic loading at relatively low strength levels (8% and 12% respectively for confinements of 35 kPa and 100kPa). For higher strength levels, cyclic loading tests are not feasible to conduct due to the fact that granular soils cannot carry tensile stresses exerted by the tensile deviatoric stress portion of the loading pattern. For these strength levels only repeated load patterns were used.

Figures 4.18 and 4.19 show the development of the resilient axial strains with RS strength levels applied. Resilient strains (ε_l^r) increase with strength levels applied and seem to remain constant regardless of the number of load applications for low and intermediate strength levels. As for high strength levels, ε_l^r seem to increase with number of load repetitions *(N)* to a maximum and then decrease with further increase in *N*.

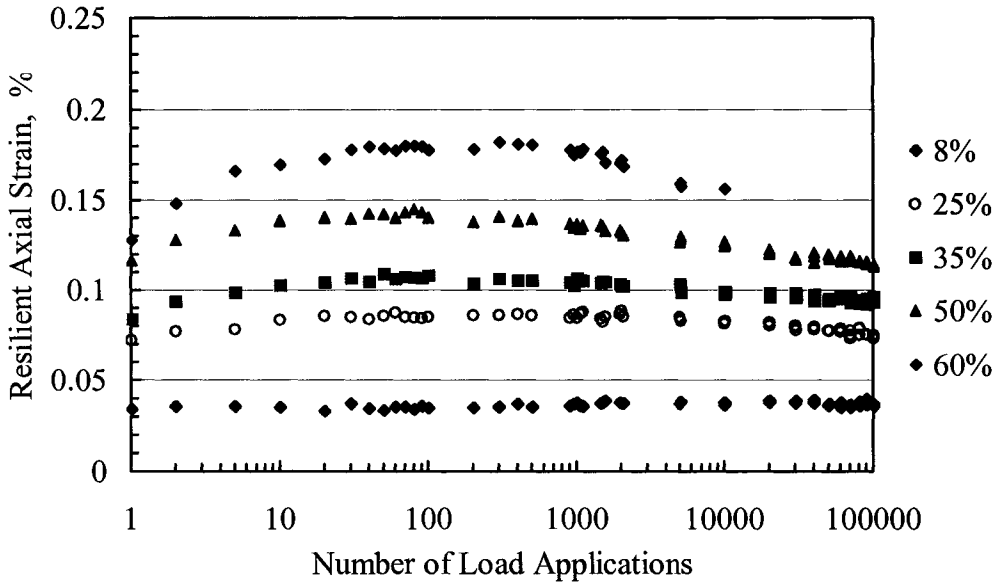

Figure 4.18: ε_1^r Variation with N at Different Strength Levels (σ_3 = 35 kPa)

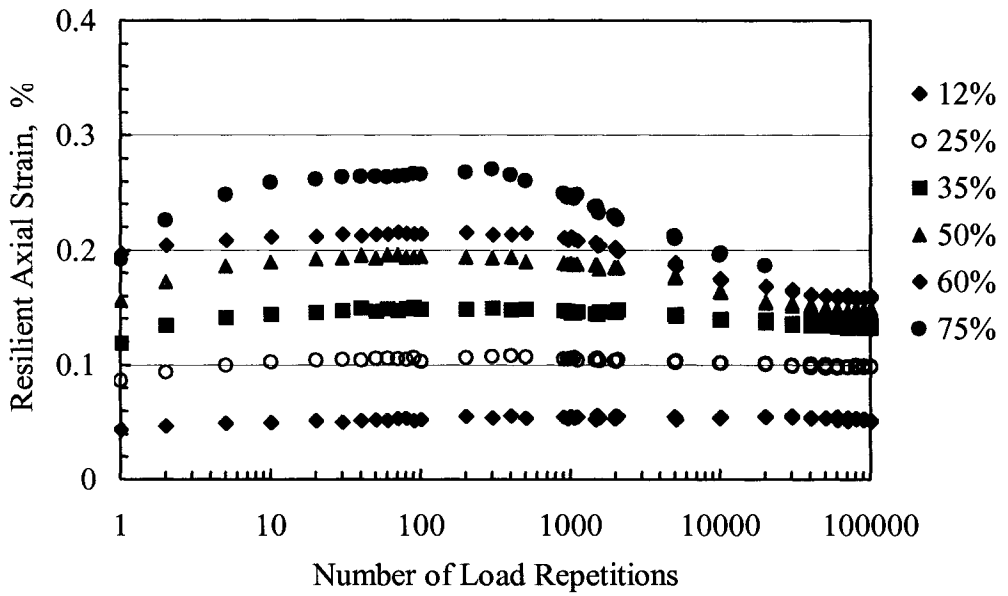

Figure 4.19: ε_1^r Variation with N at Different Strength Levels (σ_3 = 100 kPa)

4.4.2.2 Resilient Shear Strain

The resilient shear strain (γ_r) resulting from specimens tested at a repeated load pattern yielded 30% to 50% higher resilient shear strain values compared to specimens tested under similar stress level using cyclic loading pattern (Figure 4.18).

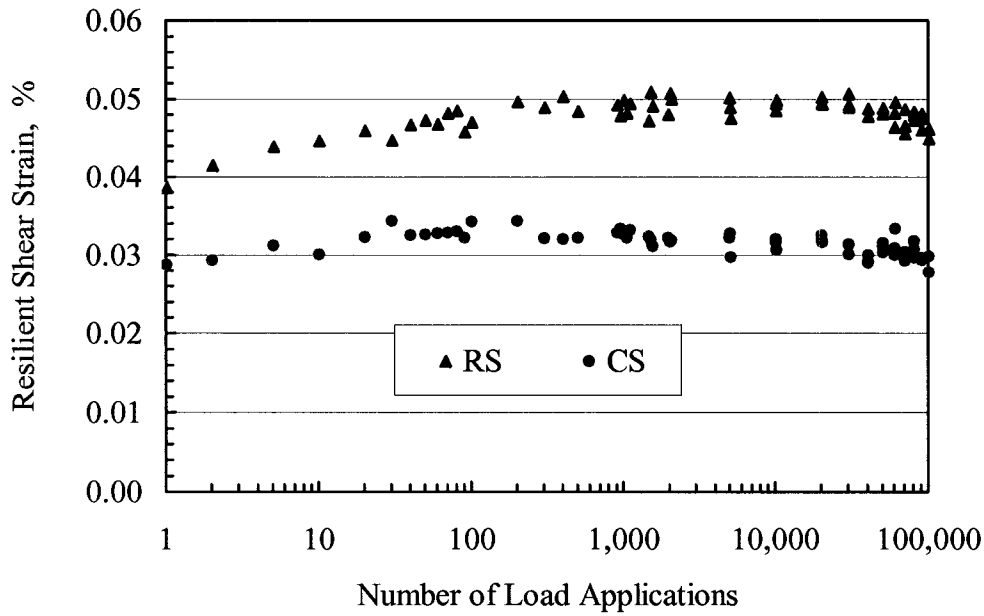

Figure 4.20: Resilient Shear Strain Variation under RS and CS Loading for Same Strength Level = 12% (σ_3 = 100 kPa).

For tests conducted using repeated load pattern and higher stress levels, the resilient shear strain (γ_r) increased with an increase in the strength level (*SL*) applied. For SL levels beyond 50%, the resilient shear strain remained basically unchanged regardless of the confining pressure applied (Figures 4.21 and 4.22).

Furthermore, the resilient shear strain (γ_r) remains unaffected with an increase in load repetitions for strength levels below 50%. For higher strength levels, γ_r increases with the number of load repetitions to achieve a maximum and decreases afterwards.

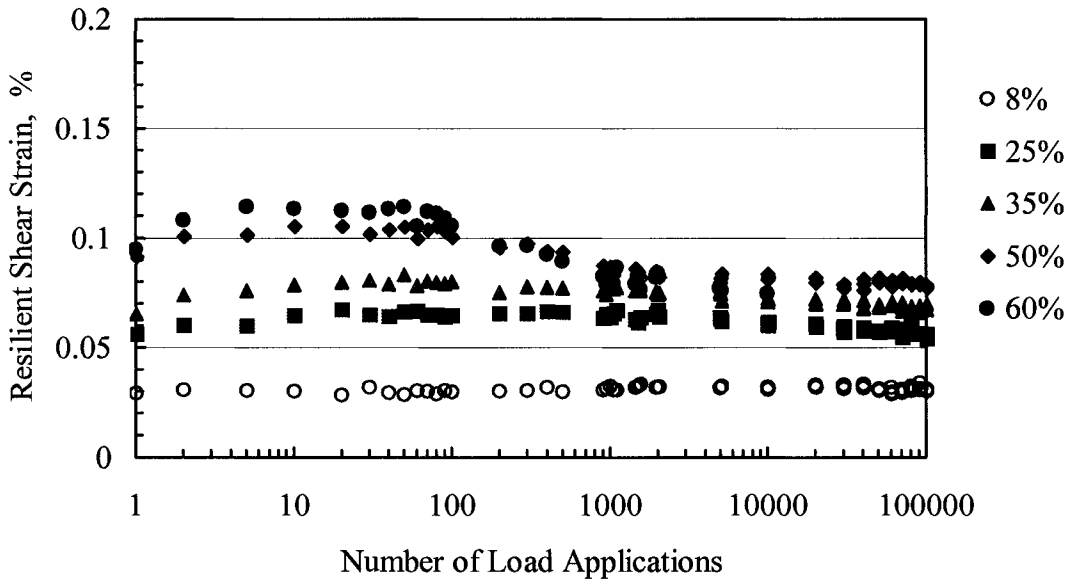

Figure 4.21: Resilient Shear Strain Variation with N for Different SL (σ_3 = 35 kPa)

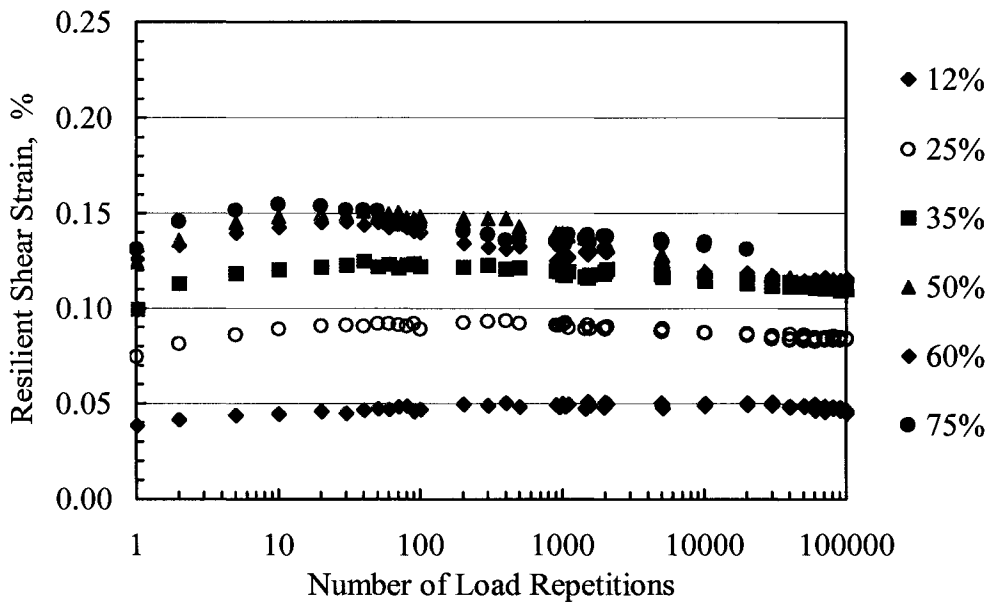

Figure 4.22: Resilient Shear Strain Variation with N for Different SL (σ_3 = 100 kPa)

4.4.2.3 Resilient Radial Strains

For the same strength level, the resilient radial strains measured in specimens subjected to repeated stress loading pattern were, on the average, 25% more than those measured in specimens tested under cyclic loading conditions (Figure 4.23).

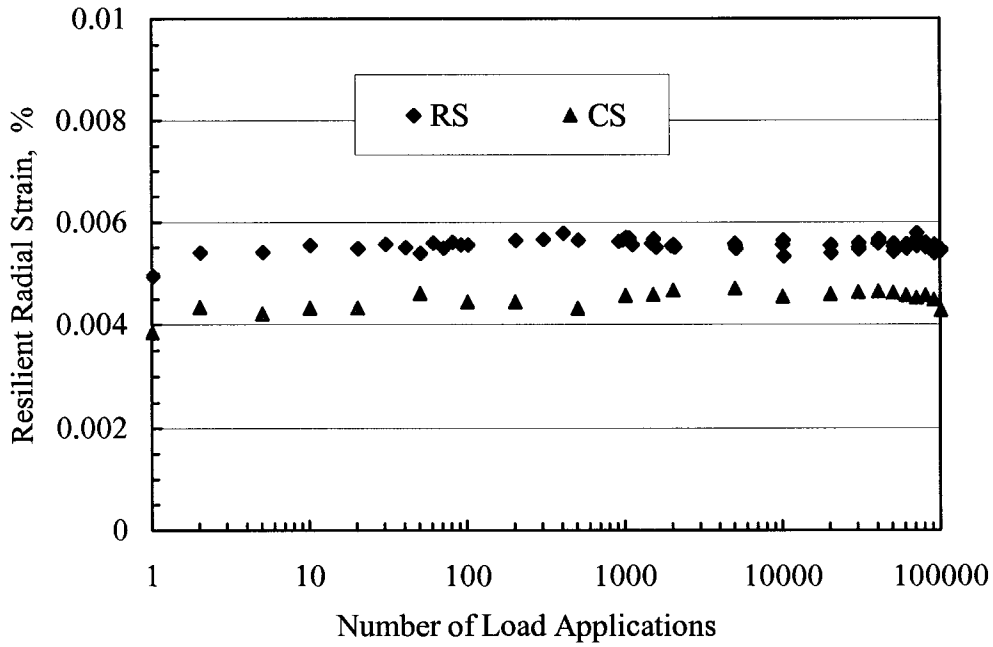

Figure 4.23: Resilient Radial Strain Variation under RS and CS Loading for Same Strength Level = 12% (σ_3 = 100 kPa).

For low strength levels, the resilient radial strains (ε_3^r) resulting from RS loading remains somewhat constant with increasing number of load repetitions (N). However, as SL increases, ε_3^r increases with N to a maximum value and thereafter decreases with further increase in the number of load repetitions applied. The same trends are observed regardless of the confinement applied (Figures 4.24 and 4.25).

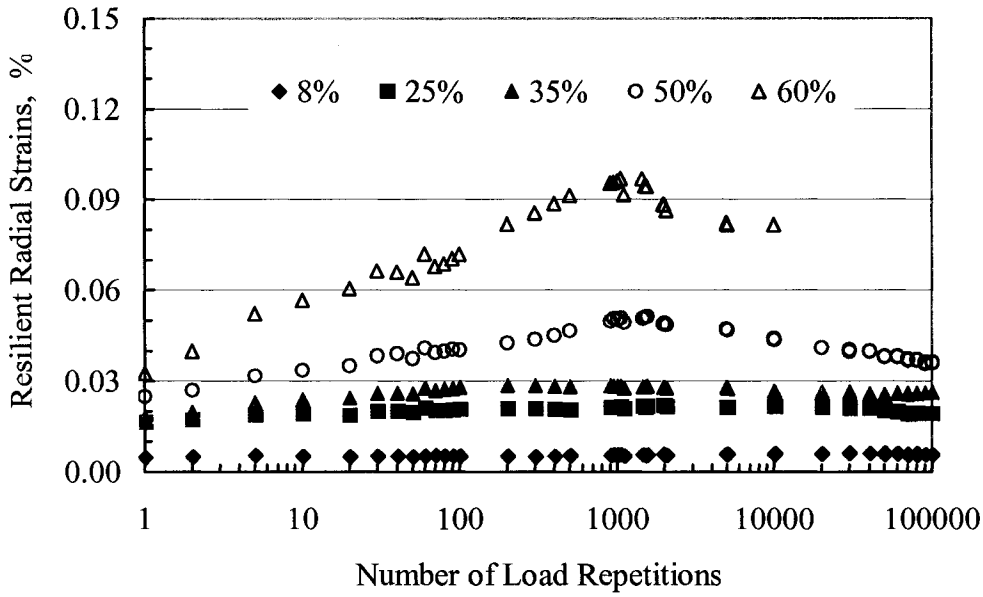

Figure 4.24: ε_3^r Variation with N under RS Loading at $\sigma_3 = 35$ kPa.

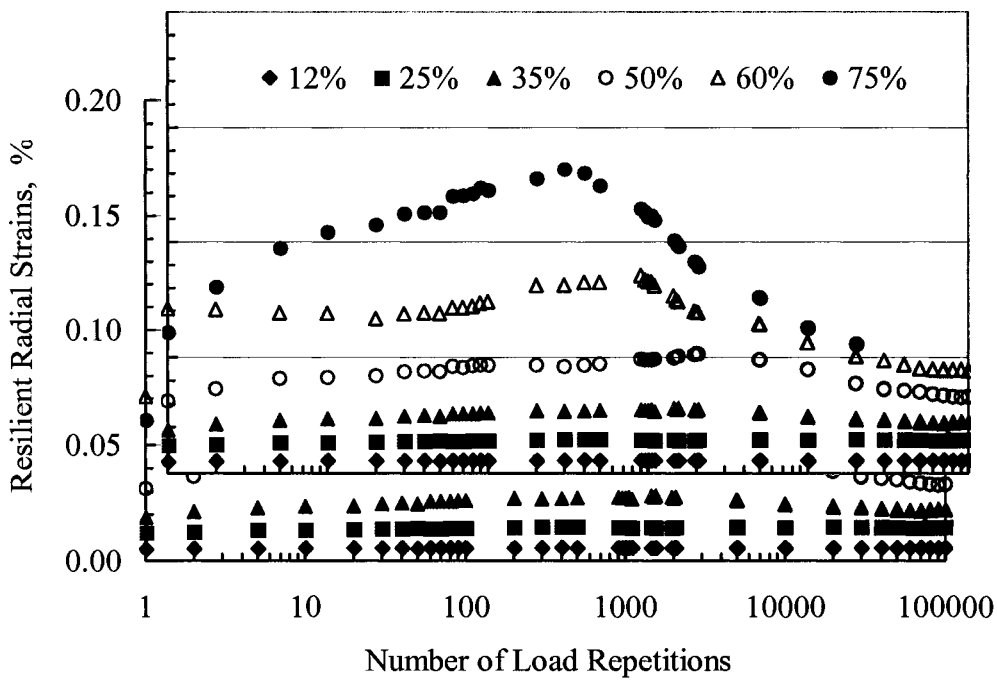

Figure 4.25: ε_3^r Variation with N under RS Loading at $\sigma_3 = 100$ kPa.

As for specimens tested under cyclic loading pattern, and for the range of strength levels used, the resilient radial strain remains mostly unchanged with increase in the number of load repetitions applied (Figure 4.26). Nonetheless, as was the case for the repeated stress pattern, an increase in the strength level applied resulted in an increase in the measured resilient radial strain.

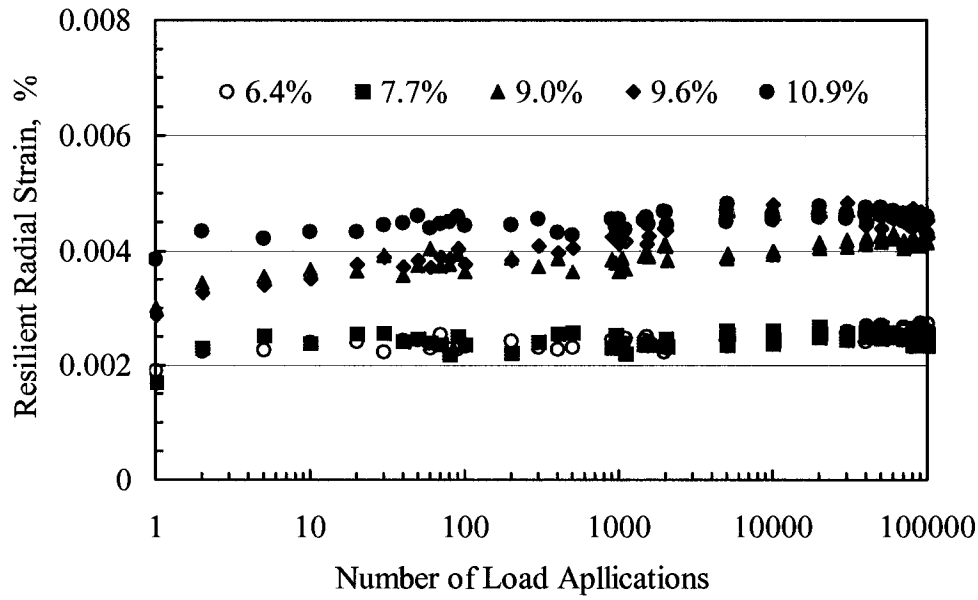

Figure 4.26: ε_3^r Variation with N under CS Loading at $\sigma_3 = 100$ kPa.

4.4.2.4 Resilient Poisson's Ratio

The resilient Poisson's ratio ν_r, resulting from RS and CS loading of specimens subjected to the same strength level, remains virtually the same with the CS loading pattern yielding slightly higher values (Figure 4.27).

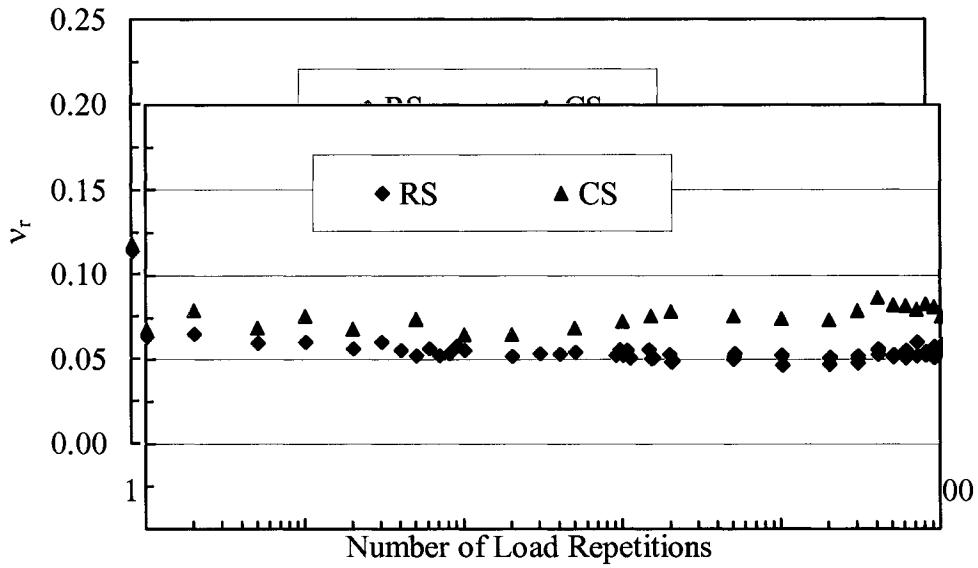

Figure 4.27: v_r Variation under RS and CS Loading for Same Strength Level =12% (σ_3 = 100 kPa).

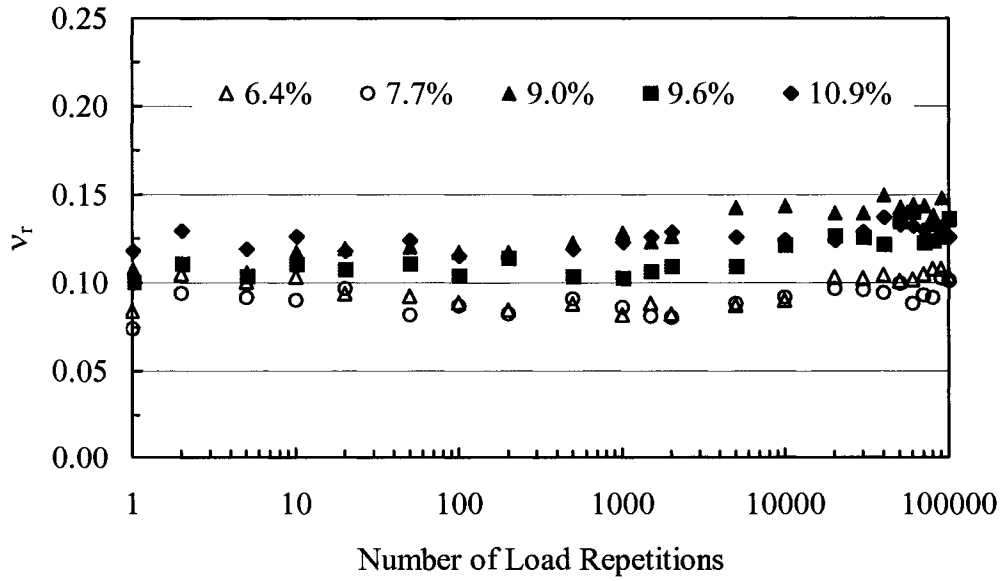

Figure 4.28: v_r Variation with N under CS Loading at σ_3 = 100 kPa.

The Poisson's ratio does not change considerably under cyclic loading conditions and for the range of strength level used in this research as shown in Figure 4.28. However, for tests performed under repeated load pattern, ν_r increases gradually with the number of load repetitions, at relatively high strength levels, reaching a maximum value before decreasing with further increase in the number of load repetitions applied. The maximum number reached, at the highest strength level applied, was in the neighborhood of 0.5 for both 35 kPa and 100 kPa confining pressures (Figures 4.29 and 4.30).

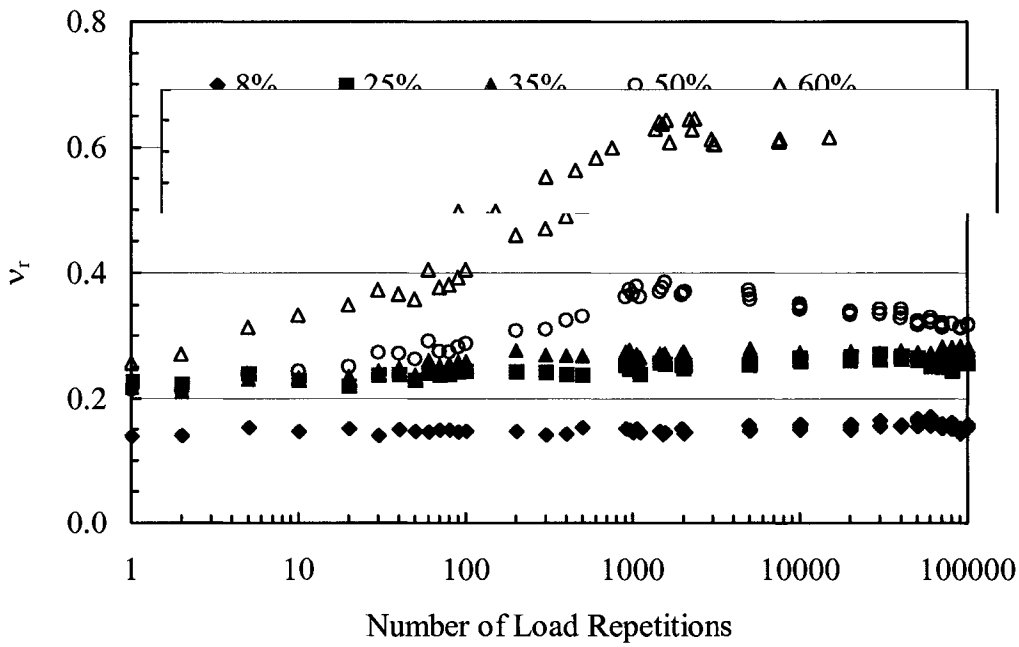

Figure 4.29: ν_r Variation with N under RS Loading at σ_3 = 35 kPa.

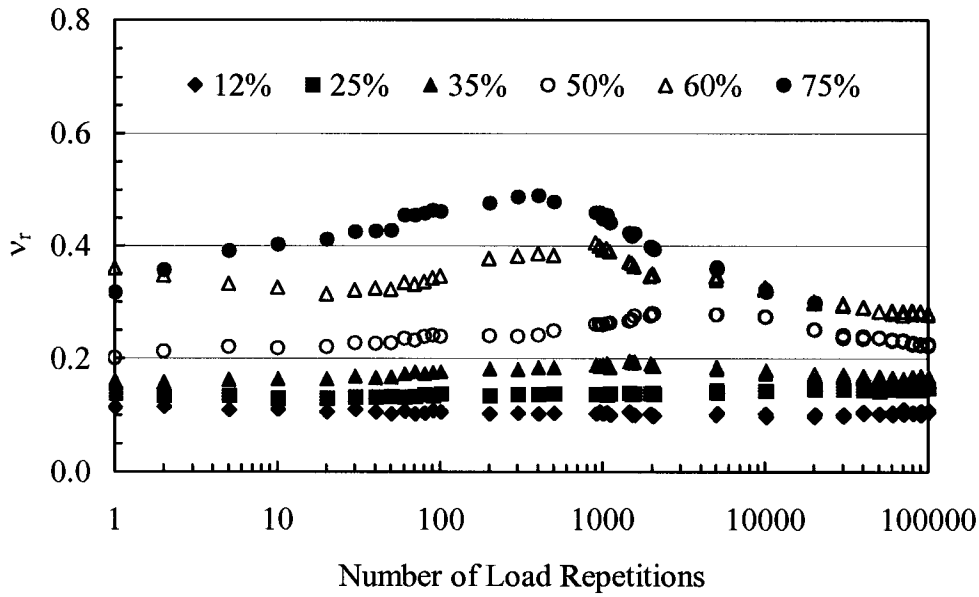

Figure 4.30: ε_r Variation with N under RS Loading at σ_3 = 100 kPa

4.4.3 Plastic Strain Accumulation

The most noticeable mode of distress developed in granular layers is permanent deformation. This distress is due to two different mechanisms that take place during the application of dynamic loading. The first is densification of the granular material due to the repetitive back and forth action of the applied load. In this scenario, the aggregates reorient themselves and roll over each other to assume the position that will result in an optimum overall geometry in order to best sustain the externally applied loads. If the optimum matrix geometry achieved cannot sustain the applied state of stress, the second mechanism takes place; this consists of the aggregates crushing against each other until the attrition of aggregates composed of the weakest mineral in the mix. This, of course, creates new matrix geometry and the process starts all over again.

The magnitude of applied loads in a typical pavement structure is not expected to be high enough to lead to the attrition of aggregates in the base course, especially

when good care is taken to choose sound materials in the granular mix. Therefore, the main mechanism that takes place is that of reorientation of the particles in order to assume denser, more efficient packing.

To understand the mechanism, and to better predict the amount and rate of permanent deformation, long term repeated triaxial tests are conducted in the lab and the resulting progressive permanent deformation is monitored with number of load applications. Both axial and radial plastic strains were monitored in the course of this research.

4.4.3.1 Effect of Type of Loading

The amount and rate of permanent deformation build up is dependent on the level of the stress applied and the type of loading. Since it was shown earlier in this study that the load pattern induced by a moving wheel is complex rather than unidirectional, it became necessary in this research to check the variation of permanent strain accumulation with different loading patterns. Identical specimens were subjected to four different loading patterns (RS, RN, CS and CN), having same initial stress level, $\sigma_d/\sigma_3 = 0.8$, and tested at two different confining stresses 35 kPa and 100 kPa. The results in terms of axial strain, radial strain and volumetric strain are given in the figures below.

Volumetric strain is given by:

$$\varepsilon_v = \varepsilon_1 + 2 \cdot \varepsilon_3 \qquad (4.3)$$

Where:

ε_1 = Axial Strain,

ε_3 = Radial Strain.

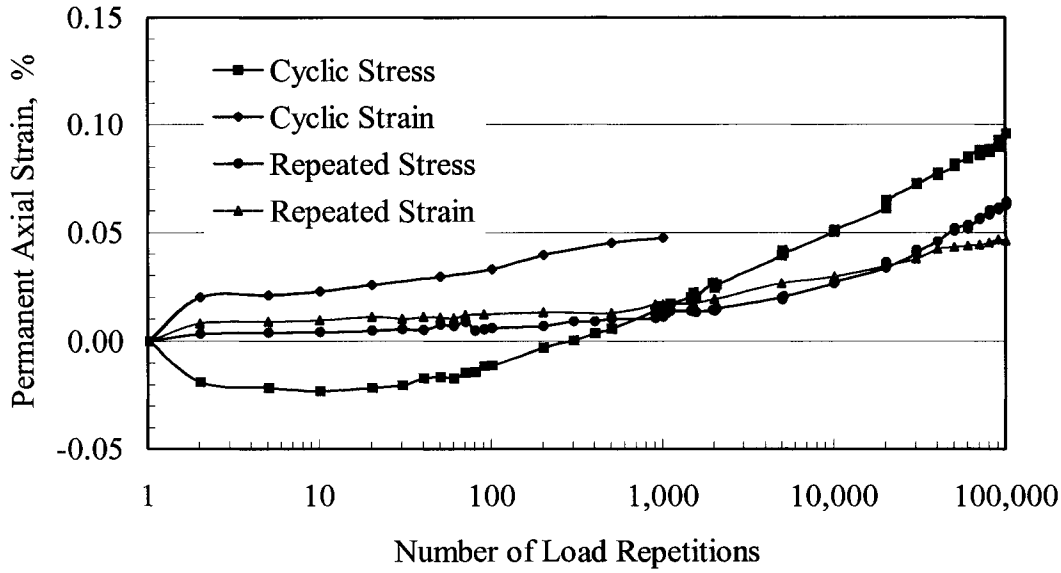

Figure 4.31: Axial Strain Accumulation for Different Load Patterns at σ_3 = 35kPa.

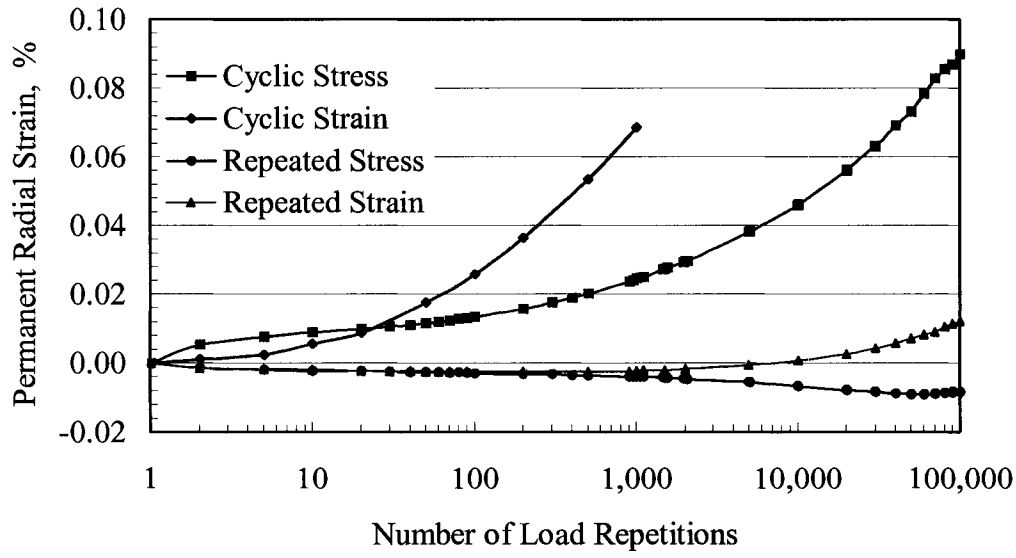

Figure 4.32: Radial Strain Accumulation for Different Load Patterns at σ_3 = 35kPa.

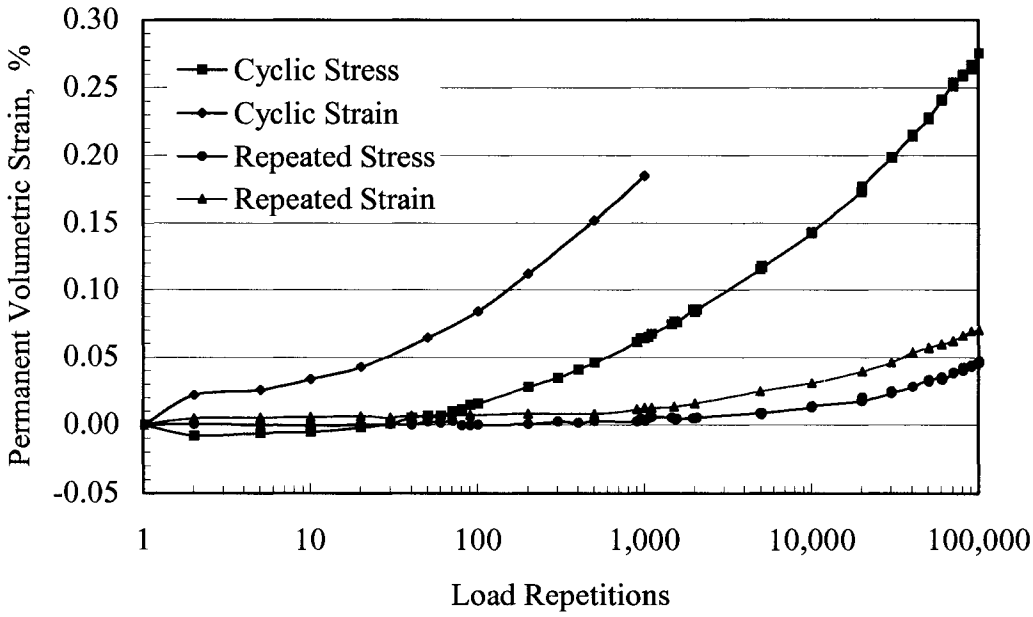

Figure 4.33: Volumetric Strain Accumulation for Different Load Patterns at σ_3 = 35 kPa.

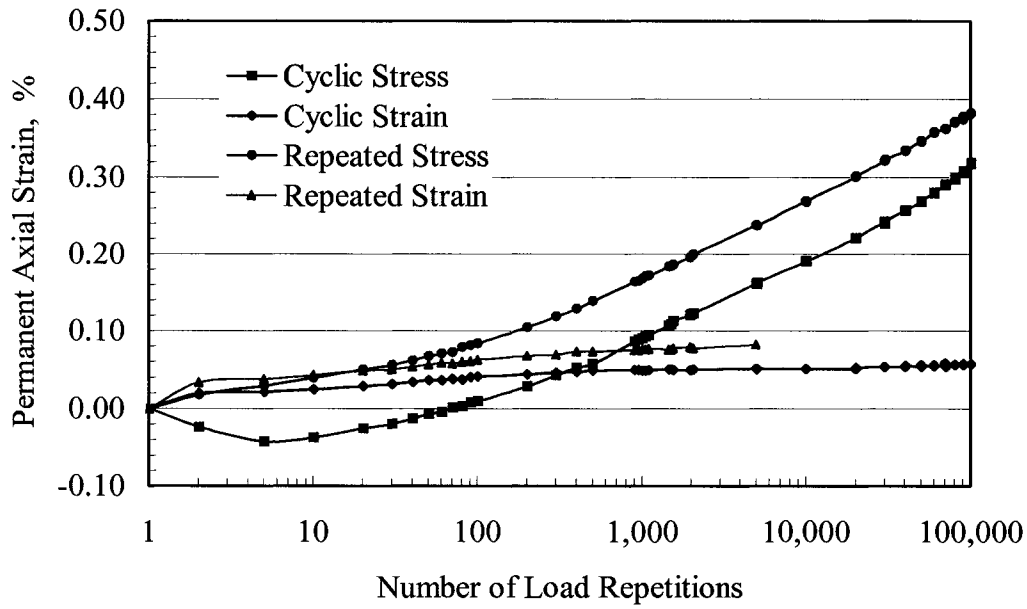

Figure 4.34: Axial Strain Accumulation for Different Load Patterns at σ_3 = 100 kPa.

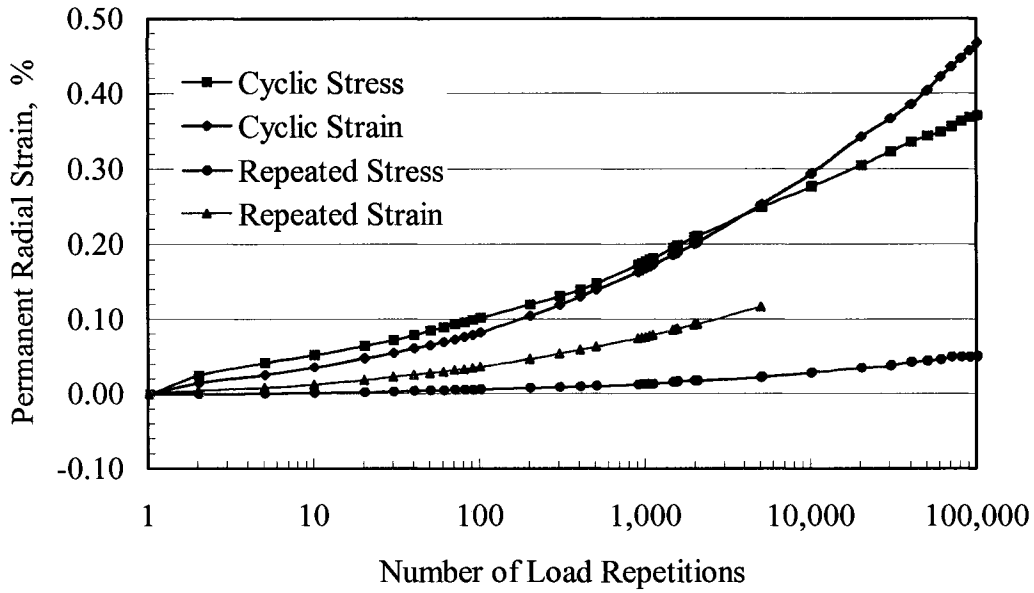

Figure 4.35: Radial Strain Accumulation for Different Load Patterns at σ_3 = 100 kPa.

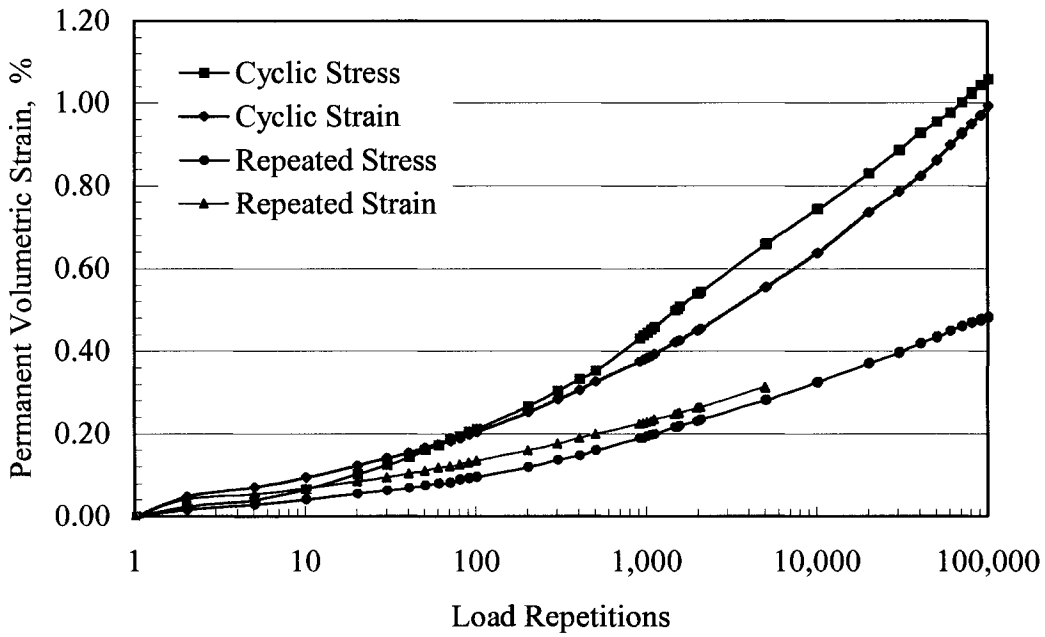

Figure 4.36: Volumetric Strain Accumulation for Different Load Patterns at σ_3 = 100 kPa.

Before discussing the results presented and their implications, few clarifications are suitable to be mentioned here. All results presented above are the average of at least three duplicate tests. Specimens subjected to cyclic strain loading at a confining pressure of 35 kPa, were stopped after 1,000 repetitions due to loss of contact between the platen and the sample due to densification. For the same reason, specimens subjected to repeated strain loading at a confining stress of 100 kPa, were discontinued after 5,000 repetitions.

Upon closer examination of the results given above, we can make the following observations:

- Specimens subjected to CS loading exhibit initially negative permanent axial strains (extension, up to 1,000 repetitions for σ_3 = 35 kPa and up to 100 repetitions for σ_3 = 100 kPa), afterwards, the accumulated axial strain increases at a higher rate.
- At the lower confining stress, specimens subjected to RN and RS loading yield comparable axial deformation, whereas their deformation at the higher confining stress differ totally, with repeated stress yielding much higher axial strain values.
- At 35 kPa confinement, samples subjected to RS loading resulted in minimal negative permanent radial strains, and those subjected to RN loading exhibited negative radial strains up to around 10,000 repetitions and, minimal positive radial strains afterwards.
- Cyclic Strain and Cyclic Stress loading produced the highest permanent radial strains regardless of the confinement.
- The volumetric strain resulting from repeated one directional (stress and strain) loading is almost the same regardless of the confinement used.
- At 35 kPa confinement, specimens subjected to cyclic stress and cyclic strain yield much higher permanent volumetric strains than those subjected to RS and RN loading. The amount of volumetric permanent strain after 100,000 CS load

applications is almost 5 times more than the amount recorded for RS and RN at the same stage of loading.

- At the higher confinement (100 kPa), specimens tested under CS and CN loading witnessed twice the amount of permanent volumetric strain measured for specimens subjected to RS or RN loading.

Plots of permanent strain versus logarithmic load repetitions are popular since they represent a convenient mean to show, on the same graph, the amount of strain measured for short term as well as long term loading. However, to better appreciate the rate of permanent strain buildup, it is better to use a simple plot of permanent strain versus load repetitions in natural scale as shown in the figure below.

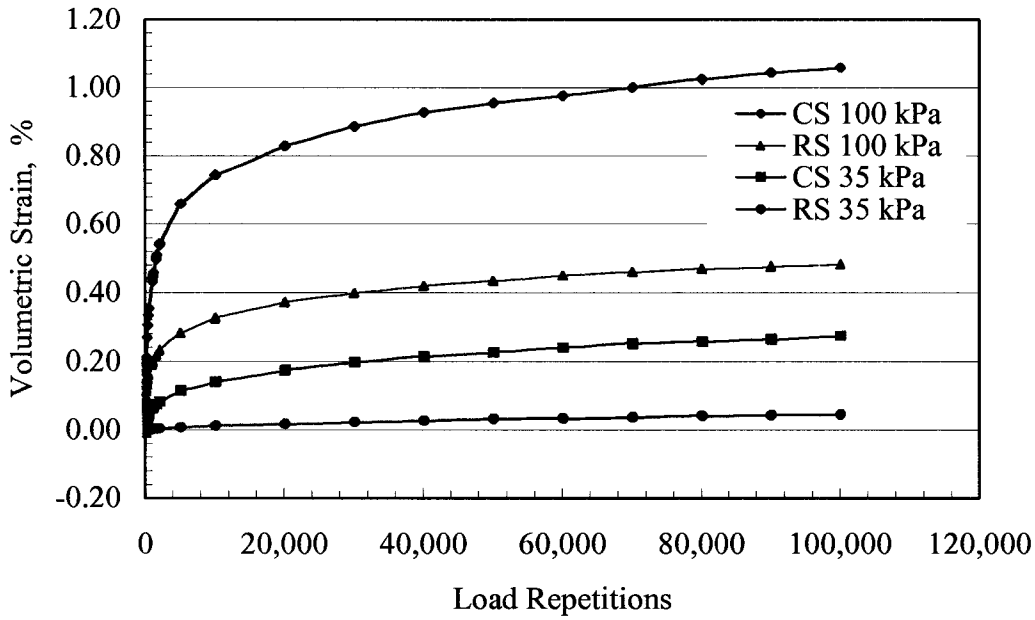

Figure 4.37: Volumetric Strain Accumulation Versus Load Repetitions for $\sigma_d/\sigma_3 = 0.8$.

Figure 4.37 shows a comparison in the amount of permanent volumetric strain accumulated due to cyclic and repeated stress loading at confinements of 35 kPa and

100 kPa. Besides loading pattern, it is evident that the confining stress is an important factor. For the same stress level, increasing the confining stress from 35 kPa to 100 kPa resulted in an increase in permanent volumetric strain by a factor of 10 in the case of repeated stress loading, and by a factor of 4 in the case of specimens subjected to cyclic stress loading.

Besides an estimate on the amount of accumulated permanent strain expected, a pavement engineer is also interested in the rate of accumulation. This information can be readily used to estimate the serviceability life of a given pavement section. Figures 4.38 through 4.43 represent the rate of axial, radial and volumetric plastic strain accumulated at a stress level of $\sigma_d/\sigma_3 = 0.8$ and confining stresses of 35 kPa and 100 kPa.

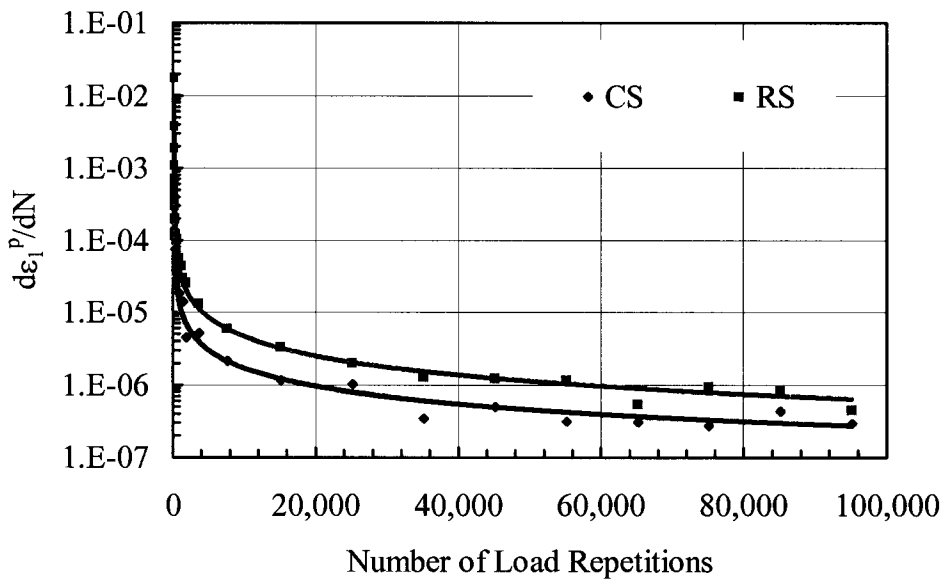

Figure 4.38: Permanent Axial Strain Rate Variation with Number of Load Applications at 35 kPa Confinement.

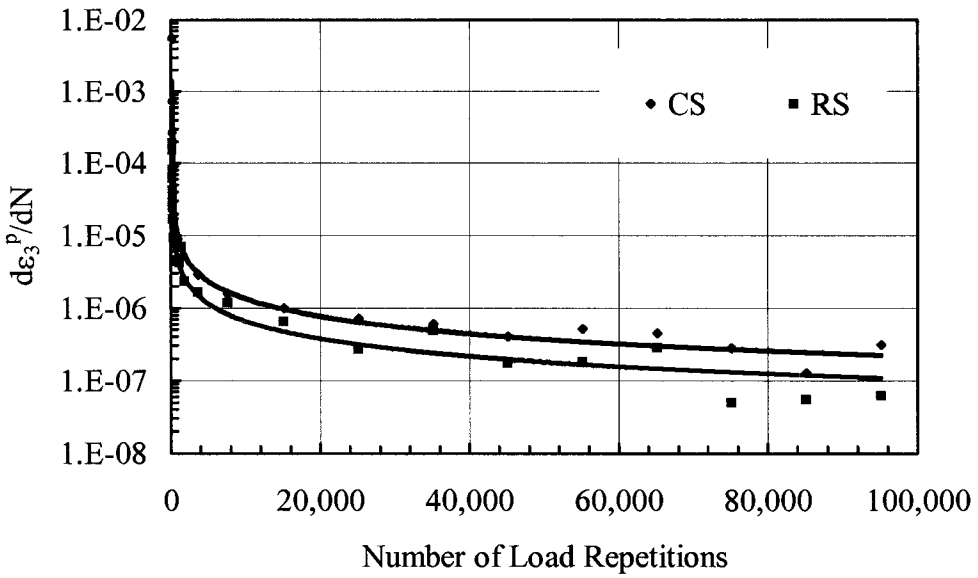

Figure 4.39: Permanent Radial Strain Rate Variation with Number of Load Applications at 35 kPa Confinement.

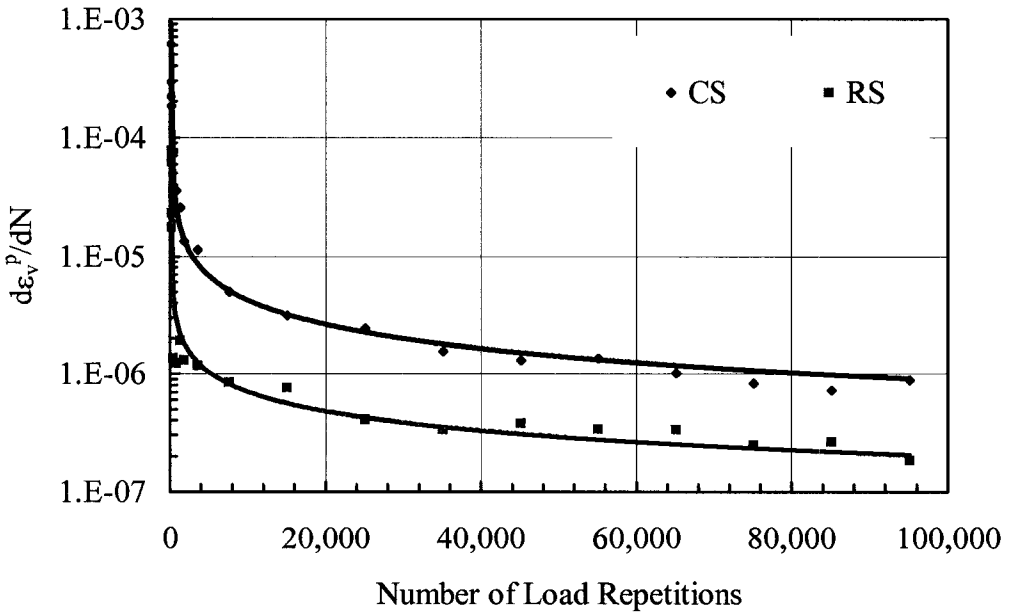

Figure 4.40: Permanent Volumetric Strain Rate Variation with Number of Load Applications at 35 kPa Confinement.

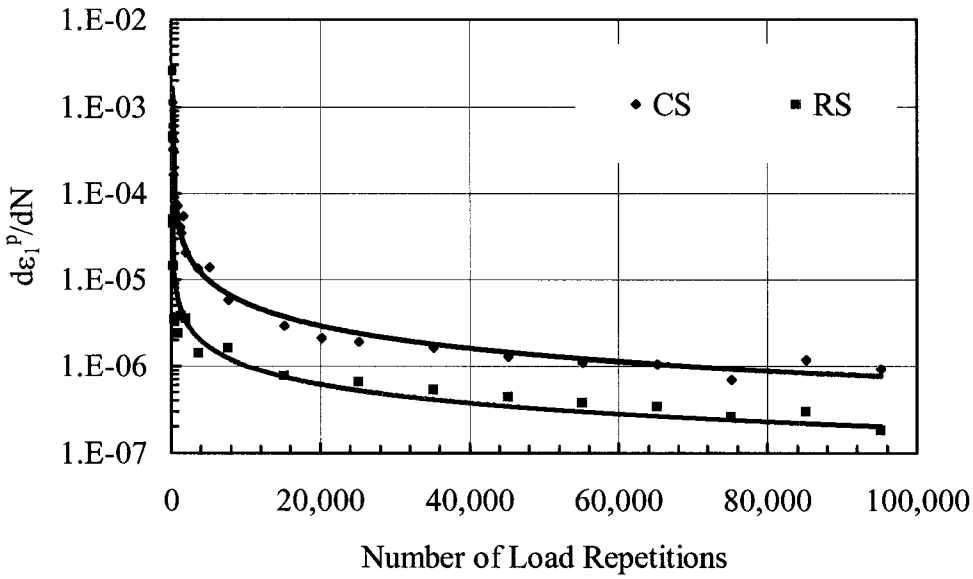

Figure 4.41: Permanent Axial Strain Rate Variation with Number of Load Applications at 100 kPa Confinement.

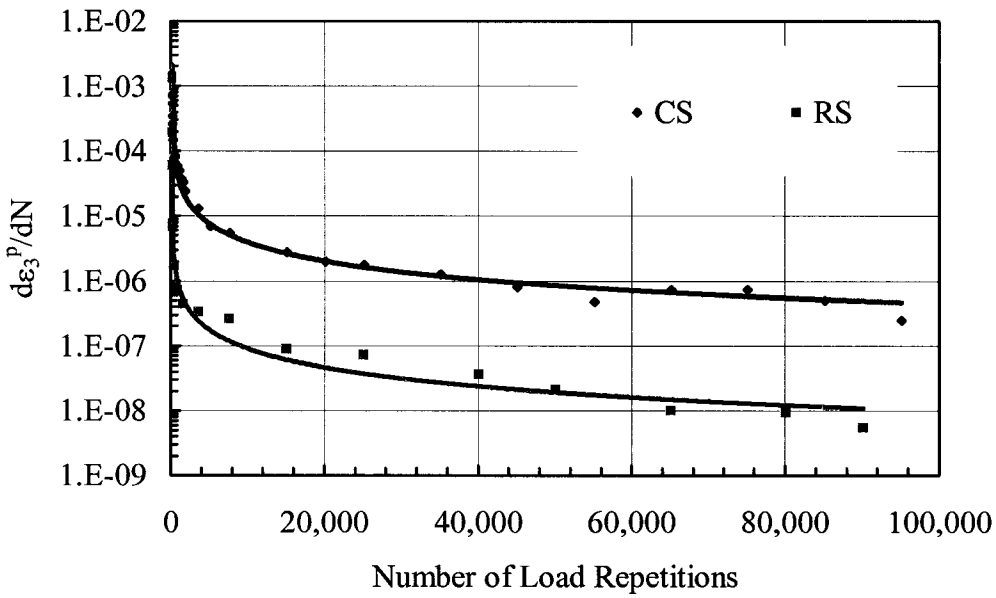

Figure 4.42: Permanent Radial Strain Rate Variation with Number of Load Applications at 100 kPa Confinement.

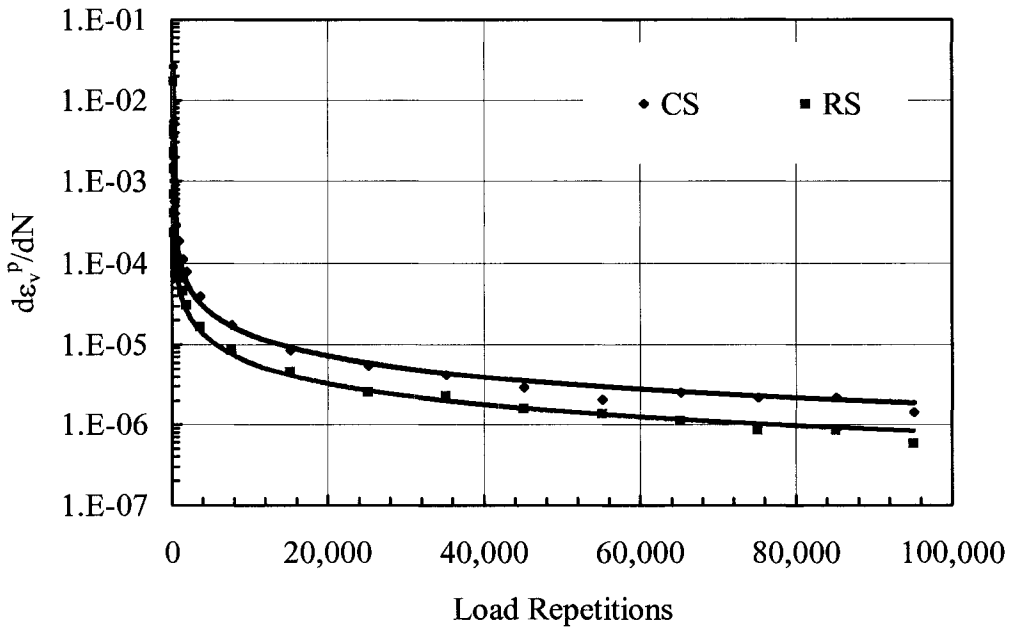

Figure 4.43: Permanent Volumetric Strain Rate Variation with Number of Load Applications at 100 kPa Confinement.

In the figures above, the rate of plastic strain build up is represented by $d\varepsilon_p/dN$. In all cases, this ratio decreases with number of load applications at a decreasing rate. The data presented for axial, radial and volumetric seems to be best fitted using a power equation of the form:

$$\frac{d\varepsilon_p}{dN} = a \cdot N^b \qquad (4.4)$$

Where: $d\varepsilon_p/dN$ = Rate of permanent (axial, radial, or volumetric) strain accumulated.

N = Number of load applications

a and b = Curve fit parameters

The various a and b parameters obtained from power curve fits as well as the associated R^2 value are given in Tables 4.3 and 4.4 below:

Table 4.3: Power Curve Fit Parameter Values for σ_3 = 35 kPa.

	σ_3 = 35 kPa					
	RS Loading			CS Loading		
	Axial	Radial	Volumetric	Axial	Radial	Volumetric
a	0.0142	0.001	0.0001	0.0029	0.0019	0.0022
b	-0.8723	-0.7955	-0.5487	-0.8075	-0.7908	-0.6777
R^2	0.985	0.975	0.956	0.974	0.976	0.976

Table 4.4: Power Curve Fit Parameter Values for σ_3 = 100 kPa.

	σ_3 = 100 kPa					
	RS Loading			CS Loading		
	Axial	Radial	Volumetric	Axial	Radial	Volumetric
a	0.0007	0.0006	0.0175	0.0138	0.022	0.0352
b	-0.7132	-0.955	-0.8675	-0.8556	-0.938	-0.8584
R^2	0.948	0.974	0.996	0.989	0.991	0.992

In order to calculate the amount of plastic axial strain accumulated during shear reversal loading, the responses normal to the 45° plane should be evaluated. The plastic strains thus calculated are compared to axial permanent strains resulting from repeated load testing at same stress level in the figure below.

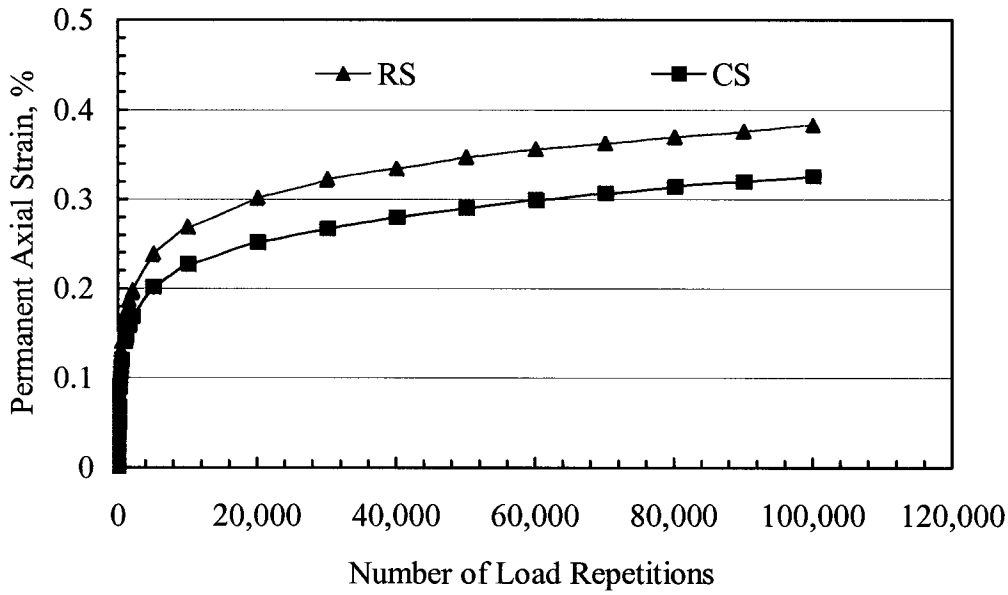

Figure 4.44: Permanent Axial Strain in RS and in CS (45° plane) for Same Strength Level = 12% (σ_3 = 100 kPa).

According to Figure 4.44, the permanent axial strain resulting from shear reversal (normal to 45° plane) of the granular material is approximately 15% less than those resulting from specimens tested under repeated load pattern.

4.4.3.2 Effect of Strength Level

In order to study the effect of stress level on the development of permanent strain, identical samples of the granular material were subjected to repeated stress and cyclic stress loading at different stress levels. In the case of repeated stress loading, the strength level (σ_d/σ_{df}), which is defined as the ratio of deviatoric stress applied over the shear strength of the material, was varied from 8% to 75% and was determined at three different confining pressures, 35 kPa, 70 kPa and 100 kPa.

As for the case of cyclic stress, a restriction on the maximum amount of deviatoric stress ($\pm \sigma_d$) applied exists such that the specimen remains in contact with

the platen at all time. The range of strength levels used in this case varied from 6.4% to 10.9% (which corresponds to stress level σ_d/σ_3 values of 0.5 to 0.85) and tests were conducted at a confining stress of 100 kPa. The reason why lower values of confining stress were not used in this case is due to the fact that low σ_3 values do not provide the luxury of using a range of strength or stress levels needed.

- Axial Strain

Permanent axial strain increases with load repetition. Higher applied stress levels result in larger axial strains. Figures 4.45, 4.46 and 4.47 show the accumulated permanent axial strains in specimens subjected to repeated stress loading and, at three different confining pressures (35 kPa, 70 kPa and 100 kPa).

In general, permanent axial strain accumulates at decreasing rate. For low stress (or strength) levels, the amount of deformation seems to level off after a given number of repetitions. After a certain strength level, the axial strain measured still increases, albeit at a low rate, even after 100,000 load repetitions. Comparing specimens tested at 35 kPa confinement, we notice that the axial strain accumulated after 100,000 repetitions for strength level of 50% is double that measured for a specimen tested at 35% strength level. And 60% strength level tests result in 3 times more permanent axial strain than tests conducted at 50% strength level after 5,000 load repetitions. This indicates that the rate of permanent axial strain accumulation is not linear with the level of stress applied but it increases at a much steeper rate.

Similar trend can be observed at higher confining stresses. However, as confinement increases the 'critical' strength level beyond which the axial strain increases at a high rate, becomes larger.

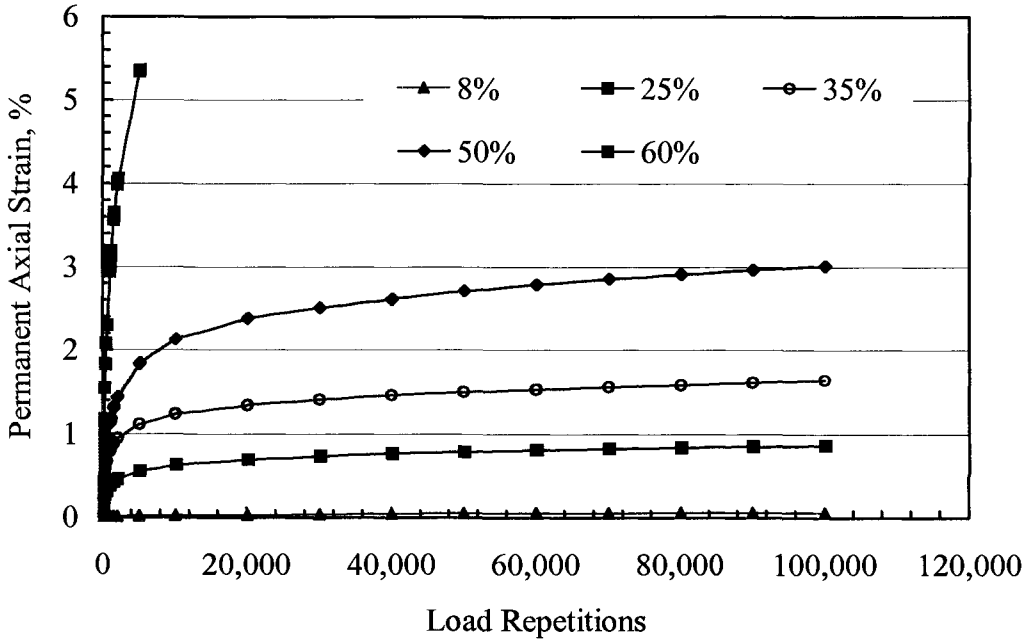

Figure 4.45: Permanent Axial Strain Build-up under RS Loading at σ_3 = 35kPa.

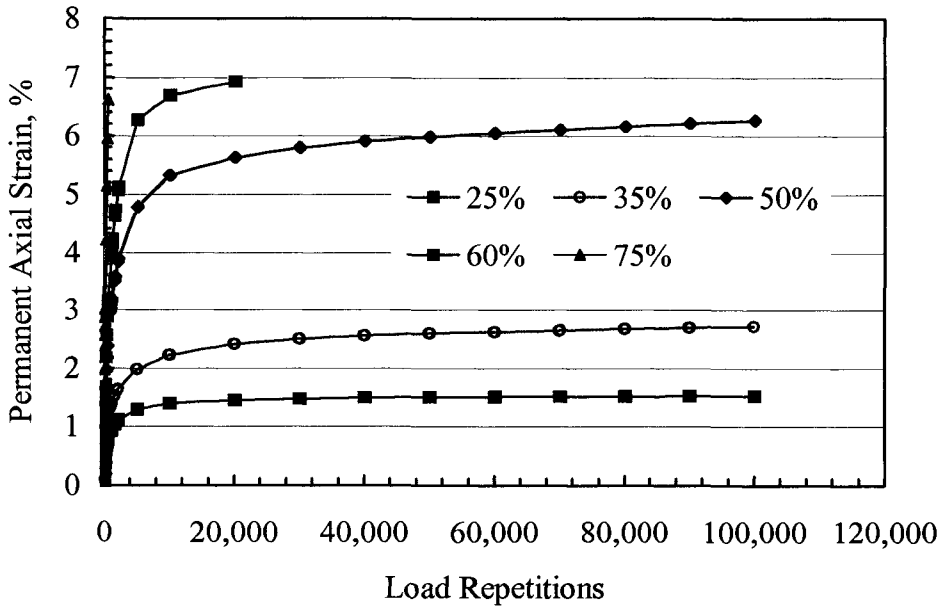

Figure 4.46: Permanent Axial Strain Build-up under RS Loading at σ_3 = 70 kPa

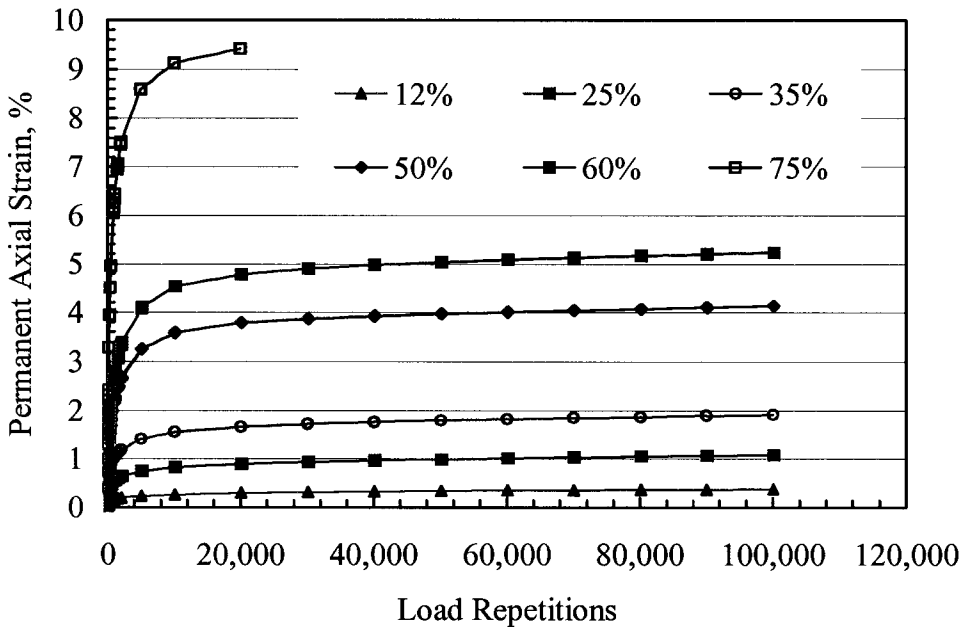

Figure 4.47: Permanent Axial Strain Build-up under RS Loading at σ_3 = 100 kPa

In order to better visualize the development of permanent axial strain and its dependence on the level of stress, a different way of presenting the collected data is here suggested, whereby the measured axial strain is plotted versus strength level used for different number of load repetitions. Figure 4.48 shows that the granular material undergoes different stages of deformation when subjected to increasing levels of stress. Up to 35% strength level, densification increases at a constant rate. Between 35% and 50% strength level, minimal densification is observed and after a stress level of 50%, the rate of densification increases at a high rate.

This general trend can be also identified for tests conducted at higher confining pressure as shown in Figure 4.49. However, the critical values of strength level causing different trends of densification are higher. They seem to be 50% and 60% respectively.

The cyclic stress tests were conducted at 100 kPa confinement, as mentioned previously, and were tested at 6.4%, 7.7%, 9.0%, 9.6% and 10.9% strength levels

(corresponding to stress levels, σ_d/σ_3, of 50%, 60%, 70%, 75% and 85%). Each specimen was subjected to 100,000 cyclic stress load repetitions or until the capacity of the testing equipment was achieved (usually, the circumferential strain gage capacity).

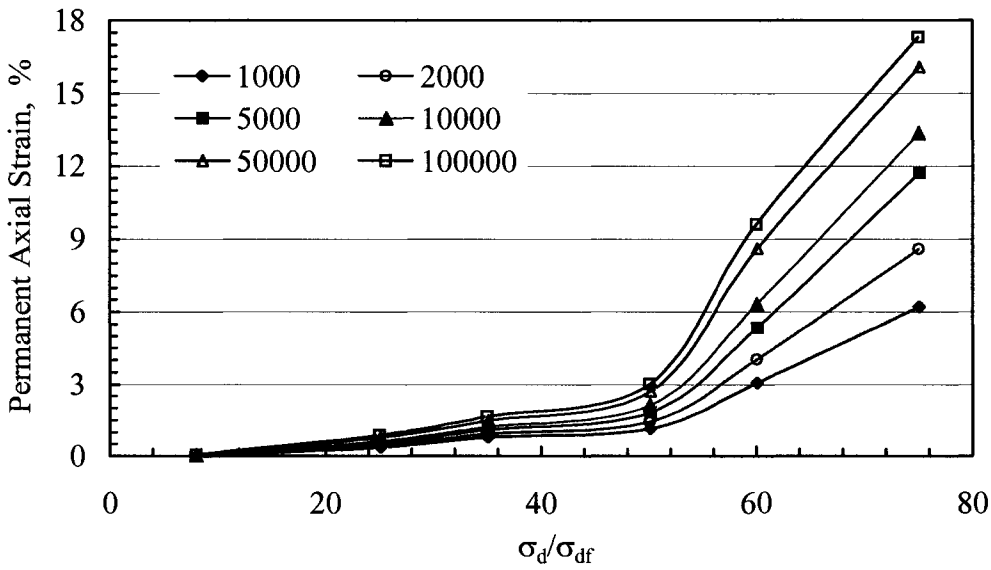

Figure 4.48: Permanent Axial Strain Variation with Strength Level at σ_3 = 35 kPa and RS Loading.

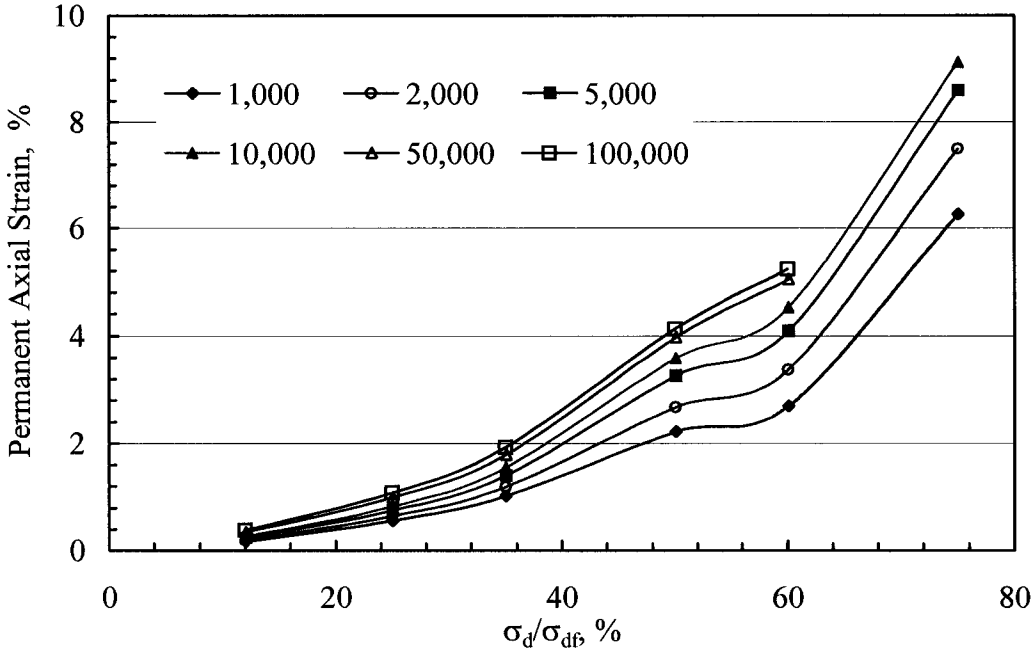

Figure 4.49: Permanent Axial Strain Variation with Strength Level at σ_3 =100 kPa and RS Loading.

The permanent axial strain (ε_l^p), in this case, is accumulated a little differently than in the case of repeated loading. Regardless of the level of stress applied, the specimen initially undergoes some extension before densification takes place. The amount of extension is the same for all stress levels used but higher stress levels need fewer load repetitions before densification sets in (Figure 4.50). Once densification starts, the general shape of the curve is quite similar to RS loading curve except that after a certain stress level (9.0%), the accumulated axial strain does not increase substantially with increase in stress level. This indicates that the sample has achieved maximum density.

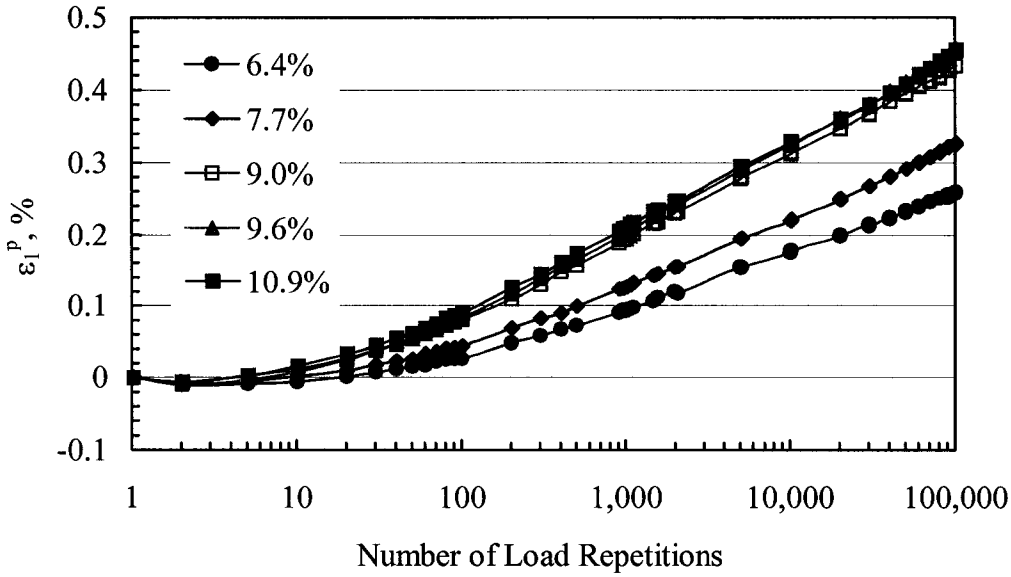

Figure 4.50: Permanent Axial Strain Variation with Number of Load Repetitions at Different Strength Levels (CS Loading).

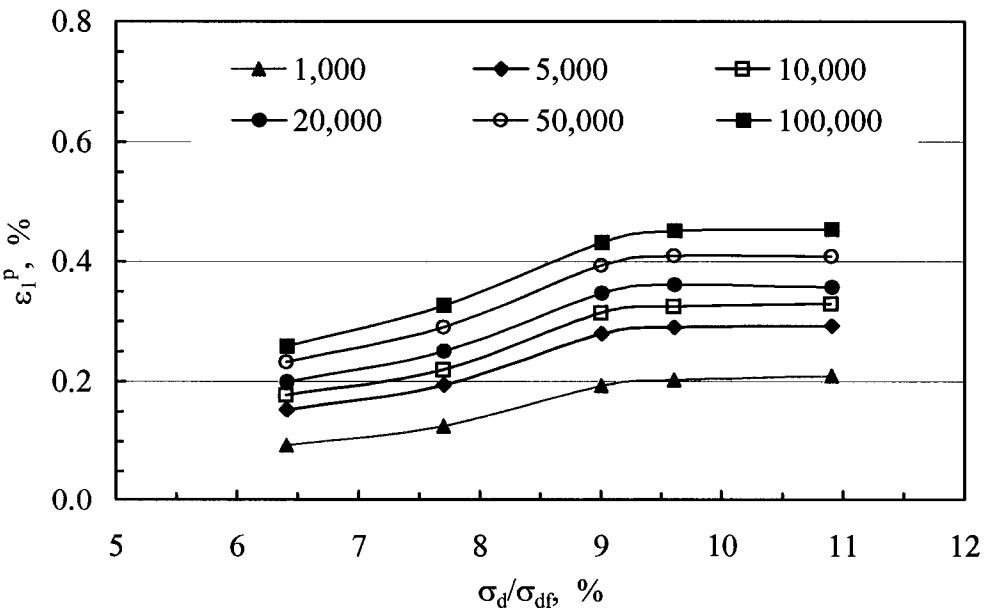

Figure 4.51: Permanent Axial Strain Variation with Strength Level at σ_3 =100 kPa (CS Loading).

Still, the different phases of densification, seen with the RS loading, can be observed when axial strain is plotted versus strength level (Figure 4.51). Densification increases with strength level at a steady rate for strength levels up to 9.0%, afterwards, consolidation of the material seems to level off. The third phase observed in the RS case is missing, because strength levels higher than 10.9% were not used. Even if we assume that RS and CS loading result in similar densification trends (for entirely different values of strength level), the amount of densification observed in each case is different. RS consistently yields higher permanent axial values than CS tests. This fact might seem at first peculiar but can be explained if radial deformation of the specimens is examined.

- Radial Strain

The permanent radial strains accumulated (ε_3^p) differ radically between samples subjected to repeated stress loading and those subjected to cyclic stress loading.

For specimens tested with repeated stress loading, negative radial permanent strains (dilation) were recorded for all strength levels used, except for tests at 100-kPa confinement. In this case, low strength level tests (25% or less) resulted in limited densification of the specimen in radial direction (positive radial strains), whereas samples subjected to higher strength levels (35% or higher) underwent dilative permanent radial strains. The amount of dilation increased with the number of repeated stresses applied (Figure 4.52) and also with strength level (Figure 4.53) for all confining pressures.

As for specimens subjected to cyclic stress, the accumulated radial permanent strain (ε_3^p) was positive (densification) for all stress levels used. The amount of radial densification increased with number of load applications at a decreasing rate (Figure 4.54). Radial densification of the material increased with stress level up to a strength level of 9.6 %, then decreased slightly after (Figure 4.55).

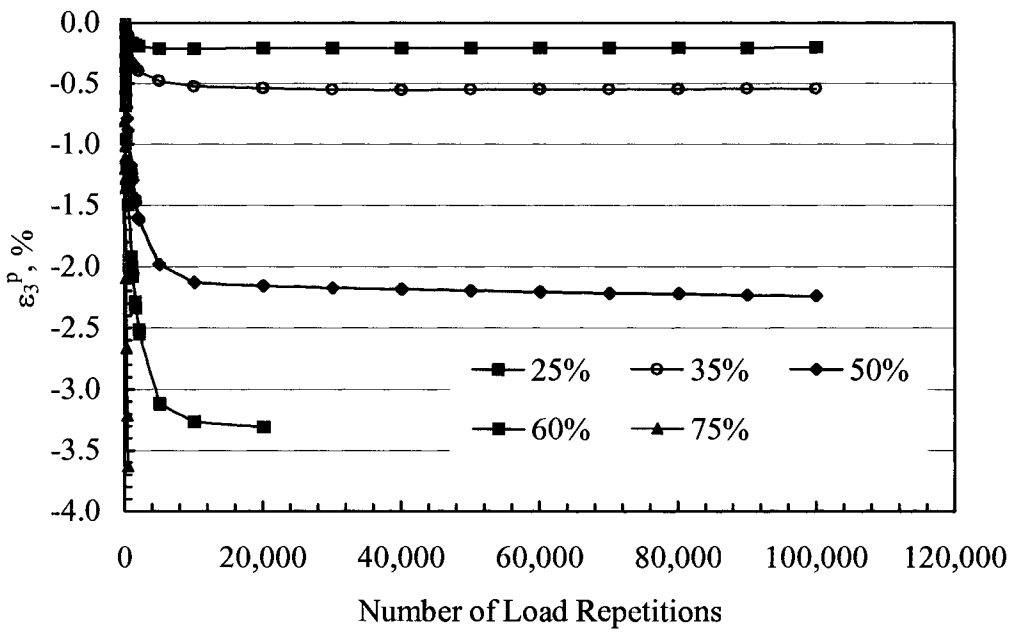

Figure 4.52: ε_3^p Variation with Number of RS Load Repetitions at Different Strength Levels (σ_3 = 35 kPa).

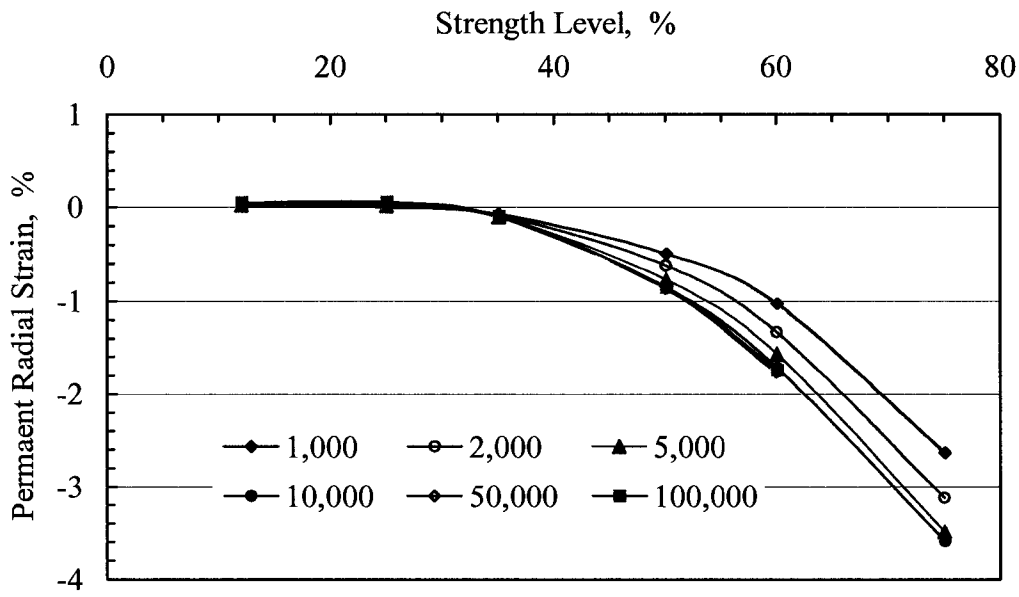

Figure 4.53: Permanent Radial Strain Variation with Strength Level at σ_3 = 35 kPa (RS Loading).

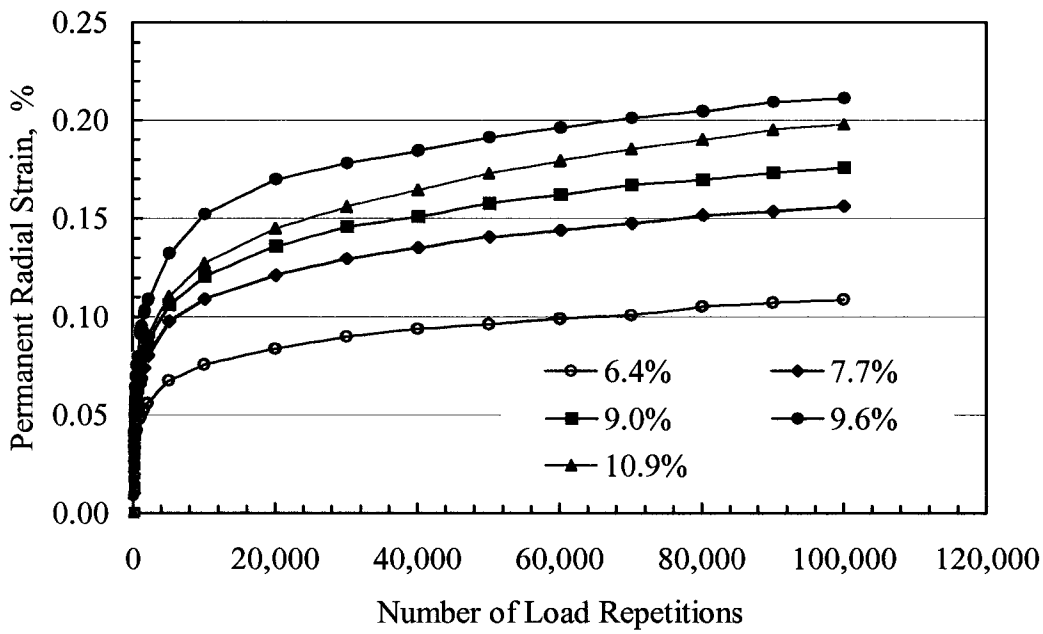

Figure 4.54: Permanent Radial Strain Variation with Cyclic Stress Load Repetitions at σ_3 =100 kPa.

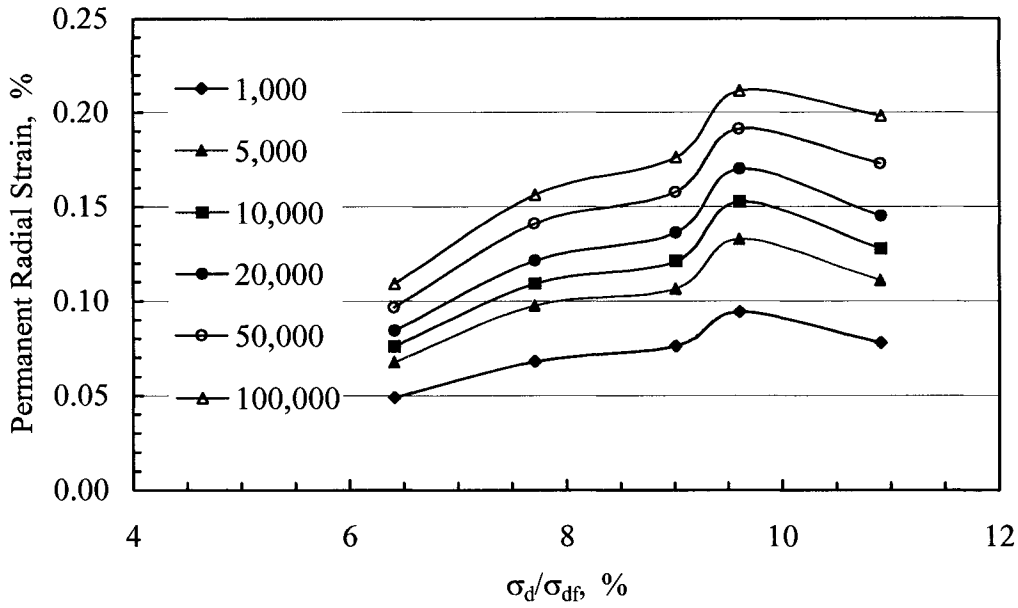

Figure 4.55: Permanent Radial Strain Variation with Cyclic Strength Level at σ_3 = 100 kPa.

- Volumetric Strain

Examining the volumetric strains developed during a test can help visualize the overall deformation of specimens under a certain loading condition.

For specimens subjected to repeated stress loading, the accumulation of permanent volumetric strain, ε_v^p, with load repetitions varies depending on the strength level used. For low strength level, ε_v^p increases with number of repetitions at decreasing rate. After a certain critical value of strength level, the variation of accumulated volumetric strain becomes more complex. For clearer picture of this variation, ε_v^p is plotted versus the log of the number of load applications in Figure 4.56. Similar results were obtained for specimens tested under higher confining pressures.

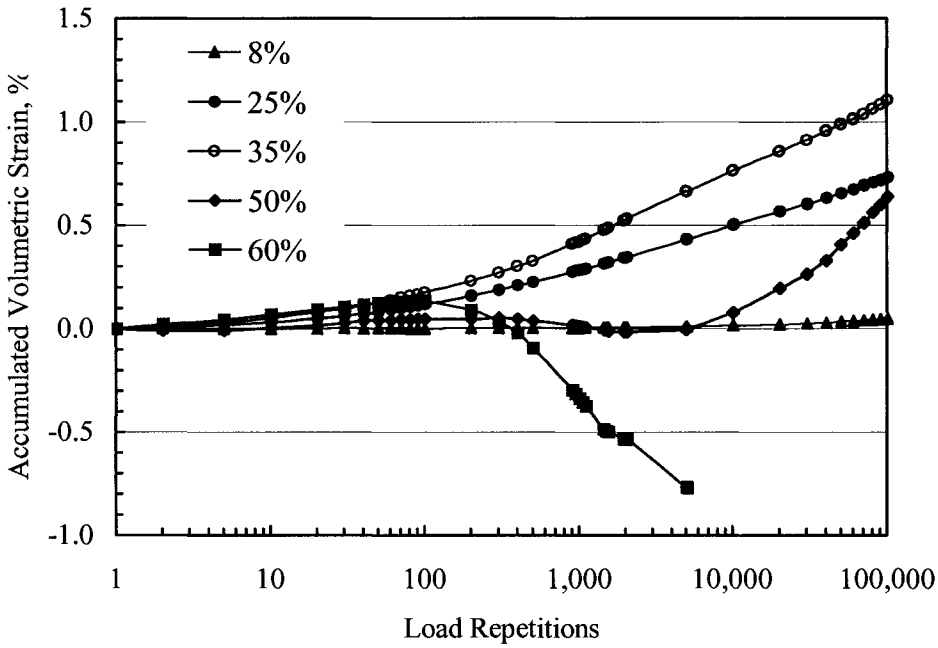

Figure 4.56: ε_v^p Variation with RS Load Repetitions at σ_3 =35 kPa

The amount of accumulated ε_v^p is very much dependent on the strength level applied during a triaxial test. Examining Figure 4.57, we notice different stages of volumetric strain accumulation. These stages occur regardless of the number of load repetitions applied. At first, ε_v^p increases with strength level to a maximum value (for a given number of load repetitions) then it decreases with increasing strength levels until it becomes negative. Datta et al. (1980) reported similar findings from tests done on dense calcareous sand. It is important to note that even though specimens subjected to strength levels beyond 35% exhibit dilation tendencies (Figure 4.57), the static shear strength of these specimens still increases as shown in Figure 4.58.

Tests performed at higher confining stresses yielded comparable results. The optimum strength level (resulting in maximum ε_v^p value) increased with increasing confining stresses (Figures 4.59 and 4.60).

It is worthwhile mentioning that tests conducted at a confinement of 100 kPa differed slightly in that after the optimum strength level (50%) was achieved, ε_v^p dropped to a minimum positive value then increased with increasing strength level. This behavior was observed for all three duplicate samples tested and can be attributed to the attrition of aggregates due to the high pressures used which changes the gradation and the aggregate matrix of the sample resulting in a different material behavior.

Even though the strength level used in cyclic stress tests was much lower compared to repeated stress tests, the accumulated volumetric strains measured exhibited comparable trends when plotted versus the strength level used. ε_v^p increased with the strength level until reaching distinctively a maximum value, then after, it tended to decrease at a lower rate (Figure 4.61). Unfortunately, due to experimental restraints, we were not able to determine values of ε_v^p associated with higher strength levels.

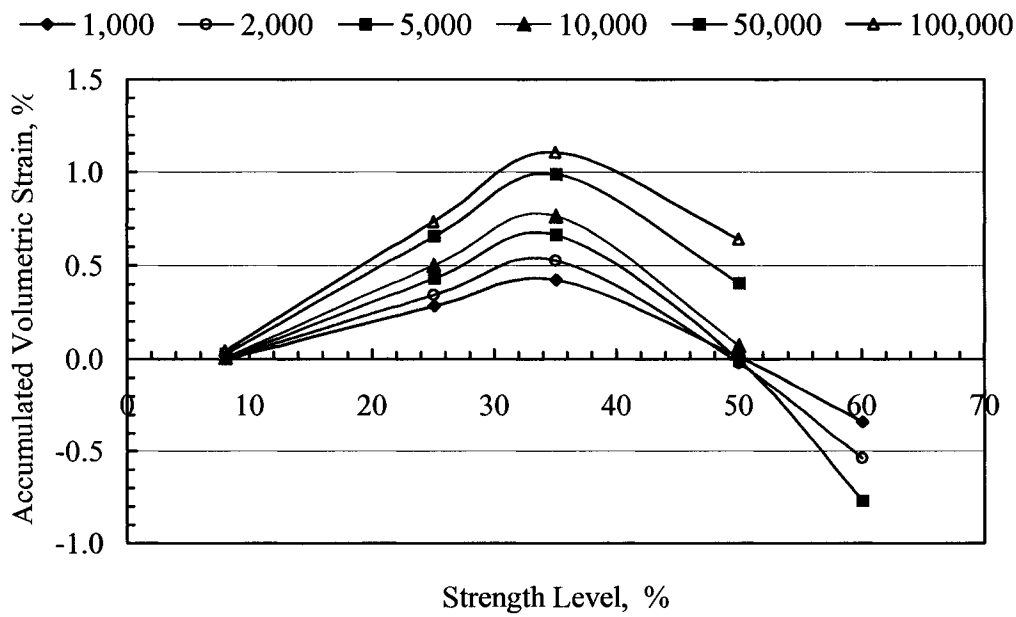

Figure 4.57: ε_v^p Variation with RS Strength Level at 35 kPa Confinement.

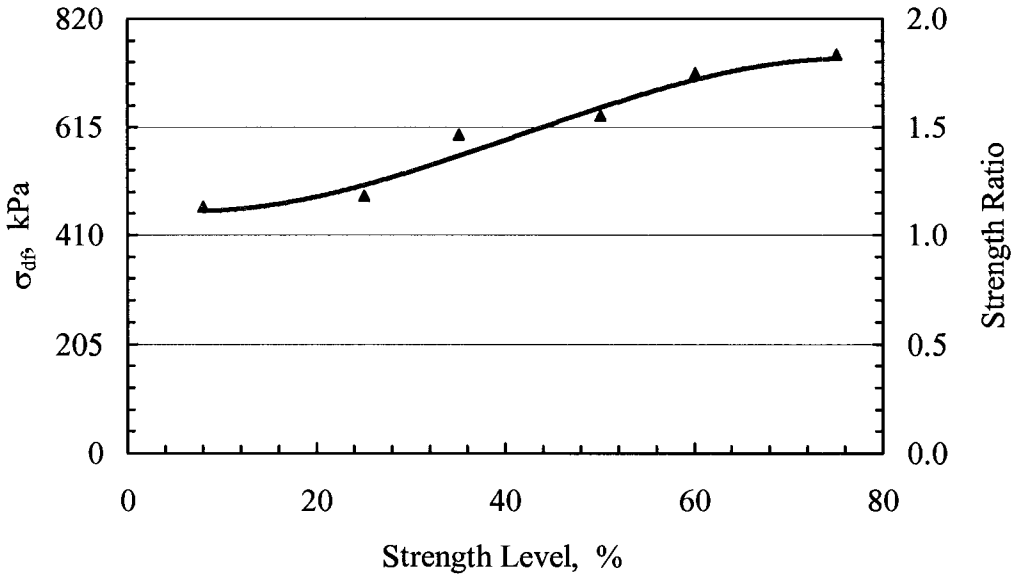

Figure 4.58: Strength Level Effect on Static Shear Strength Ratio at σ_3 =35 kPa (RS Case).

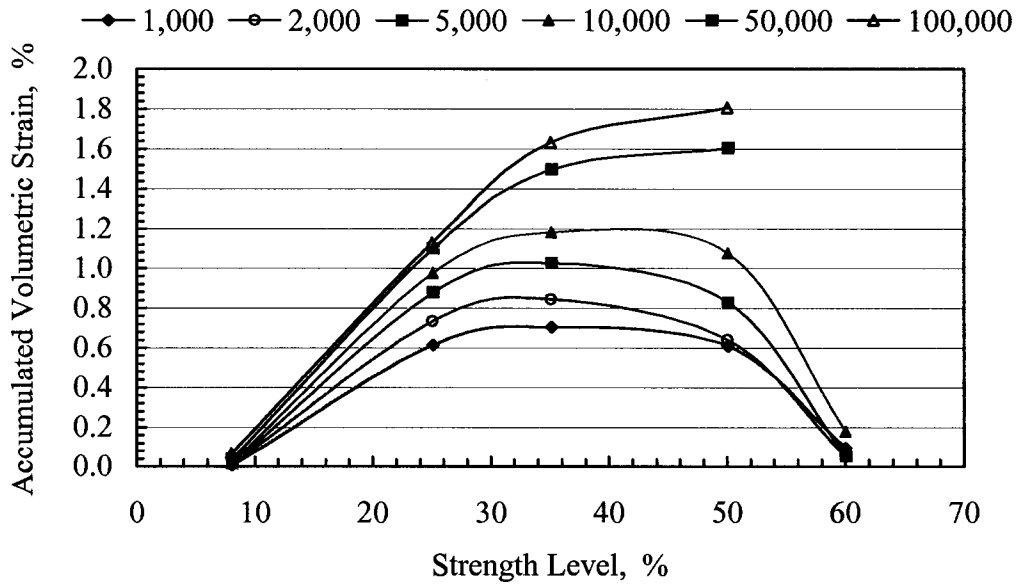

Figure 4.59: ε_v^p Variation with RS Strength Level at 70 kPa Confinement

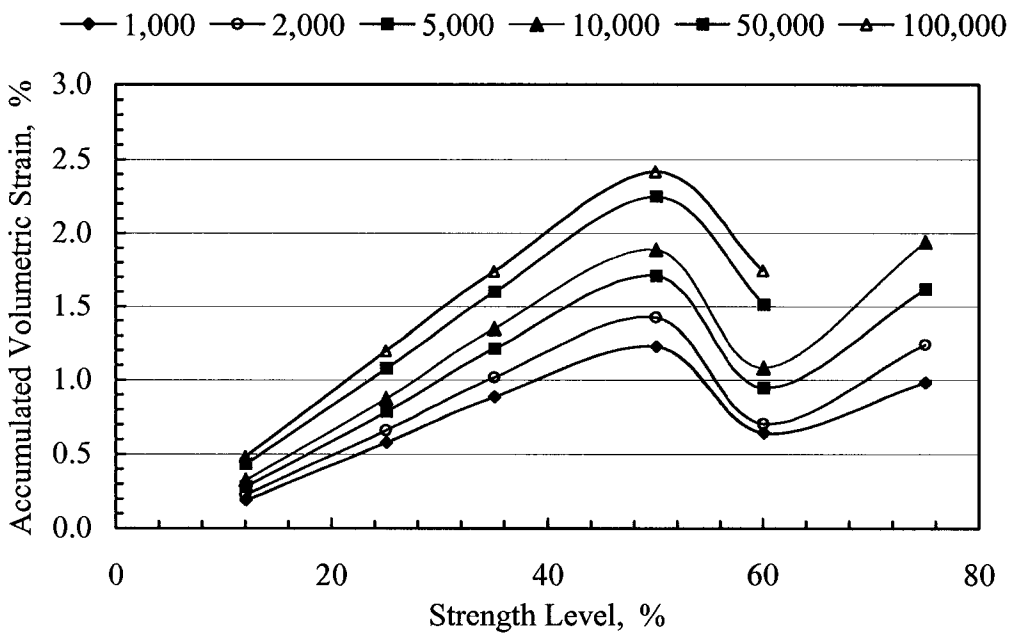

Figure 4.60: ε_v^p Variation with RS Strength Level at 100 kPa Confinement

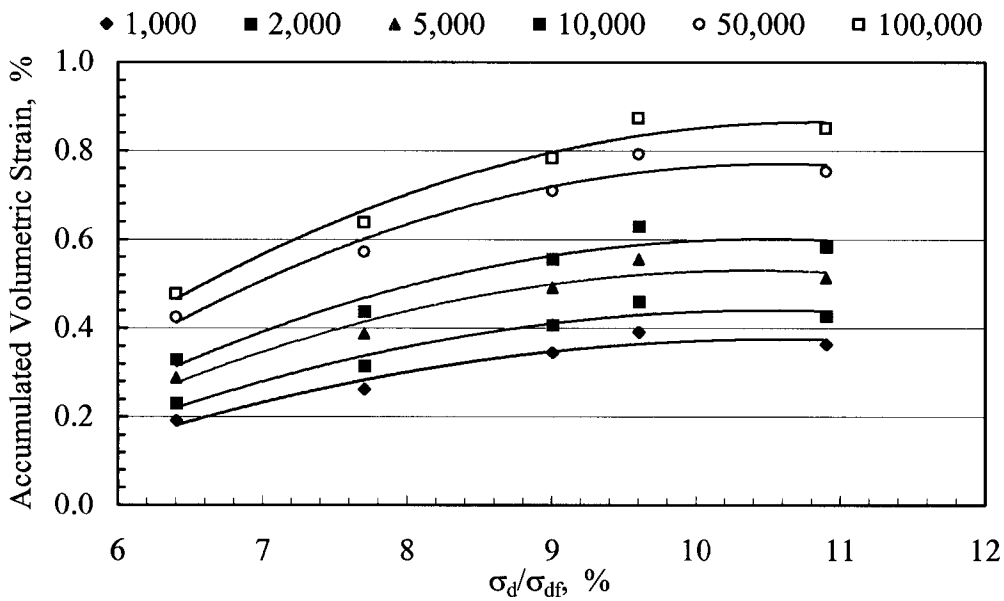

Figure 4.61: ε_v^p Variation with CS Strength Level at 100 kPa Confinement

- Poisson's Ratio

Another way to represent the relative radial and axial deformation of a specimen subjected to a given stress state can be achieved by looking at the Poisson's ratio, ν_p, which by definition is the ratio of radial to axial strain of a material:

$$\nu_p = \frac{\varepsilon_r^p}{\varepsilon_a^p} \tag{4.5}$$

Where: ε_r^p is the accumulated radial strain, and,

ε_a^p is the accumulated axial strain.

For the case of samples subjected to repeated stress loading, regardless of the confining pressure applied, the Poisson's ratio at first decreases with increasing strength level until a certain minimum value is reached and thereafter, ν_p increases with strength level to values equal or just exceeding 0.5. As mentioned earlier in Chapter Two, values of Poisson's ratio for granular materials can exceed 0.5 since the medium that we are dealing with (granular) is not continuous. Remarkably, the minimum Poisson's ratio is reached at a strength level of around 30% for all confining pressures tested (Figures 4.62, 4.63, and 4.64).

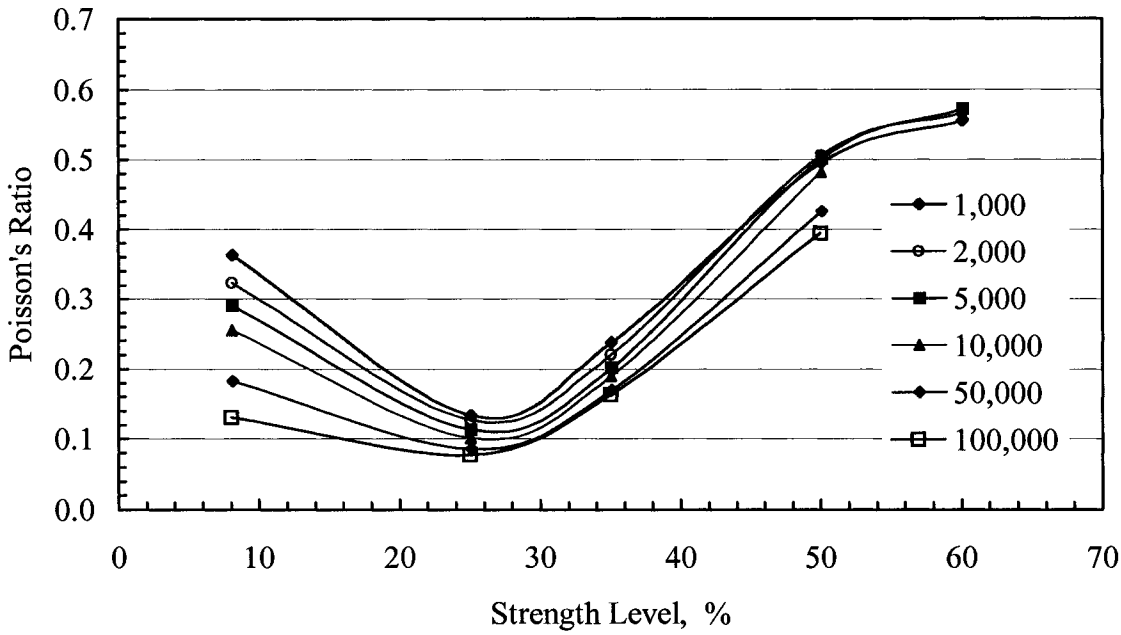

Figure 4.62: ν_p Variation with RS Strength Level at 35 kPa Confinement

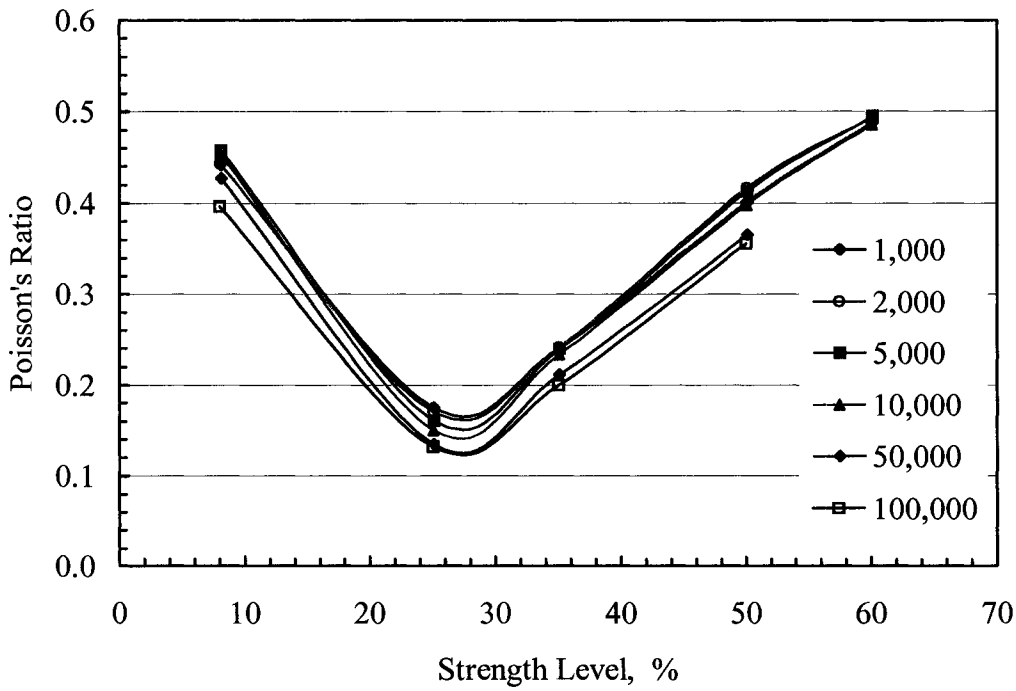

Figure 4.63: ν_p Variation with RS Strength Level at 70 kPa Confinement

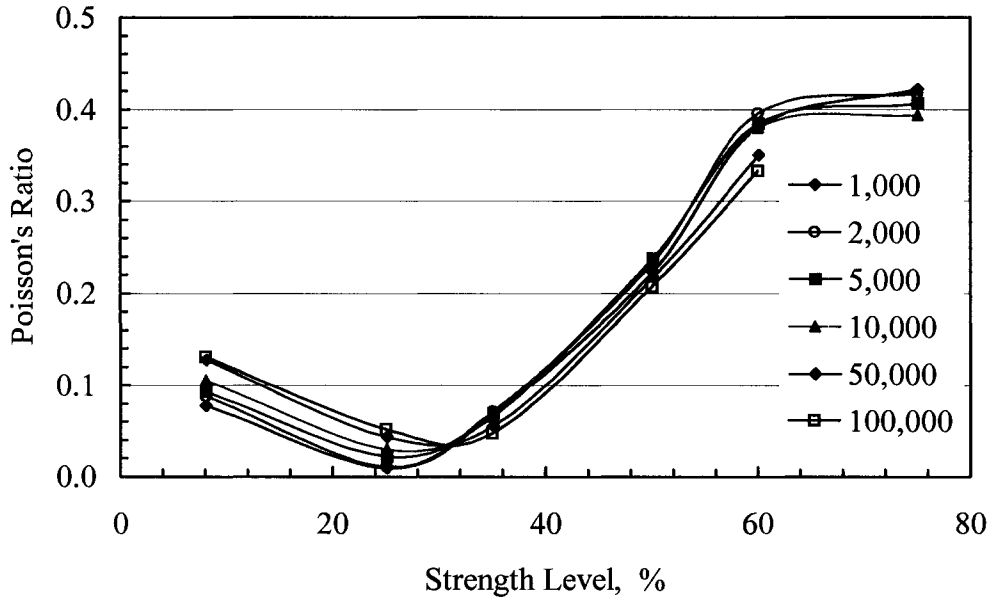

Figure 4.64: ν_p Variation with RS Strength Level at 100 kPa Confinement

As for the specimens tested using cyclic stress loading, the range of variation of Poisson's ratio with strength level was much smaller compared to the RS loading case. ν_p in this case varied between 0.4 and 0.5 as shown in Figure 4.65 below. A "critical" minimum value is reached at a strength level of 9%, after which ν_p increases for a short while before it decreases again.

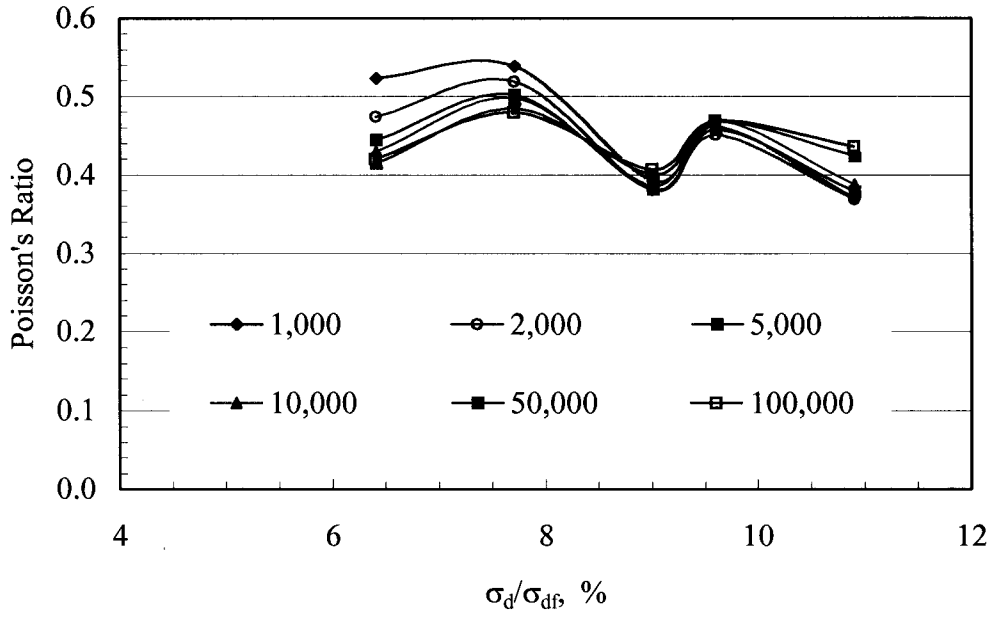

Figure 4.65: ν_p Variation with CS Strength Level at 100 kPa Confinement

4.4.4 Moduli

The variation of material characteristics and behavior during a laboratory test can be studied by looking at different moduli that are basically defined in terms of stresses applied and strains induced during the test. In pavement analysis, researchers are interested mostly in monitoring the variation of total modulus, resilient modulus, resilient shear modulus and total shear modulus of the material tested. These parameters were defined earlier in this chapter for each type of loading used in this research. The following paragraphs will address the variation of these moduli with type of loading and strength level used.

4.4.4.1 Effect of Type of Loading

The resilient modulus is an important parameter for pavement design purposes. This parameter is still widely used by pavement engineers to design a pavement section on the basis that all deformations that take place are elastic in nature. Repeated and cyclic loading tests conducted at two different confining pressures (35 kPa and 100 kPa) using same initial induced stress level ($\sigma_d/\sigma_3 = 0.8$) reveal that while RS loading does not affect the resilient modulus (M_R) of the tested soil, CS loading causes M_R values to increase with repetitions. This increase is more evident at the lower confining pressure (Figure 4.66). This phenomenon is expected since CS loading results in denser specimens (as the number of load repetitions increases) that have higher resilient moduli. It should be noted that the resilient modulus attributed to CS in Figure 4.66 is the 'loading resilient modulus' as defined in section 3.3.3.

Figure 4.67 depicts the variation of the resilient shear modulus (G_R) of the material with number of load application for both types of loading, RS and CS. Same observations made for resilient modulus can also be made here for G_R. Since for a given level of stress, cyclic loading causes more densification than repeated loading, the resilient shear modulus in the CS loading case increases with number of load applications. Here also, the 'loading resilient shear modulus', $G_R = \tau_{dl}/\gamma_r$, is used for CS to compare with resilient shear modulus of RS loading case.

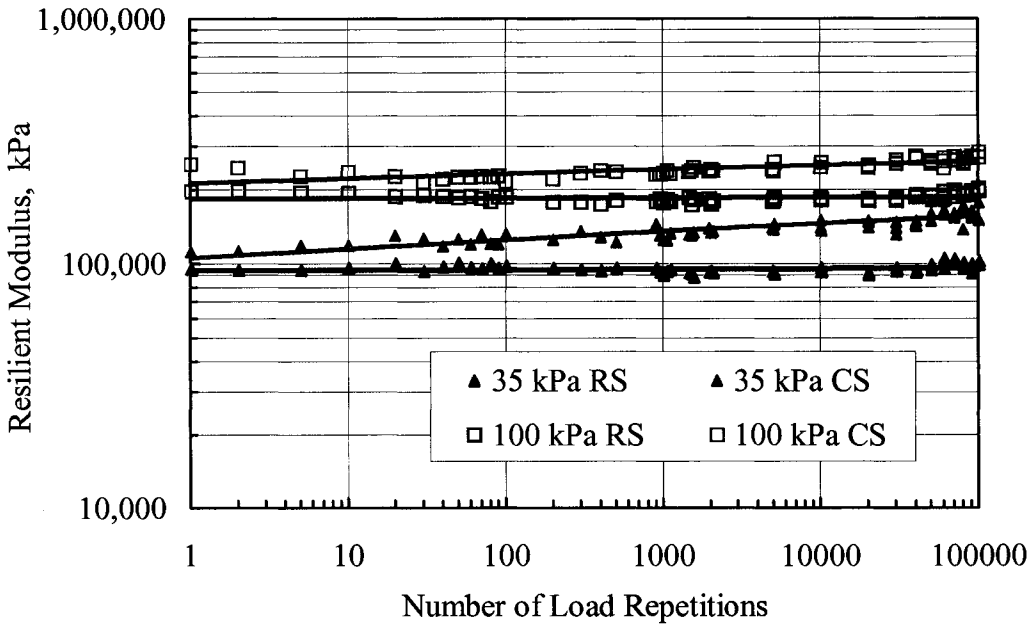

Figure 4.66: M_R Variation with RS and CS Loading at 35 kPa and 100 kPa Confinement.

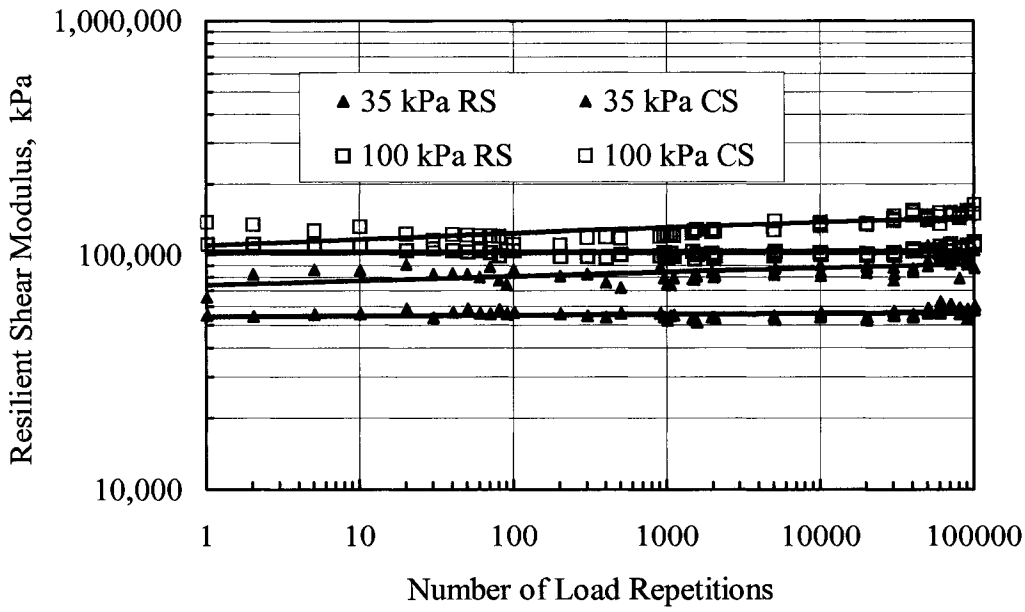

Figure 4.67: G_R Variation with RS and CS Loading at 35 kPa and 100 kPa Confinement

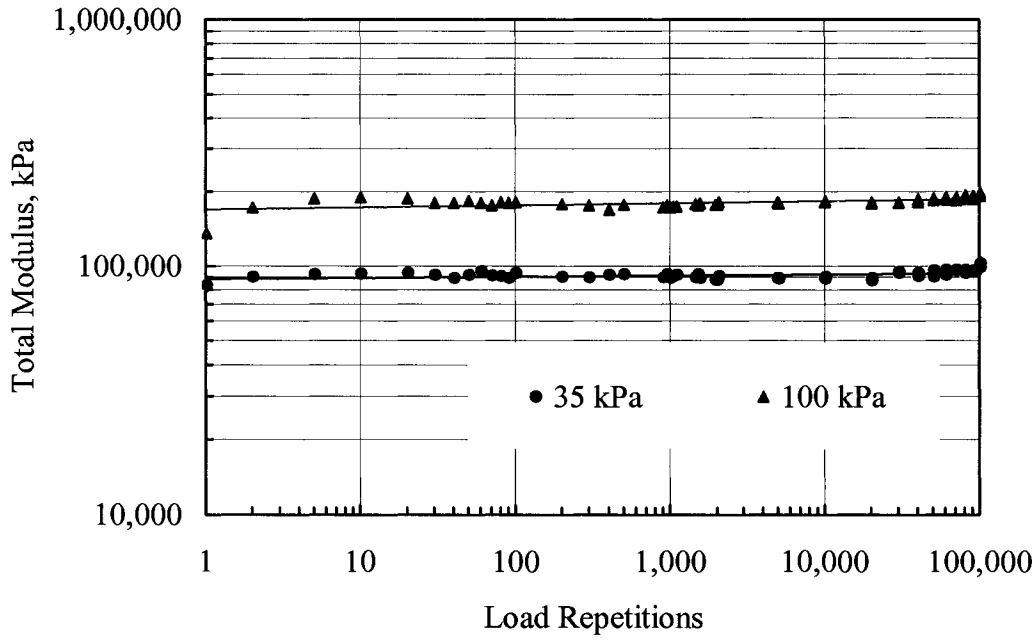

Figure 4.68: M_T Variation with RS Loading at 35 kPa and 100 kPa Confinement

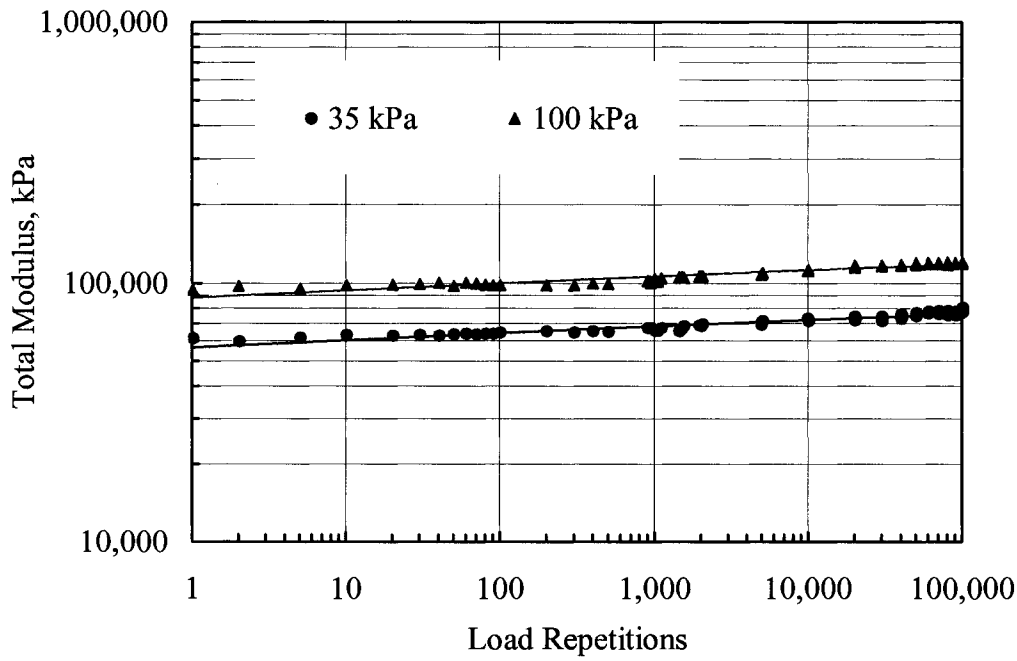

Figure 4.69: M_T Variation with CS Loading at 35 kPa and 100 kPa Confinement

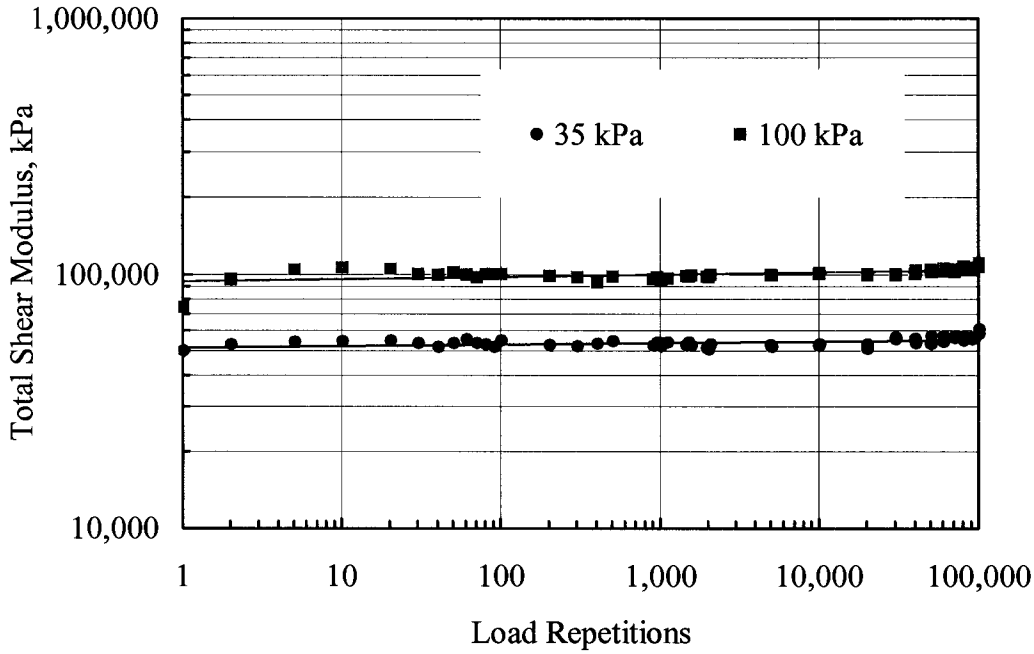

Figure 4.70: G_T Variation with RS Loading at 35 kPa and 100 kPa Confinement

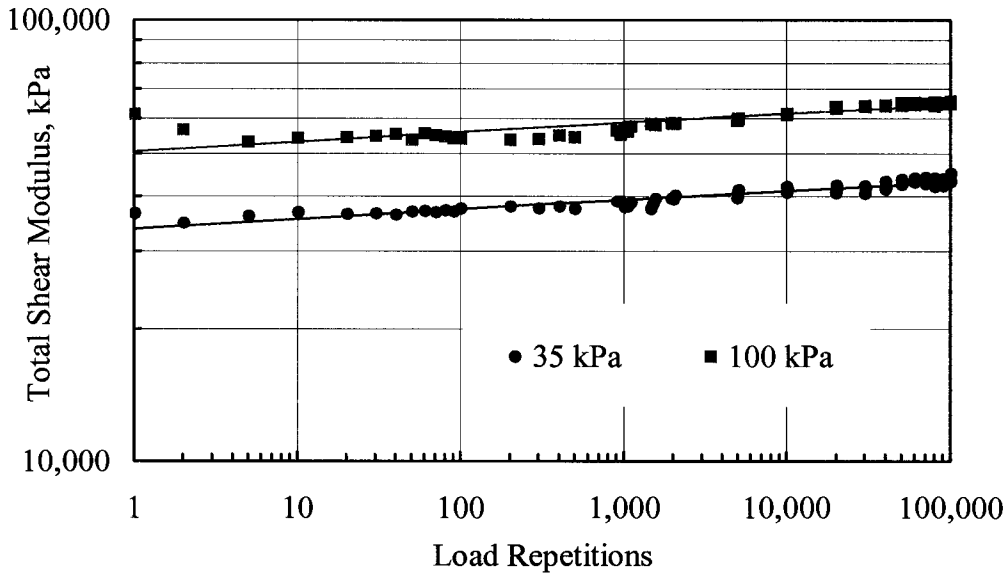

Figure 4.71: G_T Variation with CS Loading at 35 kPa and 100 kPa Confinement

The total modulus (M_T) of the granular material did not change in the RS loading case (Figure 4.67), however, in the CS loading case, M_T increased with number of load repetitions (Figure 4.69). In both cases, higher confinement yielded higher values of total modulus. The same observations can be made for the case of total shear modulus (G_T) as shown in Figures 4.70 and 4.71.

4.4.4.2 Effect of Strength Level

The effect of strength level on the various moduli is substantially different between specimens subjected to repeated loading and those subjected to cyclic loading.

For specimens tested under RS loading, the resilient modulus (M_R) and total modulus (M_T) exhibited same variation with strength level. As the strength level increased, M_R and M_T increased gradually to a maximum then decreased slightly with further increase in strength level (Figures 4.72 and 4.73). The strength level effect seems to be very important on both M_R and M_T values. For tests under 35 kPa confinement, a strength level increase from 8% to 50% resulted in an increase of 52% to 71% in resilient modulus values, whereas for the same conditions, the total modulus increased by 39% to 65% depending on the number of load repetitions.

The same type of pattern is observed for higher confining pressures with more radical increase in both M_R and M_T. A strength level increase from 12% to 60% caused the resilient modulus to increase by 158% to 180%, and at the same time, the total modulus increased by 159% to 200% for specimens under 100 kPa confinement (Figures 4.74 and 4.75). Furthermore, it can be noticed that in the case of higher confining stresses, and for a given strength level, as the number of load applications increases, the resilient and total moduli increase at decreasing rates. This is due to the densification of the material under repeated dynamic loading.

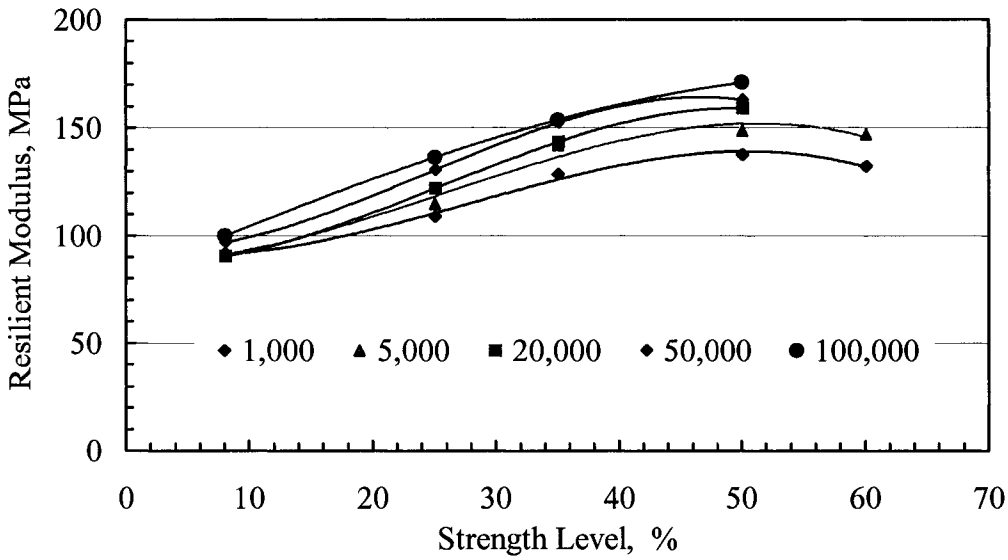

Figure 4.72: M_R Variation with Strength Level under RS Loading at σ_3 = 35 kPa.

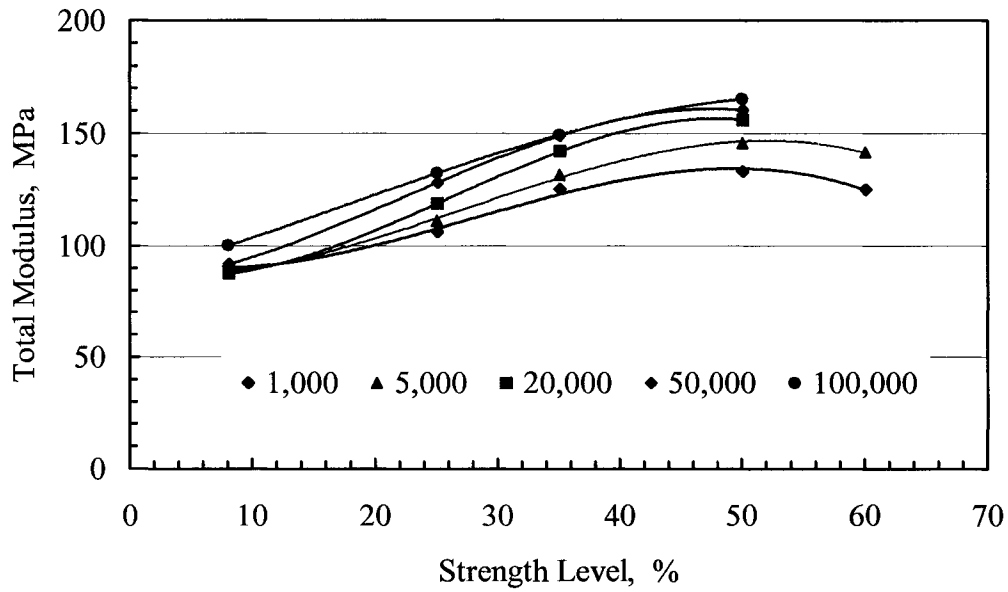

Figure 4.73: M_T Variation with Strength Level under RS Loading at σ_3 = 35 kPa

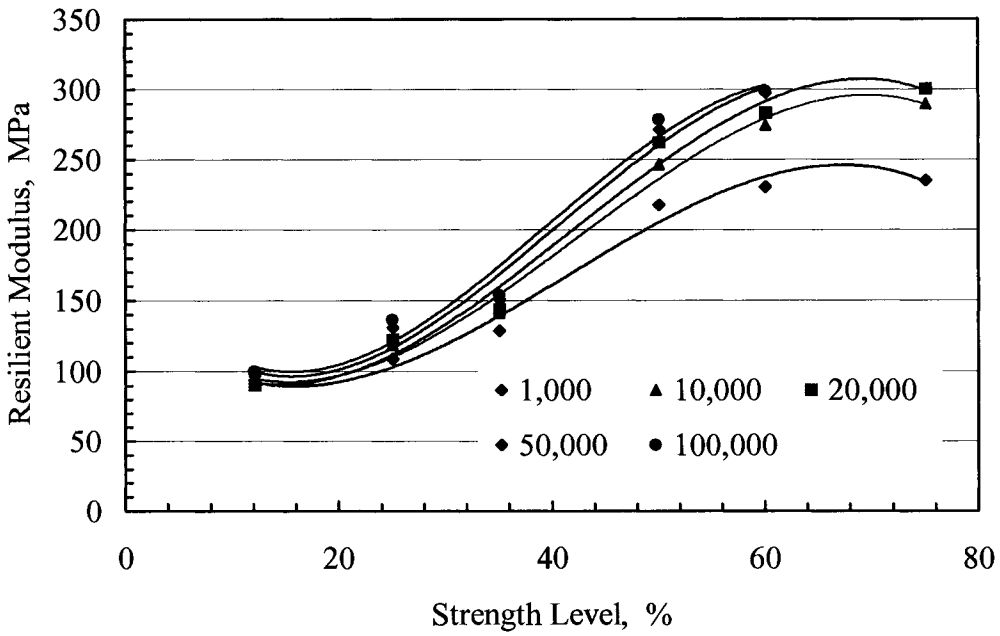

Figure 4.74: M_R Variation with Strength Level under RS Loading at σ_3 =100 kPa

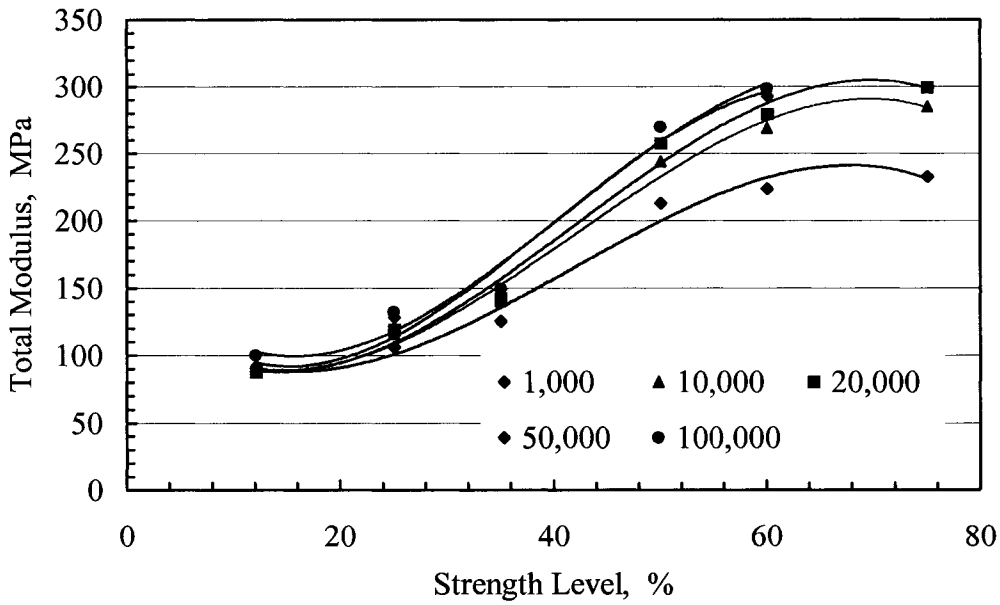

Figure 4.75: M_T Variation with Strength Level under RS Loading at σ_3 = 100 kPa

In the case of the total shear modulus (G_T) and the resilient shear modulus (G_R), as repeated load is applied, these parameters tend to increase at a steady rate with strength level up to a certain value for all confining stresses used in this research. Beyond this, two categorically different behaviors were observed. For low and intermediate confinements (35 kPa and 70 kPa), G_T and G_R increase at a higher rate (Figures 4.76 and 4.77) where as for high confinement (100 kPa), these parameters decrease with increasing strength level as shown in Figures 4.78 and 4.79.

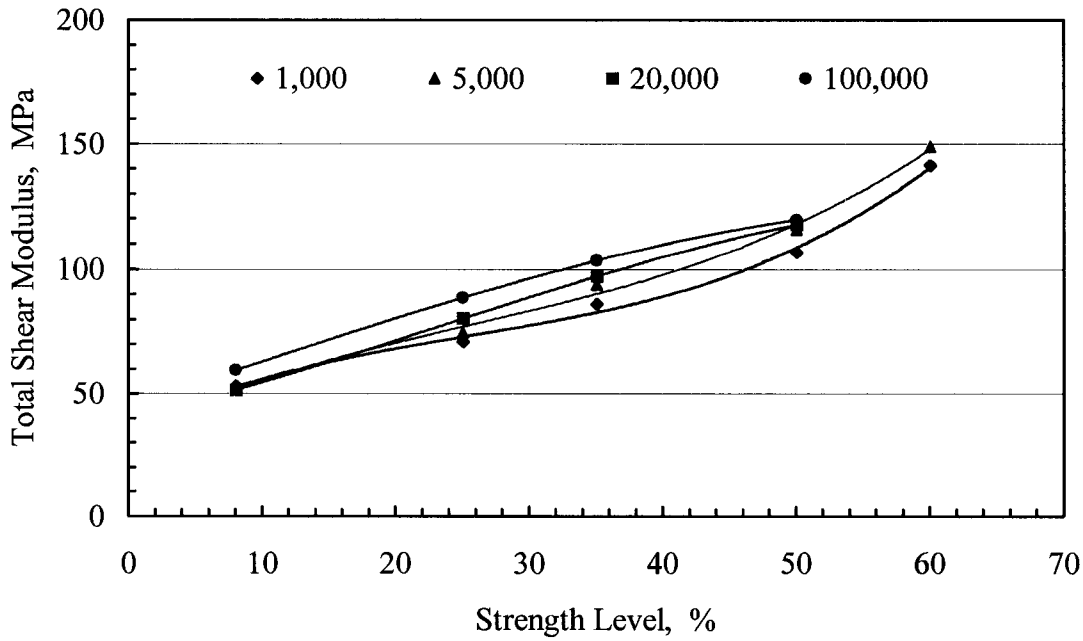

Figure 4.76: G_T Variation with Strength Level under RS Loading at σ_3 = 35 kPa

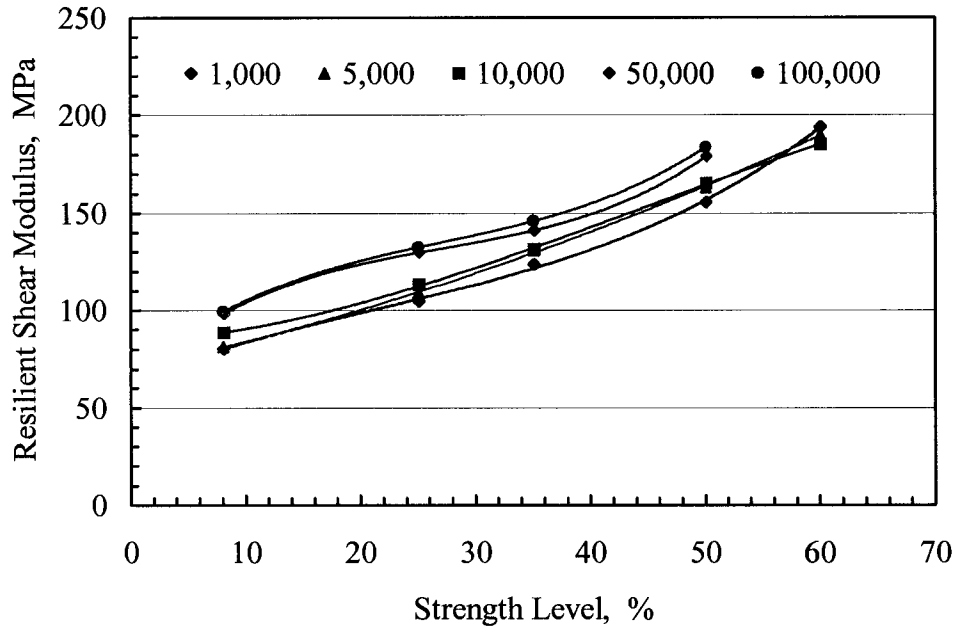

Figure 4.77: G_R Variation with Strength Level under RS Loading at σ_3 = 70 kPa

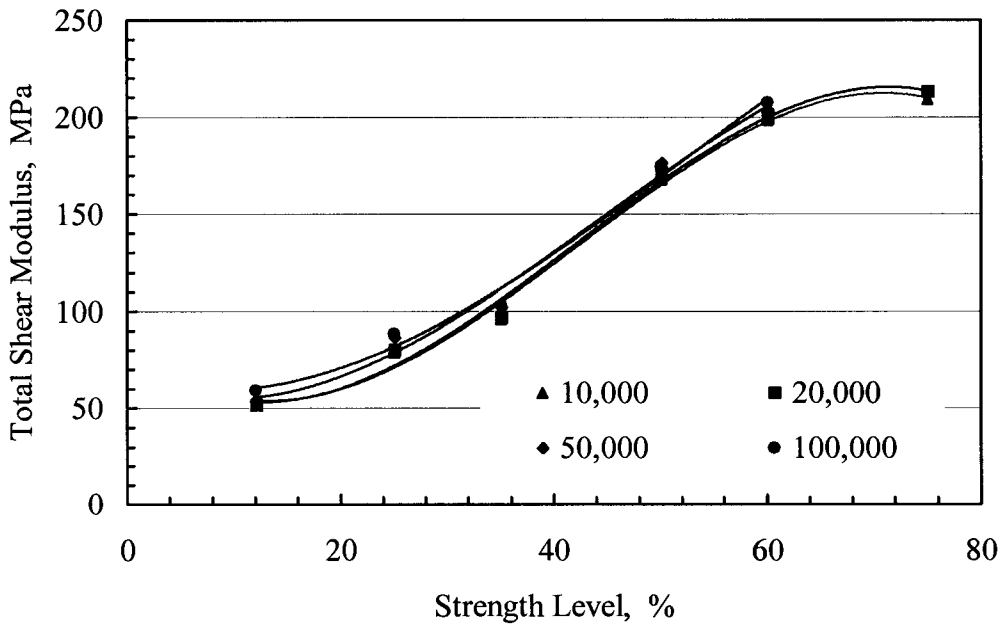

Figure 4.78: G_T Variation with Strength Level under RS Loading at σ_3 = 100 kPa

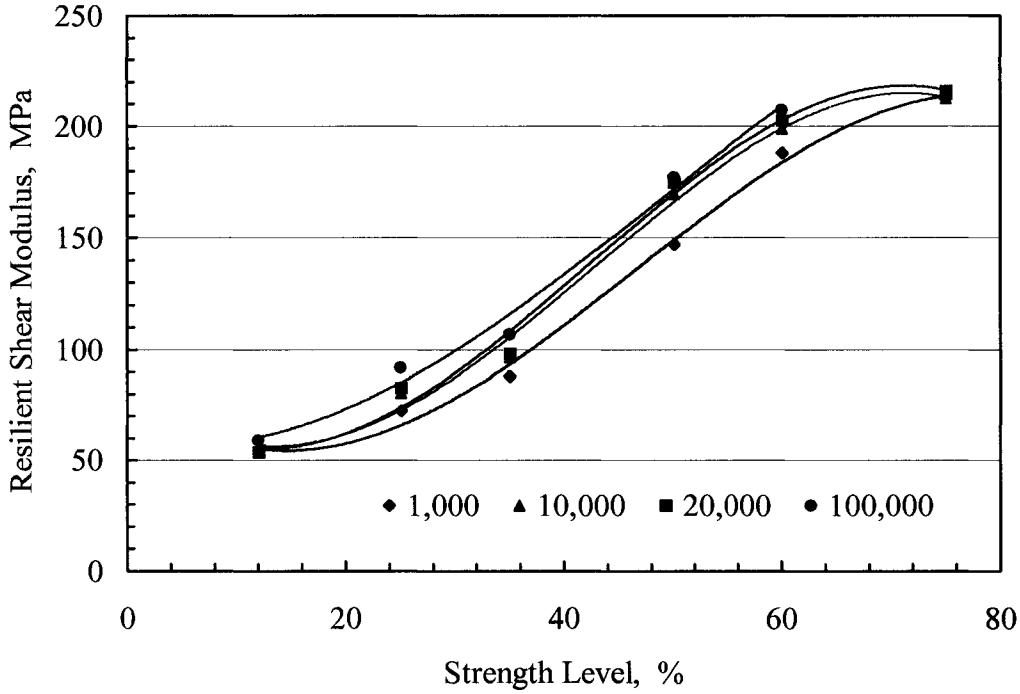

Figure 4.79: G_R Variation with Strength Level under RS Loading at σ_3 = 100 kPa

Specimens subjected to cyclic loading exhibited totally different behavior than those subjected to repeated loading. The resilient modulus, the total modulus, the total shear modulus and loading resilient shear modulus (G_R) did not seem to vary significantly with strength level and they seem only dependent on the number of load repetitions applied (Figures 4.80, 4.81, 4.82, and 4.83).

These conclusions, regarding CS loading case, can only be drawn for the sole confinement pressure (100 kPa) used in this research. Further investigation is needed to confirm the current observations.

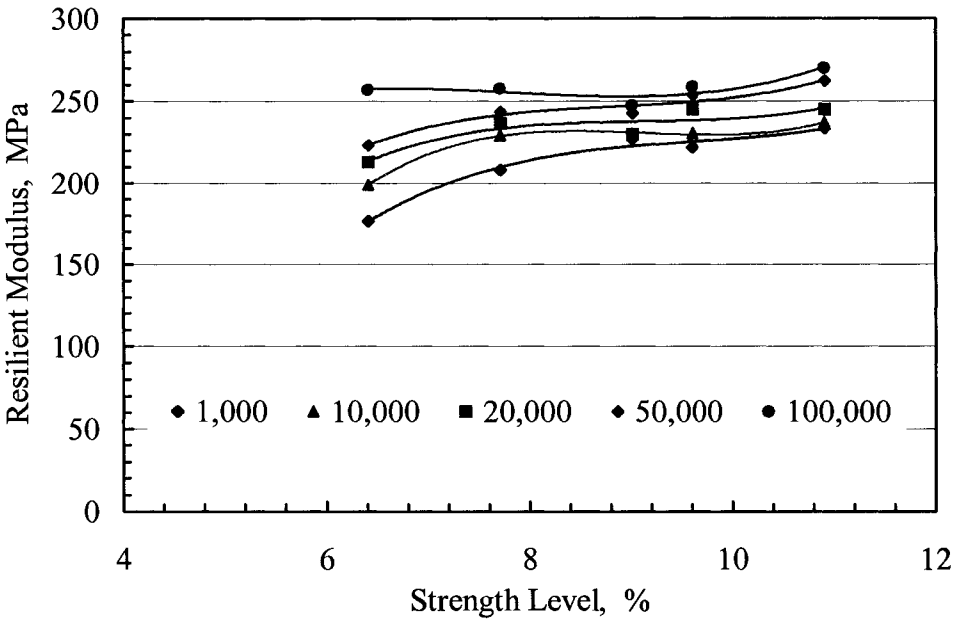

Figure 4.80: M_R Variation with Strength Level under CS Loading at σ_3 = 100 kPa

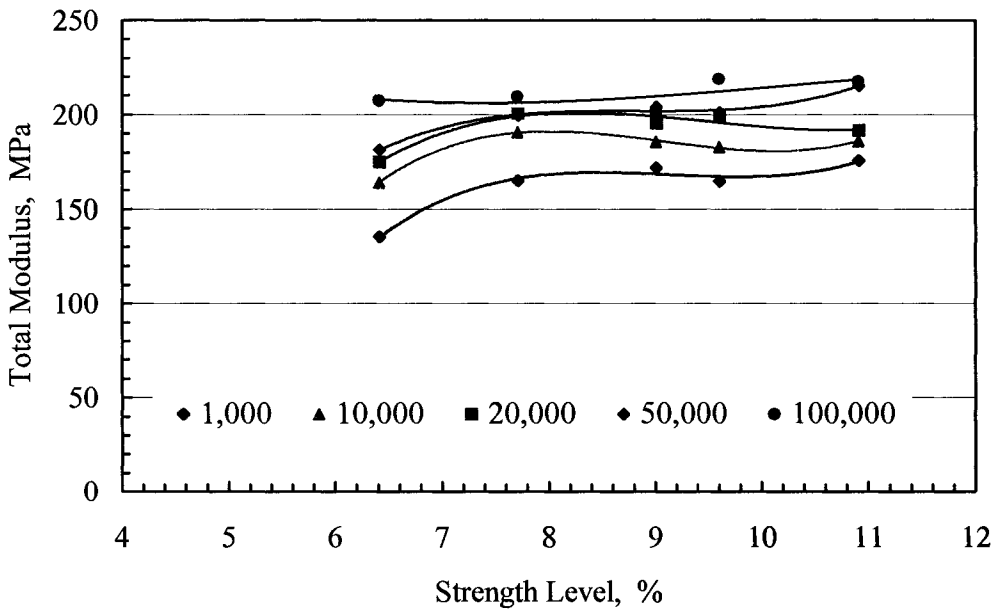

Figure 4.81: M_T Variation with Strength Level under CS Loading at σ_3 = 100 kPa

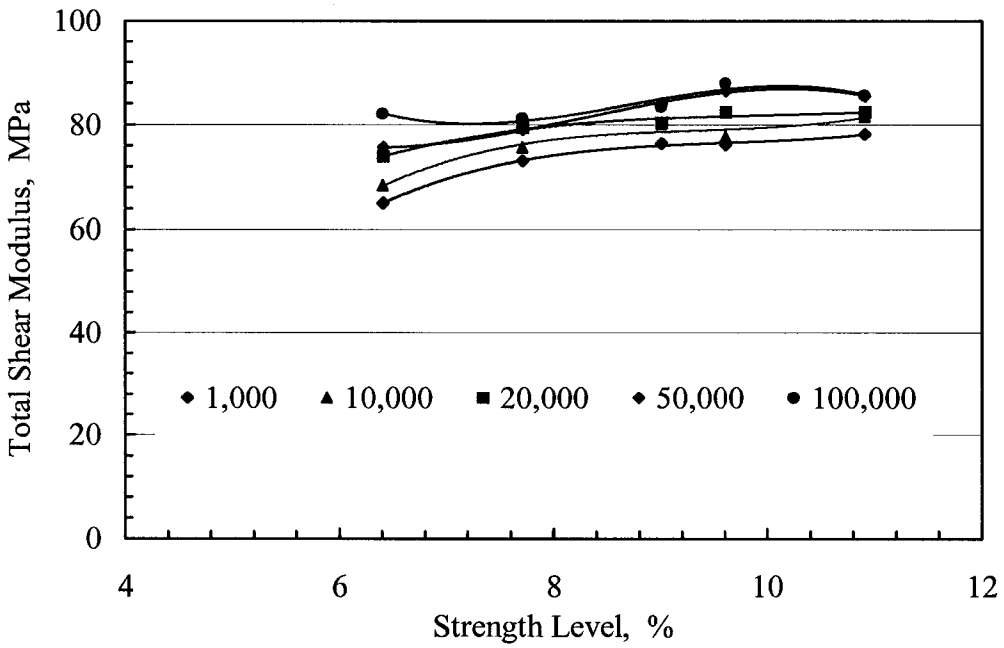

Figure 4.82: G_T Variation with Strength Level under CS Loading at σ_3 = 100 kPa

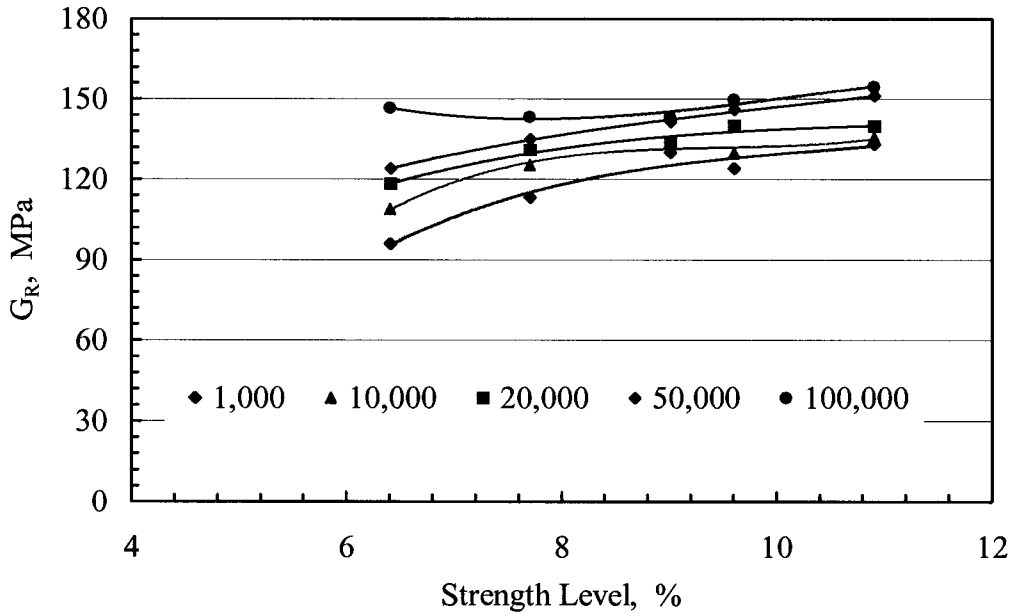

Figure 4.83: G_R Variation with Strength Level under CS Loading at σ_3 = 100 kPa

4.4.5 Damping Ratio

Damping in soils is the energy lost during a complete cycle of applied shear stresses (Seed and Idriss 1970, Hardin and Drnevich 1972). The energy loss is equal to the area enclosed by the cyclic shear stress - shear strain loop. The damping ratio reflects the damping characteristics of a soil and could be used for dynamic response analysis of pavements. With reference to Figure 4.84, the damping ratio, D, for the repeated stress loading case is given by:

$$D = \frac{1}{\pi} \cdot \frac{Area\ of\ loop\ ABCD}{Area\ of\ AEF} \tag{4.6}$$

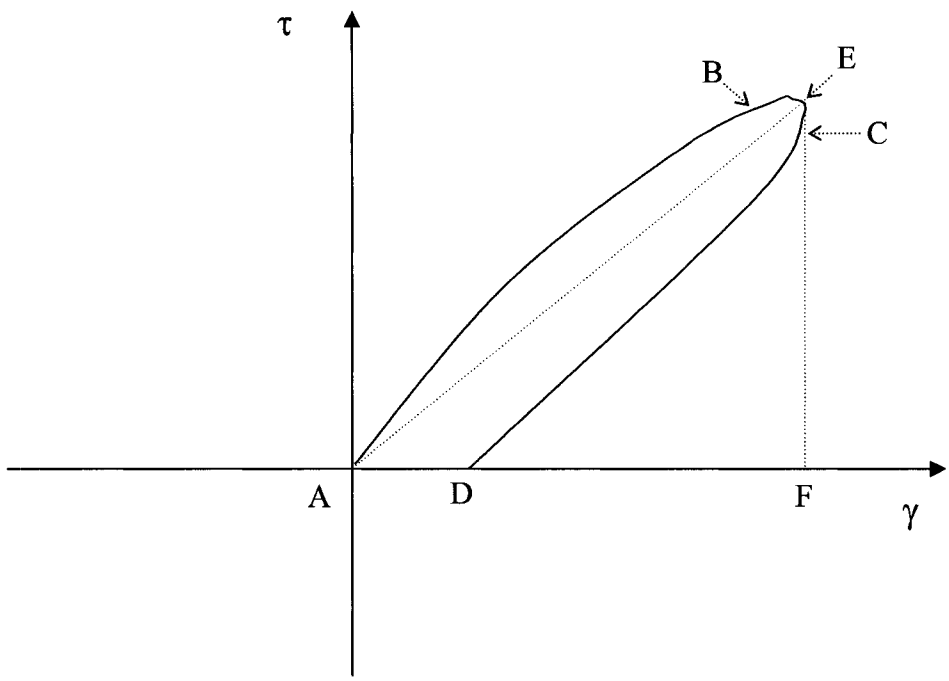

Figure 4.84: Damping Ratio Definition for Repeated Stress Loading Case.

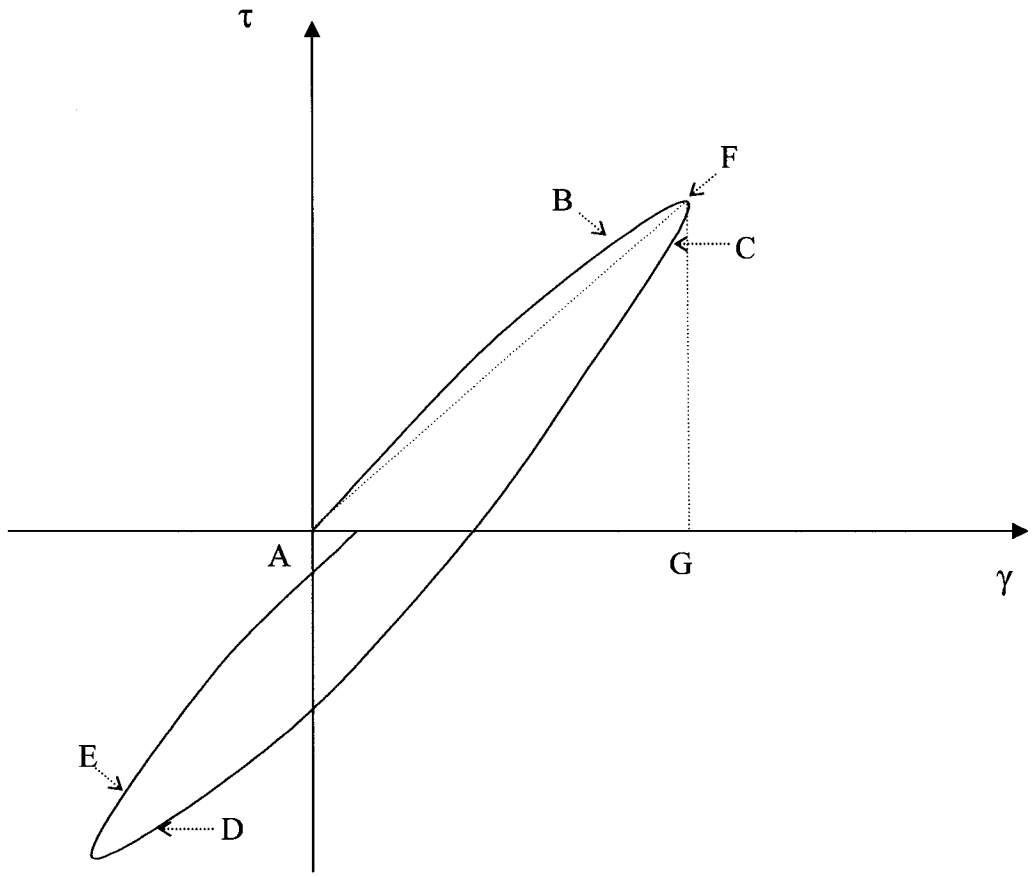

Figure 4.85: Damping Ratio Definition for Cyclic Stress Loading Case.

As for the cyclic stress loading case (Figure 4.85), the damping ratio is given by:

$$D = \frac{1}{\pi} \cdot \frac{Area\ of\ loop\ ABCDE}{2 \times Area\ of\ AFG} \qquad (4.7)$$

4.4.5.1 Effect of Repetitive Loading

The damping ratio decreases with load repetitions as the shear stress-shear strain loop decreases in size. However, the level of damping differs depending on the loading pattern used. Damping ratio values measured under cyclic stress loading are, on the average, three times higher than those measured using repeated stress loading (Figure 4.86).

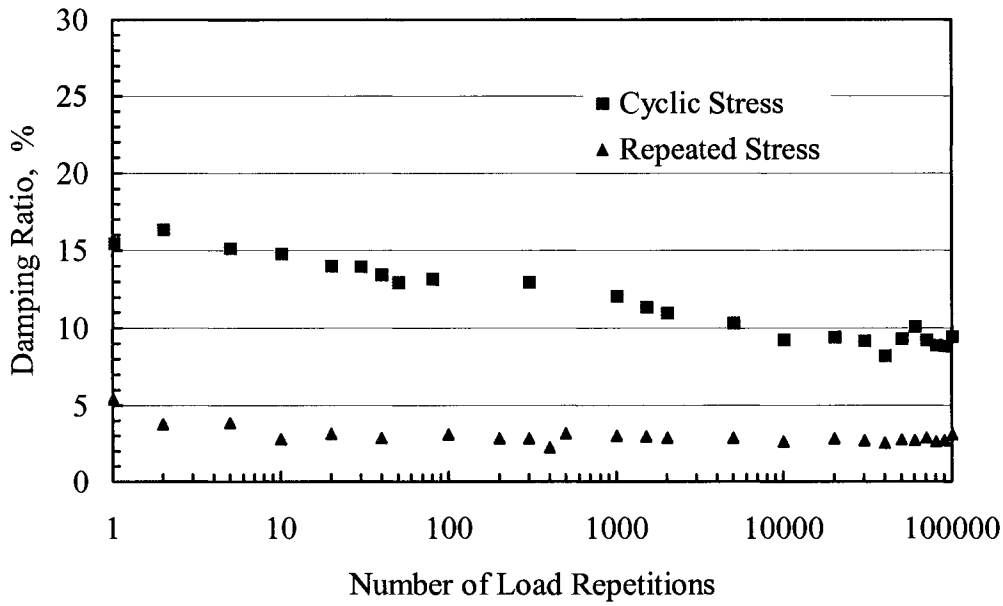

Figure 4.86: Damping Ratio Variation with Number of Load Repetitions at σ_3 = 35 kPa

For specimens tested under repeated stress loading, the decrease of the damping ratio is at relatively low rate regardless of the confining pressure used. At low confinement (35 kPa), the damping ratio decreases from 5% (after first load repetitions) to around 2.5% (after 100,000 load applications), whereas, for same confining stress, the damping ratio of specimens tested under cyclic stress conditions, decreased from around 16% to about 9% for the equal number of load applications.

The same overall behavior is also observed for tests conducted at higher confining pressures (Figure 4.87).

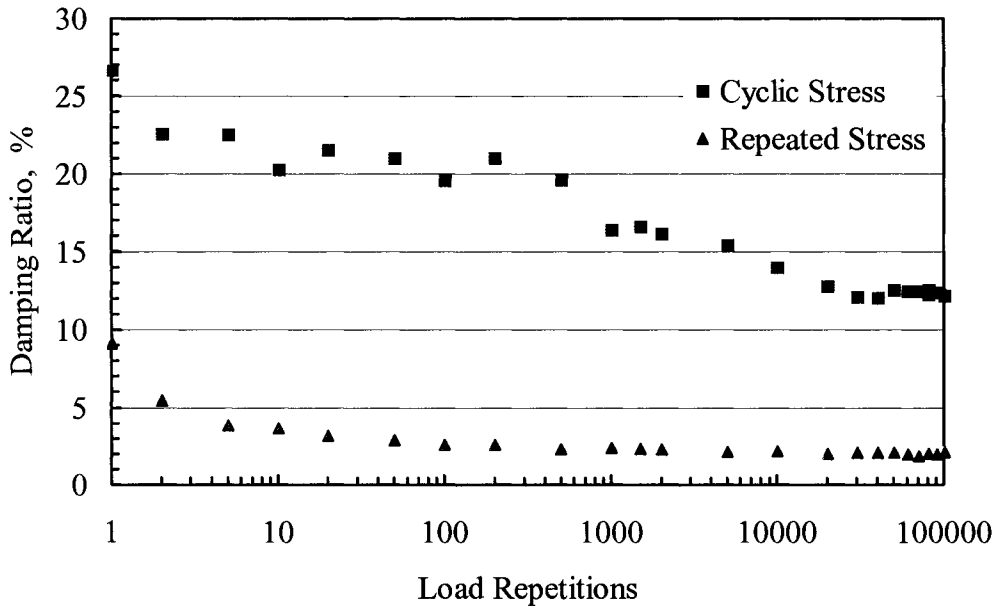

Figure 4.87: Damping Ratio Variation with Number of Load Repetitions at σ_3 = 100 kPa

4.4.5.2 Effect of Strength Level

The strength level seems to have no substantial effect on damping ratio neither for the repeated stress case nor for the cyclic stress loading case.

For specimens subjected to repeated stress loading, higher strength levels have higher initial damping ratios. As the number of load repetition increases, damping ratio resulting from different strength levels converge to a relatively unique value (Figure 4.88). In the case of cyclic stress loading, the damping ratio variation with number of load repetitions of different strength levels used, collapse into one single curve which decreases at a constant rate when number of repetitions are plotted in logarithmic scale (Figure 4.89); this compares, in the case of repeated loading, to a

curve that declines initially sharply and afterwards levels off after 100 load repetitions regardless of the confinement used.

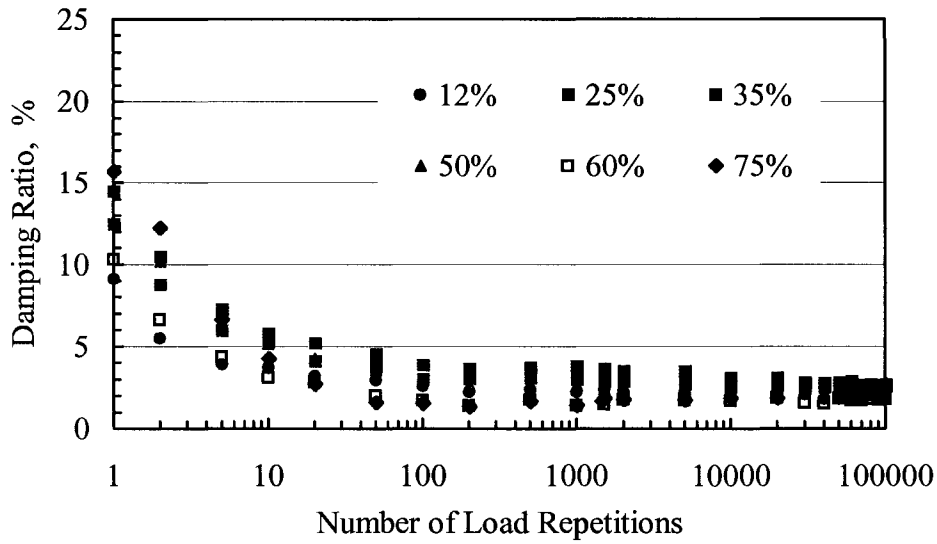

Figure 4.88: Damping Ratio Variation for Different RS Strength Levels at σ_3 = 100 kPa

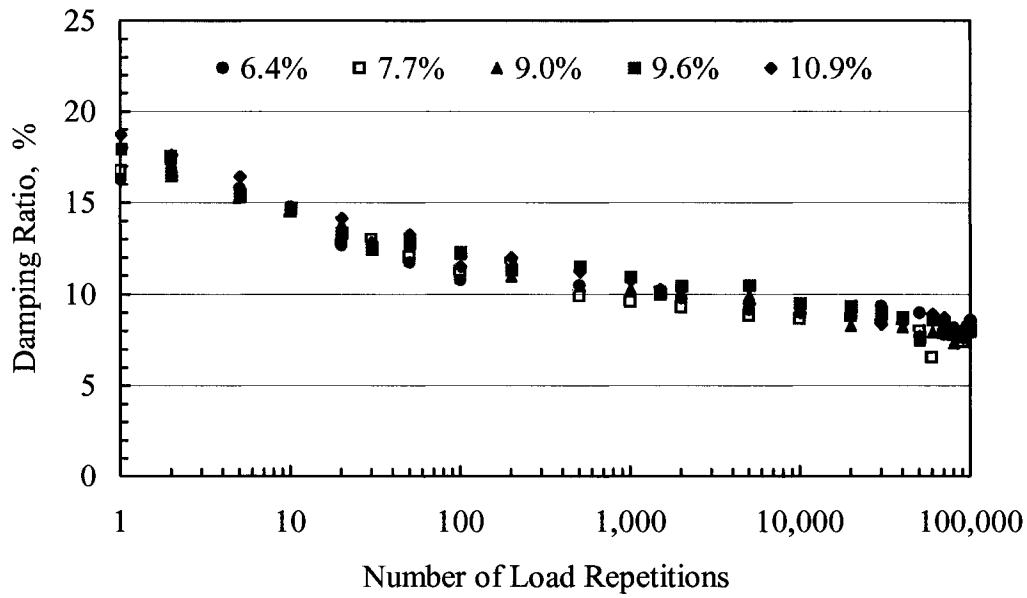

Figure 4.89: Damping Ratio Variation for Different CS Strength Levels at σ_3 = 100 kPa

4.5 Summary and Conclusions

In this chapter, an attempt has been made to present results of long-term behavior for a typical granular material under repeated and cyclic triaxial loading conditions. Of particular interest is the comparative basic dynamic response between the two different loading patterns applied, as well as the effect of increasing applied stress levels on various soil parameters. These parameters include, permanent deformations, various moduli (shear, resilient and total), and damping ratio. The results of this study will help in developing a comprehensive understanding for the purpose of providing an improved mechanistic evaluation of unbound granular layers in pavement structures. Results of this study lead to the following generalized conclusions:

1. Traffic wheel load induces a complex type of load pattern in the pavement structure that cannot be simulated with a simple repeated haversine load profile as used in traditional dynamic triaxial tests.
2. Pattern of dynamic load applied is an important factor in determining the behavior of granular materials.
3. Cyclic loading leads to densification of granular materials at much higher rate than repeated loading.
4. Resilient properties are affected by the dynamic loading history of gravels in pavement sections.
5. Shear strength of granular materials are affected by load pattern, number of load application and dynamic stress level applied.
6. Damping ratio decreases with increasing number of load applications but remains independent of strength level applied specially for granular soils subjected to cyclic loading.

Chapter Five

Analysis of Results

5.1 Introduction

In the previous chapter, the results and observations of the study were presented. These outcomes reflected the complex nature of granular materials when subjected to dynamic loading. It is the objective of this chapter to analyze and formulate the behavior of unbound granular materials when subjected to repetitive loading so that these can be used to better design and predict the deterioration or distress of granular base course layers in pavement structures.

5.2 Resilient Response

Predicting the resilient or recoverable properties of granular materials is of utmost importance since this response is used to model and design pavements. Through the years, the most popular model used to characterize the resilient properties of granular materials was the so called the k-θ model, which relates the resilient modulus M_R with the first stress invariant θ. The k-θ model was applied to the data recorded in this study and the different parameters obtained were presented in table 4.2. Currently, a more comprehensive model suggested by Uzan (1985), which incorporates the effect of shear stress or shear strain on the resilient modulus, is gaining popularity. This model (which was presented in Chapter 2 of this thesis) is given by:

$$M_R = k_1 p_0 \left(\frac{\theta}{p_0}\right)^{k_2} \left(\frac{\sigma_d}{p_0}\right)^{k_3} \quad (5.1)$$

Where: M_R = Resilient modulus,

θ = First stress invariant,

σ_d = Deviatoric stress,

p_0 = Atmospheric pressure,

And, k_1, k_2 and k_3 are curve fit parameters.

The applicability of the Uzan model was checked by applying it to the data obtained for the resilient response of the granular material from the long-term tests. The results of this exercise are given in Table 5.1. Overall, high values of R^2 were obtained for all cases studied; this indicates the suitability of the Uzan model to predict resilient properties of granular materials regardless of the load pattern and number of load repetitions applied.

Table 5.1: Uzan Model Parameters to Estimate M_R.

	Repeated Stress				Cyclic Stress			
Load Repetitions	k_1	k_2	k_3	R^2	k_1	k_2	k_3	R^2
1,000	740	0.5392	-0.0086	0.981	-	-	-	-
5,000	733	0.6222	-0.0123	0.986	1501	0.3258	0.1494	0.922
10,000	802	0.5697	0.0187	0.993	2203	0.1179	0.3894	0.993
20,000	788	0.6125	0.0082	0.992	1609	0.3270	0.1851	0.986
50,000	823	0.6238	-0.0030	0.991	1840	0.2719	0.2308	0.994
100,000	867	0.6014	0.0052	0.991	1193	0.5713	-0.0446	0.988

It is essential to find a pattern of variation of the different parameters (k_1, k_2 and k_3) with the number of load applications in order to incorporate the strain-hardening trend observed in this study in predictive numerical models. However, as it can be seen from the values presented in Table 5.1, it is difficult (if not impossible) to find a relationship relating parameters k_1, k_2 and k_3 with the number of load repetitions applied, for neither repeated nor cyclic loading cases.

The Uzan model was also used to express the resilient shear modulus, G_R, in terms of the deviatoric stress and bulk stress applied.

$$G_R = k_1' \cdot p_0 \cdot \left(\frac{\theta}{p_0}\right)^{k_2'} \cdot \left(\frac{\sigma_d}{p_0}\right)^{k_3'} \qquad (5.2)$$

Where:

G_R = Resilient shear modulus,

p_0 = Atmospheric pressure,

θ = Bulk stress,

σ_d = Deviatoric stress, and,

k_1', k_2' and k_3' are curve-fit parameters dependent on material type.

The above model was applied to the data from the repeated stress and cyclic stress load patterns. The resulting curve-fit parameters are presented in Table 5.2 below. Again the R^2 values obtained were high, suggesting that the Uzan model is suitable for the shear resilient values measured in this study. However, as was the case for the resilient modulus case, a distinctive pattern of variation between the curve-fitting parameters and the number of load applications remained elusive.

Table 5.2: Uzan Model Parameters to Estimate G_R.

	Repeated Stress				Cyclic Stress			
Load Repetitions	k_1'	k_2'	k_3'	R^2	K_1'	k_2'	k_3'	R^2
1,000	632	0.3062	0.2727	0.947	-	-	-	-
5,000	704	0.2259	0.3218	0.962	1112	0.1484	0.2776	0.990
10,000	598	0.4250	0.1810	0.988	1630	-0.0570	0.5124	0.983
20,000	615	0.4031	0.1969	0.988	1139	0.1834	0.2863	0.990
50,000	619	0.4674	0.1428	0.986	1332	0.1198	0.3480	0.999
100,000	680	0.3949	0.1803	0.982	752	0.5081	0.0005	0.990

Johnson et al. (1986) suggested including the ratio of second deviatoric stress invariant (J_2) and octahedral shear stress (τ_{oct}) in the expression used to predict the resilient modulus. They argued that the inclusion of the stress ratio accounts for the effects of both confining pressure and principal stress ratio, which is more appropriate for granular materials. The resilient modulus, in this case, is expressed as:

$$M_R = k_4 \cdot p_0 \left(\frac{J_2}{p_0 \cdot \tau_{oct}} \right)^{k_5} \qquad (5.3)$$

Where k_4 and k_5 are material constants and p_0 is the atmospheric pressure.

This expression was also used to check whether it fits the data obtained from the current research and mainly if the effect of repetitions can be incorporated in this

model. The resulting model parameters, k_4 and k_5, along with the corresponding R^2 values for both type of loading RS and CS are presented in Table 5.3.

The variation of the material variables k_4 and k_5 with the number of load applications (N) is presented in Figure 5.1 and Figure 5.2 for RS and CS load patterns respectively. k_4 was found to vary logarithmically following the curve fit equation given below:

For repeated loading pattern:

$$k_4 = 190 \cdot \log(N) + 800, \quad \ldots\ldots\ldots\ldots\ldots\ldots R^2 = 0.997 \qquad (5.4)$$

For cyclic loading pattern:

$$k_4 = 424 \cdot \log(N) + 1402, \quad \ldots\ldots\ldots\ldots\ldots\ldots R^2 = 0.966 \qquad (5.5)$$

As for the k_5 variation, it is best expressed as a simple 2nd degree polynomial function of k_4 given by:

-For repeated loading pattern:

$$k_5 = -1\times10^{-6} \cdot k_4^2 + 3.5\times10^{-3} \cdot k_4 - 2.443 \ldots\ldots R^2 = 0.992 \qquad (5.6)$$

-For cyclic loading pattern:

$$k_5 = -1\times10^{-7} \cdot k_4^2 + 0.001 \cdot k_4 - 1.237 \ldots\ldots\ldots R^2 = 0.987 \qquad (5.7)$$

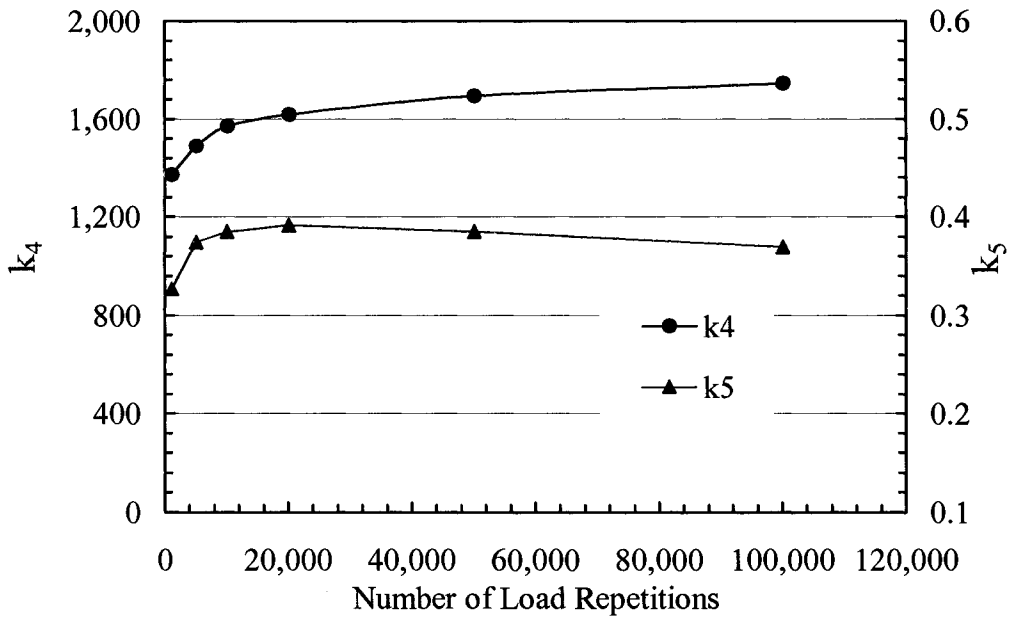

Figure 5.1: Variation of k_4 and k_5 Parameters for M_R with N for RS Load Pattern.

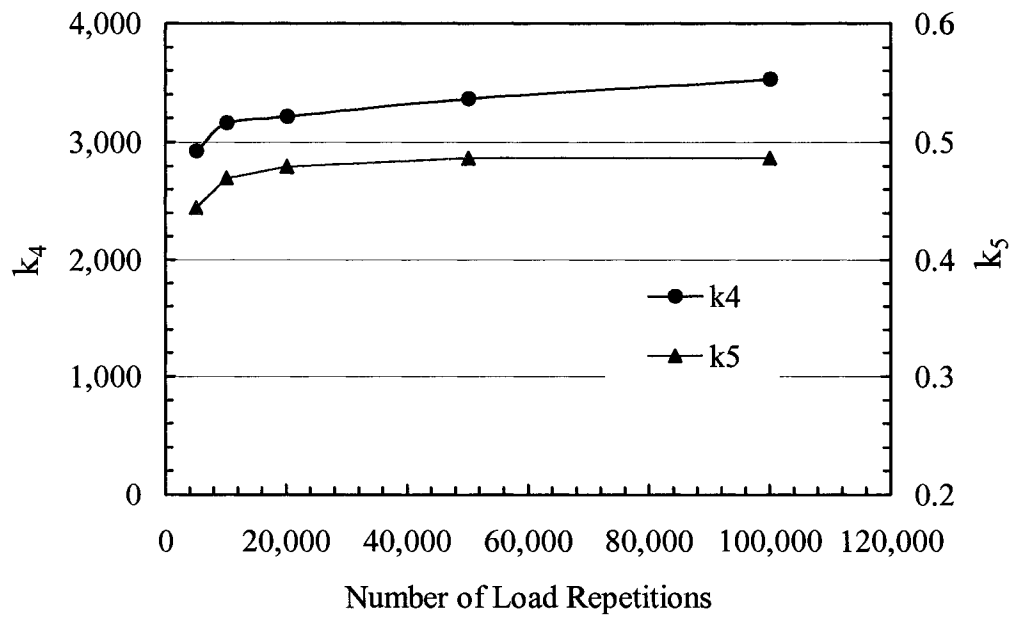

Figure 5.2: Variation of k_4 and k_5 Parameters for M_R with N for CS Load Pattern.

Table 5.3: Johnson et al. Resilient Modulus Model Parameters.

	Repeated Stress			Cyclic Stress		
Load Repetitions	k_4	k_5	R^2	k_4	k_5	R^2
1,000	1370	0.3267	0.926	-	-	-
5,000	1490	0.3745	0.931	2930	0.4446	0.895
10,000	1570	0.3850	0.945	3164	0.4712	0.892
20,000	1616	0.3919	0.925	3221	0.4800	0.891
50,000	1694	0.3850	0.965	3366	0.4870	0.952
100,000	1744	0.3692	0.954	3532	0.4869	0.945

The same model suggested by Johnson et al. (1986) for resilient model (and used above), can be utilized to estimate the resilient shear moduli measured in this research. The expression in this case is given as:

$$G_R = k_4^{'} \cdot p_0 \cdot \left(\frac{J_2}{p_0 \cdot \tau_{oct}} \right)^{k_5^{'}} \qquad (5.8)$$

Where:

G_R = Resilient shear modulus,

p_0 = Atmospheric pressure,

J_2 = Second deviatoric stress invariant,

τ_{oct} = Octahedral stress, and,

$k_4^{'}$ and $k_5^{'}$ are curve-fit parameters dependent on material type.

The resilient shear moduli data measured in this research was used to find the curve-fit parameters of the Johnson et al. expression. These parameters are outlined in Table 5.4 along with the corresponding R^2 regression coefficients, and the variations of the material variables k_4' and k_5' with the number of load applications (N), for RS and CS load patterns respectively, are presented in Figures 5.3 and 5.4.

The variation of k_4' with the number of load applications is given by:

-For RS loading pattern:

$$k_4' = 81 \cdot \log(N) + 732 \ldots\ldots\ldots\ldots\ldots R^2 = 0.976 \quad (5.9)$$

-For CS loading pattern:

$$k_4' = 274 \cdot \log(N) + 621 \ldots\ldots\ldots\ldots\ldots R^2 = 0.984 \quad (5.10)$$

As for the k_5' variation, it was again found to be best expressed as a simple 2nd degree polynomial function of k_4':

-For RS loading pattern:

$$k_5' = -1\times10^{-6} \cdot k_4'^2 + 2.1\times10^{-3} \cdot k_4' - 0.528 \ldots\ldots\ldots R^2 = 0.951 \quad (5.11)$$

-For CS loading pattern:

$$k_5 = -4\times10^{-7} \cdot k_4^2 + 1.7\times10^{-3} \cdot k_4 - 1.208 \ldots\ldots\ldots R^2 = 0.960 \quad (5.12)$$

Table 5.4: Johnson et al. Model Parameters to Estimate G_R

	Repeated Stress			Cyclic Stress		
Load Repetitions	k_4'	k_5'	R^2	k_4'	k_5'	R^2
1,000	987	0.4631	0.924	-	-	-
5,000	1021	0.4632	0.942	1622	0.4121	0.921
10,000	1048	0.4473	0.990	1744	0.449	0.893
20,000	1075	0.4494	0.955	1790	0.457	0.969
50,000	1118	0.4256	0.926	1892	0.4594	0.990
100,000	1144	0.4192	0.938	2001	0.4731	0.861

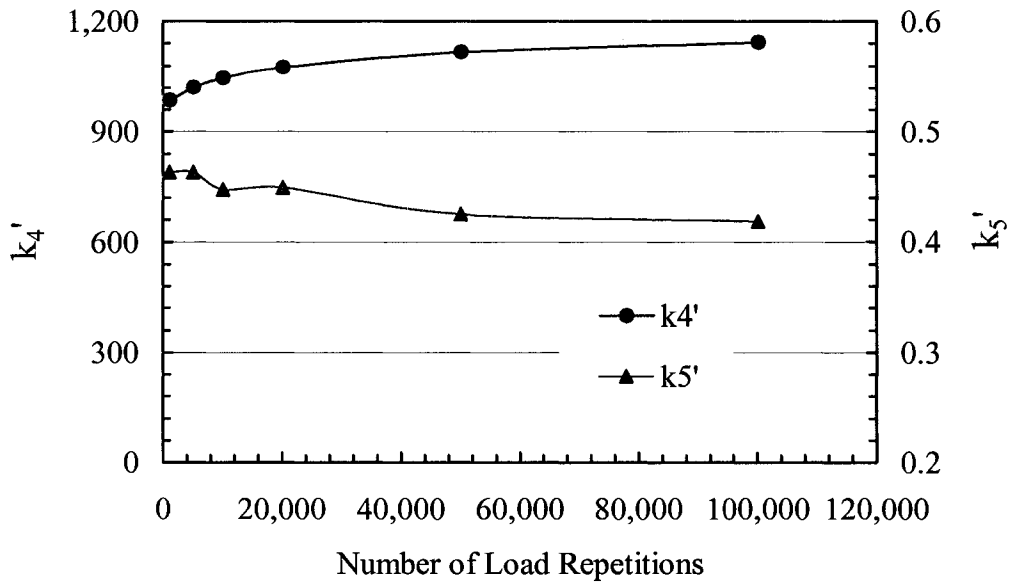

Figure 5.3: Variation of k_4' and k_5' Parameters for G_R with N for RS Load Pattern.

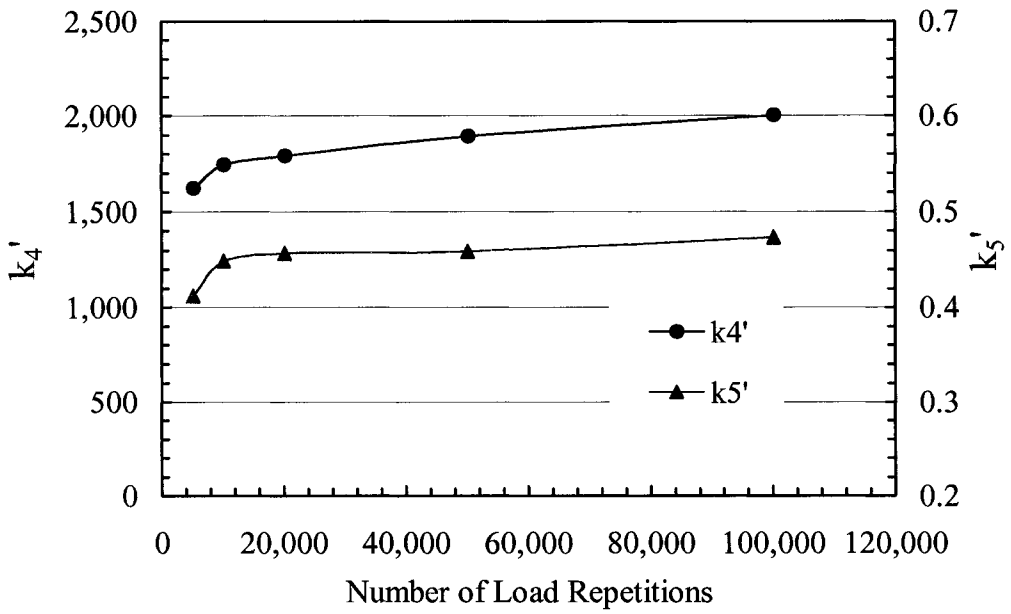

Figure 5.4: Variation of k_4' and k_5' Parameters for G_R with N for CS Load Pattern.

5.3 Total Moduli Models

The total modulus M_T is by definition the ratio of applied deviatoric stress and the resulting total strain. The total shear modulus G_T is defined and the ratio of the shear stress applied divided by the total shear strain in the system. These two moduli (as M_R and G_R) vary with the applied stress level and the number of load applications. Furthermore, these moduli are important parameters used to analyze pavement systems; therefore it would be advantageous to have adequate models to use in numerical analysis.

Once again, it was found that the model used by Johnson et al. (1986) is the most suitable expression to relate M_T and G_T to the stress state and number of load repetitions applied. The general forms of the equations proposed are:

- For total modulus:

$$M_T = k_6 \cdot p_0 \cdot \left(\frac{J_2}{p_0 \cdot \tau_{oct}} \right)^{k_7} \tag{5.13}$$

- For total shear modulus:

$$G_T = k_6' \cdot p_0 \cdot \left(\frac{J_2}{p_0 \cdot \tau_{oct}} \right)^{k_7'} \tag{5.14}$$

The variation of k_6, k_7, k_6' and k_7' with the number of load applications, for both repeated and cyclic load patterns, are presented in Figures 5.5 through 5.8.

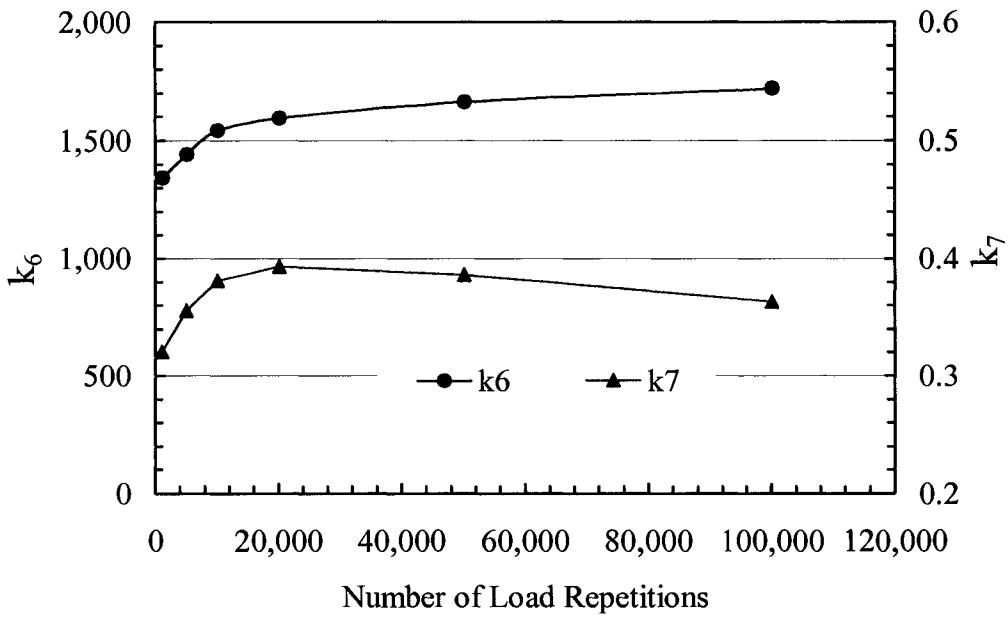

Figure 5.5: Variation of k_6 and k_7 Parameters for M_T with N for RS Load Pattern.

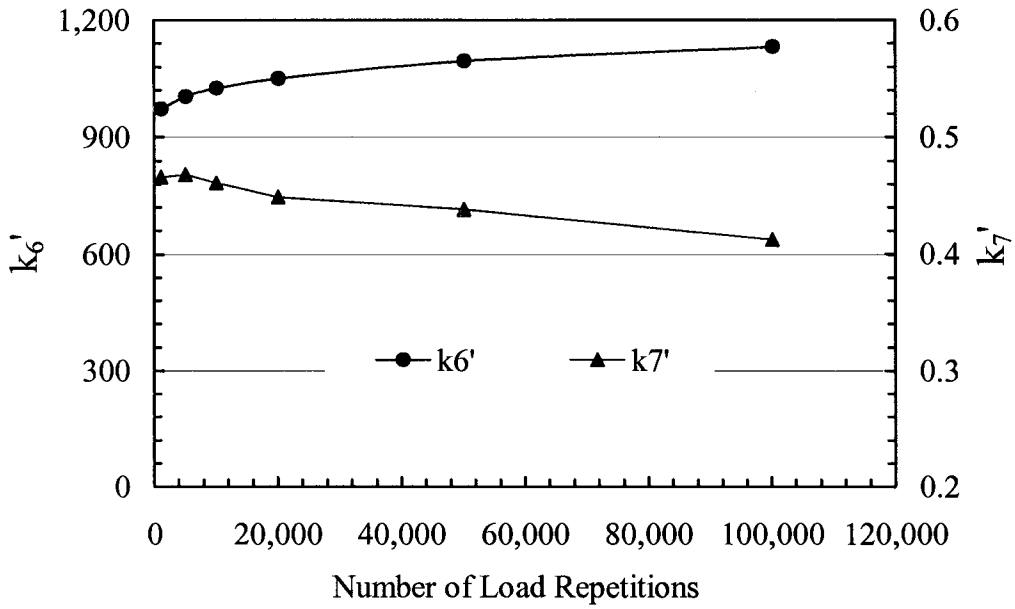

Figure 5.6: Variation of k_6' and k_7' Parameters for G_T with N for RS Load Pattern.

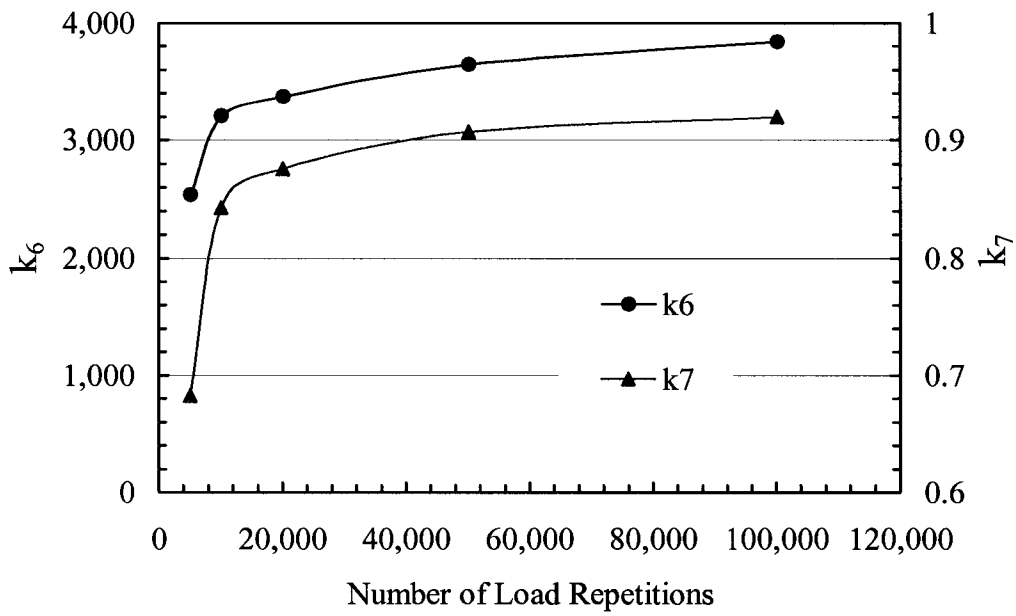

Figure 5.7: Variation of k_6 and k_7 Parameters for M_T with N for CS Load Pattern.

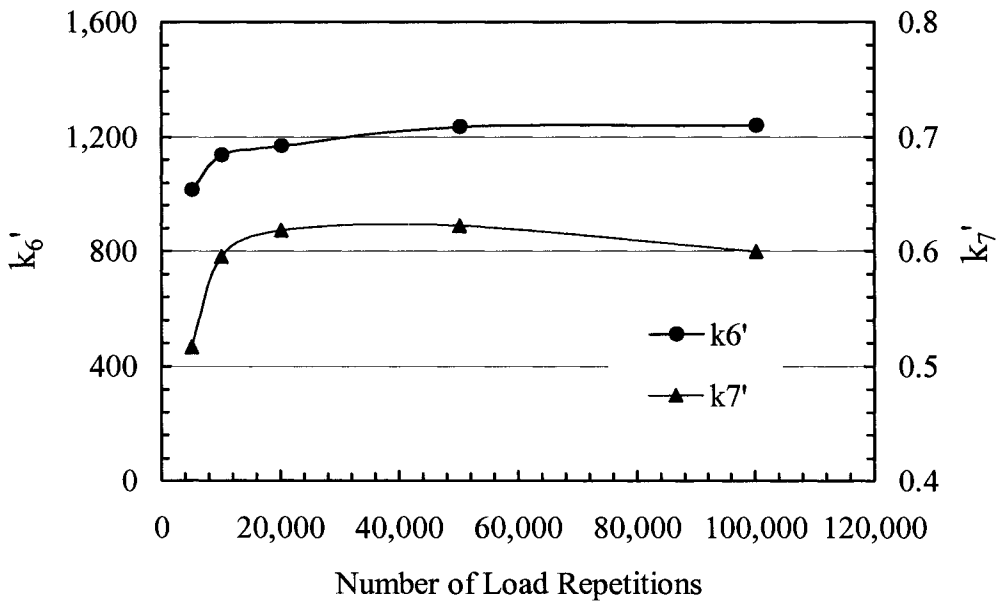

Figure 5.8: Variation of k_6' and k_7' Parameters for G_T with N for CS Load Pattern.

The equations corresponding to the variations of k_6, k_7, k_6' and k_7' are as follows:

- For total modulus M_T resulting from repeated loading:

$$k_6 = 193 \cdot \log(N) + 756 \ldots\ldots\ldots\ldots\ldots\ldots R^2 = 0.988 \qquad (5.15)$$

$$k_7 = -1\times10^{-6} \cdot k_6^{\,2} + 3.6\times10^{-3} \cdot k_6 - 2.496 \ldots\ldots\ldots R^2 = 0.960 \qquad (5.16)$$

- For total modulus M_T resulting from cyclic loading:

$$k_6 = 850 \cdot \log(N) - 635 \ldots\ldots\ldots\ldots\ldots\ldots R^2 = 0.907 \qquad (5.17)$$

$$k_7 = -1\times10^{-7} \cdot k_6^{\,2} + 8\times10^{-4} \cdot k_6 - 0.722 \ldots\ldots\ldots R^2 = 0.999 \qquad (5.18)$$

- For total shear modulus G_T resulting from repeated loading:

$$k_6' = 80 \cdot \log(N) + 716 \ldots\ldots\ldots\ldots\ldots\ldots R^2 = 0.955 \quad (5.19)$$

$$k_7' = -2 \times 10^{-6} \cdot k_6'^2 + 4 \times 10^{-3} \cdot k_6' - 1.485 \ldots\ldots\ldots R^2 = 0.977 \quad (5.20)$$

- For total shear modulus G_T resulting from cyclic loading:

$$k_6' = 166 \cdot \log(N) + 621 \ldots\ldots\ldots\ldots\ldots\ldots R^2 = 0.984 \quad (5.21)$$

$$k_7' = -3 \times 10^{-6} \cdot k_6'^2 + 6.7 \times 10^{-3} \cdot k_6' - 3.392 \ldots\ldots\ldots R^2 = 0.954 \quad (5.22)$$

5.4 Plastic Response

Failure of soils is defined traditionally as a state when the level of stress applied exceeds a given maximum allowable stress usually defined by a failure criterion such as Möhr-Coulomb, Drucker-Prager, etc.... However, there exists a situation where even though the soil structure (be it a foundation, pavement, etc...) has not yet failed according to the stress failure criteria, the accumulated strains are so large enough that the soil structure in question is rendered inadequate for the service it was designed to provide. Therefore, a certain minimum service level allowed is set to define a new serviceability failure criterion.

The variable that depicts the serviceability level in pavement structures is the accumulated vertical strain. Predicting such strains can provide pavement engineers with a good tool in designing pavement structures. Through the years, several

empirical models have been proposed. The most popular of these models will be examined in this section to check whether they fit the data recorded in this study and an attempt will be made to incorporate the level of stress applied as a variable as well as the type of loading pattern.

5.4.1 Hyperbolic Model

Kodner and Zalasko (1963) have shown that for a given confining pressure the stress-strain curves obtained from conventional, static triaxial tests performed on both granular and non-granular materials can be quite accurately approximated by a hyperbola. Duncan and Chang (1970) extended this work and have shown that a generalized hyperbolic expression can be derived expressing the measured strain in the static triaxial test as a function of the stress level applied, as:

$$\varepsilon_a = \frac{(\sigma_1 - \sigma_3) \Big/ K \cdot \sigma_3^n}{1 - \left[\frac{(\sigma_1 - \sigma_3) \cdot R_f}{2(c.\cos\phi + \sigma_3 \cdot \sin\phi)/(1 - \sin\phi)} \right]} \qquad (5.23)$$

Where:

ε_a = Axial strain,

$K.\sigma_3^n$ = Relationship defining the initial tangent modulus as a function of confining pressure σ_3 (K and n are constants),

c = Cohesion

ϕ = Angle of friction, and,

R_f = Ratio of measured strength to an asymptotic stress difference.

Encouraged by this fact, Barksdale (1972) suggested a hyperbolic relationship between the applied repetitive deviatoric stress and the accumulated plastic strain. Barksdale found out that applying this hyperbolic relationship to results from tests conducted on a variety of base course materials after 100,000 load applications, resulted in excellent agreement for low confining stresses and slightly underestimated the results of specimens tested at high confining pressures.

If we rearrange the hyperbolic equation given above so that σ_d is given as a function of ε_a^p, we obtain a general expression of the form:

$$\sigma_d = \sigma_1 - \sigma_3 = \frac{\varepsilon_a^p}{a + b \cdot \varepsilon_a^p} \tag{5.24}$$

In order to determine the values of the parameters a and b, the equation above is written in the following linear form:

$$\frac{\varepsilon_a^p}{\sigma_d} = a + b \cdot \varepsilon_a^p \tag{5.25}$$

If $\varepsilon_a^p / \sigma_d$ is plotted against ε_a^p this results in a straight-line relationship and parameters a and b are respectively, the intercept and the slope of the straight line. For $\varepsilon_a^p \to \infty$ the ultimate σ_d would be equal to the asymptote $1/b$. As for the parameter a, it is equal to the initial tangent modulus E_i (at $\varepsilon_a^p = 0$) as shown in the figure below.

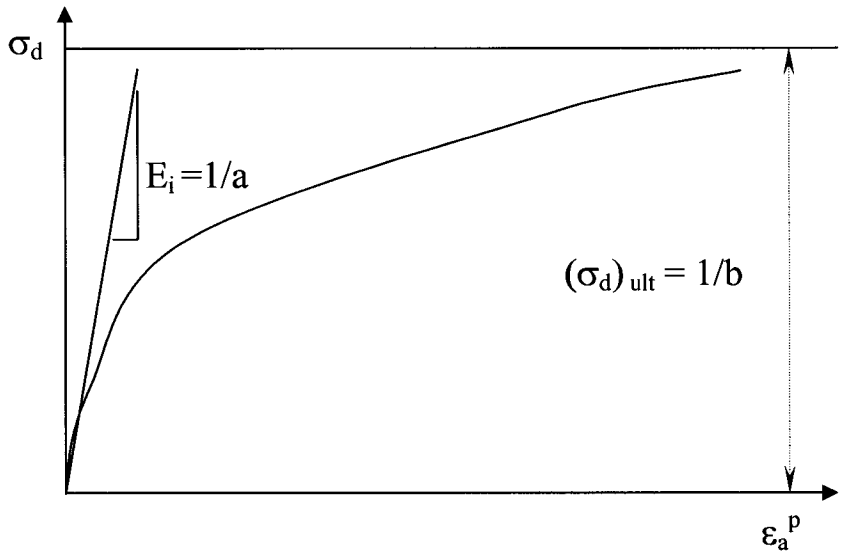

Figure 5.9: Schematic Representation of Hyperbolic Stress-Strain Model

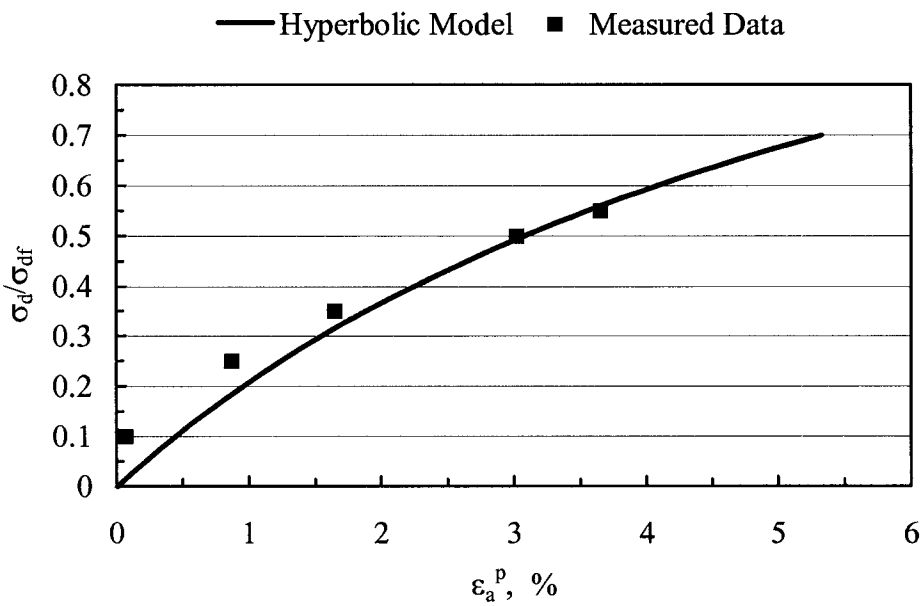

Figure 5.10: Hyperbolic Model for RS Loading at σ_3 = 35 kPa

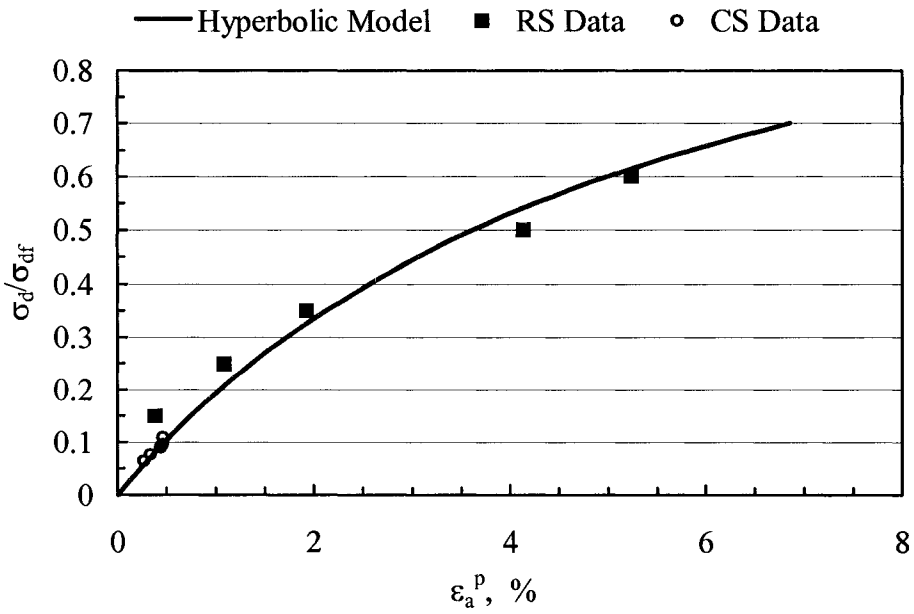

Figure 5.11: Hyperbolic Model for RS and CS Loading at σ_3 = 100 kPa

Applying the hyperbolic model to the data in this research, results in fairly good agreement with the measured plastic strain response as can be seen in Figures 5.10 and 5.11.

In order to model the accumulation of plastic strain with the number of load applications for a given stress level, Barksdale (1972) proposed a logarithmic model based on triaxial tests performed up to 100,000 repetitions. His model is still widely used for its simplicity and is given as:

$$\varepsilon_1^p = a + b \cdot \log N \qquad (5.26)$$

Where, a and b are curve-fitting variables dependent on material type and density, and N is the number of load repetitions applied.

This model was applied to the data from this research and the resulting variables are listed in Tables 5.5 and 5.6. The numbers in italic refer to samples undergoing severe expansion.

In general, the R^2-values resulting from Barksdale's model are high which would suggest that the model is suitable to be applied for prediction purposes. However, at close inspection, we notice that, for the repeated loading case, the model does well at low stress levels but is poor when applied to results of specimens tested at high stress levels (see Figures 5.12 and 5.13).

As for specimens tested under cyclic stress repetitions, the model seems to perform much better at all stress levels applied except for load repetition (N) values less than 10 where negative (expansive) permanent axial strains are recorded (Figure 5.14). This is not a serious deviation; because pavement engineers are more interested in high values of number of load applications ($N>10^4$).

Table 5.5: Barksdale's Parameters Applied to RS Case (35 and 100 kPa)

	σ_3 = 35 kPa			σ_3 = 100 kPa		
SL	a	b	R^2	a	b	R^2
8 %	-0.0203	0.014	0.817	-	-	-
12 %	-	-	-	-0.0708	0.0869	0.972
25 %	-0.1808	0.2031	0.977	-0.1202	0.2362	0.992
35 %	-0.264	0.3717	0.987	-0.1966	0.4226	0.992
50 %	-0.7613	0.7224	0.962	-0.5791	0.9664	0.980
60 %	-1.275	1.516	0.880	-1.020	1.284	0.972
70 %	-	-	-	*-1.911*	*2.683*	*0.950*

Table 5.6: Barksdale's Parameters Applied to CS Case.

	Confining Stress = 100 kPa		
Stress Level	a	b	R^2
6.4 %	-0.0561	0.0462	0.976
7.7 %	-0.0683	0.0595	0.977
9.0 %	-0.0744	0.0737	0.985
9.6 %	-0.0816	0.0805	0.987
10.9 %	-0.0777	0.0777	0.985

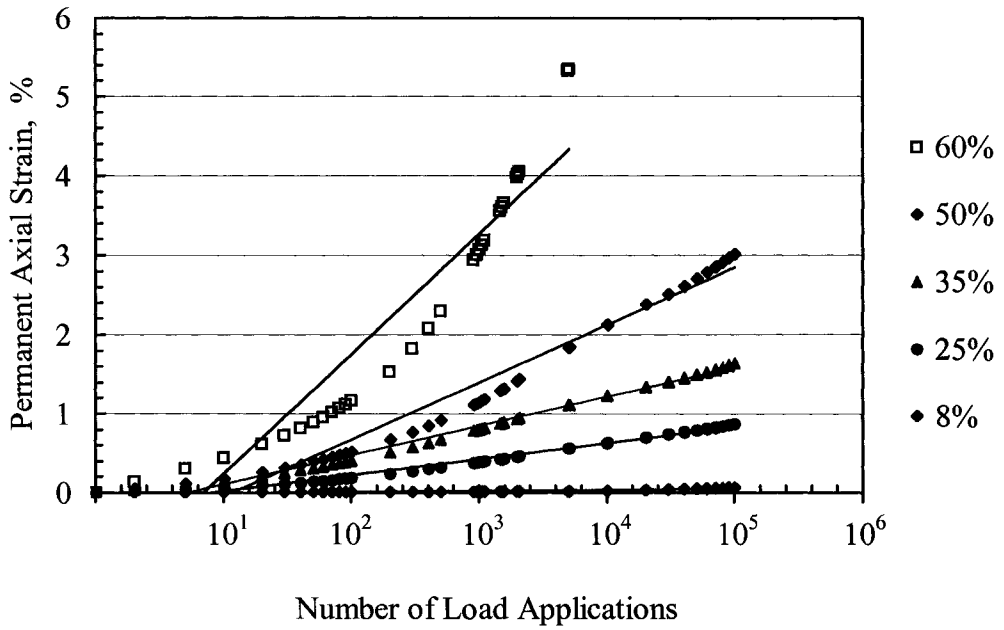

Figure 5.12: Barksdale's Model Applied to RS Tests for σ_3 = 35 kPa

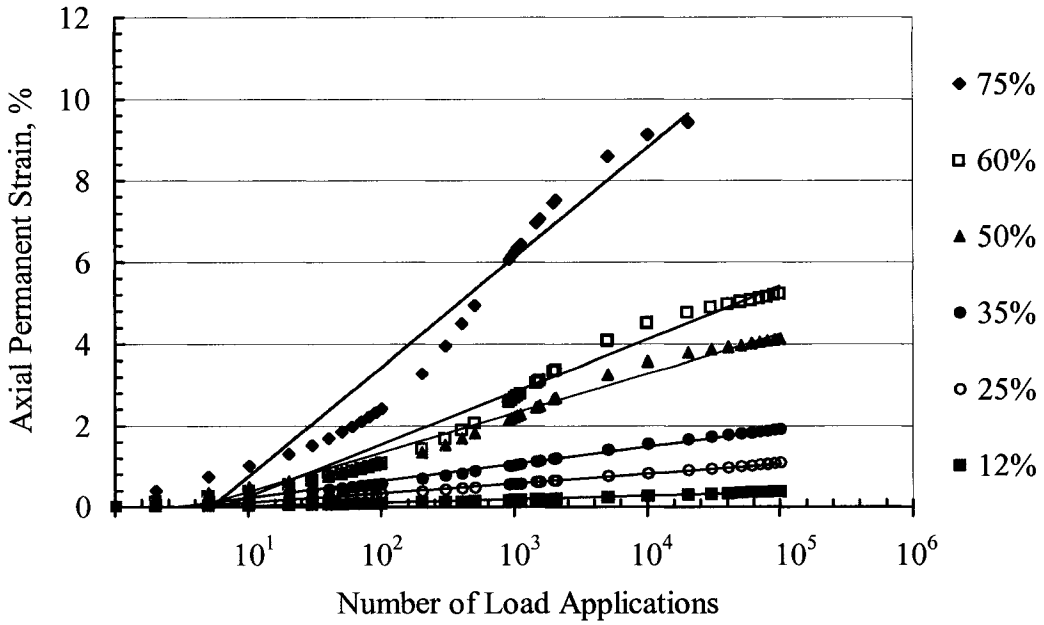

Figure 5.13: Barksdale's Model Applied to RS Tests for σ_3 = 100 kPa

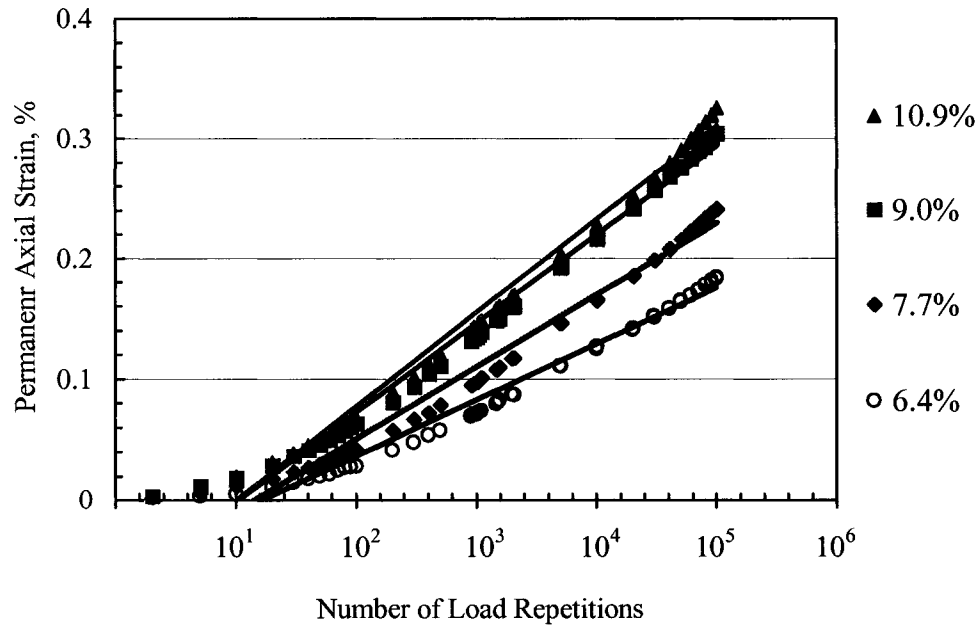

Figure 5.14: Barksdale's Model Applied to CS Tests for σ_3 = 100 kPa

The various a and b parameters presented in Tables 5.5 and 5.6 follow certain trends (Figures 5.15, 5.16 and 5.17) which can be translated into equations.

For the specimens tested under repeated loading, the relationship that best expressed parameter a in terms of the stress level (SL) turned out to be a polynomial function to the 2nd degree.

- For the case of low confining pressure (σ_3 = 35 kPa)

$$a = -5\times10^{-4}\,SL^2 + 0.0135\,SL - 0.1134 \quad \ldots\ldots\ldots R^2 = 0.993 \qquad (5.27)$$

- For the case of high confining pressure (σ_3 = 100 kPa)

$$a = -6\times10^{-4}\,SL^2 + 0.0243\,SL - 0.3009 \quad \ldots\ldots\ldots R^2 = 0.998 \qquad (5.28)$$

As for the parameter b, a power curve expression seems to best represent the relationship with the stress level (SL).

- For the case of low confining pressure (σ_3 = 35 kPa)

$$b = 1\times10^{-4}\cdot SL^{2.245} \ldots\ldots\ldots\ldots\ldots\ldots\ldots R^2 = 0.995 \qquad (5.29)$$

- For the case of high confining pressure (σ_3 = 100 kPa)

$$b = 8\times10^{-4}\cdot SL^{1.835} \ldots\ldots\ldots\ldots\ldots\ldots\ldots R^2 = 0.978 \qquad (5.30)$$

In the case of cyclic stress loading tests, parameter a is still expressed with a 2nd degree polynomial function, whereas the relationship between parameter b and

stress level SL is no longer a power function but a 2nd degree polynomial function. These equations are presented below:

$$a = -1.9\times10^{-3}\cdot SL^2 + 0.0403\cdot SL - 0.1356 \ldots\ldots\ldots\ldots R^2 = 0.970 \qquad (5.31)$$

$$b = 1.6\times10^{-3}\cdot SL^2 - 0.0322\cdot SL + 0.0861 \ldots\ldots\ldots\ldots R^2 = 0.960 \qquad (5.32)$$

The main observation that can be made here is the fact that the variation of parameters a and b with strength level is distinctively different depending on the loading pattern. Parameter a decreases at increasing rate in the case of RS loading, whereas for CS loading it decreases to a minimum (at decreasing rate). The same pattern is noticed for parameter b, which increases indefinitely with increasing stress level for the RS case, and increases to a maximum in the case of specimens subjected to cyclic loading pattern.

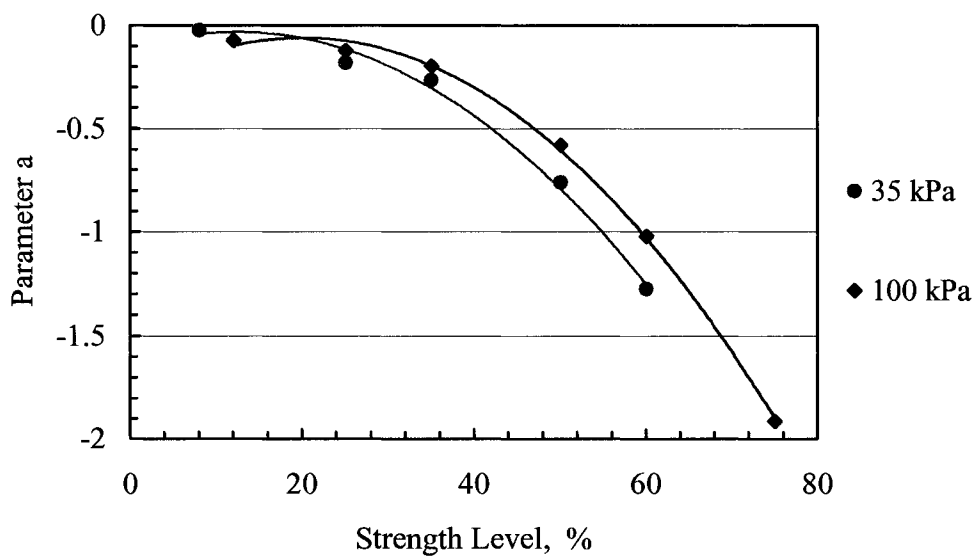

Figure 5.15: Variation of Parameter a with the Strength Level SL (RS).

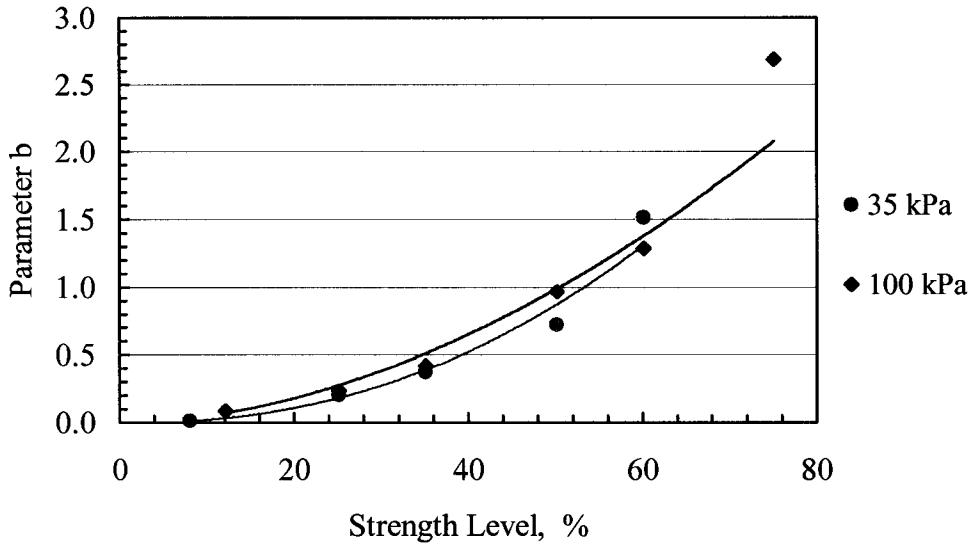

Figure 5.16: Variation of Parameter *b* with the Strength Level *SL* (RS).

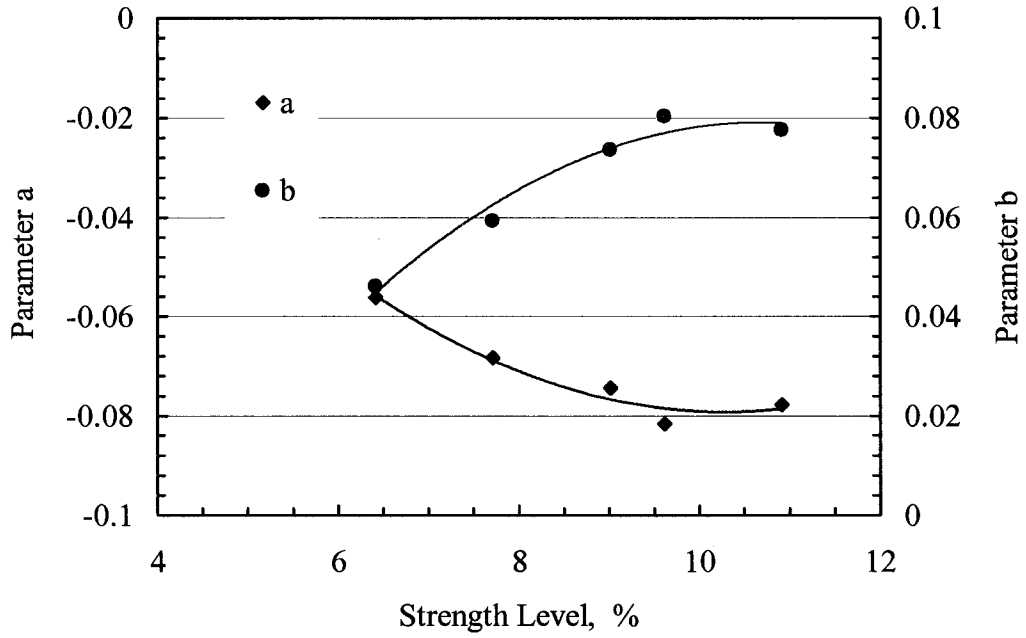

Figure 5.17: Variation of Parameters *a* and *b* with the Strength Level *SL* (CS).

5.4.2 Sweere's Model

Sweere (1990) conducted long term triaxial repeated load tests and based on his results suggested a variation of Barksdale's model since the latter did not seem to represent deformations for load repetitions beyond 10,000. The proposed model is basically a power equation relating the axial permanent strain, ε_a^p, to the number of load repetitions applied N:

$$\varepsilon_a^p = a_1 \cdot N^{b_1} \tag{5.33}$$

Where a_1 and b_1 are curve-fit variables dependent on type of material tested. The equation above can be rewritten as:

$$\log \varepsilon_a^p = \log a_1 + b_1 \cdot \log N \tag{5.34}$$

Therefore, the relationship presented by Sweere (1990) reduces to a linear equation when the data is plotted on a log-log scale.

Sweere (1990) recommends using this model for number of repetitions higher than 10^2, for fewer number of load repetitions, Barksdale's model is used. Applying the Sweere model to the data of the current research (for $N>10^2$) resulted in the parameters a_1 and b_1 listed in Tables 5.7 and 5.8. The R^2 values obtained for tests subjected to both load patterns are fairly high. This suggests that this model is a good mean to predict the accumulated plastic strain for specimens tested under either RS or CS load patterns. Plots of the results along with a curve-fit representing the Sweere model are shown in Figures 5.18 and 5.19.

Table 5.7: Parameters of the Sweere Model Applied to the Repeated Stress Case

	σ_3 = 35 kPa			σ_3 = 100 kPa		
SL	a_1	b_1	R^2	a_1	b_1	R^2
8 %	0.001	0.3598	0.994	-	-	-
12 %	-	-	-	0.0427	0.1944	0.983
25 %	0.0972	0.1949	0.972	0.1885	0.1551	0.975
35 %	0.2383	0.1713	0.968	0.3559	0.1510	0.961
50 %	0.2359	0.2273	0.974	0.7074	0.1615	0.918
60 %	0.2004	0.3917	0.994	0.7432	0.1794	0.890
75 %	-	-	-	*1.213*	*0.2241*	*0.869*

Table 5.8: Parameters of the Sweere Model Applied to the Cyclic Stress Case.

	Confining Stress = 100 kPa		
Stress Level	a_1	b_1	R^2
6.4 %	0.0145	0.2263	0.971
7.7 %	0.0209	0.2171	0.976
9.0 %	0.0334	0.1964	0.974
9.6 %	0.0375	0.1936	0.972
10.9 %	0.0364	0.1934	0.977

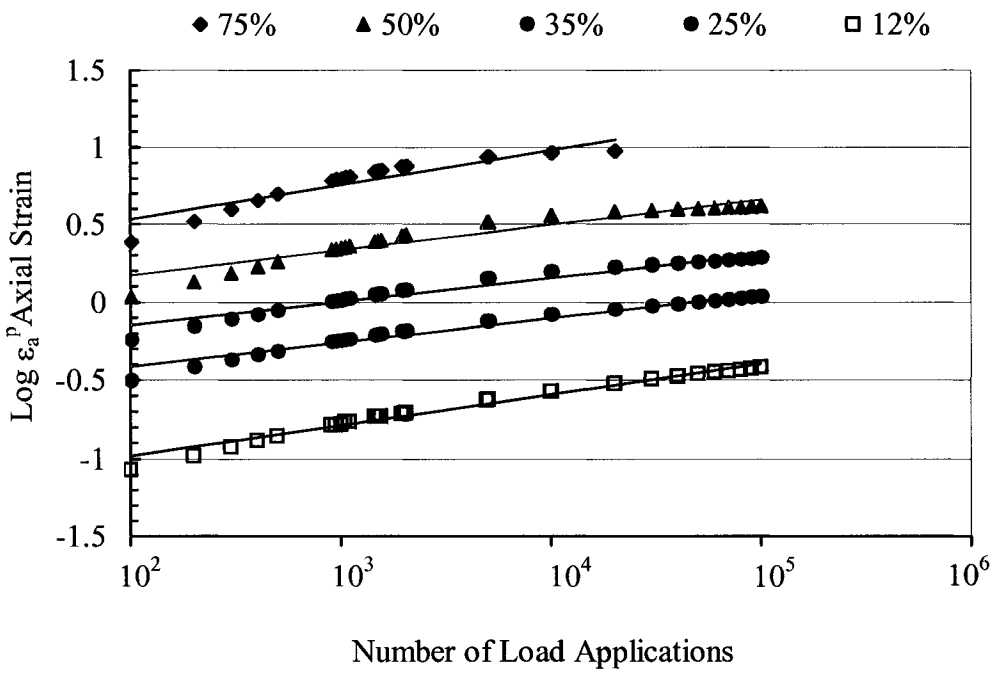

Figure 5.18: Sweere's Model Applied to ε_a^p Data for RS Test at σ_3 = 100 kPa

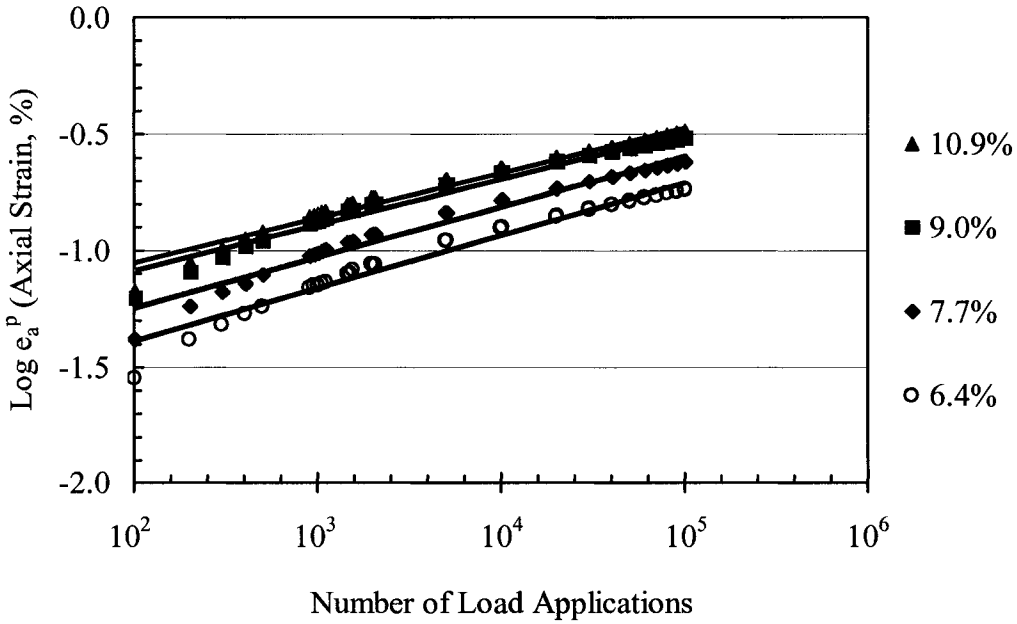

Figure 5.19: Sweere's Model Applied to ε_a^p Data for CS Test at σ_3 = 100 kPa

Figures 5.20 and 5.21 depict the variation of a_1 and b_1 with respect to the strength level applied for repeated load case. The intercept variable a_1 increases at increasing rate for high confining pressure case, whereas for the case of low σ_3, it seems to converge to a maximum (a_1 = 0.2) and stabilize. Slope b_1, under both high and low confining pressures, decreases following a 2nd degree polynomial curve to a minimum (at approximately SL=35%) then increases with increasing strength level as shown in Figure 5.21. The equations of the b_1 variation for respectively low and high confining pressure are:

$$b_1 = 3\times10^{-4}\cdot SL^2 - 0.0206\cdot SL + 0.5089 \ldots\ldots R^2 = 0.983 \qquad (5.35)$$

$$b_1 = 7\times10^{-5}\cdot SL^2 - 0.0053\cdot SL + 0.2466 \ldots\ldots R^2 = 0.988 \qquad (5.36)$$

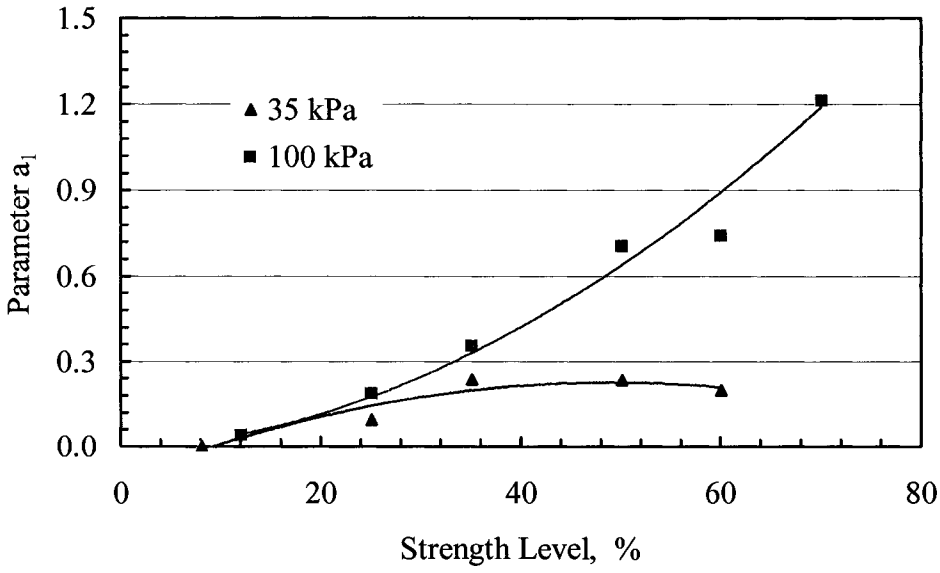

Figure 5.20: Variation of a_1 with Strength Level for RS Loading Case.

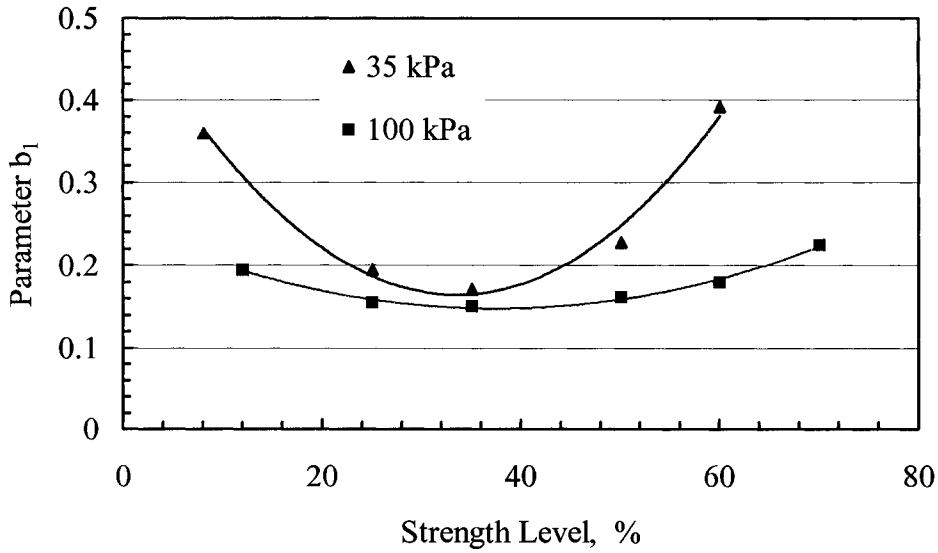

Figure 5.21: Variation of b_1 with Strength Level for RS Loading Case.

In the case of specimens subjected to cyclic loading pattern, a_1 increases linearly and b_1 decreases linearly with increasing strength level applied (Figure 5.22). The linear equations representing these variations have the following expressions:

$$a_1 = 5.5\times10^{-3}\cdot SL - 0.0198 \ldots\ldots\ldots\ldots\ldots R^2 = 0.879 \qquad (5.37)$$

$$b_1 = -8.3\times10^{-3}\cdot SL + 0.2775 \ldots\ldots\ldots\ldots\ldots R^2 = 0.877 \qquad (5.38)$$

Where SL is strength level applied and is expressed in percentage.

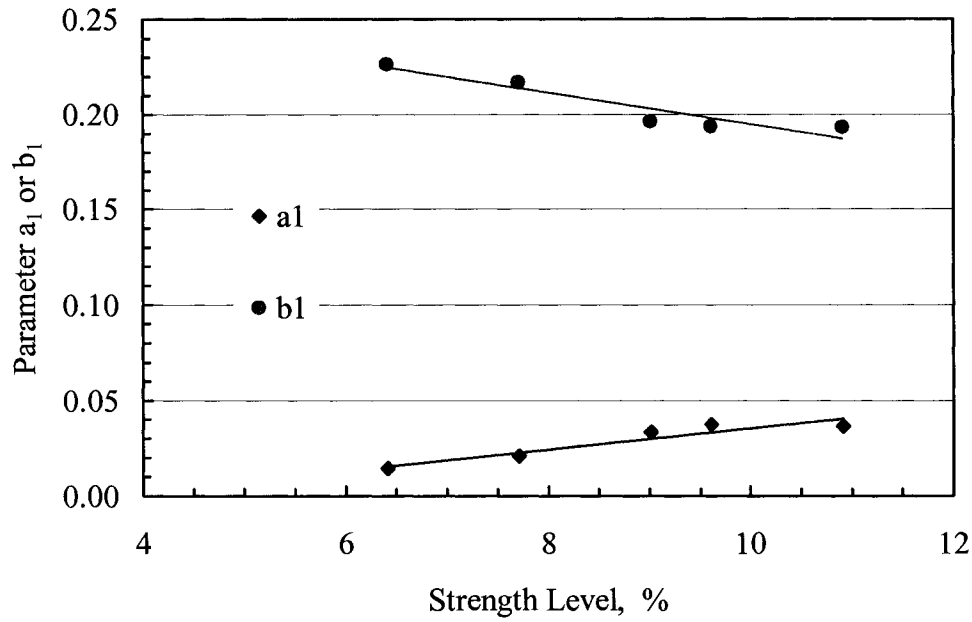

Figure 5.22: Variation of a_1 and b_1 with Strength Level for CS Loading Case.

Sweere (1990) used the same model on the permanent radial strain data collected in his research. He reported that this resulted in high R^2 values and accordingly suggested the use of the same expression to predict radial plastic strain of granular materials. Applying the Sweere model to the radial plastic strains, ε_3^p, resulting from the current research for specimens tested under RS loading, proved to be problematic mainly because ε_3^p values obtained were, in some cases, both compressive and expansive during a given test depending on the stress condition applied. Even when these strains were exclusively either compressive or expansive, the R^2 values obtained, turned out to be considerably low. As for tests performed using CS loading, the Sweere model seemed to be quite adequate when applied (Figure 5.23) and the R^2 values obtained were extremely encouraging as presented in Table 5.9 below; however, the resulting a_2 and b_2 parameters do not seem to have any trend while varying with the strength level applied.

Table 5.9: Sweere's Model Parameters Applied to ε_3^p (CS Case).

	Confinement Stress = 100 kPa		
Strength Level	a_2	b_2	R^2
6.4 %	0.0143	0.1773	0.996
7.7 %	0.0182	0.1895	0.992
9.0 %	0.0200	0.1912	0.996
9.6 %	0.0257	0.1866	0.990
10.9 %	0.0184	0.2078	0.998

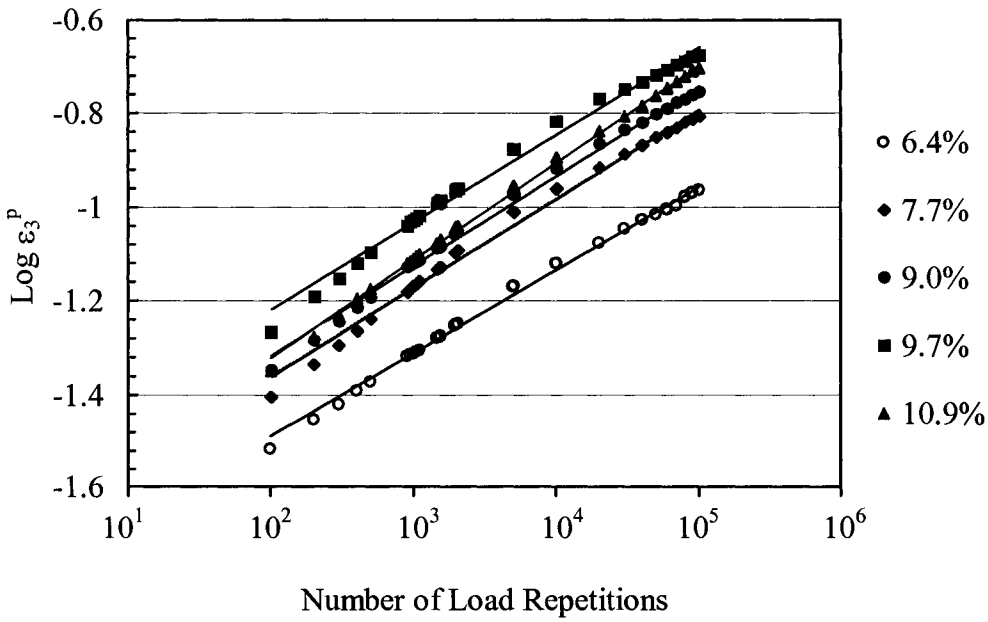

Figure 5.23: Sweere's Model Applied to Plastic Lateral Strains (CS Case).

5.4.3 Plastic Strain Model

Researchers agree that for a given type of granular soil, the factors affecting permanent strain accumulation are: the stress state, the number of load repetitions, and the stress level applied. An expression that combines these variables would be beneficial in the design of pavement structures. In this research, such an expression was derived to predict the permanent deformation accumulated based on the results of triaxial tests conducted in the lab.

To express the stress state, the function g used by Lade in his model was applied (refer to Chapter 2). This function is given by:

$$g = I_1^3 - \left[27 + \eta_2 \cdot \left(\frac{p_0}{I_1} \right)^m \right] \cdot I_3 \qquad (5.39)$$

Where:

I_1 is the first stress invariant,

η_2 is Lade's permanent deformation coefficient and is function of the failure surface and the confining stress applied,

I_3 is the third stress invariant, and,

p_0 is the atmospheric pressure.

m is a curve-fitting parameter determined by plotting $(I_1^3/I_3 - 27)$ versus p_0/I_1 at failure in log-log scale

The expression suggested in this research for estimating the accumulated axial and radial permanent strains under both repeated and cyclic loading patterns and the amount of accumulated permanent strain on the 45° plane under cyclic loading has the following form:

$$\log\left|\varepsilon^{p}\right| = a_1 \cdot \log g + a_2 \cdot \log N + a_3 \cdot \frac{I_1}{I_{1f}} + a_4 \qquad (5.40)$$

Where:

N is the number of load repetitions applied,

I_1 is the first stress invariant, and,

I_{1f} *is* the first stress invariant at failure.

a_1, a_2, a_3, and a_4 are curve-fitting coefficients.

It should be noted that absolute value of permanent strain was used in the above equation since the radial strains under repeated stress loading are negative (expansive).

The coefficients a_1, a_2, a_3, and a_4 of equation 5.40 and the corresponding R^2 values for both type of loading used are summarized in the tables below.

Table 5.10: Coefficients for $\varepsilon_p{}^1$ Model Proposed.

	Repeated Loading Pattern		Cyclic Loading Pattern		
	$\varepsilon^p{}_1$	$\varepsilon^p{}_3$	$\varepsilon^p{}_1$	$\varepsilon^p{}_3$	$\varepsilon^p{}_{45}$
a_1	0.022	-0.450	-0.691	0.434	0.604
a_2	0.255	0.253	0.281	0.218	0.310
a_3	2.96	6.66	64.3	-6.76	-8.27
a_4	-2.65	-1.87	-18.1	-0.933	-1.33
R^2	0.931	0.900	0.946	0.976	0.881

5.5 Shakedown Concept

Several researchers (Sharp and Booker 1984, Boulbibane et al. 2000, Werkmeister 2001) related the amount of permanent deformation incurred, and therefore the distress, by the pavement structure to the stress level applied. They suggested the use of Shakedown Theory to explain this relationship. The idea is that there exist three regions of stability of granular layers depending on the stress level applied. When the stress level is lower than a given value, the permanent strains accumulated in the system (granular layer) eventually reach a constant value and further load repetitions (at the same stress level) do not cause further unrecoverable deformations, therefore the system become stable and failure does not take place. At much higher stress levels, the permanent strain increases rapidly and results in the eventual failure of the granular layer in pavement structures. The third region of instability occurs at an intermediate stress level where the system accumulates permanent deformation at a decreasing rate but does not necessarily fail; this region is regarded as in a state of unstable equilibrium.

Werkmeister et al. (2001) compared permanent deformations measured in the laboratory with the types of responses usually described by the shakedown approach and accordingly suggested a design approach that can differentiate between the three regions of stability in the Shakedown Concept. The suggested design approach relies on a graph where permanent vertical strain rate is plotted versus the accumulated permanent axial strain. Three different regions in the graph are identified as:

- Range A: Plastic Shakedown
- Range B: Plastic Creep
- Range C: Incremental Collapse

As for the boundaries between these ranges, Werkmeister et al. (2001) suggests a simple linear relationship between the cell pressure and the deviatoric stress applied resulting the critical permanent strain levels described above. These 'critical limits' of shakedown deviatoric load define the lower and upper bounds of the intermediate range B and expressed as:

$$\sigma_{SD} = A_0\sigma_3 + A_1 \tag{5.41}$$

Where A_0 and A_1 are curve fit variable dependent on the material type.

The data obtained from the current research was used in plotting the graph proposed by Werkmeister et al. (2001). Figures 5.24 and 5.25 present the data of specimens subjected to repeated loading and Figure 5.26 summarizes the data for samples tested under cyclic loading conditions.

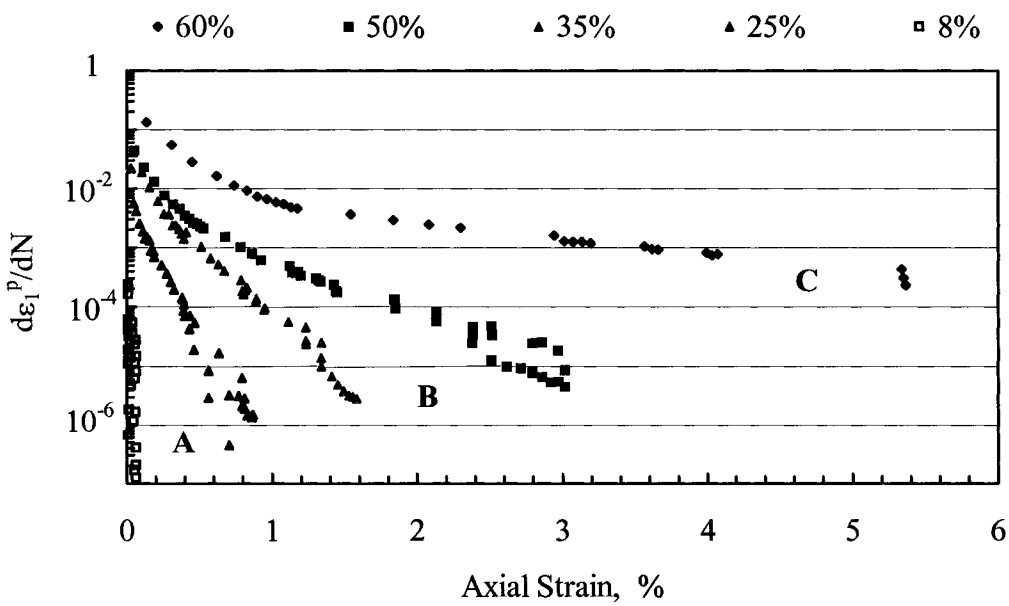

Figure 5.24: Werkmeister's Graph for Different RS Strength Levels (σ_3 = 35 kPa).

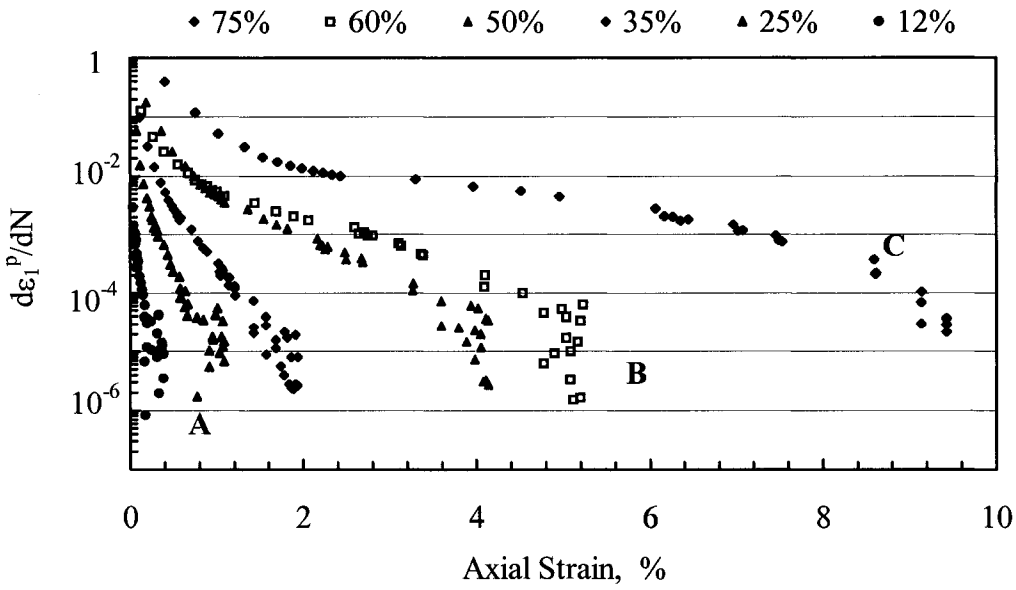

Figure 5.25: Werkmeister's Graph for Different RS Strength Levels (σ_3 = 100 kPa).

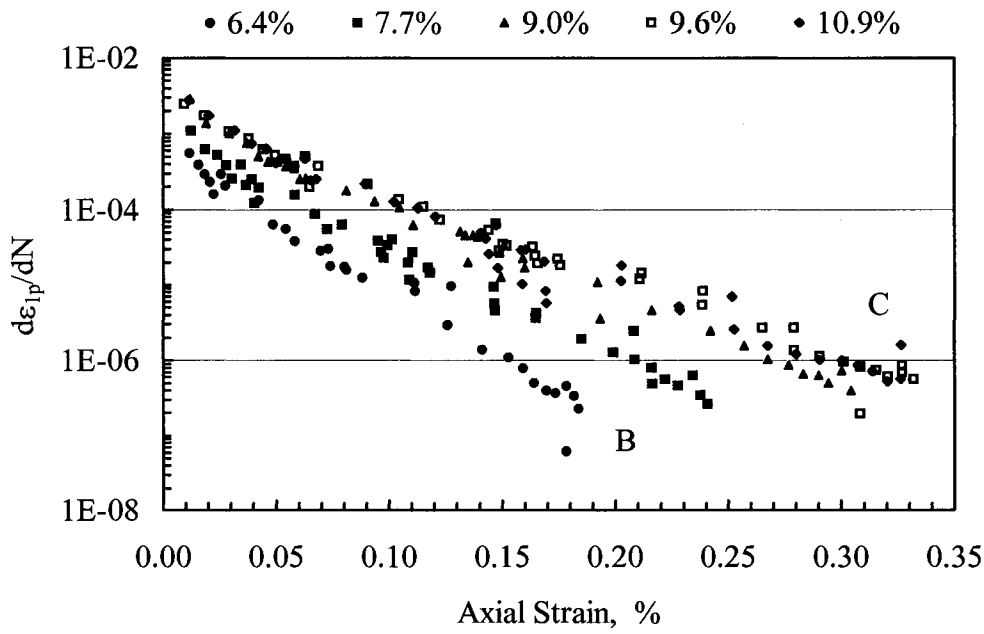

Figure 5.26: Werkmeister's Graph for Different CS Strength Levels (σ_3 = 100 kPa).

Following the guidelines given by Werkmeister et al. (2001), the tests performed under low confining stress (σ_3 = 35kPa) and presented in Figure 5.24, exhibit the following ranges: Results of stress level 8% and 25% fall in Range A, stress levels 35% and 50% are in Range B, whereas 60% stress level clearly falls in the C Range. As for tests performed at high confining pressure (σ_3 = 100 kPa), stress levels 12% and 25% fall in the A Range, 35%, 50% and 60% fall in the B Range and stress level 75% falls in the 'incremental collapse region' or otherwise termed as C Range (Figure 5.25).

As for tests where the specimen was subjected to cyclic stress loading pattern, the spectrum of strength levels applied fall in the B range as shown in Figure 5.26. These results hint again to the fact that cyclic two-directional loading is more detrimental to the granular material than repeated one-directional loading.

5.6 Volumetric Considerations

The previous analyses were done considering the axial strain of the soil mass as the critical response of the system. This is due to the fact that in pavement engineering and soil structures vertical deformation, or settlement, is the important design parameter (and easier to measure in the laboratory). However, when studying the behavior of a soil mass, the overall system must be considered and therefore the volumetric strain of the soil mass in question is a more realistic response to examine.

Studying Figures 4.57, 4.59 and 4.60, we notice that with increasing strength level applied, the specimen goes through three distinctive stages of deformation. First, densification sets in as the volumetric strain ε_v^p increases almost linearly until a maximum value is achieved (corresponding to maximum densification of the

specimen). During this stage, the aggregates start assuming the most compact packing possible, which results in relatively large axial strains whereas the accumulated radial strains are minimal.

In the second stage, the volumetric strain accumulation rate, with respect to the strength level, decreases until ε_v^p reaches zero (or a minimum, see discussion in Chapter 4). During this stage, the soil particles tend to rotate and readjust to the new stress level pushing some peripheral aggregates outward and repacking in an attempt to attain an optimum relative geometry. This mechanism causes an increase in radial strain of the specimen while the axial strain still accumulates but at a decreasing rate.

In the third stage, the accumulated volumetric strain becomes negative (expansion of the specimen). During this stage, the geometry of the aggregates cannot withstand the stress level applied and therefore they roll over each other and translate trying to sustain the pressure applied thus resulting in lateral expansion of the specimen witnessed by the large radial strains measured during this stage. These stages are illustrated as an example in Figure 5.27 below.

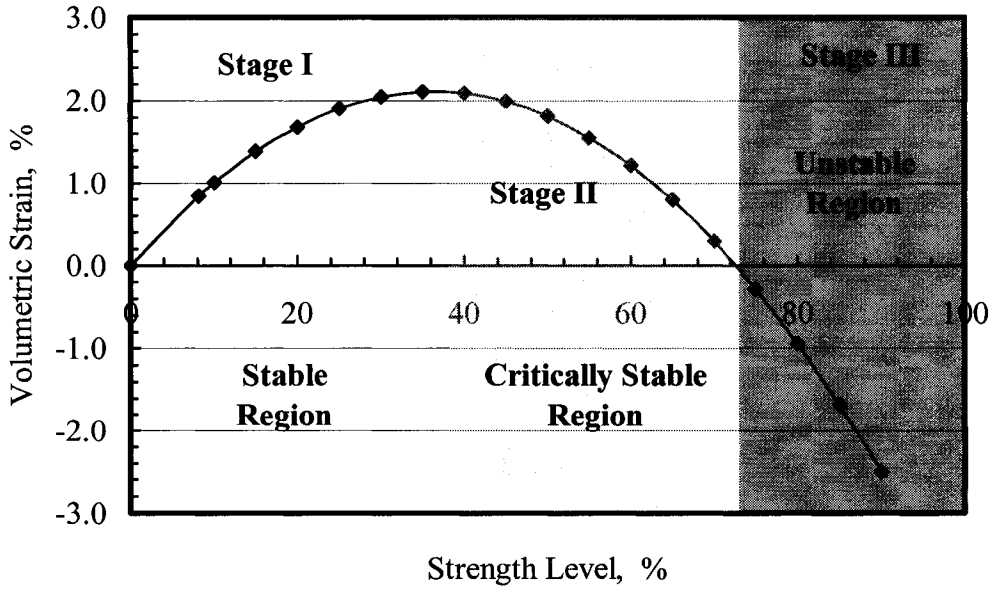

Figure 5.27: Three Stages of Volumetric Strain Variation with Strength Level.

The concept of the three stages of volumetric strain development outlined above can be explained in Shakedown Concept terms. Specimens loaded at a strength level (SL) in "Stage I" region, are stable. While specimens loaded at a strength levels in "Stage III" region are unstable and eventual "incremental collapse" is unavoidable. Whereas specimens subjected to strength levels falling in "Stage II" region are initially stable however further loading at the same level might overcome the resistance of the soil matrix and result in eventual failure of the specimen.

As for the case of tests conducted under cyclic loading pattern, examining Figure 4.61 shows that the volumetric strain increases with increasing strength level *SL* at decreasing rate reaching almost constant value. This implies that the specimen densifies with increase in *SL* until reaching a maximum density. This final stage might not represent failure in moist compacted soil conditions but is critical in the case of saturated soil tested under undrained conditions (Raad et al.1992).

5.7 Summary

In this chapter, efforts were made to find adequate models to interpret the data for different responses obtained from this research.

Uzan's resilient modulus model was found useful in interpreting the different moduli for a given number of load repetitions; however, it was unable to account for the observed strain hardening effects. On the other hand, the resilient modulus equation suggested by Johnson et al. proved to be adequate in modeling the different (total and resilient) moduli and at the same time it was possible to model in the strain hardening effect due to the repetitive nature of the load applied.

As for the permanent response case, Barksdale's hyperbolic model, which relates the accumulated plastic strain to the deviatoric stress applied, was found to be suitable in predicting the measured plastic strains for both repeated and cyclic load

patterns. However, Barksdale's equation relating the plastic strain accumulated to the number of load applications for a given stress level proved to be valid only for relatively low stress levels. Instead, Sweere's alternative power equation seemed more suitable in modeling the variation of the permanent strain with the number of load repetitions (N) applied. Moreover, a new simple model relating the accumulated plastic strain to the stress state, number of load repetitions and strength level applied, was presented.

Finally, a simple technique using the volumetric strain was presented to explain the stability of granular materials under repeated and cyclic loading. Three different stages of stability were defined, namely: stable, critically stable and unstable.

Chapter Six

Summary and Conclusions

6.1 Summary

The primary objective of this research was to better understand the behavior of granular materials and their strength degradation under traffic loading. To achieve that, a thorough review of the literature was carried out and the limitations of the current state of knowledge were identified. Furthermore, a comprehensive testing program was conducted to examine the various response parameters of a typical Alaskan base course material when subjected to the complex type dynamic loading induced by traffic.

Based on the results of these tests, models were selected to predict total as well as resilient moduli of the granular material tested and a methodology of pavement analysis incorporating such models was proposed. Furthermore, a simple but effective accumulated plastic deformation predictive model was proposed. Finally, a new and simple technique has been presented to discern the onset of instability in granular media when subjected to repetitive loading. This new technique attempts to relate the complex nature of failure of aggregates under dynamic loading to the much simpler and better-understood monotonic strength of such materials. This procedure is best demonstrated by a graph of measured volumetric strain versus the strength level (σ_d/σ_{df}) applied. From such a graph, three zones of stability are distinctively evident: a stable zone, a critically stable zone and an unstable zone.

6.2 Conclusions

The results of the research carried out in this study led to several interesting and important conclusions. These conclusions will contribute immensely to the current state of knowledge in the field and will unavoidably lead to new and improved pavement design techniques.

The most important and basic conclusions drawn from the study are summarized as follows:

- Resilient models under repeated and cyclic stress loading patterns were developed.
- Stress dependency effect on total moduli values both axial and shear was established which would allow the application of numerical techniques while accounting for kinematic compatibility between displacements and strains.
- Shear stress reversal effects which is simulated by cyclic stress loading increases density of the granular base whereas repeated stress loading conditions could cause dilatancy and failure under dynamic loading.
- Shakedown conditions are identified in terms of stable, critically stable and unstable based on build up of volumetric permanent strains under repeated loads.
- Shear strength under monotonic loading seems to be independent of applied strain rates for the granular soils tested.
- Failure under dynamic loading still occurs even though static strength increases due to strain hardening effects. Therefore, static shear strength is not a good indicator of failure under dynamic loading conditions.
- Prediction models for accumulation of permanent strain has been developed in terms of dynamic stress state applied and number of load repetitions.

- Shear reversal effects caused by traffic loading are usually ignored in conventional analysis, but based on results in this research, seem to have important detrimental effects on the behavior of granular layers.
- Repeated loading might cause more permanent axial reformation than cyclic loading at the same stress level, however, the latter results in much higher volumetric strain.

6.3 Recommendations for Future Research

As outlined above, the main objective of this research was to better understand the behavior of granular materials when subjected to the complex nature of wheel load. Based on this study, a number of conclusions were drawn, models were presented and their application in a comprehensive pavement design simulating dynamic loading were suggested. Moreover, efforts were made to identify the various stability stages of granular materials as a function of the strength level applied. This research also identified several areas requiring additional investigation. Recommendations for future research are outlined in the paragraphs below.

6.3.1 Additional Tests

In the course of this research, mainly one type of base course material typically used in Alaska was examined. The various models presented and new techniques suggested represent and describe properly the behavior of the material tested when subjected to repeated or cyclic loading conditions. It is important to verify if these models and corresponding conclusions may be applicable to a broader range of aggregates with different gradations, mineral composition and shape. This can be achieved by conducting similar laboratory tests on different materials to first support the findings and also to factor in, if needed, any soil parameter to generalize the results of the current study.

Suggested additional tests include a wider range of both confining pressures and strength levels applied as well as a series of saturated tests to better reveal the volumetric change of the specimen and the possibility of including void ratio as a parameter in the models. Moreover, since pavements in Alaska frequently witness several cycles of freeze and thaw, the set-up and triaxial cell manufactured as part of the current study, could be used to test samples that have been subjected to cycles of freeze and thaw to monitor the effect of this type of environmental impact on the various responses of granular materials under dynamic loading.

6.3.2 Field Test Verifications of the Findings in the Lab

The models suggested as well as the findings obtained from this research, can be verified and validated by results from field tests conducted on adequately instrumented pavement sections under Heavy Vehicle Simulator (HVS) loads. The results of such an endeavor could be used to validate and calibrate the models presented in this study as well as record the behavior of the base course layer under *very* long-term ($N>10^6$) load repetitions. This type of testing requires a large initial budget to setup, however, the potential results obtained are immensely beneficial in improving the current state of knowledge in the field of pavement engineering.

6.3.3 Finite Element Code

The predictive models presented in this research can be easily incorporated in a finite element code to analyze pavement structures. The finite element program to be used should allow for automatic material properties update after each cycle of calculation. Such a program if rendered user friendly can become an excellent tool for investigating and evaluating pavement sections.

6.3.4 Shakedown Theory

Results of this study suggest that specific stress thresholds govern the long-term behaviors of granular materials subjected to repetitive loading, and specifically the buildup of permanent deformation in the system. These stress thresholds, which can be expressed in terms of the static shear strength of the granular material used, outline limits between different stages of stability. This analogy agrees well with principals of shakedown theory. The extent of the analogy and the possibility of using shakedown formulation to model long-term granular behavior under traffic type loading, should be explored, and if feasible, be implemented in design procedures.

References

1. Allen J.J., "The Effects of Non-Constant Lateral Pressures on the Resilient Properties of Granular Materials," Ph.D. Thesis, University of Illinois, Unbana-Champaign, Urbana, Illinois, 1973.

2. Allen J.J. and Thompson M.R., "Resilient Response of Granular Materials Subjected to Time Dependent Lateral Stresses," TRR, 510, Transportation Research Board, Washington D.C., 1974, pp: 1-13.

3. Barksdale R.D., "Compressive Stress Pulse Times in Flexible Pavements for Use in Dynamic Testing," Highway Research Record 345, 1971, pp 32-44.

4. Barksdale R.D., "Repeated Load Test Evaluation of Base Course Materials," GHD Research Project No. 7002, Georgia Institute of Technology, 1972.

5. Barksdale R.D. and Itani S.Y., "Influence of Aggregate Shape on Base Behavior," TRR, 1227, Transportation Research Board, Washington D.C., 1988, pp: 173-182.

6. Biarez J., "Contribution de l'Etude des Propriétés Mécaniques de Sols et des Matériaux Pulvérulents," D.Sc. Thesis, Université de Grenoble, France, 1962.

7. Bonaquist R.F., "Development and Application of Comprehensive Constitutive model for Granular Materials in Flexible Pavement Structures," PhD. Dissertation, University of Maryland, College Park, Maryland, 1996.

8. Boulbibane, M., and Weichert, D., ". Application of Shakedown Theory to Soils with Non-Associative Flow Rules," Mechanics Research Communications, Vol. 24, No. 6, 1997, pp. 516-519.

9. Boulbibane M., Collins I.F., Weichert D., and Raad L., "Shakedown Analysis of Anisotropic Asphalt Concrete Pavements with Clay Subgrade", Canadian Geotechnical Journal, Vol. 37, 2000, pp: 882-889.

10. Brown S.F. and Hyde A.F.L., "Significance of Cyclic Confining Stress in Repeated Load Triaxial Testing of Granular Materials," Transportation Research Record 537, Transportation Record Board, Washington D.C., 1975, pp. 49-58.

11. Brown S.F. and Pappin J.W., "Analysis of Pavements with Granular Bases," Transportation Research Record 810, Transportation Research Board, Washington D.C., 1981, pp. 17-23.

12. Brown S.F. and Pappin J.W., "Modeling of Granular Materials in Pavements," Transportation Research Record 1022, Transportation Research Board, Washington D.C., 1985, pp. 45-51.

13. Castro G. "Liquefaction of Sands," PhD. Thesis, Harvard University, Cambridge, Massachusetts, 1969.

14. Chu H.H. and Vucetic M., "Settlement of Compacted Clay in a Cyclic Direct Simple Shear Device," ASTM Geotechnical Testing Journal, ASCE 15, No. 4, 1992, pp. 371-379.

15. Coffman B.S., Kraft D.C., and Tamayo J., "A Comparison of Calculated and Measured Deflections for the AASHO Road Test," Proceedings, Association of Asphalt Paving Technicians, Vol. 33, 1964, pp. 54-91.

16. Datta M., Rao G.V., and Gulhati S.K., "Development of Pore Water Pressures in a Dense Calcareous Sand under Repeated Compressive Stress Cycles," International Symposium on Soils under Cyclic and Transient Loading, Swansea, Great Britain, January 1980, pp. 33-47.

17. Dawson A.R., Thom N.H. and Paute J.P., "Mechanical Characteristics of Unbound Granular Materials as a Function of Condition," Proceedings of the European Symposium Euroflex 1993, Lisbon, Portugal. 1996, pp. 35-44.

18. Dehlen G.L., "The Effect of Non-linear Material Response on the Behavior of Pavements Subjected to Traffic Loads," PhD. Thesis, University of California, Berkeley, Berkeley, California, 1969.

19. Desai C.S., Somasundaram S., and Frantziskonis G., "A Hierarchical Approach for Constitutive Modelling of Geologic Materials," International Journal for Numerical and Analytical Methods in Geomechanics, Vol. 10, 1986, pp. 225-257.

20. Dobry R., Yokel F.Y., and Ladd R.S., "Liquefaction Potential of Overconsolidated Sands in Areas with Moderate Seismicity," Proceedings, Conference on Earthquakes and Earthquake Engineering: Eastern United States, Knoxville, Tennessee, September 1981, pp. 643-664.

21. Dobry R., Stokoe, K.H., Ladd, R.S., and Youd T.L., "Liquefaction Susceptibility from S-wave velocity," In-Situ Testing to Evaluate

Liquefaction Susceptibility: session no. 24, ASCE National Convention, St. Louis, Missouri, October 1981.

22. Dobry R., Ladd R.S., Yokel F.Y., Chung R.M., and Powell D., "Prediction of Pore Water Pressure Buildup and Liquefaction of Sands during Earthquakes by Cyclic Strain Method," Building Science Series 138, National Bureau of Standards, U.S. Department of Commerce, Washington D.C., July 1982.

23. Drnevich V.P., and Richart, F.E., "Dynamic Pre-Straining of Dry Sand," Journal of Soil Mechanics and Foundations, ASCE 96, No. 2, 1970, pp. 453-469.

24. Drucker D.C. and Prager W., "Soil Mechanics and Plastic Analysis or Limit Design," Quarterly of Applied Mathematics, Vol. 10, No. 2, 1952, pp. 157-175.

25. Drucker D.C., Gibson R.E., and Henkel D.J., "Soil Mechanics and Work-Hardening Theories of Plasticity," Transactions of the American Society of Civil Engineers, Vol. 122, pp. 338-346.

26. Duncan J.M. and Chang C.Y., "Nonlinear Analysis of Stress and Strain in Soils," Journal of Soil Mechanics, ASCE, Vol. 96, No. 5, September 1970, pp. 1629-1653.

27. Dunlap W.A, "A Report on a Mathematical Model Describing the Deformation Characteristics of Granular Materials," Technical Report No.1, Project 2-8-62-27, Texas Transportation Institute, Texas A&M, College Station, Texas, 1963.

28. Elsym 5, "Computer Program for Analysis of Elastic Layered Systems with Normal Loads," Coded by Gale Ahlborn, ITTE, University of California Berkeley, 1972.

29. Federal Highway Administration (FHWA), "Highway Statistics 2000", Office of Highway Policy Information, Federal Highway Administration, Washington D.C., Source: http://www.fhwa.dot.gov/ohim/hs00/index.htm, Accessed on August 28, 2003.

30. Garg N. and Thompson M.R., "Triaxial Characterization of Minnesota Road Research Project Granular Materials," Transportation Research Record 1577, Transportation Research Board, Washington D.C., 1997, pp. 27-36.

31. Griffiths D.V. and Prevost J.H., "Stress Strain Curve Generation from Simple Triaxial Parameters," International Journal for Numerical and Analytical Methods in Geomechanics, Vol. 14, 1990, pp. 587-594.

32. Habib P. and Luong M.P., "Sols Pulvérulents sous Chargement Cyclique *(Cohesionless Soils under Cyclic Loading)*," Matériaux et Structures sous Chargement Cyclique, Association Amicale des Ingénieurs Anciens Elèves de l'Ecole Nationale des Ponts et Chaussées, Palaiseau Septenber1978, pp. 49-79.

33. Hardin B.O., and Black W.L., "Vibration Modulus of Normally Consolidated Clay," Journal of Soil Mechanics and Foundations, ASCE 94, No. 2, 1968, pp. 355-369.

34. Hardin B.O. and Drnevich V.P., "Shear Modulus and Damping in Soils: Design Equations and Curves," Journal of Soil Mechanics and Foundation, ASCE 98, No. 7, 1972, pp. 667-692.

35. Hayes J.H. and Yoder E.J. "Effects of Repeated Loading on Gravel and Crushed Stone Base Material Used in the AASHO Road Test," HRB, Highway Research Record 39, 1963, pp. 82-96.

36. Hicks R.G., "Factors Influencing the Resilient Properties of Granular Materials," Ph.D. Dissertation, University of California, Berkeley, Berkeley, California, 1970.

37. Hicks R.G., and Monismith C.L., "Factors Influencing the Resilient Properties of Granular Materials," Highway Research Record, No. 345, 1971, pp: 15-31.

38. Highway Research Board, "The WASHO Road Test, Report 2: Test Data, Analysis, Findings," Highway Research Board Special Report 22, 1955.

39. Highway Research Board, "The AASHO Road Test, Report 5, Pavement Research," Highway Research Board Special Report 61E, 1962.

40. Hynes-Griffin M.E., "Pore Pressure Generation Characteristics of Gravel under Undrained Cyclic Loading," PhD Dissertation, University of California, Berkeley, Berkeley, California, 1988.

41. Ishihara K., "Soil Response in Cyclic Loading Induced by Earthquakes, Traffic and Waves," Proceedings of the 7th Asian Regional Conference on Soil Mechanics and Foundation Engineering, Haifa, Israel, Vol.2, 1983, pp. 42-66.

42. Ishihara K., "Soil Behaviour in Earthquake Geotechnics," Oxford Science Publications; 46, New York, 1996.

43. Johnson T.C., Berg R.L., and Dimillio A., "Frost Action Predictive Techniques: An Overview of Research Results," Transportation Research Record 1089, Transportation Research Board, Washington D.C., 1986, pp. 147-161.

44. Kalcheff I.V., "Characterization of Graded Aggregates as Related to their Behavior under Varying Loads and Environments," Presented at Conference of Graded Aggregate Base Materials in Flexible Pavements, Oak Brook, Illinois, March 1976.

45. Kasianchuk D.A., "Fatigue Considerations in the Design of Asphalt Concrete Pavements," Ph.D. Dissertation, University of California, Berkeley, Berkeley, California, 1968.

46. Khedr S., "Deformation Characteristics of Granular Base Course in Flexible Pavements," Transportation Research Record 1043, Transportation Research Board, Washington D.C., 1985, pp. 131-138.

47. Knutson R.H., Thompson M.R., Mullin T., and Tayabji S.D., "Materials Evaluation Study – Ballast and Foundation Materials Research Program," University Of Illinois, Urbana-Champaign, Report No. FRA-OR&D-77-02, Urbana, Illinois, 1977.

48. Kodner R. and Zelasko J., "A Hyperbolic Stress-Strain Formulation for Sands," Proceedings, Second Pan American Conference of Soil Mechanics and Foundation Engineering, Vol. I, Brazil, 1963, pp. 289-324.

49. Kolisoja P., "Resilient Deformation Characteristics of Granular Materials for Analysis of Highway Pavements," PhD. Thesis, Tempere University of Technology, Tempere, Finland, 1997.

50. Ladd R.S., "Preparing Test Specimens Using Undercompaction," Geotechnical Testing Journal, Vol. 1, No. 1, 1978, pp. 16-23.

51. Lade P. and Duncan J.M., "Cubical Triaxial Tests on Cohesionless Soil," Journal of Soil Mechanics and Foundations, ASCE 99, 1973, pp. 793-812

52. Lade P. and Duncan J.M., "Elasto-Plastic Stress-Strain Theory for Cohesionless Soil," Journal of Geotechnical Engineering, ASCE 101, No. 10, 1975, pp. 1037-1053.

53. Lade P., "Elasto-Plastic Stress-Strain Theory for Cohesionless Soil with Curved Yield Surfaces," International Journal of Solids and Structures, Vol. 13, 1977, pp. 1019-1035.

54. Lekarp F., Richardson I.R., and Dawson A., "Influences on Permanent Deformation Behavior of Unbound Granular Materials," Transportation Research Record 1547, Transportation Research Board, Washington D.C., 1997, pp. 68-75.

55. Lekarp F. and Dawson A.R., "Analysis of Permanent Deformation Behavior of Unbound Granular Materials," Proceedings of the International Symposium on Thin Pavements, Surface Treatment and Unbound Roads, Fredericton, New Brunswick, Canada, 1997, pp. 91-99.

56. Macky T.A. and Saada A.S., "Dynamics of Anisotropic Clays under Large Strains," Journal of Geotechnical Engineering, ASCE 110, No.4, 1984, pp. 487-504.

57. Majidzadeh K., Bayomy F., and Khedr S., "Rutting Evaluation of Subgrade Soils in Ohio," Transportation Research Record 671, Transportation Research Board, Washington D.C., 1978, pp. 75-84.

58. Matsui T., Ohara H., and Ito T., "Cyclic Stress-Strain History and Shear characteristics of Clay," Journal of Geotechnical Engineering, ASCE 106, No. 10, 1980, pp. 1101-1120.

59. May R.W. and Witczak M.W., "Effective Granular Modulus to Model Pavement Responses," Transportation Research Record 810, Transportation Research Board, Washington D.C., 1981, pp. 1-9.

60. Melan, E., "Theorie statisch Unbestimmter aus Ideal-Plastschen Baustoff", Sitzungsberichte der Akademie der Wissenschaften im Wien, Vol. IIa, 1936, pp: 145-195.

61. Monismith C.L., "Asphalt Mixture Behavior in Repeated Flexure," Report No. TE 66-6, University of California, Berkeley, Berkeley, California, 1966.

62. Monismith C.L., Seed H.B., Mitry F.G., and Chan C.K., "Prediction of Pavement Deflections from Laboratory Tests," Proceedings of 2nd international Conference on Structures Design of Asphalt Pavements, 1967, pp: 109-140.

63. Monismith C.L. Ogawa N., and Freeme C., "Permanent Deformation Characteristics of Subgrade Soils Due to Repeated Loadings," Transportation Research Record 537, Transportation Research Board, Washington D.C., 1975, pp. 1-17.

64. Moore W.M., Britton S.C., and Schrivner F.H, " A Laboratory study of the relation of stress to strain for a crushed limestone base material," Research Report 99-5F, Study 2-8-65-99, Texas Transportation Institute, Texas A&M University, College Station, Texas, 1970.

65. Mroz Z., Norris V.A., and Zienkiewicz O.C., "An Anisotropic Hardening Model for Soils and its Application to Cyclic Loading," International Journal for Numerical and Analytical Methods in Geomechanics, Vol. 2, 1978, pp. 203-221.

66. Pappin J.W., "Characteristics of a Granular Material for Pavement Analysis," Ph.D. Thesis, University of Nottingham, Nottingham, United Kingdom.

67. Paute J.L., Dawson A.R., and Galjaard P.J., "Recommendations for Repeated Load Triaxial Test Equipment and Procedure fro unbound Granular Materials," Proceedings of the European Symposium Euroflex 1993, Lisbon, Portugal. 1996, pp. 23-34.

68. Prévost J.H., "Plasticity Theory for Soil Stress-Strain Behavior," Journal of Engineering Mechanics, ASCE 104, No. 5, 1978, pp. 1177-1194.

69. Pyke R., Seed H.B., and Chen C.K., "Settlement of Sands under Multidirectional Shaking," Journal of Geotechnical Engineering, ASCE 101, No. 4, 1975, pp. 379-398.

70. Raad, L., Weichert, D., and Najm, W., "Stability of Multilayer Systems under Repeated Loads," Transportation Research Record, No. 1207, 1988, pp. 181-186.

71. Raad, L. Weichert, D. and Haidar, A., "Analysis of Full Depth Asphalt Concrete Pavements Using Shakedown Theory," Transportation Research Record No. 1227, 1989a, pp. 53-65.

72. Raad, L. Weichert, D. and Haidar, A., "Shakedown and Fatigue of Pavements with Granular Bases," Transportation Research Record No. 1227, 1989b, pp. 159-172.

73. Raad L., Minassian G.H., and Gartin R.S., "Characterization of Saturated Granular Bases under Repeated Loads," Transportation Research Report 1369, Transportation Research Board, Washington D.C., 1992.

74. Raad, L., and Weichert, D., "Stability of Pavement Structures under Long Term Repeated loading," Inelastic Behavior of Structures under Variable Loads, Edited by Mroz, Z., Weichert D., and Dorosz S., Kluwer Academic Publishers, 1995, pp. 473-496.

75. Rada G. and Wirtczak M.W., "Comprehensive Evaluation of Laboratory Resilient Moduli Results for Granular Material, " Transportation Research Record 810, Transportation Research Board, Washington D.C., 1981, pp. 23-33.

76. Roscoe K.H., Schofield A.N., and Wroth C.P., "On the yielding of Soil," Géotéchnique. Vol. 8, No. 1, 1958, pp. 47-54.

77. Scott R.F., "Plasticity and Constitutive Relations in Soil Mechanics," Journal of Geotechnical Engineering, ASCE 111, No. 5, 1985, pp. 563-605.

78. Seed H.B., Chan C.K. and Monismith C.L., "Effect of Repeated Load on the Strength and Deformation of Compacted Clay," Highway Research Record Vol. 34, Highway Research Board, Washington D.C., 1955, pp: 541-558.

79. Seed H.B., Mitry F.G., Monismith C.L., and Chan C.K., " Predictions of Pavement Deflection from Laboratory Repeated Load Tests," Report No. TE-65-6, Soil Mechanics and Bituminous Materials Research Laboratory, University of California, Berkeley, Berkeley, California, 1965.

80. Seed H.B., Mitry F.G., Monismith C.L. and Chan C.K., "Prediction of Flexible Pavement Deflections from Laboratory Repeated Load Tests," NCHRP Report No. 35, National Corporation of Highway Research Program, Washington D.C., 1967.

81. Seed H.B. and Idriss I.M., "Soil Moduli and Damping Factors for Dynamic Response Analysis," Earthquake Engineering Research Center, Report EERC 70-10, University of California Berkeley, December 1970.

82. Sharp R. and Booker J., "Shakedown of Pavements under Moving Surface Loads," Journal of Transportations Engineering, ASCE 110, No. 1, January 1984, pp: 1-14.

83. Sharp, R.W., "Pavement Design Based on Shakedown Analysis," Transportation Research Record, No. 1022, 1985, pp. 99-107.

84. Silver M.L., and Seed, H.B., "Volume Changes in Sands during Cyclic Load." Journal of Soil Mechanics and Foundation, ASCE 97, No. 9, 1971, pp. 1171-1182.

85. Sweere G.T.H. "Unbound Granular Bases for Roads," PhD. Thesis, University of Delft, Delft, The Netherlands. 1990.

86. Thompson M.R. and Smith K.L., "Repeated Triaxial Characterization of Granular Bases," Transportation Research Record 1278, Transportation Research Board, Washington D.C., 1990, pp. 7-17.

87. Thompson O.O., "Evaluation of Flexible Pavement Behavior of Granular Layers," Ph.D. Dissertation, University of Illinois, Urbana-Champaign, Illinois, 1969.

88. Trollope D.H., Lee I.K., and Morris J., "Stresses and Deformations in Two-Layer Pavement Structures under Slow Repeated Loading," Proceedings, Australian Road Research Board, Vol. I, Part 2, 1962, pp. 693-721.

89. Uzan J., « Characterization of Granular Materials, » Transportation Research Record 1022, Transportation Research Board, Washington D.C., 1985, pp. 52-59.

90. Vermeer P.A., "Formulation and Analysis of Sand Deformation Problems," Ph.D. Dissertation, Delft University of Technology, Delft, The Netherlands, 1980.

91. Vucetic M., "Cyclic Threshold Shear Strains in Soils," Journal of Geotechnical Engineering, ASCE 120, No. 12, 1994, pp. 2208-2228.

92. Weichert, D., and Raad, L., "Extension of the Static Shakedown Theorem to a Certain Class of Materials with Variable Elastic Coefficients." Mechanics Research Communications, Vol. 19, No. 6, 1992, pp. 511-517.

93. Werkmeister S., Dawson A., and Wellner F., "Permanent Deformation Behavior of Granular Materials and Shakedown Theory", Transportation Research Record 1757, Transportation Research Board, Washington D.C., 2001, pp. 75-81.

94. Witczak M.W. and Uzan J., "The Universal Airport Pavement Design System," Report I of IV: Granular Material Characterization, University of Maryland, College Park, Maryland, 1988.

95. Yokel F., Dobry R., Powell D., and Ladd R., "Liquefaction of Sands during Earthquakes, The Cyclic Strain Approach," Proceedings of International Symposium on Soils under Cyclic and Transient Loading, Swansea, United Kingdom, Volume 2, 1980, pp. 571-580.

96. Youd T.L., Compaction of Sands by Repeated Straining, Journal of Soil Mechanics and Foundation, ASCE 98, No. 7, 1972, pp. 709-725.

Appendix A

Petrography of the Soil Used

The following are excerpts taken from a report entitled "*Aggregate Testing for Eielson, AFB Runway Repair Including Petrographic Analysis of Coarse and Fine Aggregates*" written by Paul A. Metz, Ph.D., DIC and dated August 31, 2000.

Two samples of aggregate material were collected from the University Redi-Mix operations at their Moose Creek material site on April 25, 2000. Sample No. C-295 consists of approximately 60 kg of coarse aggregates (retained on No. 4 mesh) from a coarse aggregated stockpile. Sample C-296 consists of fine aggregates (passing No.4 mesh) from a fine aggregate stockpile.
The following five tests for deleterious materials were conducted on the materials as per ASTM procedures:

- ASTM C 117-95, 'Standard Test Method for Materials Finer than 75-μm (#200) sieve in Mineral Aggregates by Washing'
- ASTM C 123-94, 'Standard Test Method for Lightweight Pieces in Aggregates'
- ASTM C 142-78, 'Standard Test Method for Clay Lumps and Friable Particles in Aggregated.'
- ASTM C 295-90, 'Standard Guide for Petrographic Examination of Aggregates for Concrete'
- ASTM C 851-76 (CRD-C-130), 'Standard Recommendation Practice fro Estimating Scratch Hardness of Coarse Aggregate particles.'

The results of these tests indicate that samples C-295 and C-296 contain no clay lumps or friable material. The sample contains no shale. Sample C-295, medium-

grained and well-sorted gravel contains less than 0.1 % of material is finer than No. 200-mesh (75 μm). Sample C-296, fine grained and well-sorted aggregate contains 0.32% material diner than No. 200-mesh (75 μm). Sample C-295 contains no lightweight material with specific gravity less than 2.40. There is no clay ironstone present in either sample. Chert or chalcedonic quartz constitutes 1.8 % by weight of sample C-295 and 0.3% of the plus No. 50-mesh fraction of sample c-296. The chert is non-porous and has a density greater than 2.40 in sample C295 and has the same characteristics in sample C-296 as can be estimated under the petrographic microscope.

There is no claystone, mudstone, siltstone, shaly limestone, or argillaceous limestone in sample C-295 or C-296. In fact the chert is the only sedimentary rock type found in either sample. Rock fragments in the two samples include granite, diorite, gabbro, undifferentiated ultramafic rocks, felsic volcanic rocks, mafic volcanic rocks, chert, quartzite, mica schist, amphibole schist, gneiss, metamorphic quartz and quartz vein material.

There are no soft particles including organic matter in wither sample. The total deleterious material in the coarse aggregate sample is less than 0.1%.

Sample C-296 consists of the same general rock types as sample C-295, although the relative proportions are considerably different. Material finer than No. 50-mesh only contains mineral grains with no rock fragments present. This can be attributed to the coarse-grained nature of most of the parent rock types (coarse-grained igneous rocks and coarse-grained and medium to high-grade metamorphic rocks).

The smaller mesh fractions of sample C-296 contain increasing quantities of silica rich rocks and quartz clasts. This reflects the increased resistance to both

mechanical and chemical weathering of these rock types. Quartz and feldspar account for 87% of the mineral grains in the minus 50-mesh fraction.

In summary, the testing of the two samples indicates that the stockpiled material should produce good quality construction material with no measurable deleterious components.

Appendix B

Summary of Conducted Triaxial Tests

Table B-1: Summary of Conducted Triaxial Tests:

Test Group ID	Test	Material Tested	Test Variable	Sequence of Tests	Measured Parameters	Number of Tests
SS1	Static Strength	Base Course Marginal Material	ε_a, σ_3, γ_d	• Conditioning • Monotonic Loading	σ_{df}	36
SS2	Static Strength	Base Course	σ_3, SL, N	• Conditioning • RS Loading • Monotonic Loading	σ_{df}	24
SS3	Static Strength	Base Course	σ_3, SL, N	• Conditioning • RN Loading • Monotonic Loading	σ_{df}	16

Table B-1: Summary of Conducted Triaxial Tests (Continued)

Test Group ID	Test	Material Tested	Test Variable	Sequence of Tests	Measured Parameters	Number of Tests
SS4	Static Strength	Base Course	σ_3, SL, N	• Conditioning • CS Loading • Monotonic Loading	σ_{df}	24
SS5	Static Strength	Base Course	σ_3, N	• Conditioning • CN Loading • Monotonic Loading	σ_{df}	8
SS6	Static Strength	Base Course	σ_3, SL	• Conditioning • RS Loading • Monotonic Loading	σ_{df}	45

Table B-1: Summary of Conducted Triaxial Tests (Continued)

Test Group ID	Test	Material Tested	Test Variable	Sequence of Tests	Measured Parameters	Number of Tests
SS7	Static Strength	Base Course	σ_3, SL	• Conditioning • CS Loading • Monotonic Loading	σ_{df}	15
RES1	Resilient	Base Course	N	• Conditioning • Resilient	M_R	8
RES2	Resilient	Base Course	N	• Conditioning • RS Loading • Resilient	M_R	12
RES3	Resilient	Base Course	N	• Conditioning • RN Loading • Resilient	M_R	12

Table B-1: Summary of Conducted Triaxial Tests (Continued)

RES4	Resilient	Base Course	N	• Conditioning • CS Loading • Resilient	M_R	12
RN	Repeated Loading	Base Course	σ_3	• Conditioning • RN Loading	M_R, G_R, M_T, G_T, ε_1^r, ε_3^r, ε_1^p, ε_3^p , ε_v, γ_r, ν^r, ν^p, Δ	6
CN	Cyclic Loading	Base Course	σ_3	• Conditioning • CN Loading	M_R, G_R, M_T, G_T, ε_1^r, ε_3^r, ε_1^p, ε_3^p , ε_v, γ_r, ν^r, ν^p, Δ	6
RS	Repeated Loading	Base Course	σ_d, σ_3	• Conditioning • RS Loading	M_R, G_R, M_T, G_T, ε_1^r, ε_3^r, ε_1^p, ε_3^p , ε_v, γ_r, ν^r, ν^p, Δ	48

Table B-1: Summary of Conducted Triaxial Tests (Continued)

Test Group ID	Test	Material Tested	Test Variable	Sequence of Tests	Measured Parameters	Number of Tests
CS	Cyclic Loading	Base Course	σ_d, σ_3	• Conditioning • CS Loading	M_R, G_R, M_T, G_T, ε_1^r, ε_3^r, ε_1^p, ε_3^p, ε_v, γ_r, ν^r, ν^p, Δ	18

Conditioning: 1,000 stress control RS loading σ_d = 35 kPa, σ_3 = 35 kPa

Resilient: AASHTO Method T274-82

RS Loading: Repeated stress loading, RN Loading: Repeated strain loading,

CS Loading: Cyclic stress loading, CN Loading: Cyclic strain loading

ε_a: Axial strain rate, σ_3: Confining Stress, γ_d: Dry unit weight, σ_{df}: Deviatoric stress at failure, SL: Strength level, N: Number of load applications, M_R: Resilient modulus, G_R: Resilient shear modulus, M_T: Total modulus, ε_1^r: Resilient axial strain, ε_3^r: Resilient radial strain, ε_1^p: Permanent axial strain, ε_3^p: Permanent radial strain, ε_v: Volumetric strain, γ_r: Resilient shear strain, ν^r: Resilient Poisson's ratio, ν^p: Permanent Poisson's ratio, Δ: Damping ratio